PB86-211380

Catalytic Combustion
Component and System
Prototype Development

Acurex Corp., Mountain View, CA

Prepared for

Environmental Protection Agency
Research Triangle Park, NC

May 86

U.S. Department of Commerce
National Technical Information Service
NTIS

PB86-211380

EPA/600/7-86/021
May 1986

CATALYTIC COMBUSTION COMPONENT AND SYSTEM PROTOTYPE DEVELOPMENT

By

J. P. Kesselring and W. V. Krill

Acurex Corporation
Energy & Environmental Division
485 Clyde Avenue
Mountain View, California 94042

EPA Contract: 68-02-3122

EPA Project Officer: Jon E. Haebig

Air and Energy Engineering Research Laboratory
Research Triangle Park, N. C. 27711

AIR AND ENERGY ENGINEERING RESEARCH LABORATORY
OFFICE OF RESEARCH AND DEVELOPMENT
U.S. ENVIRONMENTAL PROTECTION AGENCY
RESEARCH TRIANGLE PARK, NC 27711

REPRODUCED BY
NATIONAL TECHNICAL
INFORMATION SERVICE
U.S. DEPARTMENT OF COMMERCE
SPRINGFIELD, VA. 22161

TECHNICAL REPORT DATA
(Please read Instructions on the reverse before completing)

1. REPORT NO. EPA/600/7-86/021
2.
3. RECIPIENT'S ACCESSION NO. PB86 211380/AS
4. TITLE AND SUBTITLE Catalytic Combustion Component and System Prototype Development
5. REPORT DATE May 1986
6. PERFORMING ORGANIZATION CODE
7. AUTHOR(S) J. P. Kesselring and W. V. Krill*
8. PERFORMING ORGANIZATION REPORT NO.
9. PERFORMING ORGANIZATION NAME AND ADDRESS

Acurex Corporation
Energy and Environmental Division
485 Clyde Avenue
Mountain View, California 94042

10. PROGRAM ELEMENT NO.
11. CONTRACT/GRANT NO. 68-02-3122
12. SPONSORING AGENCY NAME AND ADDRESS

EPA, Office of Research and Development
Air and Energy Engineering Research Laboratory
Research Triangle Park, NC 27711

13. TYPE OF REPORT AND PERIOD COVERED Final;
14. SPONSORING AGENCY CODE EPA/600/13
15. SUPPLEMENTARY NOTES AEERL project officer is Jon E. Haebig, Mail Drop 65, 919/541-2432. (*) Both authors are now with Alzeta Corp., 2343 Calle Del Mundo, Santa Clara, CA 95054.

16. ABSTRACT The report gives results of a project to develop the components required for catalytic combustion system operation and evaluation. The systems investigated (firetube boiler, watertube boiler, and gas turbine), when integrated with the catalytic combustor, have potential for both significant reductions in NOx emissions and increases in system thermal efficiency. The model gas turbine combustor incorporated a multiple spray nozzle fuel injector, and opposed jet igniter, an optical pyrometer for temperature control, and a graded cell catalytic combustor. The firetube boiler burner used a matrix of ceramic fibers vacuum-formed into a cylinder, and was successfully retrofitted into a 25-hp boiler. The radiative catalyst/watertube boiler was tested as a prototype for small industrial boilers with the catalyst tube either concentric with and surrounding the watertube, or surrounded by external watertubes. Significant reductions in NOx emissions were noted in all three systems. Additional work included both catalyst and substrate development for increased durability in reactors, as well as completion of a successful 1000-hour catalytic combustor test under lean combustion conditions comparable to gas turbine combustor operation.

17. KEY WORDS AND DOCUMENT ANALYSIS

a. DESCRIPTORS		b. IDENTIFIERS/OPEN ENDED TERMS	c. COSATI Field/Group
Pollution	Water Tube Boilers	Pollution Control	13B
Combustion		Stationary Sources	21B
Catalysis		Catalytic Combustion	07D
Evaluation			14G
Gas Turbines			13G
Fire Tube Boilers			13A

18. DISTRIBUTION STATEMENT Release to Public	19. SECURITY CLASS *(This Report)* Unclassified	21. NO. OF PAGES 310
	20. SECURITY CLASS *(This page)* Unclassified	22. PRICE

EPA Form 2220-1 (9-73)

NOTICE

This document has been reviewed in accordance with U.S. Environmental Protection Agency policy and approved for publication. Mention of trade names or commercial products does not constitute endorsement or recommendation for use.

Reproduced from
best available copy.

ABSTRACT

The report gives results of a project to develop the components required for catalytic combustion system operation and evaluation. The systems investigated (firetube boiler, watertube boiler, and gas turbine), when integrated with the catalytic combustor, have potential for significant reductions in NO_x emissions and increases in system thermal efficiency as well. The model gas turbine combustor tested incorporated a multiple spray nozzle fuel injector, an opposed jet igniter, an optical pyrometer for temperature control, and a graded cell catalytic combustor. The firetube boiler burner tested used a matrix of ceramic fibers vacuum-formed into a cylindrical configuration, and was successfully retrofit into an existing 25-hp boiler. The radiative catalyst/watertube boiler was tested as a prototype to small industrial-sized boilers with the catalyst tube either concentric with and surrounding the watertube, or with the catalyst tube surrounded by external watertubes. In all three systems significant reductions in NO_x emissions were noted. Additional work was performed to address both catalyst and substrate development for increased durability in reactors, and a successful 1000-hour catalytic combustor test was completed under lean combustion conditions comparable to gas turbine combustor operation.

CONTENTS

Abstract iii
Figures vi
Tables xi
Acknowledgement xii
Advisory Panel Members xiii

1 Summary 1
  1.1 Catalyst Development 1
  1.2 Fundamental Studies 2
  1.3 Gas Turbine Combustor 4
  1.4 Firetube Boiler Burner 4
  1.5 Radiative Watertube Boiler 5
  1.6 Conclusions 5
2 Introduction 7
  2.1 Catalyst Development 7
  2.2 Fundamental Studies 16
  2.3 Composite System Development 28
3 Catalyst Development 49
  3.1 High Temperature Ceramic Development for Catalytic Combustion 49
  3.2 Substrate Material Tests 102
  3.3 Catalyst Durability Tests 111
4 Fundamental Studies 126
  4.1 Experimental Setup 126
  4.2 Reaction Characterization 128
  4.3 Heterogeneous Kinetics 137
  4.4 Heterogeneous Fuel Bound Nitrogen Study 146
  4.5 Conclusions 147
5 Firetube Boiler Prototype Demonstration 154
  5.1 Introduction 154
  5.2 Prototype System Design 165
  5.3 Test Results 179
6 Watertube Boiler 196
  6.1 Introduction 196
  6.2 System Design Procedure 212
  6.3 Concentric Tube Radiant Section 236
  6.4 Nonconcentric Tube Boiler 249
7 Requirements for Future Development 266
  7.1 Status of Related Research Programs 266
  7.2 Required Further Development for System Implementation 267

APPENDIX

A Test Data 272

Preceding page blank

LIST OF FIGURES

Figure		Page
2-1	Bed temperature versus bed depth for two catalyst geometries	13
2-2	Radial distribution of CO_2 and CO concentrations at 5.08×10^{-2} cm for 3.18 mm tubes	21
2-3	Species concentration measurements in the axial direction in line with catalyst tube	22
2-4	Fuel conversion at varying preheat for platinum cylinders	23
2-5	Comparison of heterogeneous conversion of CH_4 and NH_3 . .	25
2-6	Gas turbine combustor	30
2-7	Gas turbine combustor transient operation	31
2-8	Comparison of catalytic and conventional gas turbine thermal NO_x emissions	32
2-9	Gas turbine combustor fuel NO_x emissions	34
2-10	Fiber matrix burner concept	36
2-11	Subscale combustor firetube NO emissions	37
2-12	Subscale firetube boiler burner assembly	38
2-13	Catalytic watertube boiler	40
2-14	Concentric radiative catalyst/watertube arrangement . . .	41
2-15	Radiative section thermal NO_x emissions	43
2-16	Comparison of Acurex and EER results on a NiO catalyst .	46
3-1	Vapor pressure versus temperature of selected metal oxides	60
3-2	Completely miscible -- solid solution	65
3-3	No solubility eutectic melting point	65
3-3	Formation of intermediate compound C	65
3-5	Geometric modifications to the basic honeycomb monolith	74

LIST OF FIGURES (Continued)

Figure		Page
3-6	Paper technology process	92
3-7	W. R. Grace tape rolling process	93
3-8	Model EPA-084 operating temperature	104
3-9	Model EPA-084 NO_x emissions	105
3-10	Model EPA-084 CO emissions	106
3-11	Model EPA-086 temperature cycle history	110
3-12	Durability test event chart	114
3-13	Durability test O_2 and CO_2 emissions levels	115
3-14	Durability test CO and UHC emissions levels	116
3-15	Durability test combustion efficiency performance	118
3-16	Parametric study -- effects on combustion efficiency . .	119
3-17	Thermal cycling performance	120
4-1	Common test configurations	127
4-2	Radial distribution of CO_2 and CO concentrations at 5.08×10^{-2} cm for 3.18 mm tubes	130
4-3	Species concentration measurements in the axial direction in line with catalyst tube	131
4-4	CO/CO_2 ratio for 6.35×10^{-3}m diameter platinum coated cylinders	132
4-5	CH_4 conversions to CO_2 + CO at variable throughput . . .	135
4-6	CH_4 conversion to CO, CO_2 as a function of stoichiometry	136
4-7	Heterogeneous kinetics, methane on platinum	139
4-8	Heterogeneous kinetics, propane on platinum	140
4-9	CO/CO_2 behavior with surface temperature for heterogeneous kinetics data, methane on platinum	142

LIST OF FIGURES (Continued)

Figure Page

4-10 CO/CO_2 behavior with surface temperature for heterogeneous kinetics data, propane on platinum 144

4-11 NH_3 conversion to NO at variable throughput 148

5-1 Firetube boiler with Acurex fiber burner 156

5-2 Subscale firetube boiler burner assembly 157

5-3 CTI 1 NO_x emissions 159

5-4 CTI 1 CO and HC emissions 160

5-5 CTI 3 and 4 -- NO_x emissions 161

5-6 CTI 3 CO emissions 162

5-7 J-M burner NO_x emissions 163

5-8 J-M burner CO emissions 164

5-9 J-M burner 100-hour test NO_x emissions 166

5-10 J-M burner 100-hour test CO and UHC emissions 167

5-11 Firetube boiler with J-M burner 175

5-12 Firetube boiler fiber burner assembly 176

5-13 Firetube boiler NO_x emissions 180

5-14 Firetube boiler with J-M burner NO_x emissions at various boiler loads 181

5-15 Firetube boiler with Acurex burner NO_x emissions at various boiler loads 182

5-16 Firetube boiler CO emissions versus excess air at 100 percent boiler load 185

5-17 Firetube boiler UHC emissions at 100 percent boiler load 186

5-18 Firetube boiler efficiency versus heat load 187

5-19 Firetube boiler durability test emissions and efficiency 189

LIST OF FIGURES (Continued)

Figure		Page
5-20	UHC emissions versus distance from front boiler plate . .	190
5-21	Fiber burner end following 1020-hour durability test . .	192
5-22	Fiber burner following 1020-hour durability test	193
6-1	Catalytic watertube boiler schematic	197
6-2	Catalytic watertube boiler radiant section tube arrangements	198
6-3	Graded and nongraded radiant section geometries	202
6-4	Graded and nongraded watertube system thermal NO_x comparison	203
6-5	Tube temperature profile for lean combustion at 264 MJ/hr (250,000 Btu/hr)	206
6-6	Tube temperature profile for rich combustion at 264 MJ/hr (250,000 Btu/hr)	207
6-7	Tube surface temperature profile for variable throughput testing	208
6-8	Radiant section energy transfer to watertubes	209
6-9	Radiant section fuel nitrogen conversion	211
6-10	Ceramic tensile strength comparison	225
6-11	Concentric watertube arrangement	231
6-12	Concentric watertube test fixture	233
6-13	Secondary air injector	237
6-14	1055 MJ/hr radiant section tube arrangement	238
6-15	1055 MJ/hr radiant section side view	239
6-16	Concentric tube thermal NO_x data for the 1055 MJ/hr watertube boiler radiant section	242
6-17	Modified concentric tube watertube radiant section . . .	245
6-18	Concentric watertube boiler radiant section NO_x emissions with preheat	247

LIST OF FIGURES (Concluded)

Figure Page

6-19 Concentric watertube boiler radiant section NO_x emissions without preheat 248

6-20 Catalytic watertube boiler system 250

6-21 Radiative section assembly 251

6-22 Shell details, watertube boiler 252

6-23 Convective section shell details 254

6-24 Watertube boiler radiant section test setup 256

6-25 Watertube boiler combustion efficiency 258

6-26 Watertube boiler NO_x emissions 259

6-27 Catalyst tube and gas temperatures 261

6-28 Catalyst tube and gas temperatures at low preheat 262

LIST OF TABLES

Table		Page
2-1	Noble Metal Screening Catalysts	9
2-2	Metal Oxide Screening Catalysts	10
2-3	Comparison of the Graded Cell Reactor with the Single Cell Reactor at Maximum Throughput	11
2-4	Fuel Nitrogen Test Catalysts	17
3-1	Periodic Table	57
3-2	Vapor Pressure Data of Various Oxides	59
3-3	Examples of Mixed Oxide Compounds	63
3-4	Possible Thermal Stress Conditions During Gas Turbine Operation	70
3-5	Thermal Conditions Existing at the Web Surface of a Honeycomb During Shutdown from 1644K	72
3-6	Properties of Some Common Ceramic Materials and their Thermal Stress Resistance	76
3-7	Low Thermal Expansion Materials	79
3-8	Coefficient of Thermal Expansion of Some Spinels and Perovskites	80
4-1	Heterogeneous Kinetic Parameters	145
4-2	Heterogeneous Rate Constants	146
5-1	Fiber Burner Specifications	173
5-2	Burner Performance Data	183
6-1	Historical Development of Catalytic Watertube Boiler . .	200
6-2	Watertube Boiler Design Procedure	213
6-3	Correction Factors for Heat Transfer Coefficients in Staggered Tube Arrangements	219
6-4	Predicted Tube Temperatures for Various Watertube Configurations	222

ACKNOWLEDGEMENTS

The development of prototype catalytic combustion systems described in this report has been graciously supported by many individuals. The authors would first like to thank the three EPA project officers, G. B. Martin, T. Lester, and W. S. Lanier for their interest and continuing review and support. Second, program direction was enhanced by the conduct of three advisory panel meetings and two catalytic combustion workshops. Those individuals who gave of their time to support the panel meetings in particular are listed on the following page. Finally, a large number of Acurex employees, consultants, subcontractors, and catalyst material suppliers have dedicated their efforts to this program. The success of the program has been a direct result of their efforts for which the highest of kudos are extended.

Advisory Panel Members

Name	Affiliation
W. C. Pfefferle	Consultant
S. A. Mosier	Pratt & Whitney Aircraft
J. F. Rice	Southern California Gas Company
D. A. McDuel	Southern California Gas Company
W. Wong	Southern California Gas Company
M. Bielec	Southern California Gas Company
R. Hangebrauck	IERL/EPA*
S. Cuffe	OAQPS/EPA
G. B. Martin	IERL/EPA*
T. Lester	IERL/EPA*
W. von KleinSmid	Southern California Edison Company
S. M. DeCorso	Westinghouse Electric Company
P. Pillsbury	Westinghouse Electric Company
N. Dibelius	General Electric Company
M. B. Hilt	General Electric Company
W. V. Krill	Acurex Corporation
R. M. Kendall	Acurex Corporation
J. P. Kesselring	Acurex Corporation
G. C. Snow	Acurex Corporation
E. B. Merrick	Acurex Corporation
M. J. Friedman	Acurex Corporation
S. J. Anderson	Acurex Corporation
H. Tong	Acurex Corporation
W. Hung	Solar Turbines International
R. Chronowski	Cleaver Brooks
W. E. Krauss	Cleaver Brooks
G. Halley	Kewanee Boiler Corporation
R. Neill	AiResearch Manufacturing Company
J. Sanborn	AiResearch Manufacturing Company
A. Dreisziger	Peabody Gordon-Piatt
F. E. Snyder	York-Shipley, Inc.
M. Gilligan	York-Shipley, Inc.
K. Petry	York-Shipley, Inc.

(*)Now, AEERL/EPA.

R. Niedzwiecki	NASA/Lewis Research Center
D. N. Anderson	NASA/Lewis Research Center
R. Tacina	NASA/Lewis Research Center
L. C. Angello	Electric Power Research Institute
A. Goodley	California Air Resources Board
M. Ahuja	California Air Resources Board
R. Rosenberg	Gas Research Institute
J. E. Drewry	Gas Research Institute
R. A. Vogt	Gas Research Institute
W. Axtman	American Boiler Manufacturers Association
B. Wallace	Naval Ship R&D Center
K. R. Burns	Engelhard Corporation
R. Schwartz	John Zink Company

SECTION 1

SUMMARY

The U.S. Environmental Protection Agency has sponsored research and development work in the area of catalytic combustion for over eight years. This work has focused on the development of catalytic combustion technology by developing a thorough understanding of the operation of catalytic combustors, screening a large number of catalyst and substrate materials to determine performance limitations, and then combining the basic understanding of the catalytic combustor with catalyst performance data and heat transfer considerations to design practical combustion systems. These systems have the potential benefits of lowered emissions of NO_X and CO and increased thermal efficiency. Composite systems tested and described here include a model gas turbine combustor, a fiber burner installed for retrofit or new firetube boiler applications, and a model watertube boiler. The testing of these systems was accompanied by durability testing of the burners.

1.1 CATALYST DEVELOPMENT

Catalyst development is one of the keys to the commercial acceptability of the catalytic combustor. Prior to the development of the catalytic combustor there was little need for catalysts capable of operation at temperatures above 1400K for extended periods of time, and little information was available on high temperature catalyst compositions or on suitable substrate carriers for the catalysts. A total of 12 noble metal and 20 metal oxide catalysts were tested to determine catalyst lightoff temperature, preheat temperature required for sustained catalyst operation, maximum throughput for the combustor without causing catalyst extinguishment, and emissions performance of the different combustors. Typical test times for each catalyst were 50 hours, and all of the noble metal catalysts tested showed significant decreases in activity during this period. However, high heat release rates were still achievable at the end of the test period.

Two of the noble metal catalysts were tested to evaluate the performance of the graded cell catalytic combustor concept, developed here and described in U.S. Patent 4,154,568. As predicted, the graded cell reactor was able to sustain stable combustion at volumetric heat release rates 2.7 times greater than those achieved with a single cell reactor. In addition, the graded cell reactor had a much more uniform axial temperature profile through the honeycomb monolith than the single cell reactor.

While metal oxide catalysts generally have lower activity than noble metal catalysts at temperatures of 1400K, they should have greater durability than noble metals and good activity at temperatures above 1600K. In fact, at high enough temperatures uncoated ceramic monoliths should have catalytic properties. Test times for the oxide catalysts investigated were again on the order of 50 hours, and high heat release rates were generally obtained at test conditions of 1700K bed temperature. However, interactions between the coated metal oxide catalysts and the substrate ceramic materials usually led to poor thermal shock characteristics and fracture of the substrate material. Since the weakened substrate was a result of catalyst-substrate interaction, it appeared that testing of substrate materials with an active component as an integral part of the substrate would be of interest. Eight of these "active monolith" materials were prepared as either bundled tubes or drilled disks and combustion tested. All test specimens showed acceptable catalytic activity, with combustion data similar to the coated oxide systems tested. Thermostructural promise was also shown by these materials, but better fabrication techniques (such as extrusion) are required before further testing should be done.

1.2 FUNDAMENTAL STUDIES

Fundamental studies were initiated under this program to provide greater understanding of the chemical processes of catalytic combustion. Development of this information increases the ability to predict combustor performance and allows analyses leading to system optimization. The phenomena studied here include a determination of heterogeneous hydrocarbon and nitrogen oxidation rates, a comparison of the extent of reaction with predicted mass transfer rates, and a determination of heterogeneous oxidation rate constants.

In order to isolate surface reaction events from the simultaneous gas-phase reactions that occur in practical high-temperature catalytic combustors, a test setup incorporating catalyst-coated cylinders in crossflow was used. Exhaust gas analysis was made with continuous gas analyzers for CO, CO_2, O_2, NO_X, and HC. Tests were run over a range of stoichiometries from fuel-rich to fuel-lean.

Test results showed that the use of cylinders in crossflow was an effective technique for studying the heterogeneous portion of catalytic combustion. In the higher temperature ranges of operation (near stoichiometric), the surface reaction rate on the cylinder in crossflow configuration is limited by lean reactant diffusion. In this regime, the combustion of methane was promoted to completion by the catalyst with carbon dioxide as the major product. This data is most useful for understanding normal, steady state operation encountered in honeycomb monolith type catalysts. It will allow further optimization in the amount of surface area required for a specific energy release rate.

The measured conversion rates were significantly underpredicted by calculated lean reactant mass transfer limitations. This may be due to the use of a mass transfer coefficient which does not fully account for freestream turbulence levels or high surface temperatures. Regions of flow stagnation or recirculation, possibly attached to the cylinders, may also promote higher conversion rates. However, other data, including carbon monoxide formation behavior, are not clearly supportive of this concept.

Small amounts of hydrogen in the reactant flow gave precise catalyst surface temperature control over ranges in which methane and propane heterogeneous kinetics could be quantified. The experimentally measured activation energies were 7.54×10^7 J/kg-mole for methane and 7.42×10^7 J/kg-mole for propane. These values compare favorably with those reported by other workers. Also, the relative magnitudes agree with experience in which propane ignition occurs earlier and at a lower temperature and is more difficult to blow out than methane on a given catalyst. This surface reaction rate information is required for efficient design of catalyst entry regions. The Nusselt number (Sherwood number for mass transfer) is large in these or other zones where flow stagnation may occur, giving high mass transfer rates. Additionally, kinetic information is necessary to predict lightoff characteristics and maximum throughput capabilities before catalyst blowout.

1.3 GAS TURBINE COMBUSTOR

The model gas turbine combustor tested under this program incorporated a multiple spray nozzle fuel injector for No. 2 diesel fuel, an opposed jet igniter, an optical pyrometer for temperature control, and a graded cell honeycomb catalytic combustor. The system was successfully tested over pressures from 1 x 10^5 to 5 x 10^5 Pa (1 to 5 atm), a combustor outlet temperature of 1700K, combustor inlet temperatures of 589 to 672K, and a maximum heat release rate of 4.78 x 10^5 J/hr. NO_X emissions obtained with this system were typically less than 15 ppm and resulted primarily from the nearly 100 percent conversion of the small amount of nitrogen in the liquid fuel. Combustion efficiencies above 99.985 percent were obtained at all test conditions.

Separate durability testing of a terbium-cerium-thorium (TCT) honeycomb catalyst which used a noble metal entrance segment for low temperature lightoff on propane showed successful performance for over 1000 hours at a pressure of 10^5 Pa (1 atm) and an inlet velocity of 13.4 m/sec. Emissions at the end of the test period were 2 ppm NO_X, 17 ppm CO, and <1 ppm HC. The test was concluded with five successful on/off cycling tests.

1.4 FIRETUBE BOILER BURNER

A 1055-MJ/hr fiber burner was prepared and installed in a York-Shipley 245 kW (25 hp) firetube boiler. The fiber burner, a matrix of ceramic fibers vacuum-formed into a cylindrical configuration, radiates flamelessly to the firetube wall during operation. Following preliminary tests of the boiler with conventional burner and parametric tests of the fiber burner, the system was operated for over 1000 hours at 100 percent load and 15 percent excess air. At these conditions, emissions were 13 ppm NO_X, 29 ppm CO, and 10 ppm HC. This represents a decrease in NO_X emissions of almost 80 percent and is coupled with an efficiency increase of nearly 2 percent. In addition, because the fiber burner operates at lower excess air than the conventional burner and is capable of more uniform radiant energy transfer, the boiler with fiber burner could be successfully operated at 120 percent of load and operated in an extremely quiet manner.

1.5 RADIATIVE WATERTUBE BOILER

A radiative catalyst/watertube boiler was developed and tested as a prototype to small industrial-sized boilers. Systems, both with the catalyst tube concentric with and surrounding the watertube, and with the catalyst tube surrounded by external, nonconcentric watertubes, were built and tested. The catalyst tube consisted of a catalyst-coated ceramic cylinder, while the watertube was a concentric cylinder arrangement that operated on natural circulation of the water and steam.

The most successful system tested used concentric catalyst and watertubes and was capable of operation to 1319 MJ/hr with thermal NO_X emissions less than 20 ppm at excess air levels greater than 25 percent. A problem arose where both concentric and nonconcentric system designs had ceramic tube fractures after several hours of operation. Further work to minimize this problem will be required.

1.6 CONCLUSIONS

The results of this program as described above, including a large body of data on individual catalyst performance and fundamental behavior of catalytic combustors, has brought the commercial application of catalytic combustors to certain systems much closer. The use of ceramic fiber burners in gas-fired equipment with a water-backed heat receiver, as is the case in domestic water heaters and firetube boilers, appears to require only successful field demonstration before full-scale commercialization efforts can begin.

Further laboratory demonstration of honeycomb catalysts used in gas turbine systems is required, but major advances have been made under the current program. The use of catalytic combustors in watertube boilers requires significant effort to eliminate ceramic tube failure and flameholding problems prior to field demonstration.

SECTION 2

INTRODUCTION

During the first two years of the program, significant achievements were made in catalyst development, fundamental studies, and composite system development. These activities were the basis for composite system testing and prototype system demonstration in the third and fourth program years. A summary of the first two years' development activities are described in the following subsections.

2.1 CATALYST DEVELOPMENT

Throughout the present (References 2-1, 2-6) and prior (Reference 2-2) programs in catalytic combustion, catalyst material development has been a key element. Implementation of catalysts in system combustors requires prolonged activity and material durability. Specific material requirements depend on the system configuration and operating conditions.

The effect of operating temperature on catalyst life has been a prominent constraint in material development throughout this program. Low temperature catalysts may be suitable for many gas turbine and boiler combustion applications. These low temperatures (below 1589K), however, require catalysts of relatively high activity to complete oxidation reactions. Higher operating temperatures may be required for other systems. In these systems, catalyst compounds may have thermostructural and chemical stability problems.

To develop and evaluate materials for use at operating temperatures of 1256 to 1922K (1800 to 3000°F), tests of substrates coated with noble metal catalysts, substrates coated with metal oxide catalysts, and active monoliths (where the catalyst is integral with the ceramic substrate) were performed. The test models are listed in Tables 2-1 and 2-2. Nearly all models were monolithic in configuration and of graded cells when appropriate materials were available. They were tested in a small scale atmospheric test facility as described in Reference 2-3. Test procedures were standardized to determine lightoff, preheat temperature, maximum throughput, and combustion temperature requirements for natural gas and, for some models, diesel fuel. Combustion tests were supplemented by BET surface area measurements (as described in Reference 2-2), scanning electron microscopy, and elemental analysis by X-ray energy dispersion.

2.1.1 Noble Metal Catalyst Screening

During the first 24 months of the program, a total of 12 noble metal catalysts were tested. The coatings were prepared by Oxy-Catalyst, Inc., E. I. DuPont, UOP Inc., Houdry/Air Products, and Acurex. A variety of substrates were used, including Kanthal, DuPont alumina Torvex, Corning cordierite and zirconia spinels (MCB-7 and MCB-10), General Refractories mullite, and Alfred University alumina sponge. The results of the tests can be generalized as follows.

The use of noble metals for catalytic combustion is restricted to temperatures below 1589K (2400°F) due to increased noble metal volatilization at higher temperatures. A gradual loss of the catalyst material is observable as decreasing activity at lightoff, reduction of measured surface area by a factor of 10 following 20 hours of combustion, and microscopic observation of material loss at the surface. Both metal vaporization and mobility (lack of adhesion) appear to contribute to catalyst loss at high temperature. Although low surface area always results, adequate combustion capability may remain. Stable and complete combustion with low emissions is achievable with only small amounts of noble metal present (tests suggest as little as 0.01 weight

TABLE 2-1. NOBLE METAL SCREENING CATALYSTS

Identification number	Materials Catalyst	Substrate	Manufacturer	Test date	Facility
EPA-001, -002	Pt	Corning MCB-7	Oxy-Catalyst	10/18-10/20/78	HP[1].
	Pt-Rh	Kentucky metals Kanthal			
-013	Pt-Rh	Kentucky metals Kanthal	Oxy-Catalyst	12/14/78	HP
-003	Pt	DuPont alumina	DuPont	12/7-12/12/78	HP
-024	Pt-Rh	DuPont alumina	DuPont	4/17-4/18/79	HP
-007	Prop.	Corning MCB-7	UOP	11/3-11/20/78	HP
-015	Prop.	Corning cordierite	UOP	1/3-1/10/79	HP
-020, -021	Prop.	DuPont alumina	UOP	3/20-4/2/79	HP
-009	Prop.	General Refractories mullite	UOP	4/3-4/24/79	atm[2].
-008	Prop.	Corning MCB-10	UOP	4/24-2/27/79	atm
-031	Pt	Corning MCB-12	Houdry	5/11-5/22/79	HP
-056	Pt	Alfred alumina sponge	Acurex	10/25-10/29/79	atm

1. High pressure test facility
2. Atmospheric test facility

TABLE 2-2. METAL OXIDE SCREENING CATALYSTS

EPA No.	Materials		Manufacturer	Test Dates	Facility
	Catalyst	Substrate			
012	Proprietary	Proprietary	Acurex	5/9-5/17/78	HP
010	(La-Sr-Pt)CoO_3 Perovskite	DuPont alumina	DuPont	10/26-10/21/78	HP
006	Mn-La-Cu	DuPont alumina	Pfefferle	11/27-12/1/78	HP
005	Mn-La-Cu	3M zircon mullite	Pfefferle	12/19/78	HP
016	$LaCrO_3$/Pt	DuPont alumina	Acurex	4/6-4/13/79	atm
022	NiO/Pt	Corning MCB-12	Acurex	4/30-5/4/79	atm
032	Cr_2O_3	DuPont alumina	Acurex	5/10-5/11/79	atm
030	Cr_2O_3/Pt	Corning MCB-12	Houdry	5/24-5/25/79	HP
034	Base metal-Pt	Corning MCB-12	Grace	6/11-6/14/79	HP
033	Base metal-Pt	DuPont alumina	Grace	6/22-6/26/79	HP
017	Cr_2O_3-NiO	Norton SiC	Acurex	7/10-7/12/79	atm
023	Base metal	Corning MCB-12	Oxy-Catalyst	7/17-8/6/79	atm
035	None	Corning MCB-10 (Y_2O_3 stabilized ZrO_2)	Corning	7/24-7/30/79	atm
041	$MgAl_2O_4 \cdot NiAl_2O_4$		Trans-Tech	8/13-8/15/79	atm
042	$LaAlO_3 \cdot MgCrO_3$		Trans-Tech	8/17-8/21/79	atm
045	$MgAl_2O_4 \cdot Fe_3O_4$		Trans-Tech	8/21-8/23/79	atm
043	None	Corning MCB-12 (zirconia spinel)	Corning	8/28-8/29/79	atm
046	$MgAl_2O_4 \cdot MgCr_2O_4$		Trans-Tech	8/30-8/31/79	atm
047	None	Alumina	DuPont	9/5/79	atm
048	$MgAl_2O_4 \cdot Fe_3O_4$	40% Cr cermet	Trans-Tech	9/11-9/12/79	atm
055	None	Carborundum silicon carbide	--	10/11-10/12/79	atm
057	Cr_2O_3	Corning MCB-1	Acurex	11/12-11/19/79	atm
072	$Al_2O_3 \cdot Cr_2O_3$		Trans-Tech	5/9/80	atm
071	$FeCr_2O_4 \cdot MgCr_2O_4$		Trans-Tech	5/14-5/21/80	atm
070	70% $Al_2O_3 \cdot$30% Cr		Trans-Tech	6/3-6/5/80	atm
081	Cr_2O_3	Proprietary	Acurex	5/21-8/27/80	atm
075	Proprietary	Corning MCB-12	Houdry	6/11-6/13/80	atm

percent may be sufficient for some fuels). With natural gas, emissions less than 5 ppm of CO, UHC, and NO_x are typical. Volumetric heat release rates were limited to approximately 8×10^6 J/hr-Pa-m^3 (22×10^6 Btu/hr-atm-ft^3) for the configurations tested.

Although all of the catalysts had some apparent activity at low surface area, none exhibited exceptional lifetimes. Tests were limited to less than 50 hours, and significant changes in activity were apparent. Also, none of the ceramic substrates survived without fracturing by thermal shock. The Kanthal (metal) substrate is capable of operation to 1589K. However, techniques to develop a sufficiently durable coating for this metal monolith are still required.

Two of the noble metal catalysts were tested to evaluate the performance of the graded cell concept (U.S. Patent No. 4,154,568) as developed under EPA Contract 68-02-2116 (Reference 2-2). The catalysts were a UOP preparation on one graded set and one small cell set of DuPont alumina Torvex.

As predicted, the graded cell concept was able to sustain stable combustion at higher volumetric heat release rates than the single cell model. The results at maximum throughput are given in Table 2-3.

TABLE 2-3. COMPARISON OF THE GRADED CELL REACTOR WITH THE SINGLE CELL REACTOR AT MAXIMUM THROUGHPUT

Parameter	Graded cell reactor	Single cell reactor
Fuel flow, Kg/hr (lbm/hr)	6.89 (15.21)	2.50 (5.51)
Space velocity, 1/hr	427,100	167,900
Volumetric heat release, J/hr-Pa-m^3 (Btu/hr-atm-ft^3)	7,450,000 (20,244,000)	2,573,000 (6,991,000)

The high heat release rates are achieved in the graded cell due to its ability to maintain reaction rates at the entrance region of the bed at high velocities. This effect is illustrated in Figure 2-1 where temperature profiles are quite uniform for the graded cell reactor over a range of velocities. In contrast, the single cell reactor cannot maintain reactions at its entrance except at much lower velocities. The tests also showed comparable lightoff temperatures and higher combustion efficiency at high throughputs for the graded cell model, demonstrating the applicability of the concept to high throughput systems.

2.1.2 Metal Oxide Catalyst Screening

Approximately 20 metal oxide catalysts were tested during the first two years of the program. These catalysts were prepared by coating oxides of La, Sr, Mn, Cu, Cr, Co, or Ni on ceramic substrates of Corning mullite-alumina-titanate (MCB-1), Corning zirconia spinel (MCB-12), 3M zircon mullite, Norton silicon carbide, or Carborundum silicon carbide as well as several proprietary ceramics. In addition, some of the ceramic monoliths were tested without any coating to compare their activity to the activity of coated catalysts. In some tests, platinum was added to the oxide composition to enhance low temperature activity.

The lower inherent activity of the metal oxide catalysts is apparent at lightoff and during steady state operation. Higher temperatures are required to initiate substantial heat release; many models were lit off by an auxiliary flame (opposed jet igniter). At steady state, higher combustion temperatures are required to achieve hydrocarbon oxidation rates comparable to those of the noble metals. For these reasons, operation of the metal oxides is generally restricted to temperatures above 1533K (2300°F). The operating range can be enhanced by addition of noble metal components, usually at the lower temperature, upstream end of the catalyst. The lower activity of metal oxides was also exemplified by the very high operating temperature

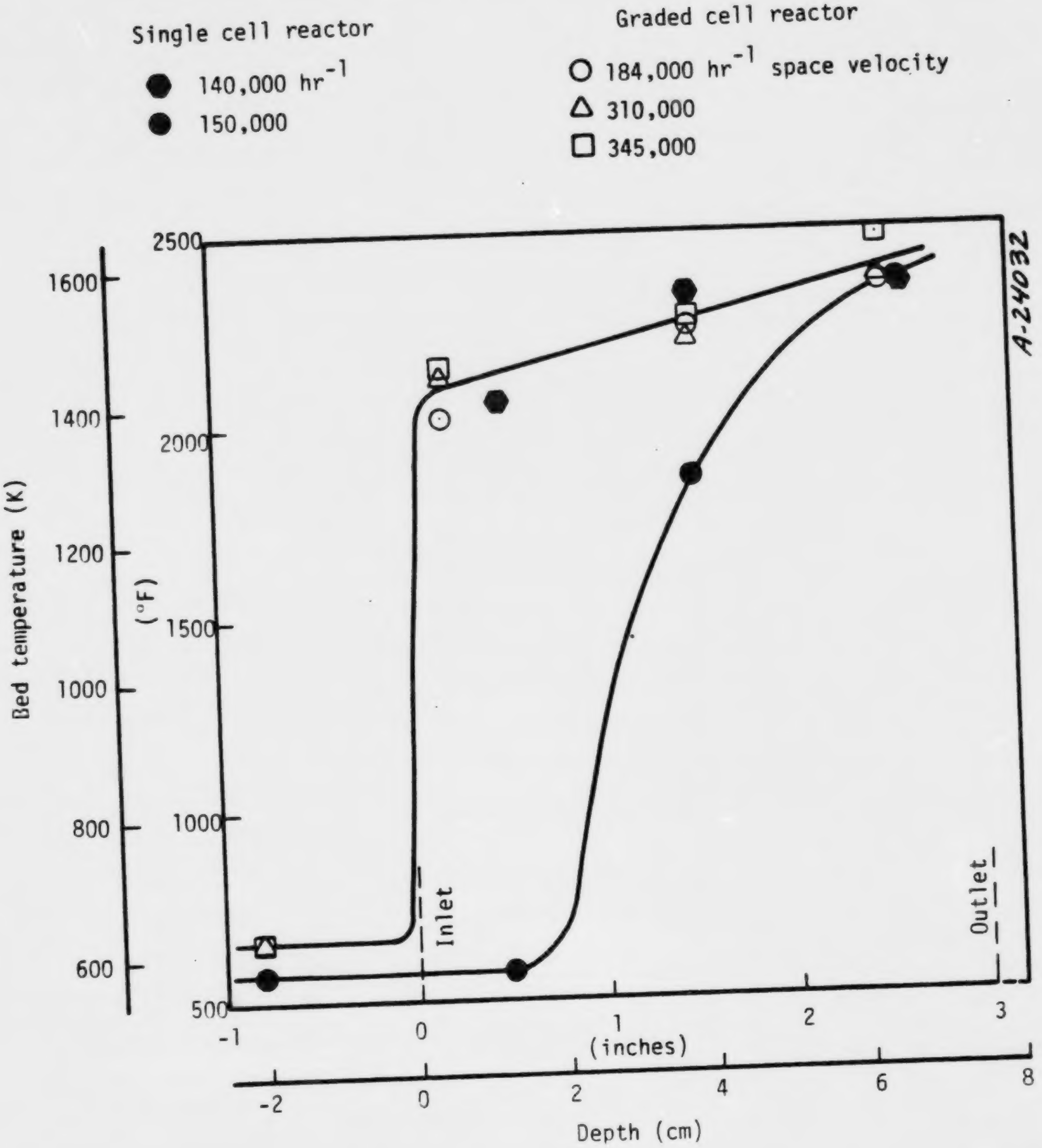

Figure 2-1. Bed temperature versus bed depth for two catalyst geometries.

requirements of the bare substrates. These are oxides of generally lower activity than those listed above (such as Al, Si, and Zr) that provide relatively complete combustion only at temperatures in excess of 1700K (2600°F).

When operating at the stated temperatures, the metal oxide catalysts exhibited equal combustion efficiencies to those of the noble metal catalysts. However, somewhat higher thermal NO_x occurred in some cases as a result of the higher combustion temperatures. Also, higher volumetric heat release rates were generally possible with the higher operating temperatures, with some oxide models approaching 40×10^6 J/hr-Pa-m^3.

Of the oxides tested, those of cobalt, chromium, manganese, and nickel appear most active, being able to sustain reactions at very low values of surface area (less than 0.005 m^2/g). In fact, measurable surface area is of little importance. Significant surface sintering can occur without great loss in activity, and the high melting temperatures of the oxides enhance their stability at the required higher operating temperatures.

With the high activity of these oxides at temperatures above 1533K, however, reactions with the substrate materials were common. Reactions of cobalt with alumina and silica are very rapid and greatly affect the structural integrity of the underlying substrate. These catalyst/substrate interactions often result in compounds with lower eutectic melting temperatures than either the catalyst or substrate compounds, limiting the upper use temperature of the prepared catalyst. For this reason, and because of poor thermal shock characteristics of many of the substrate materials tested, the active monolith catalyst concept described in Section 3 was tested during the second year of the program.

As shown in Table 2-2, eight active monolith materials prepared by Trans-Tech Inc. were tested under the program. These included oxides of Mg, Al, La, Fe, and Cr and were fabricated either as drilled disks or tube bundles of a single cell diameter.

All models showed acceptable catalytic activity as evidenced by the ability to run at surface temperatures comparable to those of the coated oxide catalysts and with comparable variations in preheat and mass throughput. As with other oxide catalysts tested, a higher level of preheat energy was required for ignition, but combustion efficiency was high at steady state operating conditions. NO_x levels were low for all models tested.

Thermostructurally, the material formulations appear promising. The crude, drilled monoliths fractured most readily at the thickest sections, but not as badly as with many commercial monoliths tested under this program. These new materials fabricated in monolithic form may have better structural characteristics due to the more uniform web thicknesses and lower material densities that could be achieved. Alternate fabrication techniques were to be pursued during the third year of the program as described in Section 3. Of all catalysts tested, these active monoliths appear to have the greatest potential for long combustor life.

2.1.3 Fuel Nitrogen Testing

Earlier studies of fuel nitrogen conversion to nitrogen oxides by catalytic combustion (References 2-2 and 2-3) indicated that the degree of fuel-NO_x control is dependent on several characteristics. Under fuel-lean conditions, all catalysts provide high conversion of the fuel nitrogen to NO_x (80 to 100 percent conversion). Under fuel-rich conditions, lower conversion rates are possible and provide hope for staged low NO_x systems burning fuels with high nitrogen content. The stoichiometry at which minimum conversion occurs is dependent on such factors as operating temperature, pressure, and catalyst type.

To further investigate the potential for fuel-NO_x control, the fuel nitrogen task was devoted to developing conversion characteristic data for a variety of catalysts. Eight catalysts were selected for testing based on the results of catalyst screening. They are listed in Table 2-4. Model EPA-060 was tested at pressures to 0.30×10^6 Pa (3 atmospheres) for comparison to EPA-058.

For these catalysts, test results showed that the conversion rates, although minimum under rich conditions, were not sufficiently low to warrant further system development. Although reductions in fuel nitrogen conversion could be achieved in a two-stage, rich-lean system with these catalysts, the 20 to 30 percent conversion levels achieved are probably comparable to those achievable with staging in conventional combustors. Operation at pressure resulted in somewhat higher conversions under rich conditions. Conversion levels below 10 percent would indicate a definitive advantage with the catalytic combustor.

Conversions below 10 percent were achieved by a wall heat loss control technique. This concept, its test results, and application to staged combustors is discussed in Section 2.3.4.

2.2 FUNDAMENTAL STUDIES

During the second year of the program, fundamental studies were initiated to provide greater understanding of the chemical processes of catalytic combustion. The development of this detailed information enhances the ability to predict combustor performance and allows analyses leading to system optimization. The phenomena that have been studied in greater detail in this program include a determination of heterogeneous hydrocarbon and nitrogen oxidation reactions, a comparison of the extent of reaction to predicted mass transfer rates, and a determination of heterogeneous oxidation rate constants. The results of these studies for the first two program years are summarized below.

TABLE 2-4. FUEL NITROGEN TEST CATALYSTS

EPA No.	Materials		Manufacturer	Test dates	Facility
	Catalyst	Substrate			
049	$LaAlO_3 \cdot LaCrO_3$		Trans-Tech	9/17-9/22/79	atm
050	$MgAl_2O_4 \cdot NiAl_2O_4$		Trans-Tech	9/25-10/3/79	atm
053	None	Proprietary	Proprietary	10/9/79	atm
051	$MgAl_2O_4 \cdot Fe_3O_4$		Trans-Tech	11/21-11/28/79	atm
058	Mn-La	Corning MCB-12	Catalysis Research	12/5-12/14/79	atm
060	Mn-La	Corning MCB-12	Catalysis Research	12/3/79-1/3/80	hp
004	Pt	DuPont alumina	DuPont	12/18/79-1/7/80	atm
025	Pt-Rh	DuPont alumina	DuPont	12/28/79	atm

2.2.1 Experimental Setup

To achieve an isolation of surface reaction events from the simultaneous gas-phase reactions that occur in practical high-temperature catalytic combustors, specialized catalyst configurations and analytical equipment were developed for the task. Two catalyst geometries were selected: cylinders in crossflow and monolithic honeycombs. The cylinder configuration was used for the majority of experiments. Supplemental data were taken with the monolithic configuration.

The size and spacing of the cylinders were chosen so that about 5 percent fuel conversion would occur by heterogeneous combustion. At this condition, insufficient heat is generated to initiate gas phase ignition as rapid mixing downstream of the cylinders cools and dilutes the surface combustion products. The cylinder in crossflow configuration also allows the use of standard correlations and analogies for the prediction of heat and mass transfer to the surface. These parameters are necessary to verify gas composition measurements and to calculate kinetic constants under the heterogeneous kinetics task as described later. Either three 3.18 mm diameter or two 6.35 mm diameter cylinders were mounted transversely in a 5.08 cm diameter duct. Each cylinder was instrumented with an internal type R thermocouple. The cylinders were alumina (procured from Coors Porcelain Company) and coated with an alumina washcoat. The catalyst coating of either platinum or nickel oxide was applied at a loading of approximately 0.6 percent by weight.

The experimental testing was conducted in the Acurex subscale 3 atmosphere test facility. The facility provides a preheated, premixed fuel/oxidizer mixture for catalytic combustion as well as instrumentation for the monitoring of catalyst performance. The catalyst test section was lined with an insulating refractory material and contained windows for viewing the catalyst from the sides and from the exhaust end. These windows allowed verification of the existence and uniformity of heterogeneous combustion on the catalyst. Also, the presence of gas phase combustion could be qualitatively evaluated.

A specialized gas sampling probe was constructed with an aerodynamic type nozzle tip with a throat diameter of 1.09 mm. A hermetically sealed bellows sample pump provided suction to choke the gas flow at the nozzle and hold the sample pressure within the probe to less than 37.3 kPa (280 Torr). The aerodynamic cooling is combined with water cooled walls to give an overall quenching rate of approximately 10^6 K/sec. The probe and nozzle were constructed of stainless steel for strength and good heat transfer properties. The probe mounting fixture allowed the probe to traverse in two dimensions relative to the catalyst. This allowed sampling of either a fully mixed or unmixed product stream from behind the cylinders.

Exhaust gas analysis was performed primarily by continuous analyzers for CO, CO_2, O_2, NO_x, and HC and supplemented by ion electrodes for NH_3 and HCN. Electrode measurement accuracy was evaluated during the program to be within ±4 percent.

The described experimental setup was used throughout the fundamental studies, and the results of early screening tests, heterogeneous fuel nitrogen tests, and initial heterogeneous kinetics measurements are described in the following sections.

2.2.2 Screening Tests

The primary objective of the screening tests was to verify that the catalyst configurations were effective in isolating heterogeneous reaction events and to evaluate the range of conditions over which the primary variables could be controlled. Further, these tests allowed experimental verification as to whether the dominant product from heterogeneous combustion of methane was carbon monoxide or carbon dioxide. Experimental evaluation of the mass transfer rate of methane to the catalyst surface was also conducted in the screening tests.

Test results for CO and CO_2 combustion products of methane on platinum-coated cylinders are shown in Figure 2-2 as measured across a plane

0.05 cm downstream of the cylinders. The cyclical profiles indicate a clear definition between surface combustion products and the unreacted freestream. At each location, CO and CO_2 concentrations are both maximized directly behind the cylinder with CO_2 as the dominant product. These results are representative of all matrix conditions tested with variations only in the absolute product concentrations. For methane-rich mixtures ($\phi_{FA} > 1.0$), however, the CO measurement was of the same order of magnitude as the CO_2. The sharp division between concentrations directly behind a cylinder and in the freestream (midway between cylinders) becomes less pronounced at increasing downstream positions as a result of cross-stream mixing. At the furthest downstream point, the profiles are essentially flat indicating a well-mixed condition. The well-mixed downstream concentration of CO_2 was also found to be below the integrated value of Figure 2-2 (0.5 percent), verifying that gas-phase combustion was not occurring in the wakes of the cylinders.

Measurements of CO_2, CO, and gas temperature were also made in the streamwise direction for the 3.18 mm diameter cylinders. Figure 2-3 shows the variation in gas species concentrations in the streamwise direction behind one cylinder. Carbon dioxide and carbon monoxide decrease while UHC concentrations increase with axial distance due to mixing of the combustion products with the unreacted freestream. These results verify that downstream combustion does not exist under the test conditions, and changes in measured species are due solely to cross-stream mixing.

The measured percent of input methane converted to CO and CO_2 was also compared to a prediction based on mass transfer, assuming conversion only at the surface and diffusional control. Under these assumptions, the percentage conversion of methane is equal to the ratio of the methane mass transfer rate to the cylinder surfaces and the total mass flowrate of methane in the test section. The results are shown in Figure 2-4. The predicted conversions are somewhat below the experimental results, which may be attributable to several factors. Additional oxidation of a small amount of CH_4 may occur in the gas

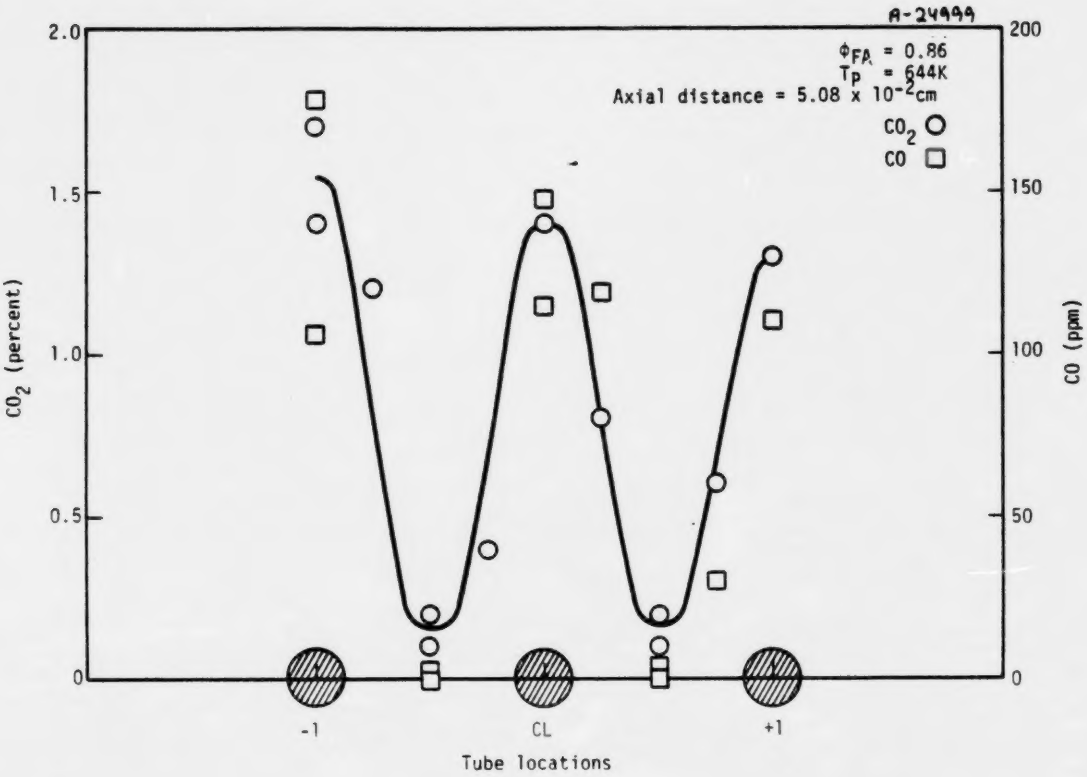

Figure 2-2. Radial distribution of CO_2 and CO concentrations at 5.08 x 10^{-2}cm for 3.18 mm tubes.

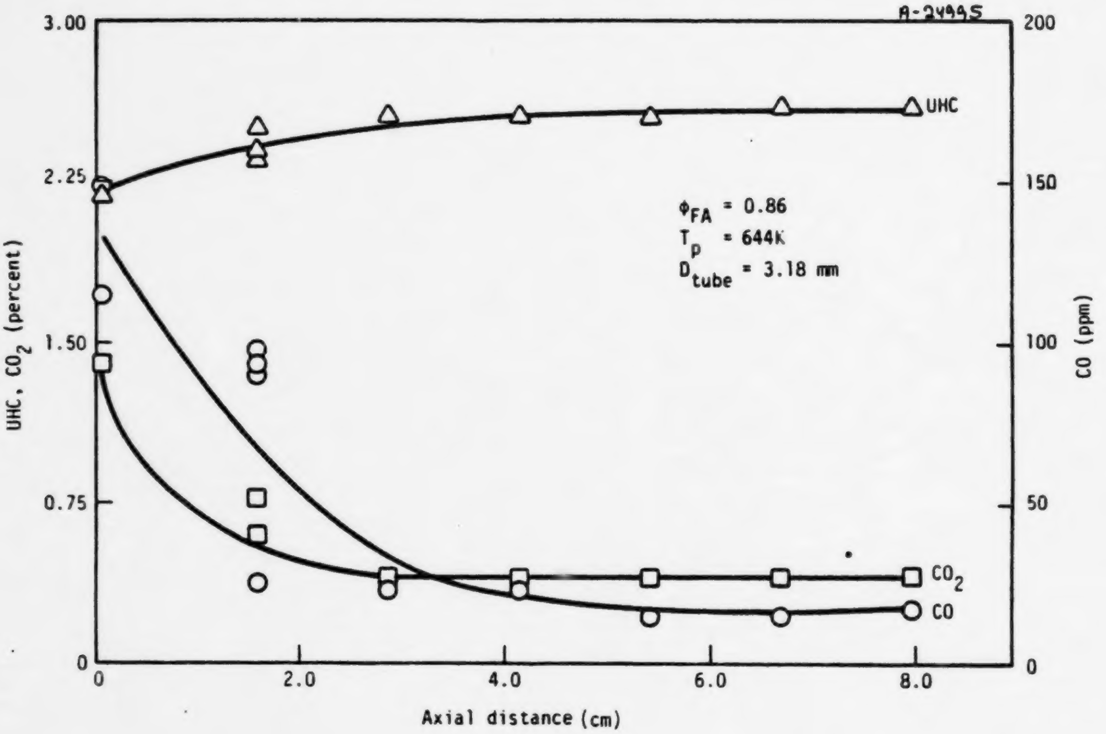

Figure 2-3. Species concentration measurements in the axial direction in line with catalyst tube.

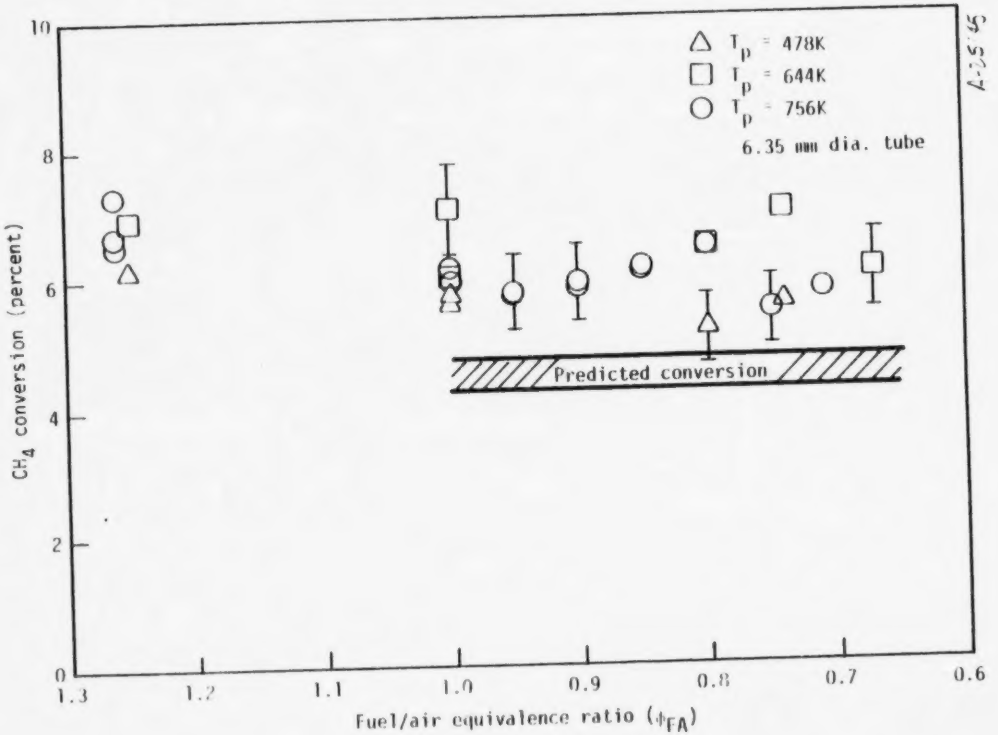

Figure 2-4. Fuel conversion at varying preheat for platinum cylinders.

phase near the catalyst surface. Other possibilities include the departure of the actual cylinder in crossflow arrangement from the idealized assumptions (i.e., end effects, interaction between cylinders, freestream turbulence), and inaccuracies of the transfer coefficient correlations used.

Unlike the platinum catalyst, the nickel oxide catalyst gave negative results in the crossflow cylinder configuration. Surface combustion could not be sustained on the less active catalyst due to radiant losses keeping the catalyst below its normal operational temperature of ~1644K. Tests were also conducted on a NiO coated monolith. Although operation of the 2.54 cm long segment (5.08 cm diameter cells) was stable, surface reactions could not be sufficiently isolated from nearby gas phase reactions to obtain comparative data.

2.2.3 Heterogeneous Fuel Bound Nitrogen Study

In this task, the nature of the fuel bound nitrogen conversion process at the surface was explored. Investigations into the heterogeneous fuel nitrogen oxidation were conducted through comparative measurements of the nitrogen species with the other major products. Additionally, the question of whether the nitrogen surface reaction mechanism is limited by diffusion or chemical kinetics was addressed.

The baseline test fuel was methane doped with ammonia to nominally 1.27 percent by volume. The platinum cylinder in crossflow configuration was the primary test setup, chosen to isolate the heterogeneous surface reactions.

NH_3 conversion results are shown in Figure 2-5, comparing the conversion of the NH_3 dopant to NO with the conversion of CH_4 to CO and CO_2 over a range of reactant stoichiometry. The NH_3 conversion data are lower than the CH_4 conversion data over the range tested. Moreover, the nitrogen conversion falls with decreasing oxygen availability while the methane conversion does not show corresponding behavior. These comparative trends are consistent with

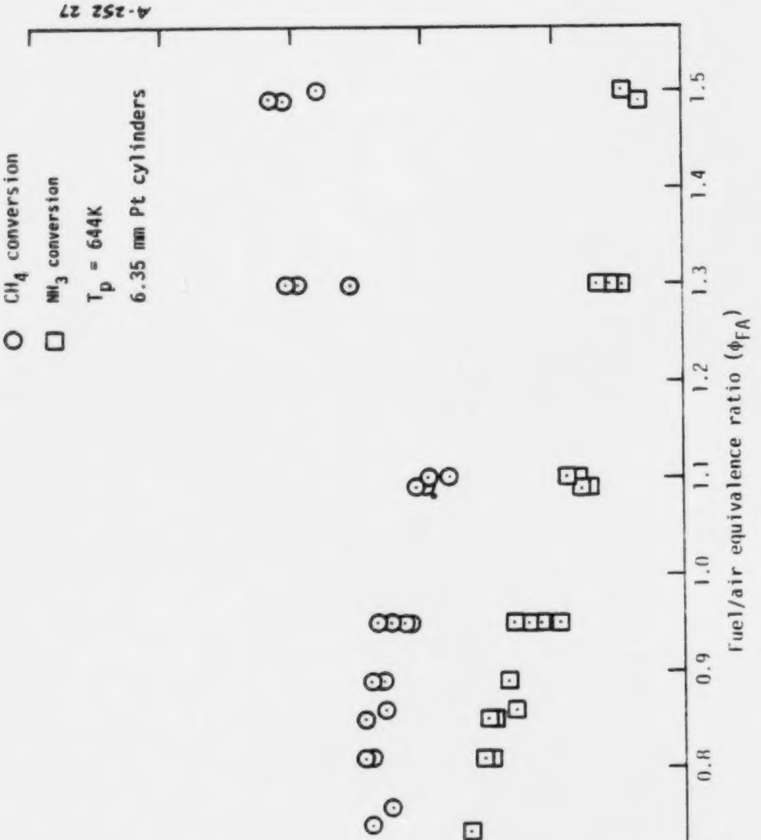

Figure 2-5. Comparison of heterogeneous conversion of CH_4 and NH_3.

a higher oxygen consumption rate of the methane over that of the nitrogen in the range of surface temperatures tested. It was also observed that preheat has no effect on the data trend even though it changes the gas-phase temperature adjacent to the surface, indicating that the $NH_3 \rightarrow NO$ mechanism may be controlled solely by surface events for the conditions tested.

The data trend exhibited by Figure 2-5 represents the decreased level of fuel nitrogen conversion obtained under fuel-rich conditions in many combustion systems. Further evaluation of the chemical mechanisms responsible for the observed conversions are of interest for system optimization. For example, a possible CO/NO_x reduction reaction was investigated for the test conditions of Figure 2-5 by doping of the system with CO. No changes in NH_3 conversion were noted, however, and other dopant studies are required. Although the current experimental system represents an appropiate scheme for obtaining this catalytic combustion mechanistic data, testing on this task was not continued during the final year of the program.

2.2.4 Heterogeneous Combustion Kinetics

If the kinetic rate constants for the heterogeneous reaction of fuel and air during catalytic combustion can be determined accurately, then system performance prediction and optimization can be done unambiguously. Such information would allow definition of the size and configuration of a catalytic reactor for desired energy conversion in a specific application. Additionally, if comparative rates of hydrocarbon combustion and pollutant formation (particularly NO_x) are available, then the system may be tailored to enhance combustion efficiency and minimize pollutants. This task was designed to experimentally measure the kinetic rate constants for the global heterogeneous reaction of natural gas and propane.

Two methods of obtaining heterogeneous reaction rate data were investigated: a catalyst blowout method and a controlled surface temperature technique.

The blowout method is described in Reference 2-1. It is sensitive to small changes in preheat temperature, fuel/air ratio, and catalyst condition and depends on quantitative definition of radiative heat transfer from the catalyst. These conditions were difficult to control in the monolithic configuration and, therefore, the controlled surface temperature technique was developed.

To measure the heterogeneous reaction rate of a fuel (such as methane) accurately, the reaction must be in the kinetically controlled regime to minimize the effect of the mass diffusion resistance. The approach was to operate over a low temperature range in which the reaction rate is below the mass transfer rate of methane to the surface and assume that the reaction mechanism remains unchanged. This condition is unstable for a self-sustained system, however, since the rate of energy release at the surface is not high enough to overcome heat losses. Therefore, an external means to maintain and control the catalyst surface temperature is required. The simultaneous surface combustion of a fuel which does not interfere with the reaction mechanism of methane was used in this study to control the catalyst temperature.

The surface temperature of the platinum coated cylinders in crossflow was controlled by combustion of a lean mixture of hydrogen in air. Initial data were taken on 6.35 mm diameter cylinders where the amount of hydrogen in the reactant mixture was varied from 2.9 to 4.3 percent by volume. This resulted in catalyst surface temperatures of 826K to 1171K at a preheat temperature of 410K and an approach velocity of approximately 6.1 m/s. A small amount of methane was introduced so that the methane/air equivalence ratio was fixed at the lean condition of $\phi_{FA} = 0.45$. The consumption rate of methane, which depends on the surface temperature, was then measured by the production of CO and CO_2.

Preliminary data for methane combustion on a platinum catalyst was taken during the second year of the program. An activation energy of 78.4 kJ/mole was obtained and was in acceptable agreement to published values, verifying the developed technique. The data were refined further in the final year; the numerical results are presented in Section 4.

Several important results were developed during the first year of fundamental studies. These results can be summarized as:

- The cylinder in crossflow configuration has proven successful in isolating heterogeneous catalytic combustion.
- Carbon dioxide is the dominant product from fuel-lean heterogeneous catalytic combustion of methane on platinum. Carbon monoxide concentration is of the same magnitude as that of CO_2 under rich conditions.
- Calculated mass transfer rates of methane to the catalyst surface underpredict experimental rates by 10 to 30 percent.
- The heterogeneous conversion of NH_3 dopant to NO is below the corresponding methane conversion and decreases with decreasing oxygen availability.
- The activation energy experimentally found for heterogeneous combustion of methane on platinum was comparable to that of other investigators.

Tests to further support these conclusions were completed in the third year of the program as described in Section 4.

2.3 COMPOSITE SYSTEM DEVELOPMENT

Four small scale integrated combustors -- gas turbine, firetube boiler, watertube boiler, and staged combustion -- were developed and tested. In the final year of the program, the boiler combustors were implemented in demonstration units. The following sections describe composite combustor developments during years 1 and 2 of the program.

2.3.1 Gas Turbine Combustor

Development of the gas turbine combustor was completed in the program second year. Initial development of a single can combustor for steady state operation was followed by a multiple spray nozzle fuel injector for more uniform fuel/air mixing, an opposed jet igniter to allow transient operation at startup, and an optical pyrometer for combustor exit temperature control. The final combustor configuration is shown in Figure 2-6 as installed in the high pressure facility test sections. The catalyst is 12.7 cm in diameter and 10 cm long to maintain those volumetric heat release rates determined in the catalyst screening tests. Most successful operation was achieved with manganese/lanthanum oxide, nickel oxide, or chromium oxide catalysts on Corning MCB-1 or MCB-12 substrates.

In operation, preheated air flow is introduced at the head end of the combustor. Gaseous fuel is injected through the opposed jet and ignited by the spark plug. Distillate fuel is introduced at the fuel nozzles to raise the temperature of the catalyst. At the lightoff temperature, the opposed jet is extinguished and combustion becomes fully catalytic. Operating conditions included pressures of 1×10^5 to 5×10^5 Pa (1 to 5 atmospheres), combustor outlet temperatures to 1700K (2600°F), 589K to 672K (600°F-750°F) combustor inlet temperatures, and 1371 MJ/hr (1.3×10^6 Btu/hr) maximum heat release rate. The opposed jet was operated at a startup combustor heat release rate of 264 MJ/hr (2.5×10^5 Btu/hr) at a velocity of approximately 20 times the the mainstream velocity.

The transient operating cycle of the combustor is shown in Figure 2-7. The time to reach steady state operation can be varied by the rate of fuel introduction at startup. NO_x emissions associated with the opposed jet decrease sharply during catalytic combustion to the 15 ppm level indicated.

Comparison of the steady state NO_x emissions to those of conventional gas turbine combustors is shown in Figure 2-8 as a function of combustor inlet temperatures. Significant reductions in thermal NO_x with distillate fuels were achieved at the inlet temperatures tested. These low emissions were maintained simultaneously with high combustion efficiencies -- above 99.985 percent at all test conditions.

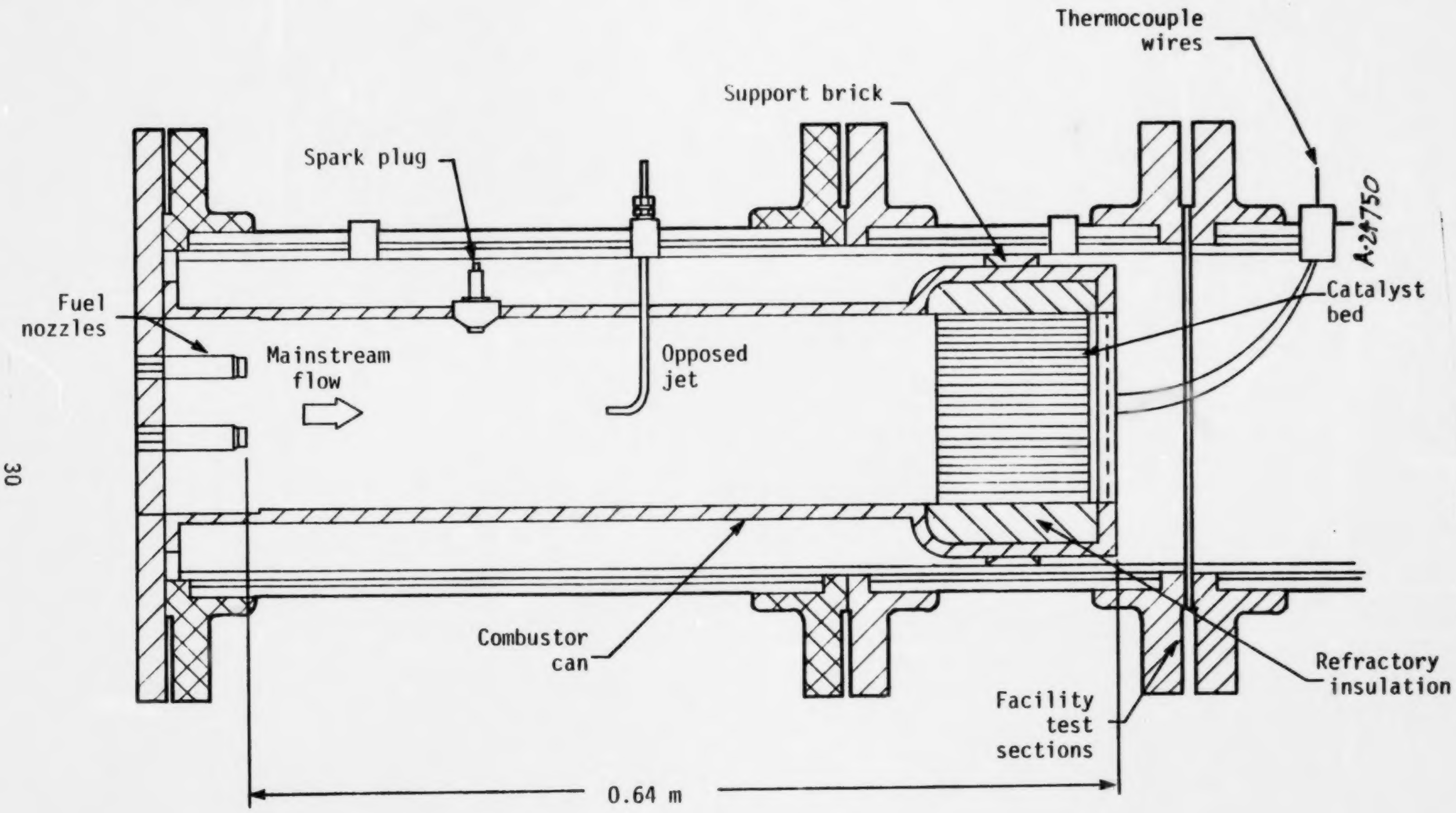
Thermocouple wires
Support brick
Spark plug
A-24750
Catalyst bed
Fuel nozzles
Mainstream flow
Opposed jet
Combustor can
Refractory insulation
Facility test sections
0.64 m

Figure 2-6. Gas turbine combustor.

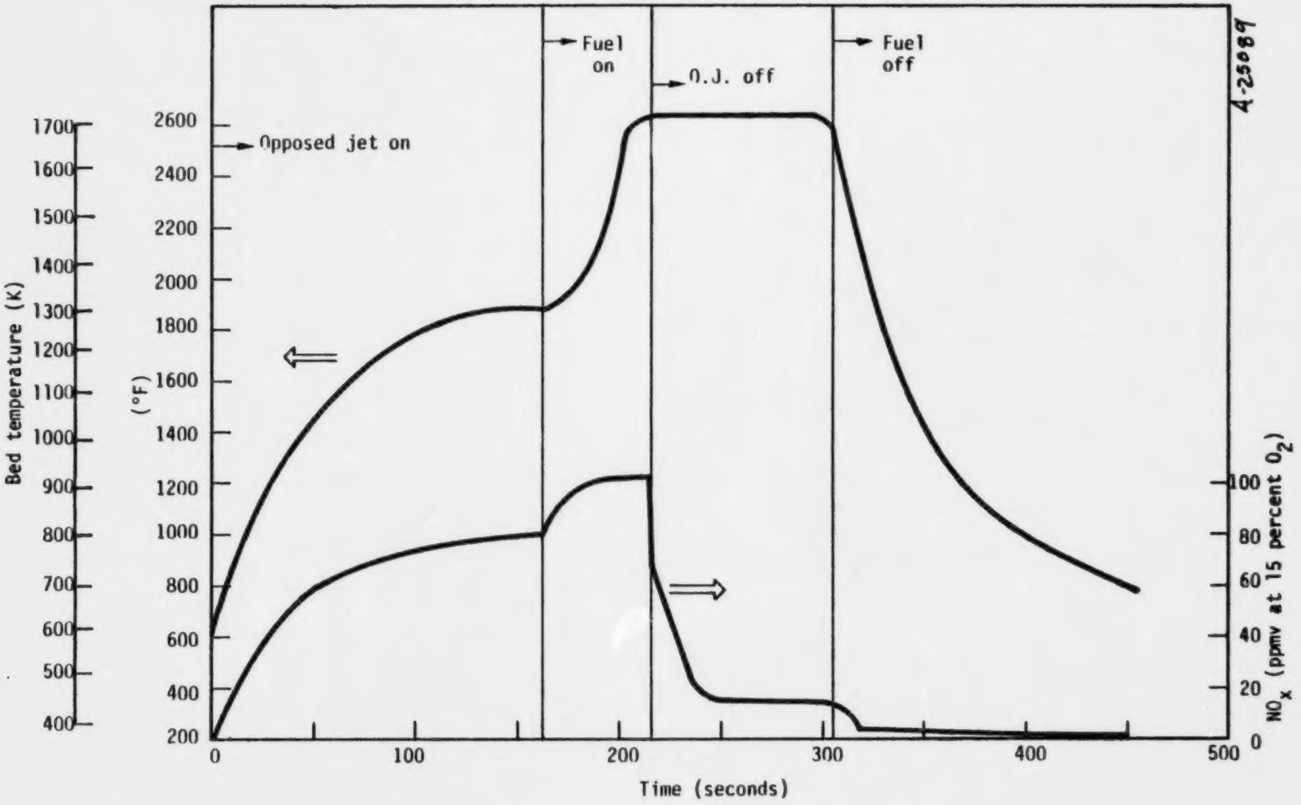

Figure 2-7. Gas turbine combustor transient operation.

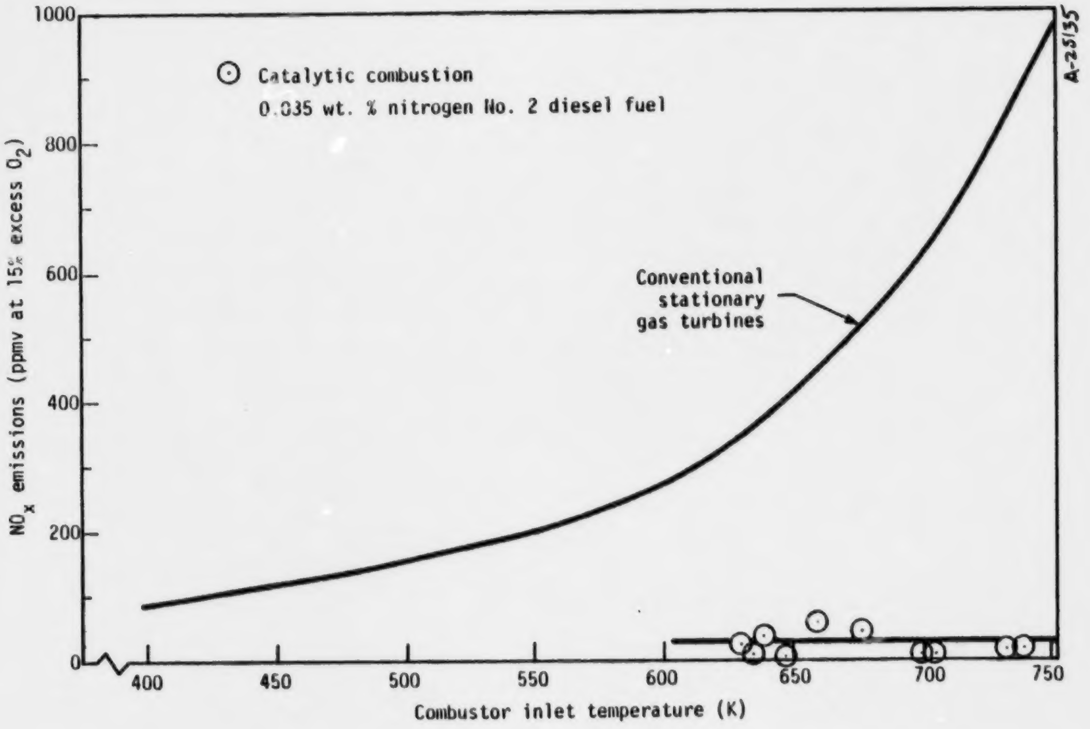

Figure 2-8. Comparison of catalytic and conventional gas turbine thermal NO$_x$ emissions.

Tests were also conducted with distillate fuels with higher nitrogen content for comparison of NO_x emissions to current standards (Reference 2-4). The results are shown in Figure 2-9 for fuels with 0.125 and 0.535 weight percent nitrogen as a function of combustor pressure. For the 0.125 percent nitrogen fuel, the catalytic combustor easily meets current regulations. However, at 0.535 percent nitrogen, the 80 to 100 percent conversion of fuel nitrogen to NO_x that occurs under lean conditions exceeds the standard. Therefore, for combustion of high nitrogen fuels in the gas turbine, staging is required.

Operation of the gas turbine combustor demonstrated that the system had fast response to system transients with combustor residence time (40 ms) and pressure drop (less than 3 percent of total pressure) comparable to those of existing systems. However, it was not possible to operate the combustor over the entire range of fuel/air mixture ratios found in some machines (0.006 to 0.025), the catalyst being limited by combustion stability at the low end and allowable material temperature at the high end of the range. To meet the full range of load variation, two possible techniques have been identified: air distribution and fuel staging. These techniques have been discussed in Reference 2-5. Further development would require machine retrofit and has not been addressed in the current program.

2.3.2 Firetube Boiler

During the first year of the program, suggestions were received from the technical advisory panel for application of catalytic combustion to firetube boilers. Several concepts were developed and reviewed with manufacturers to determine their appropriateness to existing applications. The fiber matrix burner concept was selected for development due to its immediate applicability to gas firing and its secondary potential for distillate fuel firing. Development of burner materials and subscale burner configurations were performed during the second year.

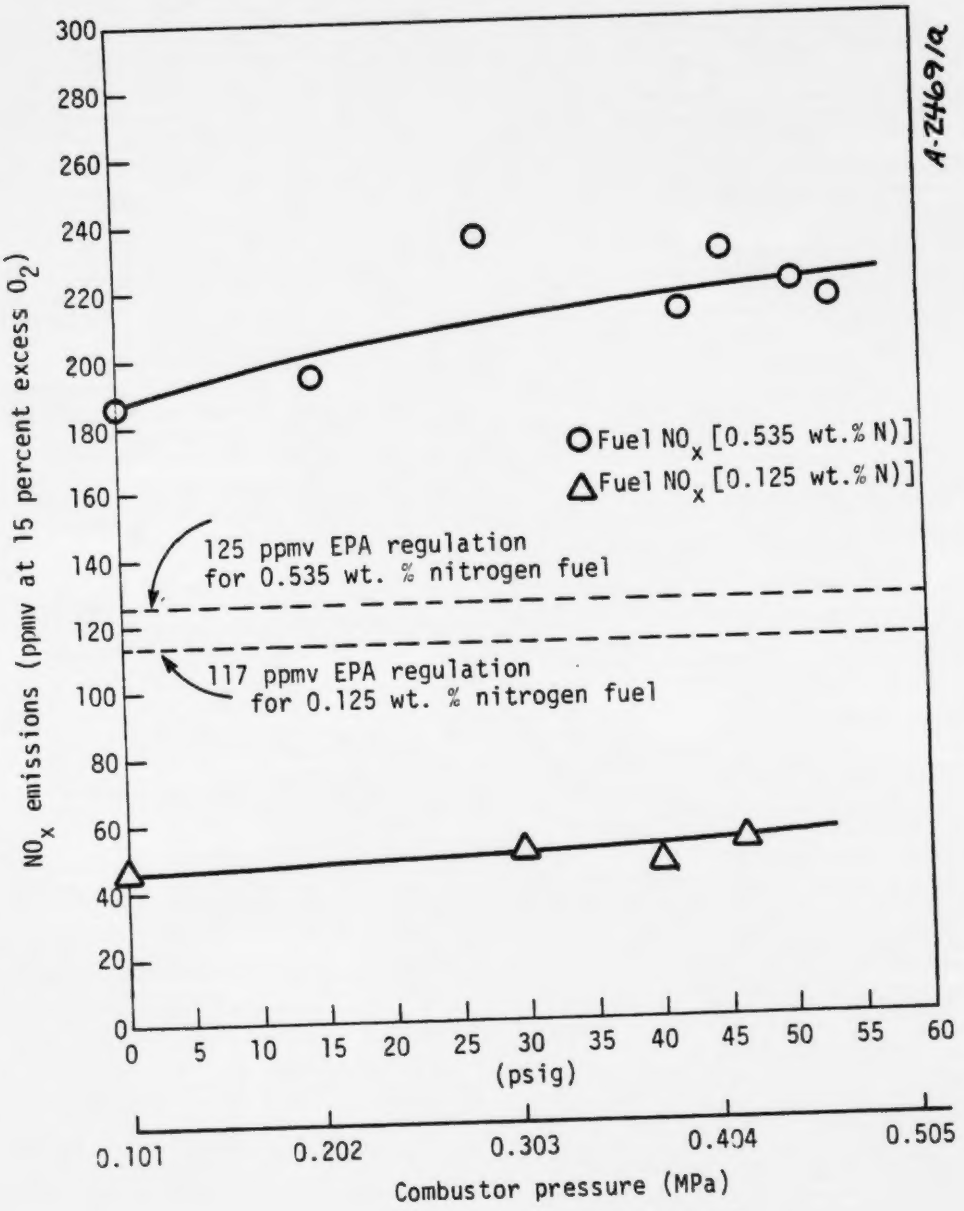

Figure 2-9. Gas turbine combustor fuel NO$_x$ emissions.

The firetube fiber matrix burner concept is shown in Figure 2-10. The fiber material is vacuum-formed into a cylinder, closed at one end. A fuel and air mixture is introduced at the open end. The reactants flow into the cylinder, through the porous fiber matrix, and react in a combustion zone on the outer surface of the material. Energy is transferred by radiation and convection across an open annulus between burner and firetube.

Vacuum-formed flat plate fiber materials were obtained from several manufacturers to optimize burner performance. These materials were tested at heat release rates of 189,000 to 458,000 W/m^2 (60,000 to 145,000 $Btu/hr\text{-}ft^2$) based on burner outer surface area. Stable operation with acceptable heat transfer, combustion efficiency, and NO_x emissions were achieved. Typical NO_x emissions are shown in Figure 2-11. Values of less than 5 ppm were achieved on natural gas from approximately 115 to 170 percent theoretical air at 206,000 W/m^2. Operation with distillate oil appeared feasible at air inlet temperatures above 600°F for vaporization of the oil.

Based on the results of the flat plate burner tests, a subscale cylindrical burner was constructed as shown in Figure 2-12. The 0.15 m diameter matrix was mounted in the water-cooled test section of the high pressure test facility to simulate the firetube waterwall.

Although combustion and emissions performance was similar to that achieved in the flat plate burner tests, the matrix materials showed mechanical degradation with use (sintering and erosion) that eventually led to flashback of the combustion zone through the matrix material. Additional materials of greater durability were identified and tested during the third year of the program. Tests of Johns-Manville and Chemo-Thermic burners from subscale to boiler retrofit are described in Section 5.3. These tests also identified the optimum burner heat release rate of 2.53×10^5 W/m^2 (80,000 $Btu/hr\text{-}ft^2$) based on burner surface area.

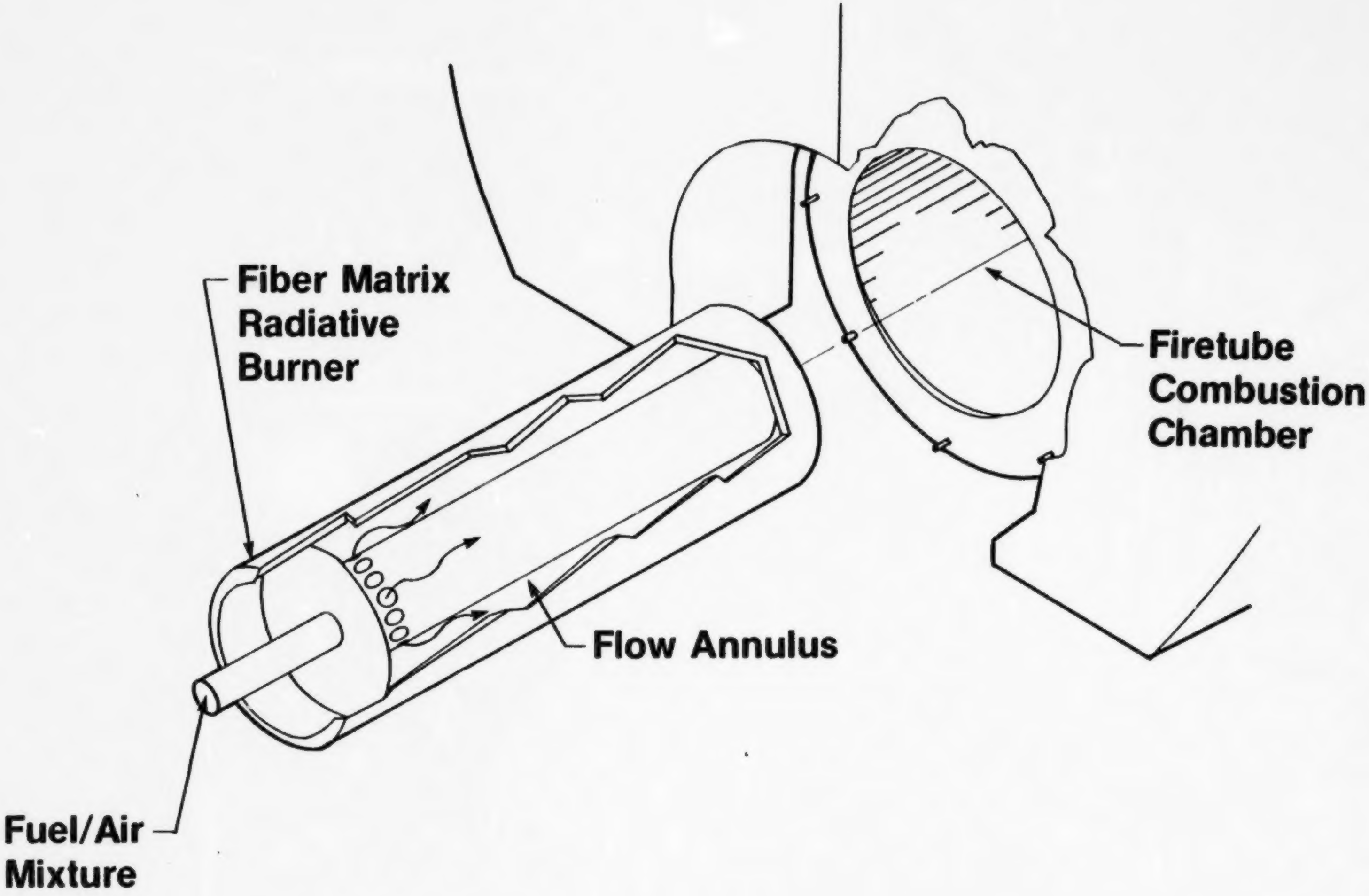
Fiber Matrix
Radiative
Burner
Firetube
Combustion
Chamber
Flow Annulus
Fuel/Air
Mixture

Figure 2-10. Fiber matrix burner concept.

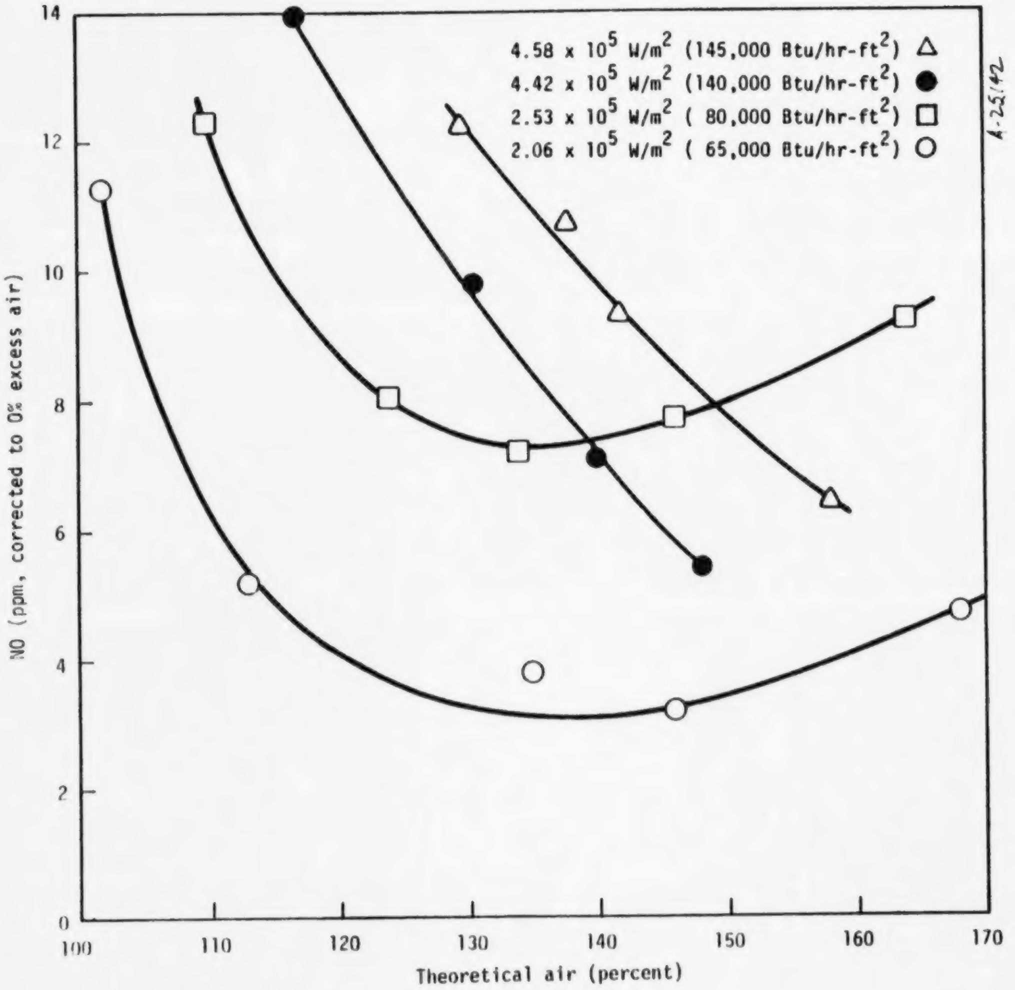

Figure 2-11. Subscale combustor firetube NO emissions.

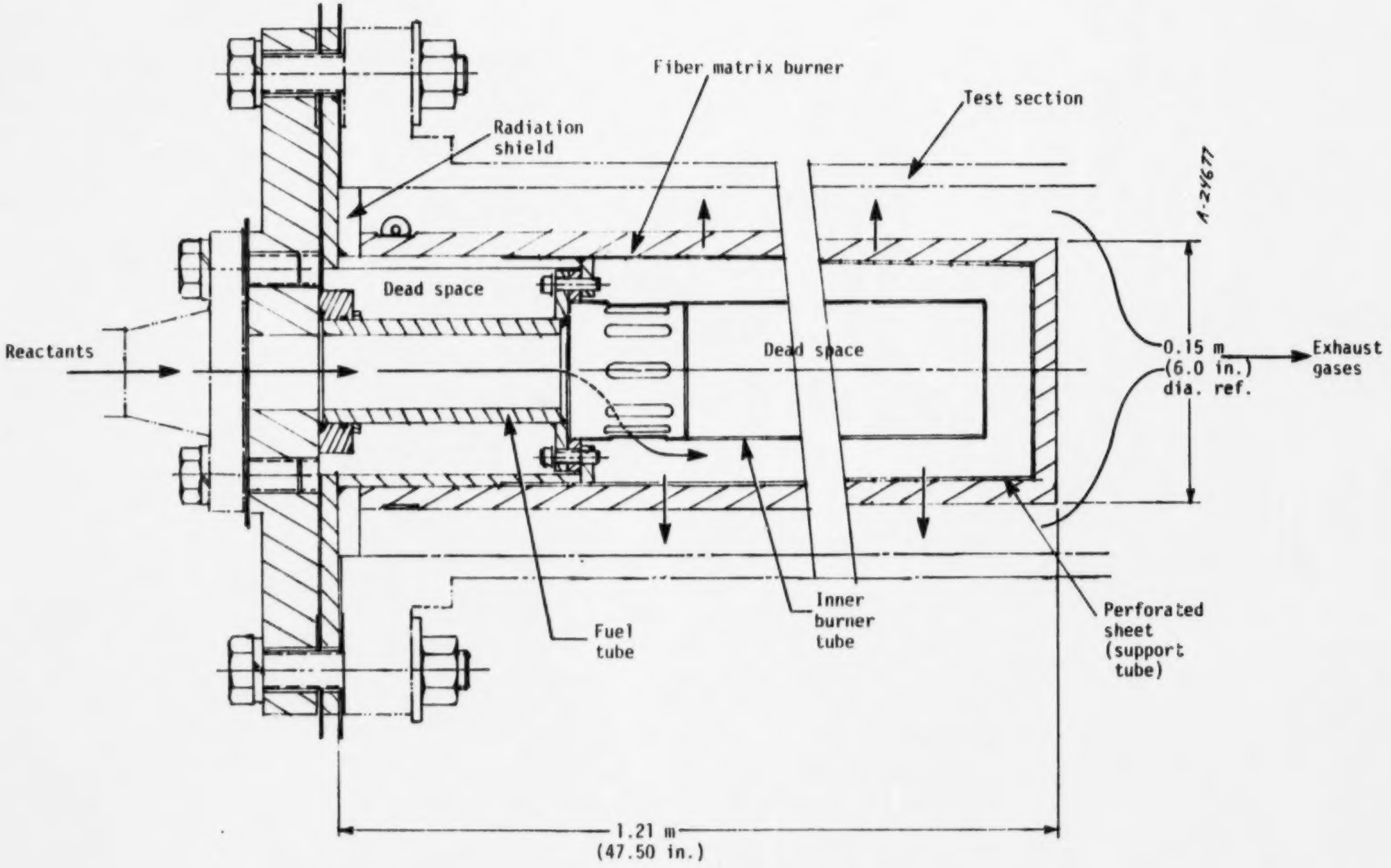
Fiber matrix burner
Test section
Radiation shield
A-24677
Dead space
Reactants
Dead space
0.15 m (6.0 in.) dia. ref.
Exhaust gases
Fuel tube
Inner burner tube
Perforated sheet (support tube)
1.21 m (47.50 in.)

Figure 2-12. Subscale firetube boiler burner assembly.

2.3.3 Watertube Boiler

The original radiative catalyst/watertube system was further developed under the current program for application to watertube boilers. The first two years' activity (summarized in References 2-7 and 2-8) included testing of a concentric catalyst/watertube configuration, identification of silicon carbide as the preferred catalyst tube material, optimization of the tube spacing to reduce NO_x emissions, and conceptualization of full scale system configurations. This work is discussed below. Third and fourth year activities focused on additional testing and scaleup demonstration of the developed concepts and are described in Sections 6.3 and 6.4.

The watertube boiler concept is shown in Figure 2-13 with catalyst and watertubes in the radiative section, an optional monolithic catalyst stage, and downstream convective section. For gaseous and distillate fuels, the monolithic stage may not be required. For high nitrogen content fuels the monolithic combustor is required, and the system is operated in a staged mode with secondary air injection just ahead of the monolithic second stage. A premixed fuel/air mixture is passed into the system and lit off by an opposed jet igniter.

To facilitate distillate oil firing in the radiative section, the tube arrangement was modified such that the catalyst tubes were concentric with the boiler watertubes. A plan view of one arrangement is shown in Figure 2-14. This configuration was initially tested with natural gas fuel with alumina as the ceramic tube material. Combustion efficiency improved significantly to 95 percent over the earlier nonconcentric design (~35 percent). Low thermal NO_x emissions and the potential for fuel NO_x control by staging the combustion were apparent.

Significant thermal fracturing of the alumina tubes occurred, however, as a result of temperature gradients developed across the tube walls. The developed thermal stresses were calculated and compared to the strength of the material. Under some operating conditions, insufficient safety factors

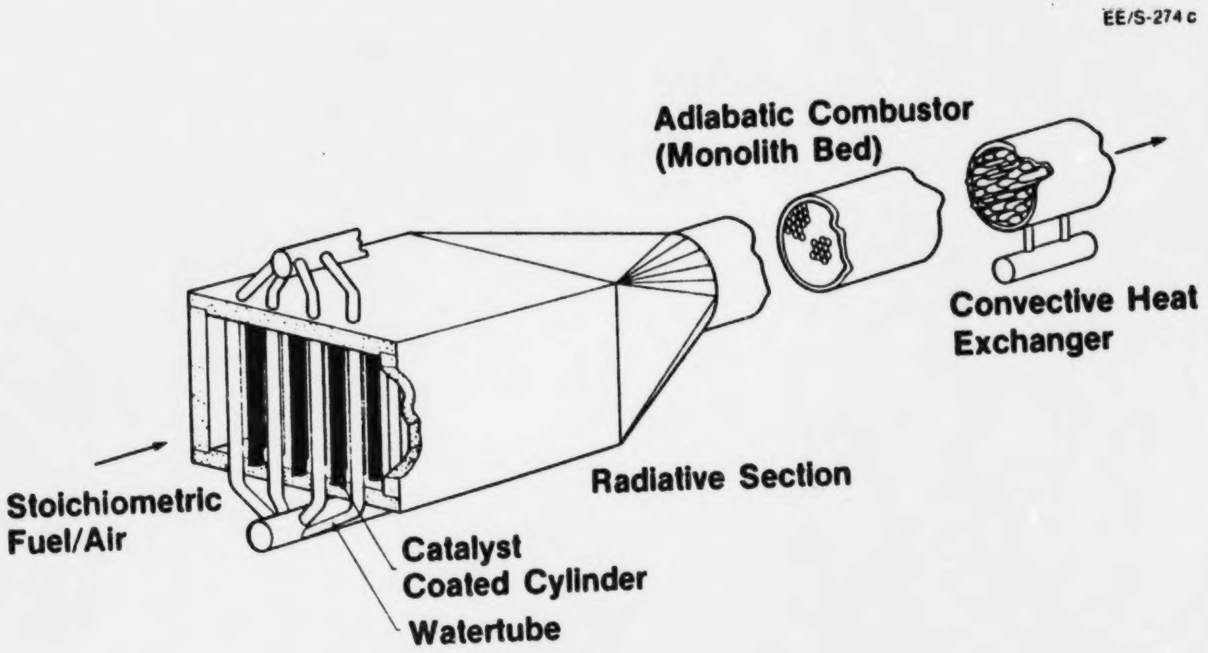
EE/S-274 c
Adiabatic Combustor
(Monolith Bed)
Convective Heat
Exchanger
Radiative Section
Stoichiometric
Fuel/Air
Catalyst
Coated Cylinder
Watertube

Figure 2-13. Catalytic watertube boiler.

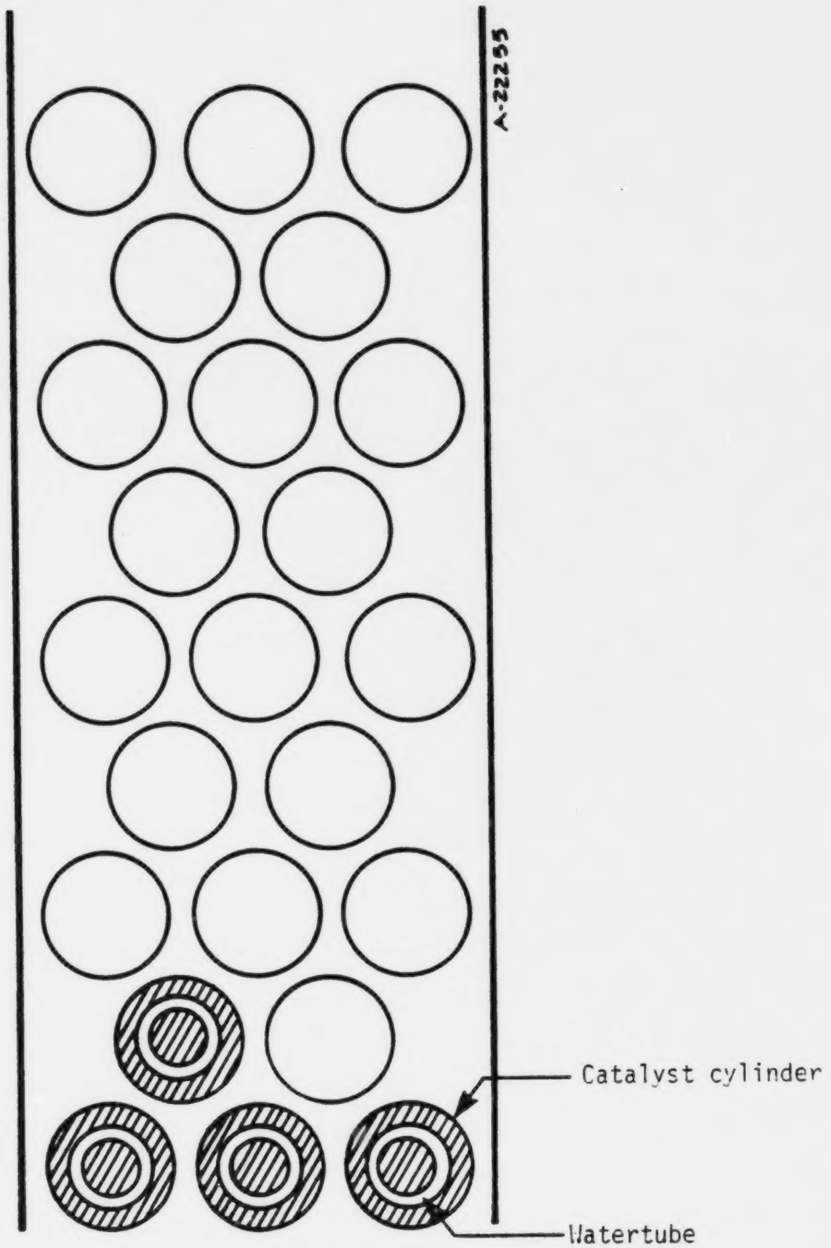
A-22255
Catalyst cylinder
Watertube

Figure 2-14. Concentric radiative catalyst/watertube arrangement.

existed. Similar analyses for other ceramic tube materials showed that silicon carbide maintained adequate strength at the application temperatures. Therefore, special silicon carbide tubes (Norton Co.) with a porosity of 70 percent were procured for further testing.

In the subsequent test series with the SiC tubes, the tube material (coated with a chromium oxide catalyst) showed no thermal fracturing problems. The tube arrangement was also varied, increasing the distance between tubes at the first three rows of the reactor to increase system maximum throughput. The larger spacing, however, resulted in increased gas-phase reactions in these regions, increasing combustion temperatures and thermal NO_x emissions. Additional testing with uniform tube spacing throughout resulted in NO_x emissions as in Figure 2-15. These levels were decreased further during testing in the third year.

The first two years' development resulted in a radiative section with durable catalyst materials and adequate combustion performance. Combustion efficiency was boosted to 99 percent with approximately 50 percent of the liberated heat being radiated to the watertubes. Tests were successful with both gaseous and distillate fuels.

2.3.4 Two-Stage Combustor

A two-stage combustor concept was developed and tested under EPA Contract 68-02-2116, showing the ability to control fuel nitrogen conversion to NO_x in a catalytic rich-lean combustor. Foreseeable applications include both boilers (watertube and firetube) and gas turbines. For watertube boilers, the first stage could be operated at any desired rich stoichiometry, controlling the catalyst temperature by the amount of heat transfer to the watertubes. Watertubes located between stages extract additional heat to allow the second stage catalyst to operate at low excess air (5 to 15 percent). In contrast, the gas turbine combustor would utilize a monolithic (adiabatic) first stage

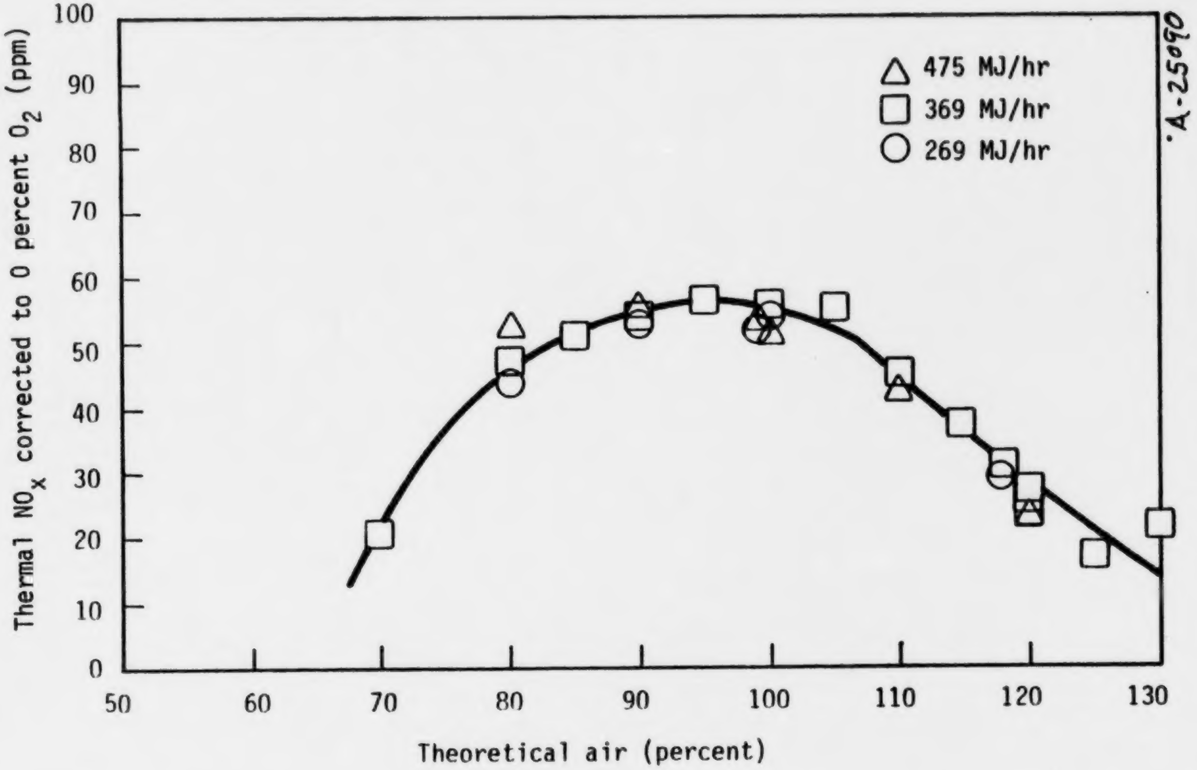

Figure 2-15. Radiative section thermal NO_x emissions.

catalyst that requires operation at a richer stoichiometry (below 60 percent) for temperature control. Similarly, the gas turbine second stage must operate at high excess air (100 to 150 percent) with large quantities of secondary air injection to satisfy turbine inlet temperature requirements.

Early fuel nitrogen testing had shown that two-stage combustion was most effective with the primary stage operating at 75 to 90 percent theoretical air. The adiabatic flame temperatures associated with this range of stoichiometries is clearly above the desired operating temperature and would not only produce unacceptably high levels of thermal NO_x, but would also destroy materials currently available for catalyst fabrication. Therefore, for systems such as the gas turbine that utilize a monolithic catalyst support, a technique for providing heat transfer from the catalyst surfaces must be devised. One concept that has been explored during the first two years of this program is the catalytic flameholder.

The flameholder initiates combustion reactions within a monolithic support and provides initial energy to support the majority of heat release downstream of the catalyst in the gas phase. The surfaces of the catalyst are kept below adiabatic flame temperatures by radiation to surrounding surfaces and convection to surrounding gases. Tests were run in the first two program years to show the feasibility of the concept. Monolithic flameholders were operated successfully at stoichiometries of 50 to 200 percent theoretical air. Configurations included large cell ceramic monoliths of 2.5 to 5.0 cm in length and a converging-diverging metallic (Kanthal) channel model made by Oxy-Catalyst Inc. Although sufficient radiative cooling was achieved in the ceramic monoliths over the wide range in stoichiometry, high thermal NO_x emissions resulted from combustion in the gas phase downstream of the flameholder (Reference 2-1). The high downstream temperatures were also responsible for higher than normal fuel nitrogen conversion (above 50 percent under rich conditions) in these tests.

Attempts to lower the NO_x emissions from these systems by increasing the flameholder length (to enhance catalytic reactions) and by quenching the downstream gas-phase reactions are largely unsuccessful. Although increasing reactor length had the effect of decreasing thermal NO_x, higher catalyst temperatures resulted downstream that required additional cooling to control NO_x. Increasing downstream cooling had the effect of cooling reactions at the catalyst surface rather than in the gas phase. Therefore, a system where cooling alleviated thermal NO_x production could not be achieved.

In summary, the test results indicated that it is not possible to operate a catalytic flameholder without diluent at 75 percent theoretical air to minimize fuel nitrogen conversion to NO_x while simultaneously controlling thermal NO_x formation. Consequently, a two-stage, rich-lean combustion system using a monolithic catalyst may have to employ a full graded cell reactor as the first stage and operate at 50-60 percent theoretical air or at higher stoichiometries with active cooling.

During the second year of the program, an alternate concept was developed to achieve this objective. The concept utilized control of heat losses surrounding the catalyst to achieve very low conversions while operating over a wide range of rich stoichiometries.

The concept was initially observed at Energy and Environmental Research Corporation (EERC) for a 2.5 cm diameter nickel oxide, graded cell catalyst mounted in a reactor with exterior wall back heating to minimize heat losses radially through the walls surrounding the catalyst. The reactor was subsequently shipped to Acurex where the EERC results were verified.

The trends in both Acurex and EERC tests are shown in Figure 2-16. Conversions of approximately 5 to 10 percent were achieved from 40 to 85 percent theoretical air by control of heat losses. On tests with a platinum catalyst, similar results could not be achieved, and a conversion minimum of approximately 30 percent was apparent under rich conditions. For the nickel

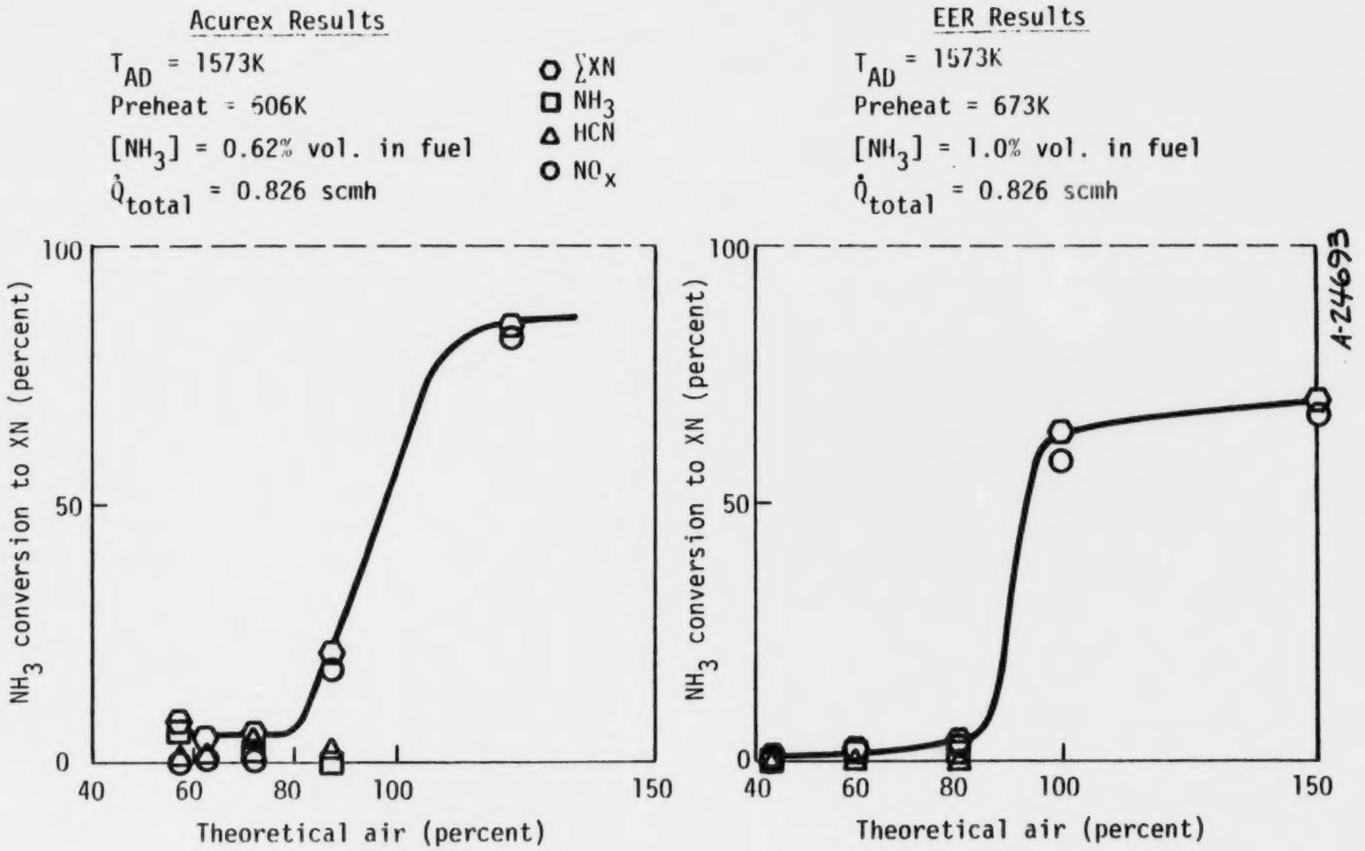

Figure 2-16. Comparison of Acurex and EER results on a NiO catalyst.

oxide catalyst, low conversions were further achieved in Acurex tests despite variations in fuel nitrogen content and combustion temperature.

The effect of wall heat loss was further quantified by variation of the amount of heat loss and noting its effect on nitrogen conversion. An approximately linear relationship between conduction losses through the wall and absolute quantities of NO_x produced was observed. The data also indicated an increasing O_2 content in the exhaust with increasing heat loss, suggesting that the higher NO_x produced may result from oxidation of NO_x precursors downstream of the catalyst.

Since the actual heat loss is proportional to the ratio of the exterior surface area of the catalyst to the catalyst volume, increasing the catalyst diameter should decrease the effects of heat loss on nitrogen conversion. This effect was confirmed in tests of a 7.6 cm diameter nickel oxide catalyst which achieved lower conversions than the 2.5 cm catalyst in the absence of heat loss control. The conversions achieved for the 7.6 cm catalyst (10 to 20 percent) were significantly greater than the 5 percent conversion measured in the controlled case, however.

The use of wall heat loss control to achieve low fuel NO_x may be particularly advantageous in gas turbine combustors where first stage monolithic catalysts may require operation over a wide range of rich stoichiometries. Means of controlling heat losses in machine configurations, however, require further consideration. This concept was not developed further during the remainder of the program. Additional development of staged combustors has focused on the watertube boiler system that uses a nonmonolithic catalyst configuration and intrabed cooling in the first stage. These activities are discussed in Section 6.

REFERENCES FOR SECTION 2

2-1. Kesselring, J. P., et al., "Development of Improved Catalyst Systems," Published in "Proceedings Fourth Workshop on Catalytic Combustion (Cincinnati, OH, May 1980)," EPA-600/9-80-035, NTIS-PB81-176067, August 1980, pp. 236-265.

2-2. Kesselring J. P., et al., "Design Criteria for Stationary Source Catalytic Combustion Systems," EPA-600/7-79-181, NTIS-PB80-147317, August 1979.

2-3. Chu, E. K., et al., "Fuel NO_x Control by Catalytic Combustion," EPA-600/7-81-151, NTIS-PB82-102351, September 1981.

2-4. Goodwin, D. R., et al., "Standard Support and Environmental Impact Statement. Volume 1: Proposed Standards of Performance for Stationary Gas Turbines," EPA-450/2-77-017A, NTIS-PB 272 422/7BE, September 1977.

2-5. Anderson, S. J., et al., "Development of a Small-Scale Catalytic Gas Turbine Combustor," ASME 81-GT-43, March 1981.

2-6. Snow, G. C. and H. Tong, "High Temperature Durable Catalyst Development," Published in "Proceedings: Fifth Workshop on Catalytic Combustion (San Antonio, TX, September 1981)," EPA-600/9-84-002, NTIS-PB84-145580, January 1984, pp. 32-69.

2-7. Krill, W. V., et al., "Prototype Catalytic Systems," published in "Proceedings Fourth Workshop on Catalytic Combustion (Cincinnati, OH, May 1980)," EPA-600/9-80-035, NTIS-PB81-176067, August 1980, pp. 302-321.

2-8. Friedman, M. A., et al., "Development of a Catalytic/Radiative Watertube Boiler," published in "Proceedings: Fifth Workshop on Catalytic Combustion (San Antonio, TX, September 1981)," EPA-600/9-84-002, NTIS-PB84-145580, January 1984, pp. 333-352.

SECTION 3

CATALYST DEVELOPMENT

Catalyst development, one of the keys to the commercial acceptability of the catalytic combustor, was carried forward by directing ceramic development work, conducting material tests on manufacturer-supplied substrates, and performing long term durability tests on selected catalyst materials. This section describes the results of this catalyst development work.

3.1 HIGH TEMPERATURE CERAMIC DEVELOPMENT FOR CATALYTIC COMBUSTION

Since the introduction of catalytic combustion as a high combustion efficiency, low emissions technique for fuel conversion, there have been significant developments in many system applications such as gas turbines, Stirling engines, fuel cell anode exhaust cleanup, water heaters, watertube and firetube boilers, and home furnaces (References 3-1, 3-2, 3-3). During this period, however, catalyst manufacturers have made relatively small developmental changes in the catalyst used for these high temperature operations. Manufacturers of catalyst/support systems are not totally convinced of the market potential of catalytic combustion and are unwilling to make the expenditures required for a comprehensive materials development program. Also, the manufacturers have not been convinced that existing low temperature catalyst materials cannot be adapted for higher temperature use. Since experience in the use of state-of-the-art materials has been obtained in various catalytic combustion programs, it has become apparent that existing materials have a poor chance of surviving the severe environments imposed by high temperature catalytic combustion. There is a need for better understanding of the materials involved and for closer interactions between the material manufacturers and the users. This study was therefore undertaken to consolidate information regarding catalytic combustion materials, to interact with manufacturers who have capacilities and interest in fabricating catalyst systems, and to provide an approach for future developments in high temperature catalyst materials technology.

3.1.1 Introduction

Prior to the development of the catalytic combustor, there was little need for catalysts capable of operation at temperatures over 1367K (2000°F) for extended periods of time. Indeed, 1089K (1500°F) had generally been thought to be the upper limit for oxidation catalysts. Thus, during the early stages of catalytic combustor development, only a very limited number of suitable high temperature catalytic compositions were known or available, and little information was available as to how some of the common oxidation catalysts would behave at high temperatures. The initial approach was to use materials technology developed for low temperature catalytic reactions such as in auto emissions cleanup. A discussion of the type of materials available and their properties is given in Reference 3-1.

In general, the catalyst system consists of an inert substrate coated with a catalytically active material dispersed in a high surface area washcoat. While several substrate geometries such as pellets, fiber pads, tubes, and honeycombs are available, the honeycomb shape is the choice wherever high mass throughputs and low pressure drops are required (such as in gas turbine applications). Commercially available honeycomb substrates are made of cordierite, mullite, alumina, and zirconia-based materials. They generally have good thermal stability under the conditions of emissions cleanup. The catalytic material is made up of elements from the noble metal group -- in particular, platinum and palladium -- while the high surface area washcoat is generally γ-alumina. While this noble metal/γ-alumina/substrate system works well for emissions control, operation at the higher temperatures of catalytic combustion created many problems. At elevated temperatures, the washcoat material tends to sinter, and the noble metals agglomerate, leading to low surface areas, low dispersions, and a subsequent decrease in activity. The noble metals are also very volatile at elevated temperatures, especially in an oxidizing environment. As a result of this increased volatility, platinum in air at 1672K (2550°F) would lose weight at the rate of 0.02 g/m^3 air for air flowing past the platinum (Reference 3-4). To overcome these problems, the substrate is sometimes loaded with a large amount of catalyst to compensate for catalyst loss. Alternatively, the γ-alumina washcoat is stabilized by the addition of other materials such as rare earth oxides (Reference 3-5) to prevent sintering. Even when these methods are used, however, noble metals are not expected to be useful above 1589K (2400°F). The longest life test run on noble metal catalysts at 1589K thus far has been for one thousand hours (Reference 3-6), and other tests on noble metals during catalytic combustion showed rather short life spans (References 3-2, 3-7).

At temperatures exceeding 1589K, other oxidation catalysts were considered. Various oxides from the transition metal and rare earth groups were tested and screened for potential activity and problems (Reference 3-2). In general, the metal oxides were not as active as the noble metals and required higher preheat temperatures and operating bed temperatures. The transition metal oxides tested, such as chromium, nickel, and cobalt, demonstrated rather high volatilization rates and were rapidly depleted from the substrate. Some of the metal oxides interacted destructively with the substrate through the formation of low melting eutectics. Manganese oxide, for example, forms a low melting mixture with silica, a common component of substrate materials. In fact, many of the transition metal oxides tend to form eutectic melts with silica at temperatures below 1922K (3000°F). Another problem is the high mobility of many metal oxides at elevated temperatures. As a result, some of the oxide coatings may migrate throughout the support, disrupting the structure and causing structural collapse. Cobalt oxide coatings on Torvex alumina supports gradually diffuse throughout the support during catalytic combustion, perhaps contributing to early structural breakup of the honeycomb. It is uncertain, however, whether migration of catalyst in the support is in all cases detrimental to structural integrity, or whether it might maintain sufficient catalytic activity as a dispersed phase in the support itself. In some cases studied where migration did occur, the catalyst was so volatile that the surface was depleted of catalyst while the interior of the substrate still contained catalyst material. In these cases, the catalyst system had very little activity left.

Due to a lack of high temperature data on many of the catalysts, however, it is difficult to predict a priori how a given catalyst-substrate system will behave during catalytic combustion. General comments on volatility and instability are based on the results of screening experiments performed thus far. Indications are that noble metals and even transition metal oxides are too mobile and volatile to be used at high temperatures and must somehow be modified to improve stability. Little comment can be made on rare earth oxides due to the lack of conclusive data. Experiments with a thorium and cerium oxide mixture have produced seemingly contradictory results in that in one set of experiments, the mixture was active and stable and in another was inactive and unstable (Reference 3-7). This is due again to a lack of understanding of the material and its interactions with the environment at elevated temperatures.

More recently, in an attempt to improve the stability of noble metals and transition metal oxides, it has been proposed that these materials can be tied up by formation of a compound with other oxides. For example, a noble metal or a transition metal ion can be introduced into a perovskite or spinel structure. The formation of a compound may reduce the tendency to volatilize or interact with other materials. Little information is available as to how some of these compounds would behave catalytically and how stable they are under combustor conditions. Tests on some perovskite formulations on emissions cleanup systems (Reference 3-8) and on several perovskite and spinel formulations during catalytic combustion (Reference 3-2) showed generally promising results. As a further step, it has been proposed that it may be possible to fabricate the entire substrate from catalytically active materials to form an "active monolith." For example, a mixture of spinel ($MgAl_2O_4$) and magnesium chrome spinel ($MgCr_2O_4$) can be used as the basic ingredients in the formation of a honeycomb substrate. The presence of chromium could make the ceramic active without an added coating of catalyst. Several simple shapes (tube bundles, discs drilled with holes) were made from a selected group of active oxides such as lanthanum chromia and lanthanum aluminate ($LaCrO_3$ + $CaAlO_3$) or magnesium aluminate and iron oxide ($MgAl_2O_4$ + Fe_3O_4) and tested (Reference 3-2). Again, they all demonstrated promising catalytic activity. Unfortunately, all the shapes tested so far had poor thermal stress resistance and fractured badly.

A problem that has not been addressed so far is the thermal shock resistance of the catalysts tested. As mentioned above, all the "active" substrates fabricated into tubes and discs fractured badly. In fact, all the support materials tested so far (whether active or inactive) fractured to some extent. Silicon carbide honeycomb, supplied by Norton, had the best thermal stability and survived combustion testing with very little fracturing. Unfortunately, the support is very dense, and the catalyst coating completely disappeared at the end of the combustion test (~14 hours), probably due to poor adhesion and/or catalyst volatility. It is uncertain whether a more porous silicon carbide substrate for improved catalyst adhesion would significantly decrease its thermal stability. Substrate materials tested so far (such as alumina, mullite, and stabilized zirconia) all fracture unacceptably. Cordierite has good thermal stress resistance but an unacceptably low use temperature (<1590K). More recently, improvements in the formulation of some of these compounds and advances in new proprietary formulations have produced substrates with improved thermal stress resistance. A better understanding of material properties, material geometry, system operating conditions, and closer interactions with manufacturers are still needed, however, before thermal stress resistant structures can be fabricated. This is especially true for "active" monolith systems where little material property data are available for many of the active compounds, and there is almost no experience in the fabrication of these compounds into honeycomb structures.

It is apparent that there are no currently available catalyst systems that can meet all the requirements for high temperature (>1590K) catalytic combustion. These requirements can be summarized as:

- A high use temperature (>1590K)
- High combustion efficiency, low emissions
- Structurally stable; thermal stress/shock resistant; no destructive interactions with the flow environment (e.g., chemical attack)
- Catalytically stable; low volatilization; no destructive interactions with the flow environment (e.g., poisoning); no destructive interactions with the substrate (in the case of coated catalysts).

It is now generally recognized that catalyst development for catalytic combustion is a critical issue that must be addressed in a timely manner. A review of the achievements to date, the problems encountered, and the promising directions to take is therefore necessary. The objectives of this task are to:

- Survey the state of the art in materials development for catalytic combustion
- Survey other high temperature materials technology for possible extrapolation to catalytic combustion use
- Identify critical areas requiring further development
- Formulate a plan for future development work.

3.1.2 Critical Areas for Catalyst Development

The development of catalysts suitable for catalytic combustion requires the simultaneous consideration of several factors including catalyst activity, stability, and structural integrity as well as methods that are available to fabricate various shapes of acceptable quality. For example, materials considered good catalysts may have very poor stability in severe thermal environments, while materials with good thermal stress resistance may be difficult to fabricate into a catalytically active structure. Finding catalysts that satisfy all the criteria defined above requires an understanding of each of the problems and the methods available to overcome them.

3.1.2.1 Catalyst Selection

Catalyst Activity

Catalyst activity is one of the key properties to consider in catalyst selection, whether the catalyst is to be used as a coating or as the basic component of an active monolith. It is generally difficult to project a material's potential for catalytic combustion, since catalysis is a complex phenomenon involving the surface, the chemical composition, and the overall structure of the material (References 3-9, 3-10). Even so, in many cases, it seems that catalytic activity can be correlated with the number and type of localized defects in the solid (Reference 3-11). Such defects could be surface defects. For example, a crystal can be cleaved along one of its crystalline planes, leaving unsatisfied bonding. The Ni^{2+} ion in nickel oxide has sixfold octahedral coordination in the bulk, but in the surfaces of the three main cleavage planes (100, 110 and 111), the coordination of Ni^{2+} is reduced from NiO_6 to NiO_5, NiO_4, and NiO_3, respectively. In order to recover the sixfold coordination of the bulk, the nickel oxide readily chemisorbs various gaseous species such as O_2, thereby initiating catalytic reaction. For metal oxides, the controlled production of anionic or cationic vacancies seems to be of particular importance in determining catalytic activity. Two approaches are possible for production of these defect structures, as described below.

Nonstoichiometric defect structures can be formed from a metal oxide containing a metal in a mixture of oxidation states such as Fe_2O_3 and Fe_3O_4. They are nonstoichiometric in that the ratio of metal to oxygen is not quite what an ideal formula demands. An unambiguous assignment of valence cannot be given to the metal ion so that a "perfect" crystal structure can be formed, and because the crystal structure is not perfect, a defect structure is formed. Two examples of nonstoichiometric defect structures are $LaCo_{1-x}O_3$, which contains Co in +3 and +2 states, and $LaCr_{1-X}O_3$, which contains Cr in +3 and +6 states.

The other kind of defect structure is formed by the introduction of impurity ions of valence different from that of the replaced ion. For example, Li^+ ions introduced in solid solution in the divalent oxide NiO serve to generate Ni^{+3} ions. It may be important to control the valence of the introduced metal ion to increase selectivity and activity. It was found that for N_2O decomposition with Mn_2O_3, the Mn^{3+} ions are more active than Mn^{4+} ions for decomposition (Reference 3-12). The amount of Mn^{3+} ions can be controlled by adding LiO and MgO_2 in solid solution combination with the Mn_2O_3.

The above discussion is a simplistic view of defect structures and their catalytic activity. The actual sequence of events taking place during catalysis and the roles of the surface, catalyst composition, and structure in those events are still largely unknown. In any case, the capability of a material to exhibit multiple valency under different conditions appears to play a key role in determining catalytic activity. This restricts the choice of catalytic materials to the transition metal elements and their compounds including those of the lanthanide and actinide series. These are shown in Table 3-1. Within the transition elements themselves, some have a greater number of oxidation states compared to others and are probably more active catalysts. Among the more active oxidation catalysts are platinum group

TABLE 3-1. PERIODIC TABLE

	METALS												NONMETALS					
			TRANSITION METALS															
PERIODS	I A	II A	III B	IV B	V B	VI B	VII B	VIII			I B	II B	III A	IV A	V A	VI A	VII A	0
1 0	1.00797 H [1] 1																1.00797 H [1] 1	4.0026 He[2] 2
2 2	6.939 Li [3] 1	9.0122 Be[4] 2											10.811 B [5] 3	12.01115 C [6] 4	14.0067 N [7] 5	15.9994 O [8] 6	18.9984 F [9] 7	20.183 Ne[10] 8
3 2, 8	22.9898 Na[11] 1	24.312 Mg[12] 2											26.9815 Al[13] 3	28.086 Si [14] 4	30.9738 P [15] 5	32.064 S [16] 6	35.453 Cl [17] 7	39.948 Ar[18] 8
4 2, 8	39.102 K [19] 8, 1	40.08 Ca[20] 8, 2	44.956 Sc [21] 9, 2	47.90 Ti [22] 10, 2	50.942 V [23] 11, 2	51.996 Cr[24] 13, 1	54.9381 Mn[25] 13, 2	55.847 Fe[26] 14, 2	58.9332 Co[27] 15, 2	58.71 Ni [28] 16, 2	63.546 Cu[29] 18, 1	65.37 Zn[30] 18, 2	69.72 Ga[31] 18, 3	72.59 Ge[32] 18, 4	74.9216 As[33] 18, 5	78.96 Se[34] 18, 6	79.904 Br[35] 18, 7	83.80 Kr[36] 18, 8
5 2, 8, 18	85.47 Rb[37] 8, 1	87.62 Sr [38] 8, 2	88.905 Y [39] 9, 2	91.22 Zr [40] 10, 2	92.906 Nb[41] 12, 1	95.94 Mo[42] 13, 1	(99) Tc[43] 14, 1	101.07 Ru[44] 15, 1	102.905 Rh[45] 16, 1	105.4 Pd[46] 18	107.868 Ag[47] 18, 1	112.40 Cd[48] 18, 2	114.82 In[49] 18, 3	118.69 Sn[50] 18, 4	121.75 Sb[51] 18, 5	127.60 Te[52] 18, 6	126.9044 I [53] 18, 7	131.30 Xe[54] 18, 8
6 2, 8, 18	132.905 Cs [55] 18, 8, 1	137.34 Ba[56] 18, 8, 2	[57-71] *	178.49 Hf[72] 32, 10, 2	180.948 Ta[73] 32, 11, 2	183.85 W [74] 32, 12, 2	186.2 Re[75] 32, 13, 2	190.2 Os[76] 32, 14, 2	192.2 Ir [77] 32, 15, 2	195.09 Pt [78] 32, 17, 1	196.967 Au[79] 32, 18, 1	200.59 Hg[80] 32, 18, 2	204.37 Tl[81] 32, 18, 3	207.19 Pb[82] 32, 18, 4	208.980 Bi [83] 32, 18, 5	(210) Po[84] 32, 18, 6	(210) At[85] 32, 18, 7	(222) Rn[86] 32, 18, 8
7 2,8,18,32	(223) Fr [87] 18, 8, 1	(226.05) Ra[88] 18, 8, 2	[89-103] †	[104]	[105]	[106]	[107]	[108]										

* LANTHANIDE SERIES	138.91 La[57] 18, 9, 2	140.12 Ce[58] 20, 8, 2	140.907 Pr[59] 21, 8, 2	144.24 Nd[60] 22, 8, 2	(145) Pm[61] 23, 8, 2	150.35 Sm[62] 24, 8, 2	151.96 Eu[63] 25, 8, 2	157.25 Gd[64] 25, 9, 2	158.924 Tb[65] 27, 8, 2	162.50 Dy[66] 28, 8, 2	164.930 Ho[67] 29, 8, 2	167.26 Er[68] 30, 8, 2	168.934 Tm[69] 31, 8, 2	173.04 Yb[70] 32, 8, 2	174.97 Lu[71] 32, 9, 2
† ACTINIDE SERIES	(227) Ac[89] 18, 9, 2	232.038 Th[90] 18, 10, 2	(231) Pa[91] 20, 9, 2	238.03 U [92] 21, 9, 2	(237) Np[93] 23, 8, 2	(242) Pu[94] 24, 8, 2	(243) Am[95] 25, 8, 2	(245) Cm[96] 25, 9, 2	(245) Bk[97] 26, 9, 2	(248) Cf [98] 28, 8, 2	(253) Es[99] 29, 8, 2	(254) Fm[100] 30, 8, 2	(256) Md[101] 31, 8, 2	(253) No[102] 32, 8, 2	(257) Lw[103] 32, 9, 2

metals, chromium, nickel, manganese, cobalt, iron, and copper. In the rare earth series, cerium, terbium, and praseodymium, and to a lesser extent samarium, europium, and ytterbium exhibit multiple valency.

It is important to address how catalytic activity is affected by the formation of a solid solution or compound of an active oxide with other oxides. For example, can the activity of Cr_2O_3 be compared to the activity of $Cr_2O_3 + Al_2O_3$ or $LaCrO_3$ in the absence of test data? A series of perovskite compounds containing mixtures of oxides were tested by DuPont and shown to support oxidation reactions (Reference 3-8). Unfortunately, no comparison was made to active oxides alone, so it is difficult to tell whether activity was increased or decreased with the formation of the perovskite.

Catalyst Stability

Some of the most active catalysts for oxidation reactions are also the most volatile. Although little reliable data on vapor pressures are available, many compounds potentially useful as catalyst or substrate materials have significant vapor pressures at the elevated temperatures of catalytic combustion. In addition, the oxidizing atmosphere and high volumetric flowrates over the substrate will further enhance the rate of depletion of some of the compounds. In many cases, this depletion would be unsatisfactory since this implies a loss of activity and/or a loss of structural integrity (e.g., loss of the stabilizer from ZrO_2 matrix). Even some of the transition metal oxides such as Cr_2O_3 and NiO were significantly depleted as surface coatings during catalytic combustion, leading to complete loss of ability to sustain combustion. To assess the stability of any catalyst or substrate material, it is imperative to obtain information on the rate of volatilization (although limited high temperature data are available). Initial screening experiments under actual conditions would be needed in most cases.

Table 3-2 lists the vapor pressures of various oxides at two different temperatures. Figure 3-1 is a plot of vapor pressure as a function of

TABLE 3-2. VAPOR PRESSURE DATA OF VARIOUS OXIDES
(References 3-13, 3-14, 3-15)

Compound	Vapor pressure (x 10^6 atm)	
	1644K (2500°F)	2006K (3150°F)
Al_2O_3	0.001	1
SiO_2	80	2,000
MgO	2	700
ZrO_2	$<10^{-3}$	0.01
BeO	--	12
BaO	60	10,000
LiO	2,000	--
CeO_2	--	<800
La_2O_3	0.05	30
HfO_2		$>10^{-8}$
TiO_2		>0.01
ThO_2		0.01
V_2O_3		>0.1
Y_2O_3		>0.001
Cr_2O_3	70	9,000
NiO		100,000
Fe_2O_3	70	10,000
PtO_2	960	8,400

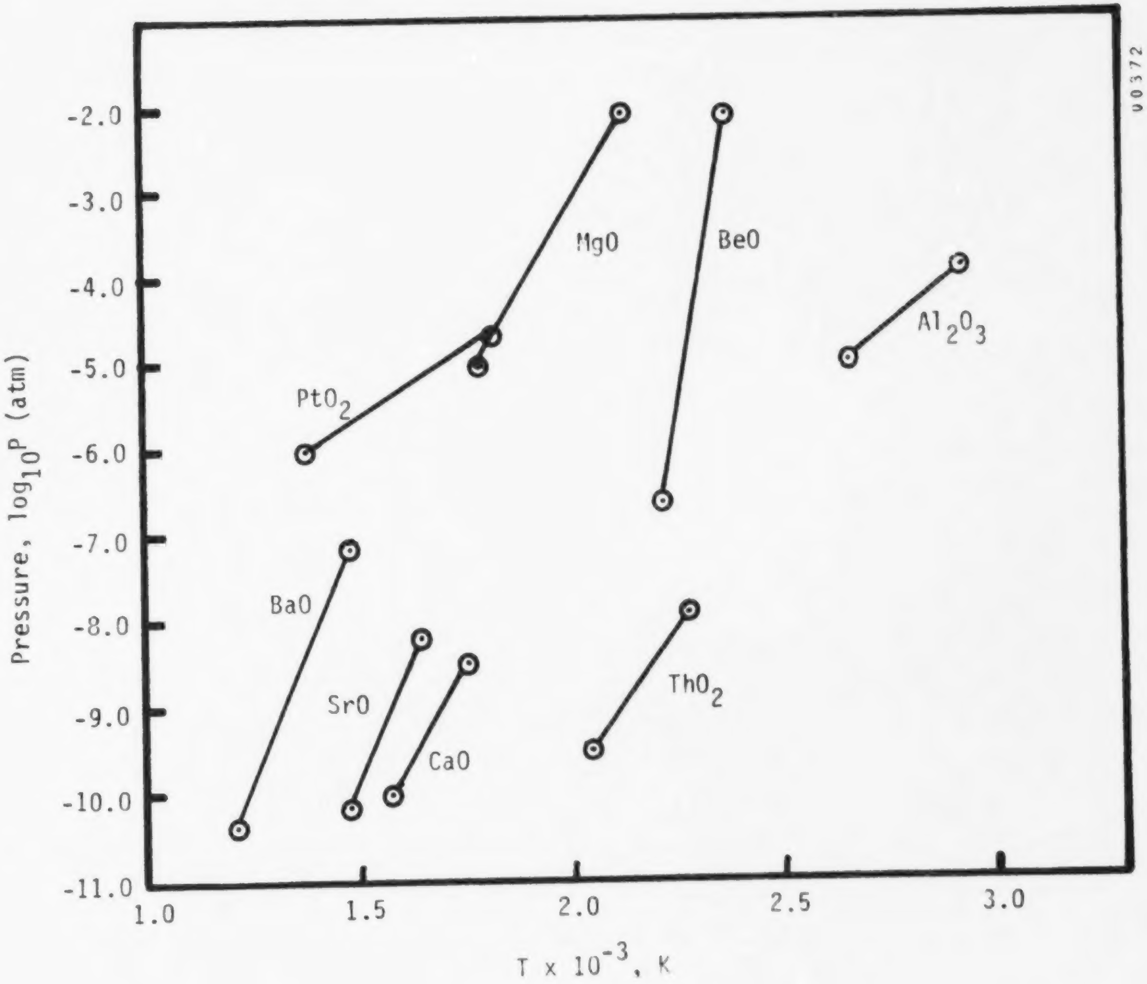

Figure 3-1. Vapor pressure versus temperature of selected metal oxides (after Reference 3-16).

temperature for some of the oxides in Table 3-2. The data provide qualitative comparisons of oxide behavior at elevated temperatures. Volatilization can occur by several mechanisms. The simplest mechanism is sublimation of the solid to gaseous molecules with identical composition, such as with ThO_2. The solid may also vaporize to gaseous molecules with a different composition from the solid, as in the decomposition of Li_2O to Li and O_2 with small amounts of LiO as well. It should be noted that the rate of volatilization of many of the compounds is very much dependent on the atmosphere surrounding it. Thus, Cr_2O_3 shows appreciable volatilization in oxygen but none in argon (Reference 3-14). This has been attributed to the formation of CrO_3, a very volatile oxide, from Cr_2O_3 under oxidizing conditions. There is some evidence in the same study that Fe_2O_3 may be more stable than Cr_2O_3 in an oxidizing atmosphere, since little weight loss of Fe_2O_3 was observed in air. The volatility of platinum metal is increased by a factor of 10^4 in the presence of oxygen at 1773K (2732°F). This has been attributed to the formation of PtO_2, which is highly volatile (Reference 3-15). Some of the rare earth oxides have low vapor pressures and should be rather stable during catalytic combustion. Very little information on volatility, however, is available for the rare earth oxides, such as cerium, terbium, praseodymium, samarium, europium, and ytterbium, which are potentially active. In one study, cerium oxide was found to be rather volatile (vapor pressure $\sim 8 \times 10^6$ atmospheres) under the high temperature environment of magnetohydrodynamics (Reference 3-17). However, this was tested at a temperature of >1920K and an oxygen partial pressure of $<10^{-5}$ atmospheres. The rare earth oxides should therefore be an interesting group to consider both for their potential activity and lower volatility.

One way to reduce the volatilization tendency of an oxide is to combine it with other oxides to form a solid solution or a compound. For example, Cr_2O_3 and Al_2O_3 are readily miscible to form a solid solution. If the solution formed is ideal, the effectiveness of the solid solution in reducing the volatilization of a component is probably rather low. For an ideal solution, the partial pressure of each component would be proportional to the mole fraction of the component according to Raoult's Law:

$$p_A = P_A x_A$$

where p_A = partial pressure of component A at temperature T

P_A = vapor pressure of A at temperature T

x_A = mole fraction of A in solution

This would imply that the actual vapor pressure of component A would be lowered, and thus less A would be removed. Since there is less A to start with in a solid solution of A, the time it takes to deplete A from a solid solution may not be significantly different compared to depleting pure A.

If A has strong attractive forces for the other oxides in the solid solution, the solution is highly nonideal and does not obey Raoult's Law. The partial pressure of A in this case would be significantly lower than predicted from ideal solution behavior. For the case of strong "negative" deviations from Raoult's Law, formation of a solid solution may help stabilize A in the solution and slow the depletion rate. The affinity of A for the other oxides may be so strong that compounds are actually formed. Compound formation, in some cases, is expected to depress the rate of volatilization of an oxide by an order of magnitude.

The major classes of mixed oxide compounds include spinels, perovskites, corundum-ilmenites and a large variety of silicate-based materials. Spinels have the general formula AB_2O_4, where A and B represent metal ions, and a variety of compounds can be formed by varying A and B. A large number of compounds can also be formed in the perovskites (ABO_3) and corundum-ilmenites (ABO_3). Table 3-3 provides some examples of the compounds which can be formed by suitable combinations of various oxides. How and whether a mixture of

TABLE 3-3. EXAMPLES OF MIXED OXIDE COMPOUNDS

Spinel: AB_2O_4 (Cubic close packed)	Perovskite: ABO_3 (Cubic close packed)	Ilmenite: ABO_3 (Hexagonal close packed)
$MgAl_2O_4$	$LaCrO_3$	$FeTiO_3$
$MgCr_2O_4$	$CaTiO_3$	$NiTiO_3$
$NiCr_2O_4$	$YAlO_3$	$CoTiO_3$
$Mg_xCo_{1-x}Cr_2O_4$	$LaAlO_3$	$MgTiO_3$
Fe_3O_4	$YCrO_3$	$LiNbO_2$
$CoAl_2O_4$	$YMg_{0.05}Cr_{0.95}O_3$	
$NiAl_2O_4$	$La_{0.95}Mg_{0.05}CrO_3$	
$MgAl_2O_4$:$NiAl_2O_4$	$(Th_{0.1}La_{0.9})(Fe_{0.8}Al_{0.2})O_3$	
$Ni(Al_{0.3}Cr_{0.5}Fe_{0.2})_2O_4$	$SrRuO_3$	
$Ni_{0.5}Mg_{0.5}(Al_{0.5}Cr_{0.3}Fe_{0.2})_2O_4$	$(Ba_{0.1}La_{0.9})(Al_{0.9}Pt_{0.1})O_3$	

oxides will form certain structures can be determined by consideration of the sizes of the cations and anions involved and their coordination numbers. A detailed discussion is given in Reference 3-18. In all cases, however, by combining suitable amounts of different oxides to form compounds, the tendency for the volatile components to be depleted can be diminished. Coatings developed from some of these compounds should be more stable on the substrate. Substrates can also be fabricated directly from compounds containing catalytically active components to form the active monoliths discussed earlier.

Besides volatility, the melting point of the catalyst will determine the maximum use temperature in many cases. For pure components, melting point information is relatively easy to obtain, but most catalyst systems are made up of a complex mixture of components. For some binary and multicomponent mixtures, phase diagrams are available for predicting use temperatures as a function of composition (Reference 3-19). For a binary mixture, the general shapes of phase diagrams for completely miscible, completely immiscible, and intermediate compound formation cases are illustrated in Figures 3-2, 3-3, and 3-4, respectively. Completely miscible systems have melting points which are usually higher than the lower melting components (e.g., $Cr_2O_3 + Al_2O_3$). Completely immiscible systems form eutectic melts at temperatures lower than the melting point of either component (e.g., $MnO + SiO_2$). Addition of more components to the binary eutectic will depress the melting point further. The formation of eutectic melts is undesirable in some cases as it lowers the use temperature of a catalyst system significantly. Manganese oxide and silica, for example, form a eutectic that melts at 1522K (2280°F). Thus, when manganese oxide is used as a catalyst on or in a substrate containing silica, the operating temperature cannot exceed 1522K. In the choice of a catalyst system, therefore, some attention should be given to the expected melting temperature of the catalyst.

For catalyst systems in which a catalyst is to be coated on a substrate with which it is miscible, the catalyst will potentially diffuse and mix with

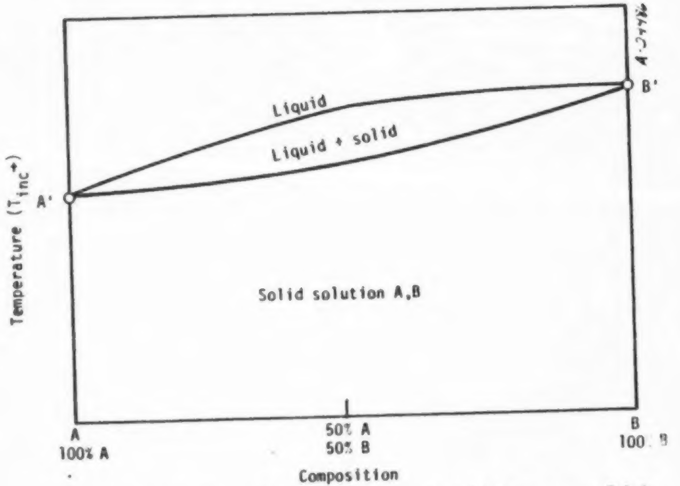

Figure 3-2. Completely miscible -- solid solution.

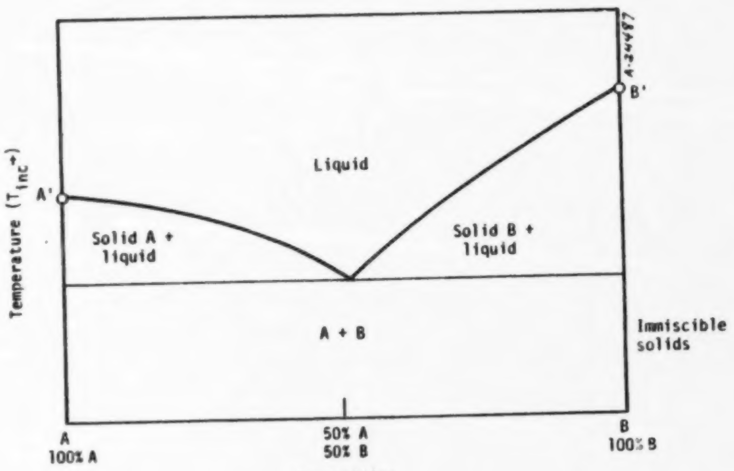

Figure 3-3. No solubility -- eutectic melting point.

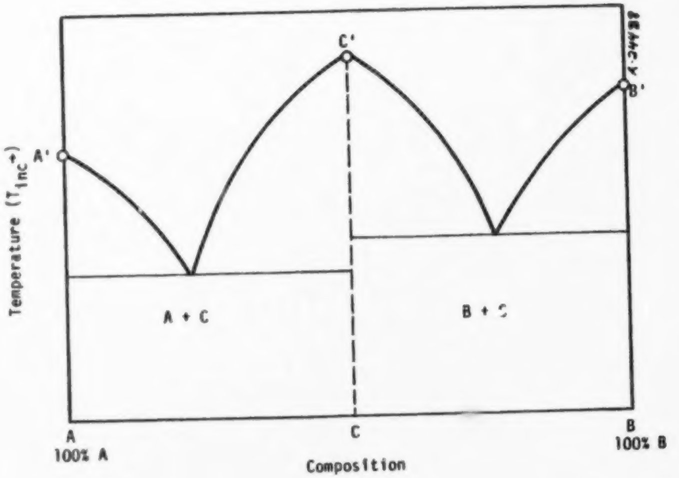

Figure 3-4. Formation of intermediate compound C.

the substrate at elevated temperatures, altering the strength and thermal shock capabilities of the substrate. It has been observed, for example, that a coating of cobalt oxide penetrated a Torvex alumina honeycomb at high temperatures and probably contributed to structural collapse. To minimize solid state reactions the melting points of the materials used should be greater than the maximum operating temperatures by a factor of at least 1.5.

Catalyst penetration into a substrate may not always cause structural damage. If the structure remains intact, the substrate should become "active" by virtue of the penetration of the catalyst. If the catalyst and substrate are mutually insoluble (or of very limited solubility), catalyst/substrate interactions would be minimized. For catalyst systems utilizing a coated catalyst, it is desirable to choose either a catalyst/substrate with very high melting points (1.5 times operating temperature) or a catalyst/substrate with high eutectic melt temperatures (greater than the use temperature).

Contaminants in the gas stream may adversely affect catalyst performance. At temperatures below 770K (926°F), base metal catalysts can be deactivated by sulfur at levels <1 ppm. At the higher temperatures of catalytic combustion, tolerance to sulfur and many other poisons (e.g., lead) increases since many of these compounds decompose at high temperatures. Halides in the gas stream form highly volatile oxyhalides with many catalysts. Chromia, for example, forms chromium oxychloride with a vapor pressure of 1 atmosphere at 661K (730°F). The presence of alkali salts in the gas stream may also deactivate the catalyst by forming low temperature fluxes and/or volatile compounds with many of the catalyst components.

On the other hand, catalysts consisting of a mixture of compounds may have significantly altered tolerance to contaminants. Traces of platinum, for example, when added to certain base metal perovskites (Reference 3-20) have been shown to increase their catalytic activity significantly while rendering the catalyst insensitive to sulfur poisoning. In formulating catalyst compositions for low volatility, high use temperature, and tolerance to poisons, a great deal will have to depend on initial screening under the actual environments of operation since high temperature data for many of the catalysts are relatively scarce.

3.1.2.2 Structural Stability

One of the key requirements for a catalyst system is overall structural stability. In particular, this implies the ability to stand up under transient as well as steady state conditions which produce large thermal stresses. For the present study, only honeycomb shaped structures are considered and the catalyst system could either be a catalyst coating on an inert honeycomb or a honeycomb fabricated from catalytic material. In either case, thermal stress failure of the structure is a major factor limiting the usefulness of honeycomb catalytic combustors. The thermal stress resistance of the honeycomb structure is a complex combination of the physical properties of the material, the material geometry, and the heat transfer effects at the material surface during operation. A careful selection of material properties, geometry, and overall system design can optimize the solid's resistance to fracture under thermal stress. It should be noted that a solid develops thermal stresses only if there are restraints on free expansion. Thermal stress develops as a consequence of strain and is the dependent variable. This is different from strain produced by mechanical stress, in which case strain is the dependent variable. This immediately suggests that any approach to minimize strain due to thermal gradients is of primary consideration.

A material with zero coefficient of thermal expansion will have no thermal stress problems since no strain is produced by thermal gradients. A material with some degree of plasticity will also be able to accommodate thermal stresses better by deformation. Since most materials develop some degree of plasticity near their melting points, thermal stress problems are usually less severe at high temperatures. If the material geometry is such that the parts are small and thin, large temperature gradients are harder to establish. In addition, if the system can be operated so that large temperature transients are avoided, the probability of steep thermal gradients is diminished. In many cases, however, there is insufficient flexibility in geometry and system design to reduce thermal stress to acceptable levels. Under these conditions, the physical properties of the material will have to be refined and/or modified or new materials chosen to satisfy system needs. Since each system and application have different requirements, each of the three factors -- geometry, system operating conditions/maximum temperature gradients expected, and physical properties of the materials considered -- will have to be examined to assess the potential thermal shock/stress resistance of a particular material. The following discussions on each of these factors address applications to high temperature (>1600K) catalytic combustion applications.

System Operating Conditions and Geometry

In many applications of catalytic combustion, careful consideration of system operating conditions and geometry may provide avenues for minimizing thermal stresses under steady state and transient conditions. It also allows some assessment of the magnitude of thermal stresses which may develop in the substrate, and the probability a given substrate material can withstand such stresses. Most refractory oxide substrates will not be able to withstand stresses in excess of 30,000 psi. In some cases, improper substrate restraints may produce unnecessarily high stresses. For example, a ceramic tube constrained at both ends will develop tremendous stresses as temperature increases, while a loosely fitting tube will be able to expand freely and undergo no stress at all. Thus, during combustion mounting, minimum restraint should be placed on the honeycomb substrate used. Thermal shock during transients can be minimized by making the web thickness sufficiently thin or by using materials with high thermal conductivity to minimize the temperature gradient across the material. A typical set of operating conditions for a gas turbine catalytic combustor during startup, shutdown, and steady state operation is summarized in Table 3-4, and stresses that can develop under these conditions are discussed below.

During startup, preheated air at 480K (400°F) flows through the honeycomb for about 70 seconds, after which the system is ready for lightoff. With one approach, an opposed jet is used as the igniter. As the jet is turned on, the temperature of the gas stream rises to 810K (1000°F). Fuel is then added slowly to the stream (opposed jet on) until the wall temperature reaches 1640K (2500°F). This usually takes place in less than 30 seconds. For webs with a thickness less than 0.2 cm and made with a typical ceramic material (thermal diffusivity $\simeq 6 \times 10^{-7}$ m^2/s), it can readily be shown that it takes less than 0.1 seconds for the center of the web to reach the temperature of the surface (Reference 3-21). Thus, as the web surface heats up due to catalytic oxidation of the fuel, the center of the web responds quickly, preventing steep thermal gradients from building up. As fuel is added, the air/fuel equivalence ratio decreases, and the catalyst walls approach the adiabatic flame temperature of the mixture. It takes about 30 seconds to bring the fuel flow up to the steady state level. The web surface temperature will thus go from 810K to 1640K in about 30 seconds, significantly longer than the response time of the temperature at the center of the web due to surface temperature fluctuations. In addition, during the heating of the substrate, the surface of the web is under compression and is much less prone to fracture since ceramic materials are much stronger in compression than in tension.

During shutdown, the situation is somewhat different. Fuel flow is shut off in less than 5 seconds, after which air flows through the honeycomb at 480K. Taking the worst possible case, the webs are still at 1640K when air at 480K first comes in contact with the surface. Assuming that the air flowing over the web surfaces can be approximated by air flowing past a flat plate with appropriate heat transfer coefficients derived for flow in square channels, the difference in temperature between the center and surface of the web can be determined (Reference 3-22). Results for honeycombs of two typical

TABLE 3-4. POSSIBLE THERMAL STRESS CONDITIONS DURING GAS TURBINE OPERATION

Startup	Steady State Operation	Shutdown
• Room temperature	• Center of honeycomb at 1640K	• Fuel off in <5 sec, air, 15.2 m/s, 480K
• Compressed air at 480K, 15.2 m/s, for 70 seconds	• Outer edges of honeycomb at 980K	
• Opposed jet, 810K		
• Fuel addition; catalyst wall reaches 1640K in 30 seconds		

cell sizes are given in Table 3-5. For small cells with thin webs (configuration A), the maximum temperature difference expected is 58K, as opposed to 29K for larger cells with thicker webs (configuration B). This temperature difference may exceed the maximum allowable difference for some ceramic materials, causing larger tensile stresses (as described in the following section on material properties).

During steady state, other temperature gradients may exist that can cause significant thermal stresses. For example, heat transfer to the support structure and surroundings may cause temperature differences from honeycomb centerline to the perimeter or in the axial flow direction. Uneven fuel/air distribution can also support these temperature variations within the structure. It is, therefore, possible to develop simple or combined axial, radial, and circumferential stresses within the structure.

There are a number of geometrical changes that can be envisioned for alleviating these stresses in honeycombs. The use of thin webs of high thermal conductivity has been discussed as a means of minimizing stresses across the web. Increased conductivity also could alleviate axial stresses along the web (if alternate material selection were possible). However, in most cases, thermal conductivity will be fixed by the selection of a specific material based on other criteria, and geometrical changes may be required to alleviate possible stresses. One technique that has been developed by Corning is the flexible cell structure that allows cell walls to bend as a means of reducing axial stress (see Reference 3-1). These structures are most readily produced by the Corning extrusion process. The ceramic sponge (Hi-Tech Ceramics, Inc.) is another example of a multidirectional structure of thin web cross section that may allow bending to relieve thermal stresses. Producing such structures free of cracks and other stress concentration factors is difficult, however, and tests have not fully verified the advantage of these structures at temperatures above 1367K.

TABLE 3-5. THERMAL CONDITIONS EXISTING AT THE WEB SURFACE OF A HONEYCOMB DURING SHUTDOWN FROM 1644K

Configuration	A	B
Cell diameter (cm)	0.16 (1/16 in)	0. 64 (1/4 in)
Web thickness (cm)	0.05	0.16
Material thermal conductivity (W/m-K)	1.1	1.1
Material thermal diffusivity (m^2/s)	6×10^{-7}	6×10^{-7}
Heat transfer coefficient (J/m^2-K-s) (for air at 15.2 m/s, 478K)	131	68
Web temperature (K),		
Center	1644	1644
Surface	1586	1615
Maximum web center to surface temperature difference (K)	58	29

Several other schemes of reducing selected stresses in honeycomb structures are illustrated in Figure 3-5. A collection of smaller honeycomb elements can reduce axial stresses (such as with the graded cell configuration) or circumferential stresses. The pie-shaped elements of Figure 3-5A are an example of segmenting. Of course, a larger number of elements results in more complex support and mounting problems which limit the practical number of segments that can be accommodated. The radial and axial flow split structures of Figures 3-5B and 3-5C are designed to minimize the radial and circumferential stresses that can develop across the structure for these two flow configurations. It may also be possible to fabricate a honeycomb structure from a fibrous insulator such that stress can be alleviated by movement of the fibers (Figure 3-5D). Refractory oxide fibers such as thoria or zirconia may be able to survive the high temperature environments encountered without undue sintering and degradation.

In summary, there exists sufficient promise in system and geometric modifications that these should be considered as viable solutions to thermal stress problems, especially under thermal conditions where material considerations alone will probably not succeed.

Material Properties

The physical properties of a material are functions of both the chemical components and the microstructure. Many parameters have been proposed to relate these material properties with thermal stress resistance (References 3-23 through 3-28). In general, however, only a few parameters prove to be of any practical use in comparing different materials. The two most useful indicators of thermal stress resistance are R and R', defined by:

$$R = \frac{\sigma_f(1 - \nu)}{\alpha E} \qquad (3\text{-}1)$$

$$R' = kR \qquad (3\text{-}2)$$

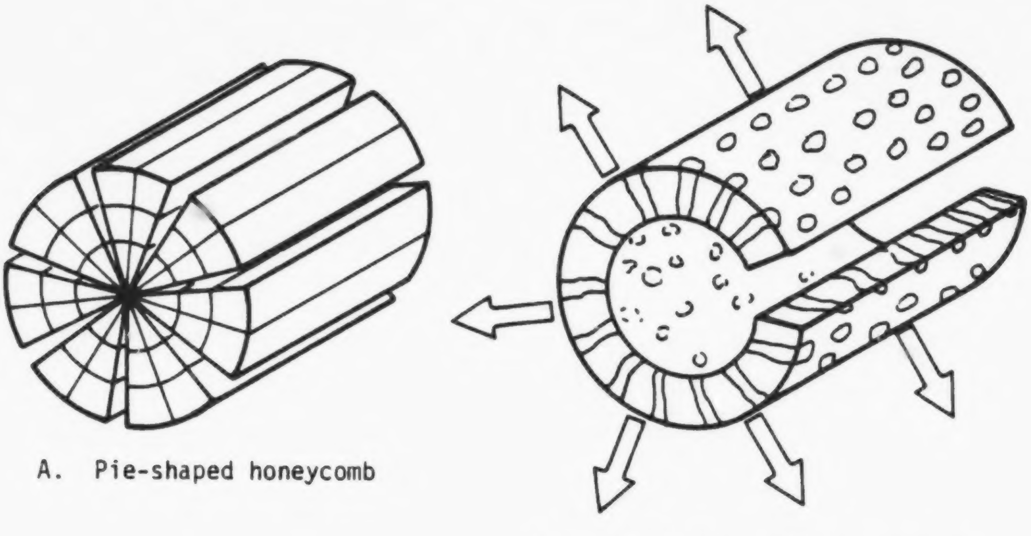

A. Pie-shaped honeycomb

B. Radial flow split structure

A-26484

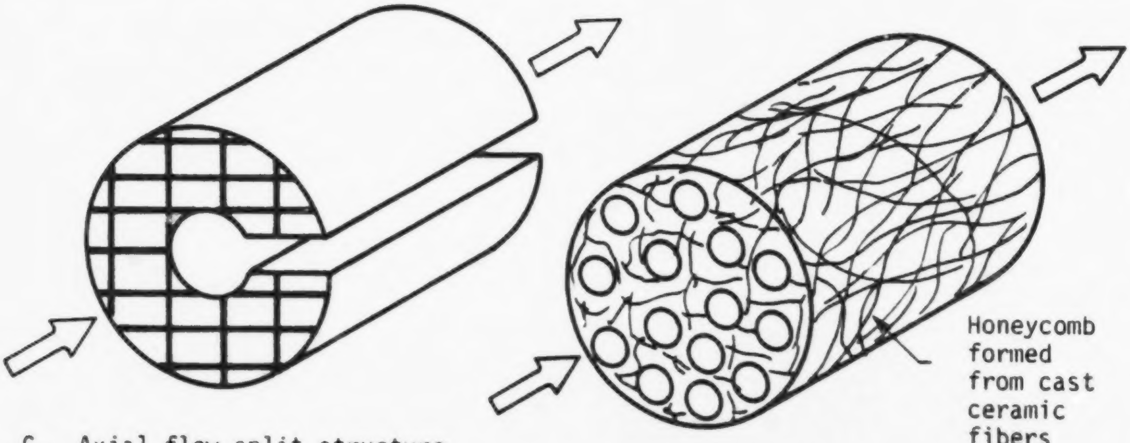
Honeycomb
formed
from cast
ceramic
fibers

C. Axial flow split structure

D. Axial flow cast ceramic fiber

Figure 3-5. Geometric modifications to the basic honeycomb monolith.

where σ_f = fracture stress

ν = Poisson ratio

α = coefficient of thermal expansion

E = Young's Modulus

k = thermal conductivity

The higher the values of R and R', the greater is the resistance to thermal stress. The expression for R is simply derived from the conditions that a material will fracture once the strain and the resultant stress produced by temperature changes exceed the fracture stress (Reference 3-28). For a point in an infinite slab of the material, this is given by:

$$\frac{E}{(1 - \nu)} \alpha \Delta T = \sigma_f \tag{3-3}$$

where ΔT = difference between temperature at the point and the average temperature.

Comparing Equations (3-1) and (3-3), it can be seen that R has units of temperature. The magnitude of R not only allows a comparison of different materials but also indicates the maximum allowable temperature difference that can exist in the material before fracture occurs. Table 3-6 shows a selection of common ceramic materials, their physical properties, and the expected thermal stress resistance. It should be emphasized that the physical properties listed may not be entirely accurate and are very dependent on the exact components of the material, the microstructure, and the method of fabrication. Thus, the measured fracture strength of a material is usually much lower than the theoretical strength due to flaws existing in the material (Reference 3-28). The percent porosity also has strong effects on the resultant physical properties (Reference 3-23).

TABLE 3-6. PROPERTIES OF SOME COMMON CERAMIC MATERIALS AND THEIR THERMAL STRESS RESISTANCE (References 3-29, 3-30)

Material	Composition	Porosity vol %	MP °C (°F)	Maximum use temperature °C (°F)	Coefficient thermal expansion x 10^6/°C	Young's modulus x 10^{-3} psi	Fracture strength x 10^{-3} psi (1000°C)	Thermal conductivity cal/s/cm/°C (1000°C)	Thermal stress resistance R
Alumina (sintered)	99.8Al_2O_3	3-7	2030 (3685)	1900 (3452)	8.6	53	22	0.014	0.68
Cordierite	2MgO 2Al_2O_3 5SiO_2		1470 (2678)	1300 (2372)	1.0	-25	11	0.0025	1.10
Mullite (sintered)	72Al_2O_3 28SiO_2	3-10	1810 (3290)	1750 (3182)	4.5	21	12	0.008	1.02
Spodumene	Li_2O Al_2O_3 4SiO_2		1026 (1878)		-1 to 1				
Spinel (sintered)	99.8$MgAl_2O_4$	3-10	2130 (3866)	1850 (3362)	8.2	35	11	0.013	0.50
Zircon (sintered)	99.5$ZrSiO_4$	5-15	2420 (4388)	1800 (3272)	4.2	30	6	0.008	0.38
Stabilized zirconia (sintered)	92ZrO_2 4HfO_2 4CaO	3-10	2550 (4622)	2200 (3992)	7.2	22	15	0.005	0.47
Silicon carbide (sintered)	αSiC (98% dense)		5126 (9259)	1530 (2800)	4.7	50	66	0.100	28.10
Silicon nitride (hot pressed)	Si_3N_4 (98% dense)		3450 (6242)	1200 (2200)	3.0	40	64	0.045	24.00
Chrome alumina cermet	77Cr 23Al_2O_3	2	1850 (3362)	1300 (2872)	8.9	37.5	20	0.050	3.00
Beryllia (sintered)	99.8BeO	3-7	2570 (4658)	1900 (3452)	8.9	45	10	0.046	1.15
Magnesia (sintered)	99.8MgO	3-7	2800 (5072)	1900 (3452)	13.5	30.5	12	0.016	0.46
Titania (sintered)	99.5TiO_2	3-7	1840 (3344)	1600 (2912)	8.7		6	0.008	
Thoria (sintered)	99.8ThO_2	3-7	3050 (5522)	2500 (4532)	9.0	21	7	0.007	0.26
Yttria (sintered)	99.8Y_2O_3	2-5	2410 (4370)	2000 (3632)	9.3				
Silica glass	99.8SiO_2	0	1710 (3110)	1100 (2012)	0.5	10.5	-15 (Rm. temp.)	0.012	34.00

Returning to Equations (3-1) and (3-2) and Table 3-6, it can be seen that low coefficients of thermal expansion and Young's modulus, and high values of strength and thermal conductivity favor resistance to thermal stress. Silica glass, silicon carbide, and silicon nitride are the most thermally shock resistant materials listed, and this conclusion is supported by experimental evidence (References 3-31, 3-32 and 3-33). Silica glass has a rather low use temperature, while silicon carbide and silicon nitride are limited by their tendency to form silica at elevated temperatures in an oxidizing environment. The use temperature of silicon carbide (limited by formation of oxides) is sufficiently high to make it an attractive material for catalytic combustion applications. It should be noted, however, that coating a silicon carbide substrate with transition metal oxides may increase its tendency to undergo oxidation.

Of the common refractory oxide materials listed in Table 3-6, mullite, cordierite, beryllia, and chrome alumina cermet appear to have the greatest thermal stress resistance. Cordierite is limited by its low use temperature, while beryllia is unstable in the presence of water vapor. Chrome alumina cermet has a tendency to undergo oxidation, but the proper proportion of chrome to alumina can minimize the extent of reaction. Cermet materials with resistance to oxidation therefore show promise for high temperature applications.

For each material considered, it is beneficial to make similar analyses of thermal stress resistance and compare them to materials whose properties and performance under actual conditions are known. A material with thermal stress resistance much lower than mullite or cordierite would probably not be suitable as a substrate, since mullite and cordierite were both tested for catalytic combustion and found to hold up well, but not well enough to prevent some fracturing. Some of the materials considered unsatisfactory by thermal stress resistance criteria can be improved by changing a few of their properties through modifications in the chemical composition and/or fabrication method. The oxidation resistance of silicon nitride, for example, can be improved by proper additions of yttria (Reference 3-34). The fracture strengths of many of the materials can be improved by optimizing the grain size, pore distribution, amount and distribution of additives, and grain boundary chemistry. There is still room for improvement for materials considered marginal for thermal stress resistance and other stability problems.

Since it is the expansion of a material under temperature changes that produces stress, it is desirable to have materials with very low thermal expansion coefficients. Such compounds exist (References 3-35, 3-36, 3-37); some examples are shown in Table 3-7. Most of these compounds have highly anisotropic expansions, generally showing a positive thermal expansion in one direction and a negative expansion in a perpendicular direction. This results in a net change in volume of zero with temperature. Unfortunately, the anisotropic behavior may produce substantial microcracking in some cases, leading to very low strength materials. Microcracking may be suppressed by using very small grains of these materials during fabrication (Reference 3-37). Some investigators also suggest that microcracking may actually contribute to the low expansion coefficients. Regardless of the reason, there exists enough promise in these materials to encourage further investigation.

Some of the materials considered to have interesting properties may be difficult to fabricate into a thermal stress resistant substrate according to the criteria set above. Most transition metal perovskites and spinels, for example, have high thermal expansion coefficients (Table 3-8) and would probably fracture if honeycombs were made from these materials. An alternative approach is to prevent extensive crack propagation (rather than to prevent crack formation) by introducing a second phase. The second phase may be a disperson of particles in a matrix of the first phase or may simply be a distribution of pores. There are several mechanisms by which the second phase may enhance the thermal shock resistance of the matrix, such as a limitation on the intrinsic crack length of the matrix so that the strength of the material is increased. This is given quantitatively by the Griffith solution

TABLE 3-7. LOW THERMAL EXPANSION MATERIALS
(References 3-35 and 3-36)

Compound	Coefficient of Thermal Expansion (x 10^6/°C)
$37Ta_2O_3 \cdot 63WO_3$	-0.7
$63HfO_2 \cdot 37TiO_2$	0
$Al_2O_3 \cdot TiO_2$	0.8
$HfO_2 \cdot Nb_2O_5$	<1
$SnO_2 \cdot Ta_2O_5$	1.7
$ZrO_2 \cdot Nb_2O_5$	2.7
$HfO_2 \cdot 3Ta_2O_5$	3.4

TABLE 3-8. COEFFICIENT OF THERMAL EXPANSION OF SOME SPINELS AND PEROVSKITES (Reference 3-38)

Compound	Mean Coefficient of Thermal Expansion (x 10^6/°C)		
	From 25°C to		
	500°C	1000°C	1200°C
$BaTiO_3$	11.3	12.5	--
$Mg_{0.25}Ni_{o.75}Cr_2O_4$	7.0	7.4	7.7
$BaZrO_3$	7.8	8.3	8.6
$SrHfO_3$	8.6	9.7	9.9
$SrCeO_3$	9.1	9.4	10.2
$LaAlO_3$	10.7	11.5	11.8
$YAlO_3$	8.0	9.1	9.6
$LaCrO_3$	7.7	8.9	9.4
$YCrO_3$	7.7	8.0	8.4
$LaFeO_3$	10.1	10.6	10.8
$YFeO_3$	10.5	11.0	11.1
$BaPrO_3$	11.1	11.8	12.8
$MgCr_2O_4 \cdot MgAl_2O_4$	7.9	8.6	9.0
$MgAl_2O_4$	8.4	8.9	9.2
$MgCr_2O_4$	6.5	7.1	7.6
$CoCr_2O_4$	6.8	7.3	7.7
$NiCr_2O_4$	6.7	7.6	8.0

(Reference 3-28) for the critical fracture stress (σ_f) for a crack with length L as:

$$\sigma_f = \sqrt{\frac{\gamma E}{\pi L}}$$

where γ = surface fracture energy required to produce unit area of new crack surface

E = Young's Modulus

A brittle glass matrix, for example, was strengthened by a dispersion of alumina particles (Reference 3-39). The second phase may also act as crack "stoppers" to limit the extent of crack propagation. This concept has been applied successfully to increasing the thermal shock resistance of refractory bricks by increasing porosity and grog (oxide particles of a larger size than the average bulk material particle) addition (Reference 3-40) or of castables by addition of steel fibers (Reference 3-41). In many cases, a significant thermal expansion mismatch between the matrix and dispersed phase also leads to extensive microcracking and a subsequent decrease in overall strenth of the material. While strength usually decreases with the introduction of microcracks, quite a few materials actually become more thermally shock resistant in that they are less prone to catastrophic cracking and are able to withstand higher temperature differences. This has been explained by various microcrack theories and mechanisms (References 3-25 and 3-42). In general, it is assumed that the microcracks may provide a means of accommodating thermal strain by relieving some of the strain energy induced by thermal expansion. Cracks will propagate once the stored elastic energy due to thermal stress exceeds the energy required to create new surfaces. However, if the number of cracks is significant, each crack will only need to dissipate a little stored energy and thus can propagate in a stable fashion. If there are only a few cracks, each crack will have to dissipate much more stored energy and cracking becomes severe. Hasselman (Reference 3-25) has also attempted to show that the effect of microcracking on the individual physical properties of the material is such that an increase in the thermal stress resistance parameters R and R' is expected. His analysis shows that the strength to modulus ratio of the microcracked body increases with the number and size of microcracks. In most cases, the coefficient of thermal expansion is expected to decrease or remain unchanged. Microcracking is expected to lower the thermal conductivity somewhat, but R' is still expected to remain above the value for noncracked material.

The balance between the extent and number of microcracks and the desired physical properties of the resultant substrate is difficult to define quantitatively or to control in practice. The idea of introducing microcracks, however, has been shown to enhance thermal shock resistance in some systems. These include dispersions of SiC in BeO (Reference 3-43), ZrO in Al_2O_3 (Reference 3-44), graphite in ZrC (Reference 3-45) and W in MgO (Reference 3-46). Microcrack theory has also been applied successfully to the manufacture of refractory bricks with high spalling resistance. Application of this theory to honeycomb fabrication may prove more difficult. In order that the honeycombs possess sufficient strength in the presence of extensive microcracking, for example, the webs must be made thicker than normal. The thicker webs, however, would mean greater temperature gradients and higher thermal stresses. Extensive developmental work will be needed and would require more long term goals before significant achievements can be made. Apart from the concepts discussed above, there are other possibilities for increasing the thermal shock resistance of substrate materials. Again, however, many of the concepts are highly exploratory and require extensive development efforts. One approach is to establish a gradual variation in composition from the surface to the interior of the substrate (chemical strengthening, Reference 3-47) such as the formation of Al_2O_3-Cr_2O_3 surface layers on Al_2O_3. The slow variation in composition provides a gradual change in the thermal expansion coefficient and a more gradual variation in developed stresses. It is also used to produce compressive stresses at the surface. At high temperature, however, it will be difficult to keep the components from migrating and eventually forming a homogeneous mix. Another possible approach is the introduction of a fluxing agent which introduces the proper plasticity at a desired temperature to the substrate. The plasticity may relieve some of the thermal stress developed.

3.1.2.3 Honeycomb Fabrication Methods

A variety of techniques are available for making ceramic honeycomb structures. In general, the fabrication procedure can be divided into four distinct processing steps, all of which must be controlled carefully to ensure a product of uniform quality and reproducibility. The four key steps are (Reference 3-48):

- Preparation of the mixture
- Forming
- Drying
- Firing

Before forming into a honeycomb shape, the mix or batch used must be in a state of aggregation which gives it the requisite rheological properties, composition, liquid content, and particulate size distribution to optimize response during forming, drying, and firing. This is achieved by choosing suitable base materials, liquid media, and processing additives and properly blending and mixing into the final batch. This is a highly proprietary area in which not only the kind of additive but the sequence of addition may be important. Criteria for selection become empirical and intuitive. Some of the key additives often used are:

- Binders for strength
- Plasticizers for water retention, rheological aids, and strength during and after forming

- Deflocculants and flocculants for pH control and particle surface charge control
- Fluxes to aid in the maturing of the material during firing at lower temperatures
- Lubricants for rheological aids and as antifracture agents
- Others such as wetting agents, antistatic agents, foam stabilizers, etc.

Once the proper mix has been formulated, a variety of forming techniques are available for making honeycomb structures. Only a few, namely extrusion, paper method, and tape rolling, are readily amenable to the production of honeycombs of thin walls and uniform quality. Several other methods, some offering promise for special applications, will also be described.

The "green" shape after forming must in general undergo a carefully controlled drying process for liquid removal. As liquid evaporates, particles are pressed closely together and shrinkage occurs. During shrinking, stresses, warping, and even cracks may develop because of local variations in liquid content. Careful control of the drying rate and drying conditions are therefore critical.

After drying, the ceramic material is normally fired to temperatures ranging from 970K to 2100K. During firing, a viscous liquid of sufficient atomic mobility in the solid is developed to permit chemical reactions, grain growth, and sintering. As sintering occurs, the porosity is reduced, and some shrinkage occurs. Care must be taken during firing to ensure that the oven or kiln furniture on which the ceramic shape is supported does not interact with the ceramic material or cause undue restriction of the ceramic shape. On the other hand, the firing environment should be such that uniform heating of the ceramic shape can be achieved. The atmosphere surrounding the ceramic shape during firing, in general, also has to be carefully controlled. Firing, therefore, is a complicated final step in which material microstructure can be controlled. In the remainder of this section, details of mixture preparation and forming techniques for honeycomb shapes are given.

Mixture Preparation

Silicate and aluminum silicate compounds are the most abundant naturally occurring minerals and are used widely in the fabrication of raw materials. Cordierite and mullite, for example, use silicate-based compounds as basic material. Sometimes, the raw materials are beneficiated by mechanical concentration, froth flotation, and other processes. For specialized materials, chemical purification and even chemical preparation of raw materials may be necessary and appropriate. Silicon carbide, for example, is manufactured by reacting sand and coke. In the production of barium titanate capacitors, chemically purified titania and barium carbonate are used. Preparation of complex oxide compounds such as some of the perovskites and spinels discussed in the previous sections may require careful combination of various oxide precursors, mixing and processing several times before a suitable, homogeneous mix can be made.

Both particle size and particle size distribution also have to be controlled closely. The particle size constituents are essential for many processes since colloidal suspensions and plastic mixes with liquid phase binders depend on small particles flowing over one another or remaining in a stable suspension. For suspensions, the settling tendency is proportional to the particle size and density while for plastic forming, the coherence of mass is determined by the capillary force of the liquid between particles which is inversely proportional to the particle size. However, if all the material were of uniform fine particle size, it would not be feasible to form a high concentration of solids. In addition, during the drying process, large shrinkages would result from too much water trapped between small particles. Mixing in a coarser material allows the fines to fill the interstices between the coarse particles, a maximum packing density being achieved with 70 percent coarse and 30 percent fine when two particle sizes are used. In general, considerations of porosity and other factors such as optimal thermal shock resistance may require mixes of different particle size distribution.

Having chosen the basic raw material and the desired particle size distribution, a variety of additives are needed before the material can be formed into a final "green"* shape. The amount and type of additives are highly dependent on the properties of the base material, the forming method, and the desired characteristics of the final product. In many cases, the optimum combination is more of an art than a science. Each manufacturer has its own recipe as well as the method and order of combination of the ingredients. Some of the more common additives and their functions are described below.

Liquid Diluent

In slip casting, a slurry of the base material in a liquid is needed. In general, water is used and the material (e.g., clay particles) is dispersed with the help of deflocculants. The amount of water used depends on the desired viscosity of the slip. In some of the paper and thermoplastic forming processes (described later), a suspension of base material is held in a polymer solution. Organic solvents such as alcohols and ethers are used as plasticizers/solvents for the polymer as well as diluents for adjusting the solution to proper viscosities.

Plasticizer/Binder

Many of the base materials may not contain sufficient plasticity for forming or enough green strength to hold together before firing. To enhance plasticity, a suitable plastic medium can be added. Three general types are used:

- Organic binders which disappear almost completely when the articles are fired, such as starch, tar, linseed oil, waxes, cellulose derivatives, and various polymers

---

*Green is used to describe formed objects before they are fired.

- Substances, generally hydroxides or chlorides, which decompose to give the oxide on being mixed. $Al(OH)_3$ and $AlCl_3$, for example, can be used with Al_2O_3, and $ZrCl_4$ can be mixed with ZrO_2. Many of these compounds are gelatinous and can impart a high degree of plasticity.
- Substances which remain in the mass after firing, with their influence reflected in the final product. Examples include clay, silicates, and other oxides.

Alternatively, the base material may be treated chemically or physically. Alumina and zirconia can be treated with an acid solution. The acid treatment modifies the surface of the particles and imparts plasticity. Bodies containing few small particles have little plasticity since the coherence of mass and its yield point are determined by the capillarity of the liquid between particles and the force is inversely proportional to particle size. In some cases, a minimum of 20 percent of particles below 1 μm diameter is said to produce the best working conditions.

Deflocculants

Deflocculants are used to disperse the base material evenly and prevent the material from settling out of solution. In making a slip casting solution of clay with water, sodium, and lithium, salts of weak acids are used. Alkyl ethers are used in the Hexcell Paper Technology as antisettling agents for metal or cermet powders.

Fluxes

Fluxes are added in small amounts to promote the maturing of ceramic bodies at lower firing temperatures. These are usually compounds which form low melting eutectics with the base material. Oxides of alkali and alkali earth metals, for example, form low melting compounds with many oxides.

Lubricants

Lubricants are used to assist in forming and at die faces to prevent sticking. For extrusion of complicated shapes and for pressing of wares, oily lubricants are usually required on the dies. When a dry body is pressed, it may require an internal lubricant. It is essential that the lubricants do not lower the material qualities. They should burn out without charring or fluxing the surface and without leaving holes.

Mixing

Once the proper amounts of constituents have been chosen, intimate mixing of materials is necessary for uniformity of properties within a body and for the reaction of individual constituents during the firing process. For preparing slurries of a fine-grain plastic mass, the usual practice is to use wet mixing, with the raw materials placed together in ball mills. Shearing stresses developed in the mixing process improve the properties of a plastic mix and ensure the uniform distribution of the fine-grain constituent. Use of a filter press or spray drying may be used to dewater the wet mixture for further processing.

Forming

A variety of ceramic forming methods can be adapted for the manufacture of honeycomb shapes. These include processes such as slip casting, pressing, extrusion, paper type technology, tape rolling, and some special techniques. Each of these processes is discussed below with respect to their promise for making honeycomb shapes of uniform and controllable properties as well as their potential for mass production.

Slip Casting

In slip casting, a slip is poured into a mold which is usually made of a porous material to facilitate solvent removal and deposition of the solids. Compaction occurs at the fluid mold interface and a rigid but fragile shape is formed. The formed shape can either be carefully removed from the mold or the mold can be made of a material which can be melted or vaporized out. Assists to the slip casting process have taken the form of applying pressure to the slip, as in pressure casting, or vacuum, as in vacuum casting. Slip casting, in general, is confined to small scale processes. Honeycombs of thin walls and uniform properties are difficult to prepare with this process due to the complexity of the geometry and the difficulty in controlling the rate and amount of solvent removal during casting and subsequent drying.

Pressing

One way of forming a ceramic shape is to compress a dry or slightly damp powder under high pressures to form a dense strong piece. Pressures in the range of 3,000 to 30,000 psi are commonly used. One drawback for a shape with high length-to-diameter ratio is pressure gradients in the axial direction during pressing, which can lead to density variations. For more uniform pressure, a modification of dry pressing is isostatic pressing, in which the sample is placed in a rubber mold inserted in a hydrostatic chamber. Hydrostatic pressure can then be applied uniformly around the sample by the surrounding fluid. The major drawback of pressing in present applications is that it is mainly used for forming simple shapes. It would be extremely difficult to form a complex honeycomb with thin walls with this method. A previous attempt to make a honeycomb monolith indirectly with this method was to press a disc shape and then drill holes through the disc. Only very crude structures can be fabricated with this method.

Extrusion

One of the best methods to make a uniform honeycomb shape with thin walls is to extrude a stiff plastic mix through a die orifice (Reference 3-49). Compaction during extrusion occurs in the extrusion chamber and in the die orifice, at high shear rates and at relatively high forming pressures. The plastic mass is deformed beyond its elastic limit but without fracture. The liquid-to-solid ratio is generally lower than for slip casting, and liquid removal is generally done after the forming process. Modifications to the basic process include the liquid removal step as an integral part of the extrusion process by use of infrared or radio-frequency energy immediately following extrusion. Even finer control of the final product (such as a preferred crystalline orientation) can be incorporated during extrusion. At present, some of the most uniform honeycombs available are made by extrusion. The major drawback is the high cost of the extruder and dies which may wear out quickly when operated improperly or when abrasive mixes are extruded. The extrusion process is mainly suited for mass production and is less desirable for developmental processes where material properties are constantly changed.

Paper Technology

A variety of techniques exist which involve stacking layers of green ceramic sheets together to form a honeycomb shape (Reference 3-50). For example, layers of corrugated and flat sheets can be stacked alternately to form a honeycomb. These green ceramic sheets are made by coating a low ash paper with the desired ceramic material mixed with an organic binder such as a thermoplastic polymer. The thermoplastic binder is preferably one which decomposes on heating without charring. Synthetic polymers such as acrylates, methacrylates, polystyrenes, and materials such as methyl cellulose are illustrative of useful thermoplastic binders. A typical coating composition will include the base ceramic (e.g., alumina), the organic binder (e.g., octadecyl acrylate), a solvent, and other additives to introduce the proper fluidity and viscosity. The coating is then applied on the support (e.g., paper) with the aid of a coating knife and dried. A portion of the sheets is corrugated by passage between hot corrugating rollers. To facilitate bonding between the ridges of corrugations on one side of a corrugated film and a flat sheet on the other, a thin dilute film of the basic coating mix is applied at the point of contact. Once the structure is dried, a temporary bond between the ridges and the sheet member is formed. The bond turns into a strong rigid weld when the structure is fired to sintering temperature. A representative process utilizing paper technology is given in Figure 3-6.

Paper technology is worth considering as an alternative to extrusion methods for making honeycomb shapes. It is adaptable to small scale or even laboratory production and is more amenable to the development of new materials. Thus, thin-walled honeycombs (as low as 0.1 mm) with uniform cell geometry can be formed.

Tape Rolling

Tape rolling processes are very similar to paper technology except that no paper is used as a carrier. The ceramic-polymer mixture is simply extruded as a flat sheet, ribs are then embossed on the sheet and the sheet rolled into a bundle. The typical process, pioneered by W. R. Grace (Reference 3-51) is shown in Figure 3-7. A typical extrusion mix consists of ceramic powders, high molecular weight linear polyethylene, and a plasticizer (e.g., mineral oil). The green form is a thermoplastic product which would slump badly when heated. The key is to remove the plasticizer by solvent extraction (e.g., hexane). With the removal of the plasticizer, the remaining two components -- ceramic and polyethylene -- are still thermoplastic, but the viscosity is so high that no distortion takes place on heating. The polyethylene can then be burned off slowly, and, finally, the product is sintered at high temperatures. Plasticizer removal and polyethylene burnout has to be done under carefully controlled conditions. Tape rolling can also produce thin-walled honeycombs (0.1 mm) of uniform quality and is one of the methods of making honeycombs worth considering, together with extrusion and paper techniques.

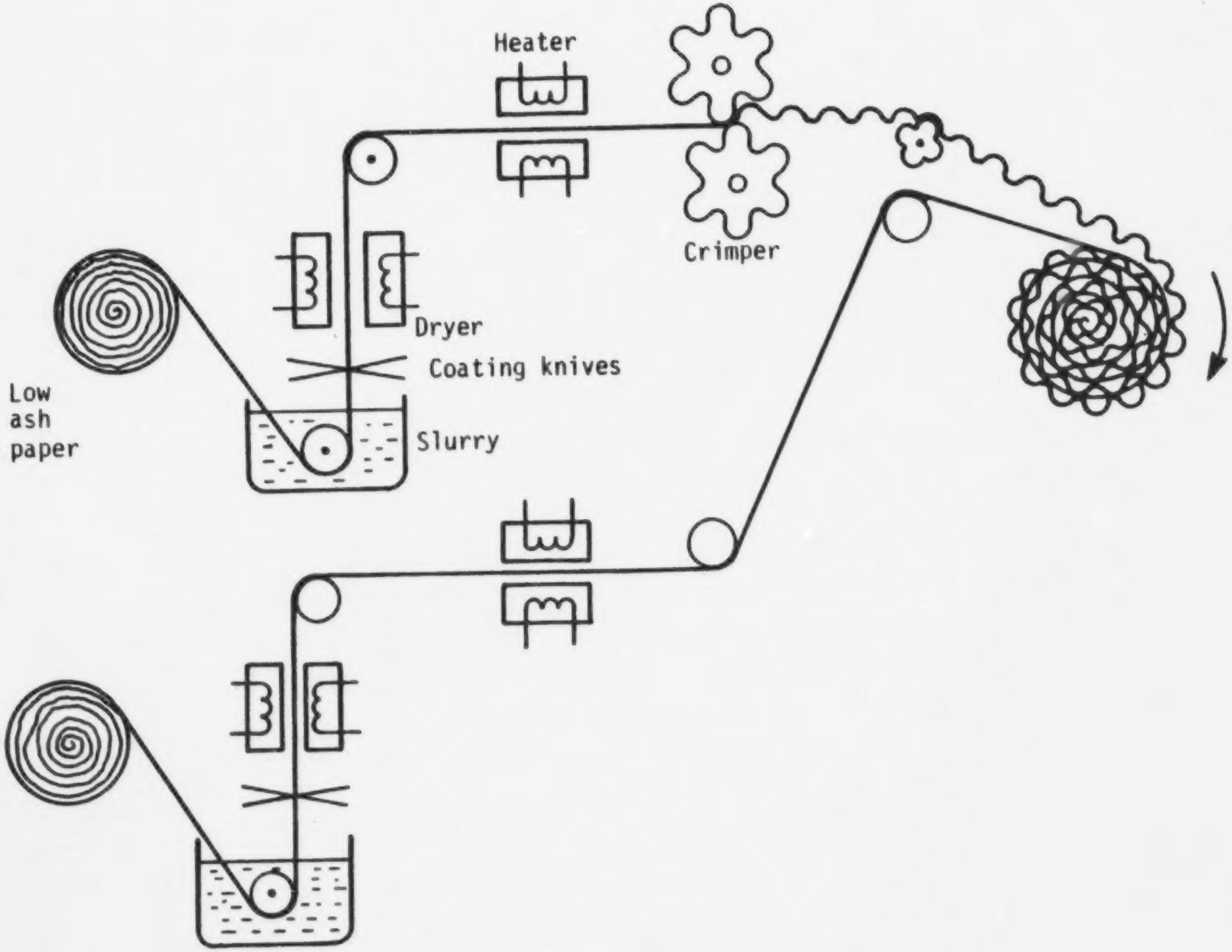
Heater
Crimper
Dryer
Coating knives
Slurry
Low
ash
paper

A264499

Figure 3-6. Paper technology process.

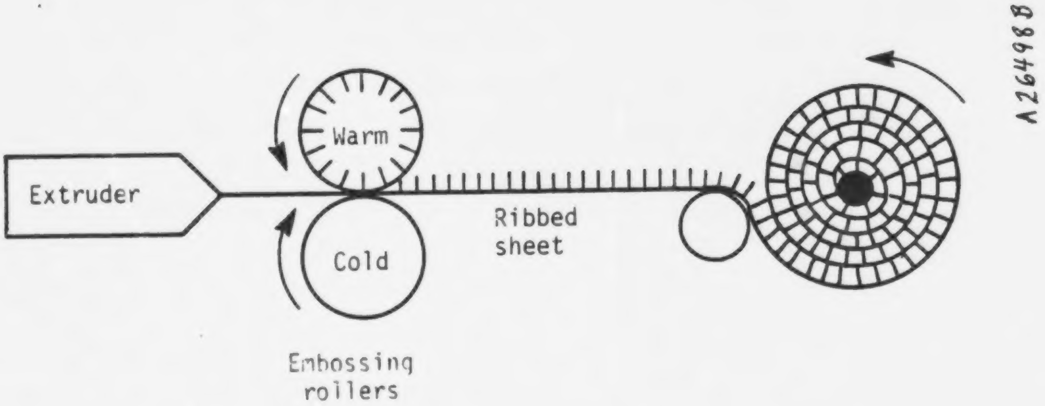
Warm
Extruder
Cold
Ribbed sheet
Embossing rollers
A264988

Figure 3-7. W. R. Grace tape rolling process.

Other Methods

Several other methods are available for making honeycombed structures. They are generally less desirable compared to the ones discussed previously, but are worth considering when special features are required.

One approach is to make a sponge-type structure by impregnating an organic sponge material with a ceramic slurry and then burning off the organic to form a ceramic skeleton (Reference 3-52). The porosity of the resultant sponge material can be adjusted to fit different requirements.

Alternatively, a dense fibrous block can be formed by vacuum casting and then holes drilled through to form a honeycomb structure. The stability of the fibers and high temperature sintering of the fibers may present problems. Formation of sponge or fiber-based structures should be considered as potentially useful approaches to increase thermal stress resistance.

3.1.3 Conclusions and Recommendations

The development of suitable high temperature catalysts for catalytic combustion is a multifaceted problem requiring expertise in catalysis, material properties, fabrication methods, and catalytic combustion. This will require cooperation and close interactions of manufacturers and the catalytic combustion user. Some front end work will be required in research and development, and there should be a smooth transition from laboratory scale to mass production. Preferably, the manufacturer will have research and development capabilities or can work closely with laboratories possessing these capabilities. The catalytic combustion user will be needed to integrate the overall technology, perform testing, and provide continuous feedback to the manufacturers. The first step in high temperature catalyst development is therefore to form a team and work out a cooperative arrangement.

The team must first develop short and long term strategies for a solution. State-of-the-art surveys of high temperature materials and discussions with manufacturers and consultants conducted under this program have provided various possibilities. In the short term, it is unlikely that good active monoliths can be developed due to a lack of data on active materials and a lack of experience in their fabrication. On the other hand, there is a good technology base for making high temperature substrates via traditional fabrication techniques. New materials are being developed for high temperature applications such as heat regenerators/recuperators, turbine components, and other advanced energy processes. Most of these materials are inactive but can be made into honeycomb shapes. There is thus a greater probability for inactive honeycombs with improved thermal shock to be developed in the near term. Since these honeycombs will be inactive, catalyst coating will remain a viable method to produce a catalyst system. This implies that better coating techniques may be needed. For the short term, geometric modifications to modify stress concentrations can also be very effective. For certain cases, there are possibilities for making active monoliths with good thermal shock resistance or for making previously unacceptable materials usable. Active monoliths remain an attractive alternative for long term development, since they eliminate the need for a coating and simplify the problems associated with the use of the coating. Their fabrication, however, will probably require extensive research and development and will be suitable mainly for achieving long range goals.

Simultaneous with the pursuit of solutions to the materials problem, there is a need to develop a logical test plan for rapid determination of material performance. It is apparent from the discussions presented that a lack of reliable materials data has precluded predictions on the performance of promising systems and has made the formulation/fabrication of suitable compositions difficult. The data base needed for catalytic combustion, however, is exceedingly large and complex. The combination of catalytic activity, stability, volatility, thermal expansion, and thermal conductivity properties for the large number of promising materials presents a formidable problem. In addition, other properties such as strength and elastic modulus are needed and are dependent on the microstructure and method of fabrication. In the short term, it is unlikely that sufficient data will be available or can be collected to give an accurate assessment of different materials. In addition to material properties data, an accurate assessment of honeycomb performance requires detailed thermal stress analysis, taking into account geometry and heat transfer effects. Some rapid screening experiments would be useful and necessary to provide a starting point for material selection. A set of logical screening experiments for potential materials should provide a valuable tool in lieu of extensive data collection.

3.1.3.1 Recommended Methods of Approach for Catalyst Development

Substrate Improvement

The traditional method of making thermal stress-resistant structures is to avoid fracture initiation by designing for substrates with high strength and thermal conductivity and low Young's modulus and thermal expansion coefficient. Some of these properties can be controlled by careful choice of composition and consideration of processing and fabrication method. This is an area where ceramic manufacturers have significant experience and background that could lead to improvements in the fabrication of materials considered promising. This is particularly true for materials which have been tested under catalytic combustion and other high temperature environments and have demonstrated encouraging results. In addition, recent emphasis on the development of advanced energy technologies and energy conservation methods have generated much interest in fabrication of high temperature components such as those used for MHD electrodes, heat regenerators and recuperators, and turbine components. New and often proprietary materials are beginning to emerge and their development should be watched closely.

Two high temperature materials under extensive development are silicon carbide and silicon nitride. Both have limited availability in honeycomb structures. The silicon carbide honeycombs tested were either highly dense and difficult to coat with a catalyst or were made from reaction sintered silicon carbide which exuded silica at elevated temperatures (1650K) in an oxidizing environment. Little effort has been devoted to making a silicon carbide honeycomb suitable for catalytic combustion applications such as making the substrate more porous and easier to coat. One problem with silicon carbide is the tendency for the carbide to be oxidized to silicon dioxide which may form low melting eutectics with some of the catalytic oxides. Care should be taken to choose only catalysts which do not flux with the silicon dioxide at the temperature of operation. Rare earth oxides, for example, generally will not form melts with silicon dioxide below 1920K. Addition of extra components will depress these melting points. Silicon nitride has a tendency to undergo oxidation at lower temperatures than silicon carbide. Recent developments have improved the oxidation resistance of the silicon nitride by addition of yttrium oxide, making it suitable for higher use temperatures.

The cermets represent another group of materials that have potential for fabrication into honeycomb shapes. Their high thermal conductivities make them attractive in terms of thermal shock resistance. Their major drawback is their low resistance to oxidation. Chrome-alumina cermet is the most common combination, and most compositions have a use temperature of less than 1500K due to oxidation. A 70% alumina-30% chromium cermet, however, has very good oxidation resistance up to 1780K. The control of proper amounts of each component may optimize oxidation resistance and in some cases be sufficient to satisfy catalytic combustion requirements.

Materials with low coefficients of expansion are worth testing since they would minimize thermal stresses developed from temperature gradients. Cordierite has a very low expansion coefficient but, unfortunately, also has a low use temperature (<1580K) and is unsuitable for high temperature applications. The same low use temperature limits the usefulness of spodumene.

Other low expansion materials are available; two such compositions are $63HfO_2 \cdot 37TiO_2$ and $Al_2O_3 \cdot TiO_2$. Both should have use temperatures above 1920K. Materials with high use temperatures can be highly anisotropic and have very low strengths, which some investigators have attributed to the development of extensive microcracking. If this is the case, the microcracking can be minimized by using very small grains during fabrication. If the strengths of these materials can be sufficiently improved, they should offer promise as thermal stress/shock resistant materials. Developmental work in fabrication will be necessary to optimize the structural properties of such compounds.

In addition to the materials discussed above, improvements to the more traditional ceramic materials (mullite, alumina and zircon) offer some promise for near term applications. This is especially true if modifications can also be made to substrate geometry to minimize stresses.

Geometric Modification

In the short term, modifications to the honeycomb structure to minimize areas of stress concentration, without altering the low pressure drop and high throughput capabilities, appears most promising. This approach is attractive since it makes use of available materials. Materials such as mullite, mullite alumina titanate, and alumina may have improved thermal stress resistance through such modifications. For example, the honeycomb can be subdivided into smaller sections, or a slit can be cut into the honeycomb to relieve radial stresses (Figure 3-5A,B,C). Other subdivisions of the basic honeycomb shape are possible and may be worth investigating depending on application. Alternatively, a honeycomb shape can be fabricated from a fibrous substrate with cylindrical channels (Figure 3-5D). Such a fibrous structure should have excellent resistance to large temperature variations as long as the fibers themselves do not sinter extensively at high temperatures. While a fibrous honeycomb for catalytic combustion has not yet been made, the sponge type substrate may be an alternative to the fibers. Such modifications as fibers and sponges to the basic honeycomb structure may even allow previously unacceptable materials to be used. An active monolith made from most spinels and perovskites of transition metals would have poor thermal shock resistance due to the relatively high thermal expansion coefficients, but making the active materials into fibers or sponges to improve their thermal stress/shock characteristics is possible.

Coating Improvement

In the short term, it is likely that most of the honeycomb supports developed with good thermal stress/shock resistance will be made from nonactive materials. The new materials developed for advanced processes such as heat recuperator/regenerator and turbine components do not have requirements for catalytic activity, although they can readily be adapted to make good honeycomb supports. On the other hand, many of the active materials such as transition metal spinels and perovskites have a limited data base, and a great deal of testing and developmental work will be needed before suitable compositions and processes can be developed. For what is known, their high thermal expansion coefficients make them difficult to form into structures with low thermal stress. It is quite likely that catalyst coating will remain an important method to satisfy catalytic combustion requirements. The many problems experienced with coatings, such as stability and coating-substrate interactions at high temperatures, will have to be addressed and coating materials as well as techniques improved. The problem of volatility may be resolved by using catalytic materials with low vapor pressures at the operating temperatures.

The method of applying the coating may also need development. The two general approaches for applying a coating are the use of slurry of the appropriate catalyst, or the use of a solution impregnation with the proper catalyst precursor, followed by calcining. In using a slurry, there is a need to explore optimal particle sizes of the slurry, slurry viscosity, and additives. The particle size should be small enough to penetrate the surface pores of the substrate and establish an anchor. For very fine pore sizes, solution impregnation with oxide precursors such as nitrates should be used. The nitrate can be converted to the proper oxide upon calcination. Some uncertainty exists as to whether compounds can be formed *in situ* from oxide precursors in all cases, and other methods of applying coatings (such as arc plasma spraying and chemical vapor deposition) should be explored as possibilities.

Active Monolith Development

The development of active monoliths remains an attractive approach since it eliminates the need for coating a substrate and therefore the problems associated with a coating. Unfortunately, there is a general lack of data for materials considered potentially active, making it difficult to predict a priori how a substrate would perform during catalytic combustion. Lack of information on these materials also makes fabrication into honeycomb shapes difficult, since extensive developmental work on mixture preparation, tooling, drying, and forming will have to be undertaken. Some of the compounds derived from ilmenite, spinel, and perovskite structures containing transition metal oxide components have demonstrated promising catalytic activity. These compounds have also shown high thermal expansion coefficients, a property undesirable for minimizing thermal stresses. Not much is known about thermal conductivity, fracture strength, and elastic modulus, these properties being dependent on the method of fabrication and microstructure. For most ceramic materials, however, the thermal conductivity, fracture strength, and elastic modulus have about the same order of magnitude and cannot be varied significantly. It is possible that there may be formulations which are active and have properties that enable them to be fabricated into a stable honeycomb structure by the traditional method of maximizing strength and thermal conductivity and minimizing

Young's modulus and thermal expansion coefficient. If the active substrate formed has poor strength properties, geometric modifications may be possible to reduce areas of stress concentration.

An active honeycomb can also be made by doping a thermally stress-resistant substrate with small amounts of catalyst during fabrication when the dopant does not alter the properties of the substrate significantly. It is also assumed that sufficient catalytic activity can develop with small amounts of catalyst, a result observed in some catalytic systems. A general lack of data precludes accurate predictions of the performance of such systems.

Microcracked Bodies

An alternative way of making thermally stress-resistant structures is to prevent crack propagation. This can be accomplished by the introduction of a network of microcracks and/or crack stoppers which help to dissipate fracture energy more uniformly and increase the work required for fracture. While the microcrack approach has been somewhat successful, good thermal stress/shock resistance remains a highly empirical approach. Variables like crack size and crack density are difficult to measure and control in practice, and extensive developmental work will be required before a microcracked honeycomb can be developed to meet the requirements of catalytic combustion. Corning, for example, has a series of honeycombs made from microcracked bodies (MCB), including yttria-stabilized zirconia, zirconia spinel, and mullite alumina titanate. Of these, the mullite alumina titanate and some of the zirconia spinels have shown promise during testing. The development of microcracked honeycombs by ceramic manufacturers should remain a viable long term possibility for making thermally stress-resistant structures.

Fabrication Techniques

Extrusion and paper/tape rolling techniques are the most promising methods for honeycomb production due to their capabilities for mass production and relative ease of quality control. Paper/tape rolling techniques are especially attractive for the present application since they are adaptable to small scale productions as well and would be ideal for research and development work. Extrusion is desirable if very large scale operation of an established formulation is needed, but for small experimental batch production the tooling is expensive, and excessive die wear is possible.

Other techniques, such as pressing and slip casting, are technically feasible but undesirable since it is relatively difficult to produce a complex honeycomb structure with thin walls using these methods. In cases where structures such as sponges or fibers are needed, existing special methods will be used.

3.2 SUBSTRATE MATERIAL TESTS

As a result of ceramic manufacturer contacts during ceramic development activities, several new ceramic formulations were obtained for testing. Two zircon-nickel perforated tiles were obtained from Hamilton Porcelains Ltd of Brantford, Ontario. In addition, monoliths were received from Coors Porcelain Co., Applied Ceramics, and Kyocera Int. The test results for each of the five materials are described in the following sections.

3.2.1 Hamilton Porcelains Model EPA-084

The Hamilton Porcelains' ceramic was in the form of a perforated tile with a hexagonal array of 2.4 mm holes, approximately 6.4 holes per square cm. Overall dimensions were 4.5 cm by 7.0 cm by 1.3 cm thick. The perforated tile is a pressed, punched, and fired configuration used for gas-fired infrared heaters. This active ceramic composition (experimental) was 75 percent zircon and 25 percent nickel. After firing at Hamilton Porcelains, the tile was removed from the oven at 1256K and plunged into water without fracturing.

Since the tile configuration is meant to be fired at low heat release rates, tests were conducted in the atmospheric facility at heat release rates as low as 1.06 MJ/hr (1000 Btu/hr) as well as rates more typical of other catalysts tested (to 54 MJ/hr). The tile was fired in an upflow configuration and lit off from the downstream face with a propane torch. No air preheat was used in any of the tests. The data are presented in Table A-1.

Four low heat release rate tests were run at 1.06 to 4.22 MJ/hr. The tile was lit off at 170 percent theoretical air where only blue flames could be established, discretely located at each cell opening. As excess air was decreased, the increase in combustion temperature raised the tile temperature until incandescence was achieved at approximately 1200K (1700°F). No downstream flames were visible at this point. This is the typical infrared heater operating condition. Further reduction in excess air resulted in flashback.

Figure 3-8 shows the tile temperature for the 1.79, 2.64, and 4.22 MJ/hr heat release rates. Higher heat release rates allow operation at higher surface temperatures but with an apparently narrower range of stoichiometry at which incandescence could be maintained.

Corresponding NO_x and CO emissions are shown in Figures 3-9 and 3-10. NO_x directly corresponds to surface temperature except during incandescence, when surface reactions are maximized. A dip in the curves of Figure 3-9 results at these conditions. NO_x is generally less than 15 ppm at 40 percent excess air or greater. CO emissions are minimized with increasing temperature except when the tile is incandescent. At that point, a large increase to over 100 ppm occurs in Figure 3-10, apparently due to the lack of burnout in a downstream homogeneous combustion zone. The tile operating temperature

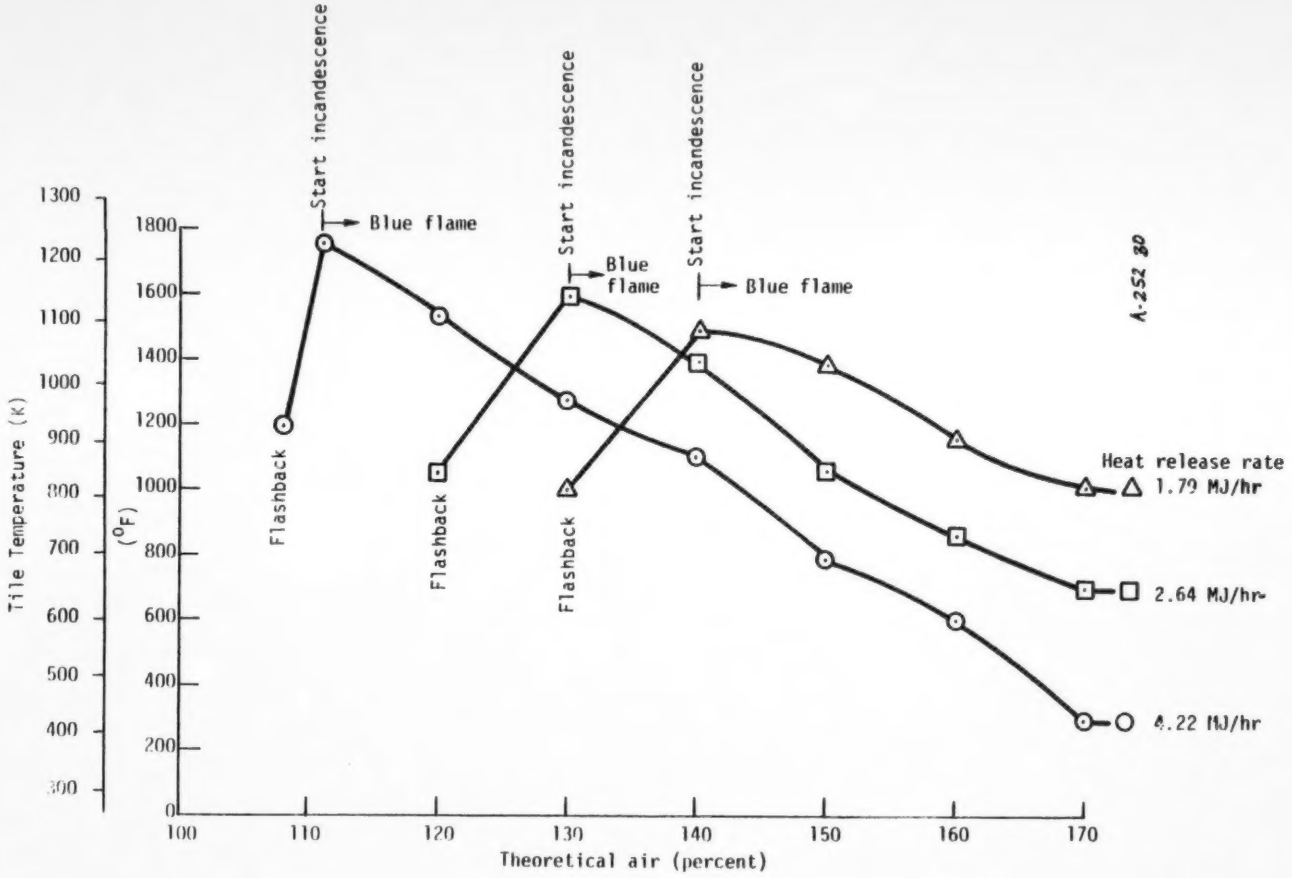

Figure 3-8. Model EPA-084 operating temperature.

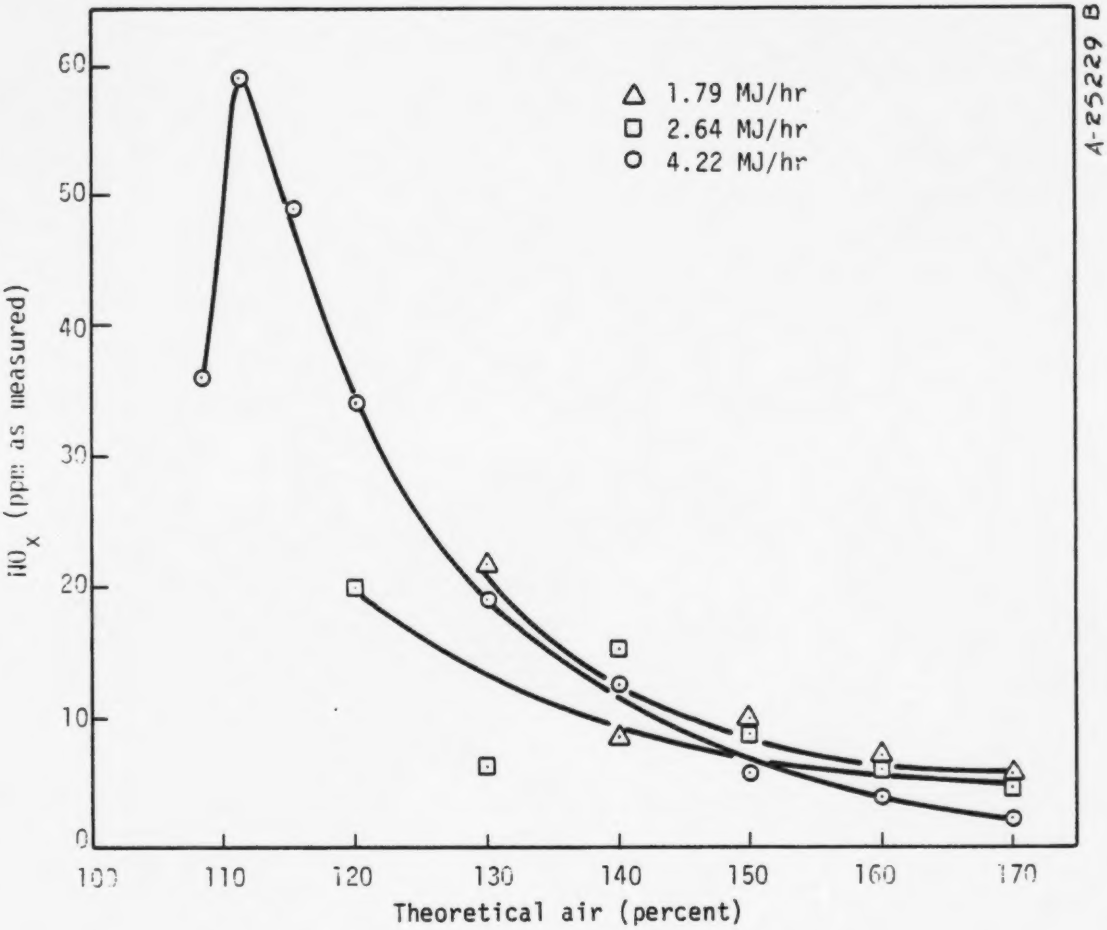

Figure 3-9. Model EPA-084 NO_x emissions.

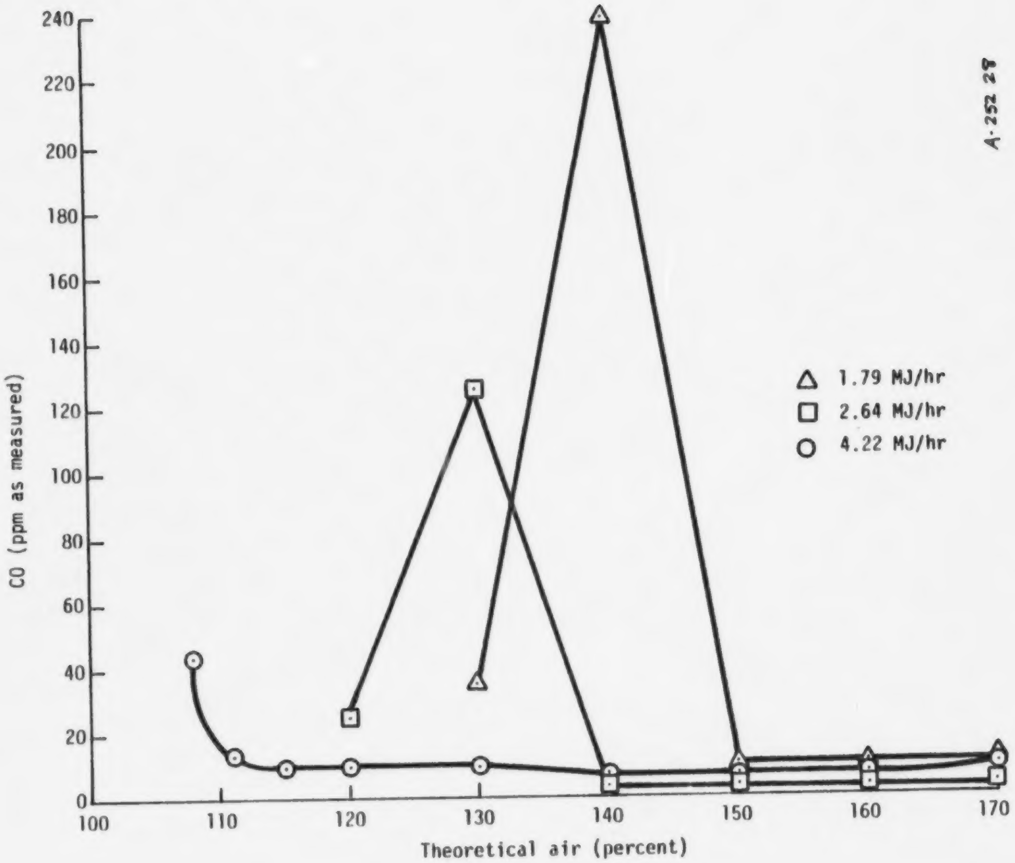

A·252 28

Figure 3-10. Model EPA-084 CO emissions.

and NO_x emissions show great similarity to fiber matrix results when operated at comparable heat release rates per unit flow area. The trend in CO is unique, however. The tile is less applicable to systems than the fiber matrix, however, due to its flat plate configurational constraint.

To further determine the catalytic activity of the tile at conditions closer to other monolithic catalysts tested, the heat release rate was increased to 53.8 MJ/hr (51,000 Btu/hr) in an attempt to reach blowout. Blowout was not achieved at the maximum available flow (29 Kg/hr) with ambient preheat, showing the activity of the nickel ceramic, even at fairly low operating temperature (1506K). Emissions, as shown in Table A-1, were generally low.

After testing, the tile was intact with a few hairline cracks in the upstream flow side. These may have occurred during operation at 1728K (2650°F) or at high throughputs when the tile began to vibrate in its holder. The body was easily broken in two by hand due to these small fractures. A small amount of erosion also appeared to occur near the inlets of the cells (again, probably affected by the high combustion temperatures). The generally high activity and structural strength make the ceramic attractive for further development.

3.2.2 Hamilton Porcelains Model EPA-085

A second Hamilton Porcelains tile contained the same zircon-nickel composition as the first material with the addition of CaO as a stabilizer. The ceramic was somewhat harder, denser, and darker in color than the first composition. Overall tile dimensions were 6.4 cm by 4.1 cm by 1.3 cm thick with a hexagonal array of 2.4 mm diameter holes.

Test results were very similar to those of the first tile (EPA-084). Data are shown in Table A-2. At all of the low heat release rates tested (1.06 to 4.22 MJ/hr), operating temperatures, conditions at flashback,

NO_x emissions, and HC emissions were essentially the same as for EPA-084. Decreases in CO emissions by approximately a factor of two were noted, however. At most of the low heat release conditions, operation was essentially blue-flame combustion, standing off from the ports in the tile.

At the higher heat release rates, the reactions were forced to occur at the tile surface by intensely heating the surface with a torch at light-off. Test results were again similar to those of the earlier model.

Following testing at the 14.8 MJ/hr (14,000 Btu/hr) heat release rate, a temperature excursion to 1783K (2750°F) resulted in localized melting on the upstream face of the tile. The tile had some hairline cracks between cells but was removed from the test holder in one piece. Also, some discoloration of the downstream face occurred, resulting in a color similar to EPA-084 as though the CaO additive was removed at the surface. Inspection of the fracture showed that the discoloration did not occur throughout the material.

A second tile was used for a final test sequence with heat release rates to 47.5 MJ/hr (45,000 Btu/hr). The surface was not blown out (i.e., combustion was not extinguished at the surface) during the test, but testing was terminated when the tile lifted out of the test holder as a result of the flow velocity. This tile also showed discoloration of the downstream face and minor hairline fracturing. The material remained hard and dense, however.

The EPA-085 tile composition appeared to be harder and slightly stronger than the first composition tested (EPA-084). The feasibility of fabrication into monolithic type configurations was subsequently discussed with Hamilton Porcelains. In order to make tiles with a void fraction similar to extruded honeycomb would require new dies with larger pins, and the resultant ceramic could have low thermostructural integrity.

3.2.3 Coors Porcelain Model EPA-086

This experimental monolith was supplied by Coors and cut to a cylinder 6.4 cm in diameter and 7.7 cm long at Acurex. The ceramic material is a proprietary composition and had 1.4 square cells per square cm. The monolith was heated by using the opposed jet to 1367K, 1478K, and 1589K (2000°F, 2200°F, and 2400°F). The 1367K test consisted of five cycles, with the monolith brought to 1367K in 3 to 4 minutes, kept there for about 2 minutes, and then cooled down under air flow. It was lit off again after the temperature had dropped to below 422K (300°F). No fractures were visible after the 1367K tests. When the same heating cycles were carried out at 1478K, fine cracks appeared at the center of the monolith (near the thermocouple) during the second cycle (at 1478K). The size and number of cracks increased during the next three cycles. When the temperature was raised to 1589K, flashback occurred and the opposed jet was shut off. The monolith did not continue combustion reactions at 1589K after shutoff of the opposed jet as some prior substrates had. A representation of the temperature cycles is shown in Figure 3-11, and test condition data are reported in Table A-3.

3.2.4 Applied Ceramics Model EPA-087

This monolith was supplied by Applied Ceramics and cut to 6.4 cm in diameter and 0.97 cm length. The composition of the ceramic material is primarily zirconia; the cell structure is approximately 47 square cells per square cm. The monolith was added to the top of EPA-086 and the heating cycles were repeated as before. The test data are shown in Table A-3. During the first 1367K cycle, the temperature exceeded 1367K due to a gasket leak. The temperature reached 1533K and returned to 1367K after about 1 minute. Fine cracks appeared at the end of this cycle. The gasket leak was repaired and four more cycles were run at 1367K. The monolith fractured into five pieces, and no testing was carried out at higher temperatures. During testing, the color of the monolith changed from flesh colored to a light yellow beige.

3.2.5 Kyocera Model EPA-088

A silicon carbide monolith was supplied by Kyocera International. Its size was 7.6 cm in diameter and 8.9 cm long, and the cell structure was 50 square cells per square cm. The monolith was tested for thermal shock

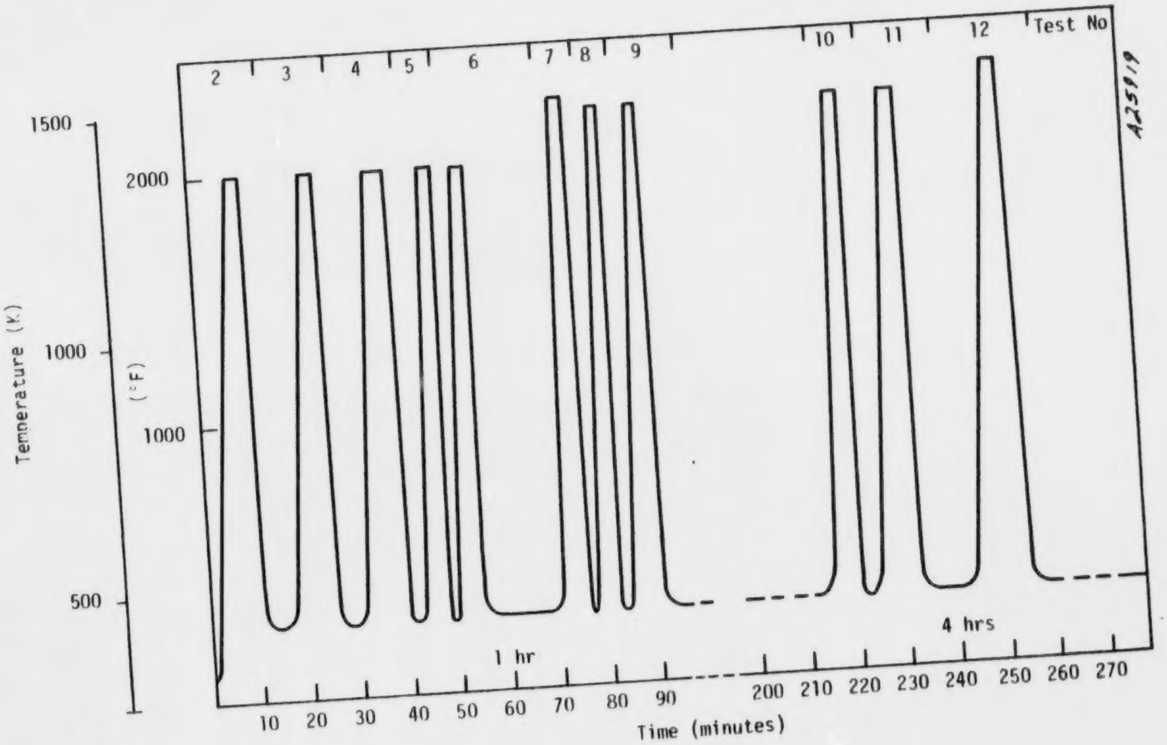

Figure 3-11. Model EPA-086 temperature cycle history.

resistance at 1367K in five cycles using natural gas. During each cycle, the monolith was lit off with the opposed jet and brought to 1367K in about 2 to 3 minutes and kept at this temperature for 1.5 minutes. After cooling under air flow, the monolith was inspected for fractures, and the cycle was repeated. After the first cycle, the monolith showed several fractures across the center of the monolith. Upon removal of the monolith at the end of the fifth cycle, it had split into two pieces. No changes were visible throughout the surface of the fracture.

3.2.6 Summary

Of the five materials tested, the Hamilton Porcelains and Coors Porcelain formulations appeared most durable. The Hamilton Porcelain tiles also showed good catalytic activity as active ceramics. The Hamilton Porcelains composition is deserving of further testing if it could be adapted to a monolithic configuration. Hamilton Porcelains is currently considering the possibility of several fabrication techniques. Since the other compositions in monolith form cracked after only a few cycles at moderate temperatures, they do not appear suitable for further testing with applied catalysts in their current compositions. The Coors ceramic did appear promising, however, and Coors has identified a new formulation expected to have greater strength in monolithic form. The Applied Ceramics and Kyocera monoliths are not considered appropriate for further testing.

3.3 CATALYST DURABILITY TESTS

One monolithic graded cell catalyst system was subjected to 1000 hours of testing to demonstrate catalyst durability. This test was conducted in conjunction with NASA Lewis Research Center Contract No. DEN3-83. Under that contract, materials were developed for a high temperature durable catalyst for use in advanced automotive gas turbine engines (Reference 3-7). Materials were sought that would withstand a 1700K (2600°F) combustion environment in excess of 1000 hours. The discussion that follows summarizes the development of the catalyst materials and the experimental results of the 1000 hour durability test.

The catalyst configuration was chosen following oven and combustion screening tests conducted under Contract DEN3-83. No. 2 diesel was used as the test fuel, and eight graded cell reactors were tested. Results of these eight screening tests are given in detail in Reference 3-7. At the conclusion, it was obvious that none of the eight reactors performed with a high degree of catalytic activity. Only three reactors were able to sustain combustion at all; the terbium-cerium-thorium (TCT) formulation on proprietary (JNM) substrate apparently gave the best performance. This judgement was based on reactor temperature and emission measurements as well as physical appearance. The structural performance of JNM substrate was at least as good as that of all the eight reactors tested. The substrate damage was probably due to overheating during lightoff instabilities rather than a steady state loss of strength. Based on the above considerations, the JNM/TCT reactor was selected for durability life testing.

The test reactor was assembled from four segments to give overall dimensions of 5.1 cm in diameter by 2.5 cm in length. The configuration was a modified graded cell arrangement beginning with an entrance segment of a UOP proprietary noble metal on a Corning MCB-1 medium cell substrate. The following three segments were graded (from large to small cell) proprietary mullite honeycomb substrates. These segments were coated at Acurex with a formulation of oxides of terbium, cerium, and thorium. This terbium, cerium, thorium (TCT) catalyst formulation is relatively low in activity, but had shown potential for sustaining its activity level for long periods at the required test temperature of 1700K. The noble metal entrance segment is much higher in activity and was chosen to improve lightoff and low temperature performance. Surface temperature of the entrance segment was held below the adiabatic flame temperature by radiative and convective heat transfer. The bulk reactant mixture is effectively preheated by the entrance segment, allowing the TCT portion of the reactor to complete the fuel burnout.

The durability test was conducted at the nominal conditions of:

- Preheat → 717K to 744K (830°F to 880°F)
- Pressure → 1×10^5 Pa (1 atmosphere)
- Face velocity → 13.4 m/s (44 ft/s) (actual)
- Stoichiometry → 230 percent theoretical air
- Fuel → propane (C_3H_8)

The durability test was completed with a total of 1012.5 hours of combustion operation logged. The testing consisted of 1001.6 hours of steady state operation at the above conditions. Seven parametric test sequences were also performed during the 1001.6 hours of operation. This was followed by additional testing which included five on/off cyclic tests, a final parametric test, and a short period of operation on diesel fuel. Figure 3-12 gives a chronology of events including six shutdowns that occurred.

The emissions performance of the reactor during the life test is given in Figures 3-13 and 3-14. The plots show only a fraction of the total amount of data, as measurements were recorded approximately every 2 hours. Figure 3-13 shows that the O_2 and CO_2 levels remained fairly level throughout the test, indicating the steady state operation. The parametric tests appear as points of reduced CO_2 and increased O_2 as the fuel/air ratio was decreased. The drift in oxygen level was probably due to a malfunctioning O_2 analyzer which ultimately failed at about 890 hours. A comparison of CO_2, CO, and UHC levels with input fuel flow results in a carbon balance of within 5 to 8 percent for most of the data. The average carbon monoxide concentration in the exhaust sample apparently increased slightly throughout the test, as indicated in Figure 3-14. This was probably due to slow catalyst deactivation. The unburned hydrocarbon measurements appear to be instrument noise. UHC concentrations remained essentially zero during steady state operation. Figure 3-14 does not show the effects of parametric testing.

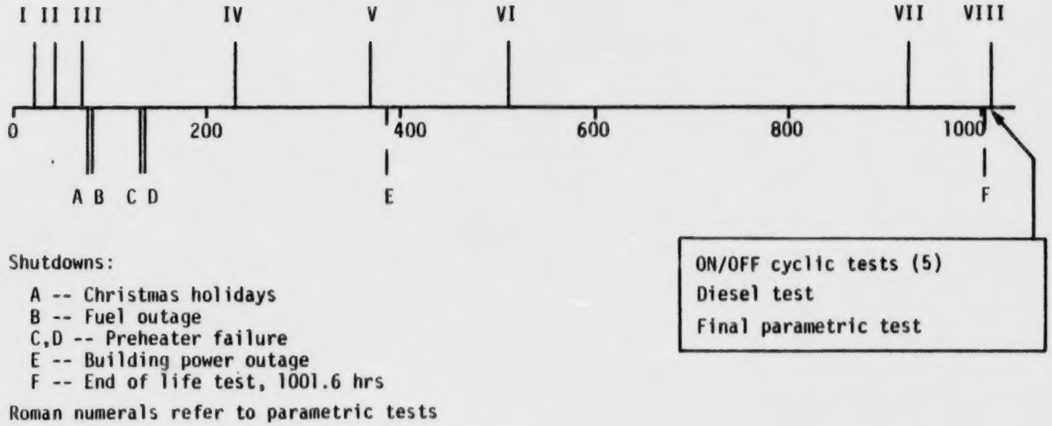

Figure 3-12. Durability test event chart.

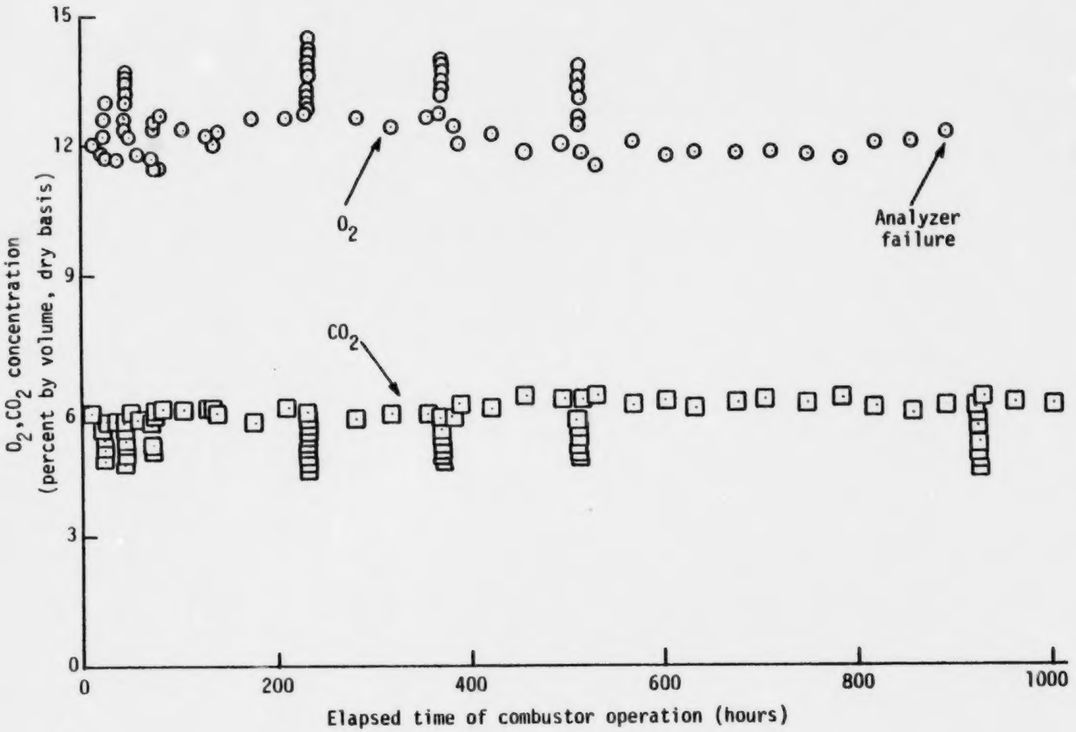

Figure 3-13. Durability test O_2 and CO_2 emissions levels.

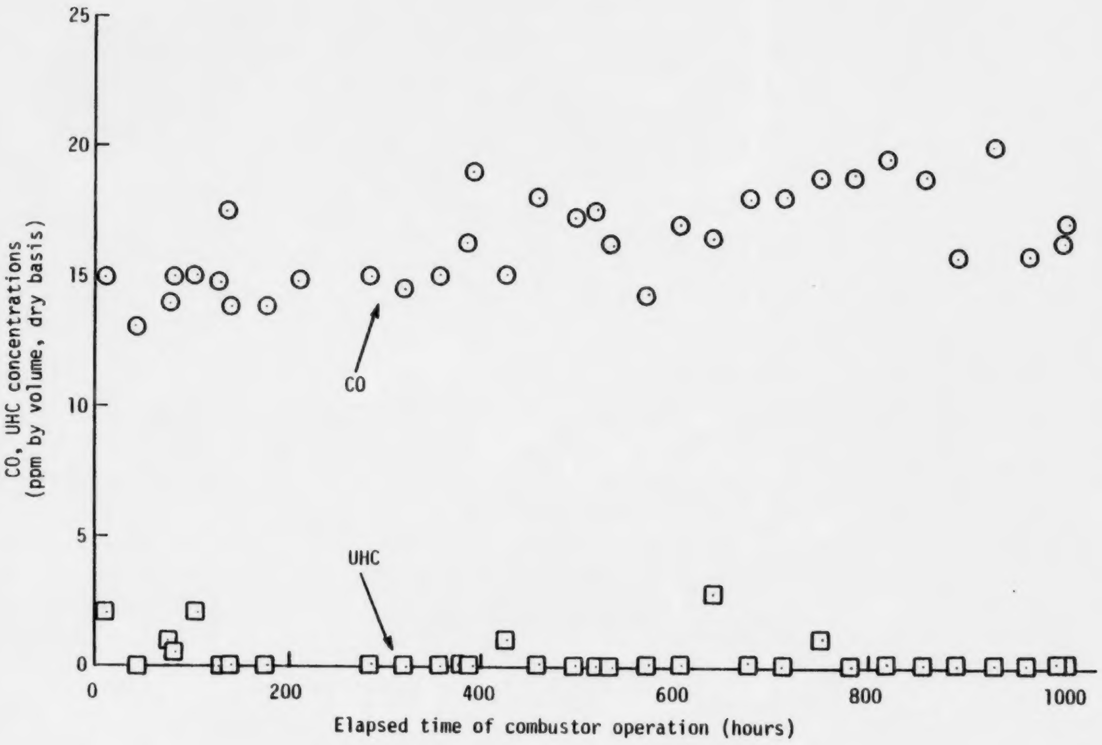

Figure 3-14. Durability test CO and UHC emissions levels.

In spite of the slight carbon monoxide increase, Figure 3-15 shows that the calculated combustion efficiency remained high throughout the test. The only major influence on combustion efficiency was the parametric tests.

NO_x emission levels are not shown since a malfunctioning chemiluminescent analyzer did not allow successive measurements. The instrument was functional at the test beginning, and concentrations of from 1 to 3 ppm were recorded. A temporary repair at 740 hours gave a measurement of 4 ppm. The analyzer was fully operational prior to the on/off cyclic tests and measured levels ranged from 2 to 5.4 ppm.

Eight parametric tests were conducted in which the fuel/air ratio was progressively decreased until an increase in carbon monoxide or unburned hydrocarbons was detected. The point at which combustion degradation occurs is representative of the level of catalyst activity. With all other parameters constant, a comparison of minimum fuel/air ratio or minimum catalyst temperature achieved from test to test indicates changes in catalyst activity. A representative plot of combustion efficiency versus catalyst temperature is shown in Figure 3-16. This test was conducted after 45 hours of operation and shows a rapid decline in combustion efficiency below a catalyst temperature of 1297K (1875°F).

Following the durability test, the reactor was removed for visual inspection and photographs. The surface appeared much lighter in color, indicating a probable loss of catalyst coating. Structurally, the monolith had distorted slightly and fused to the refractory holder, but major cracks, loss of substrate, or other damage had not occurred.

The catalyst was reinstalled for the on/off cyclic tests which resulted in the performance plot of Figure 3-17. Prior to each lightoff of the catalyst, the bed temperature was brought to about 756K (900°F) by passing preheated air over the reactor for about 1 hour. The first lightoff was performed with the opposed jet igniter while the subsequent four lightoffs

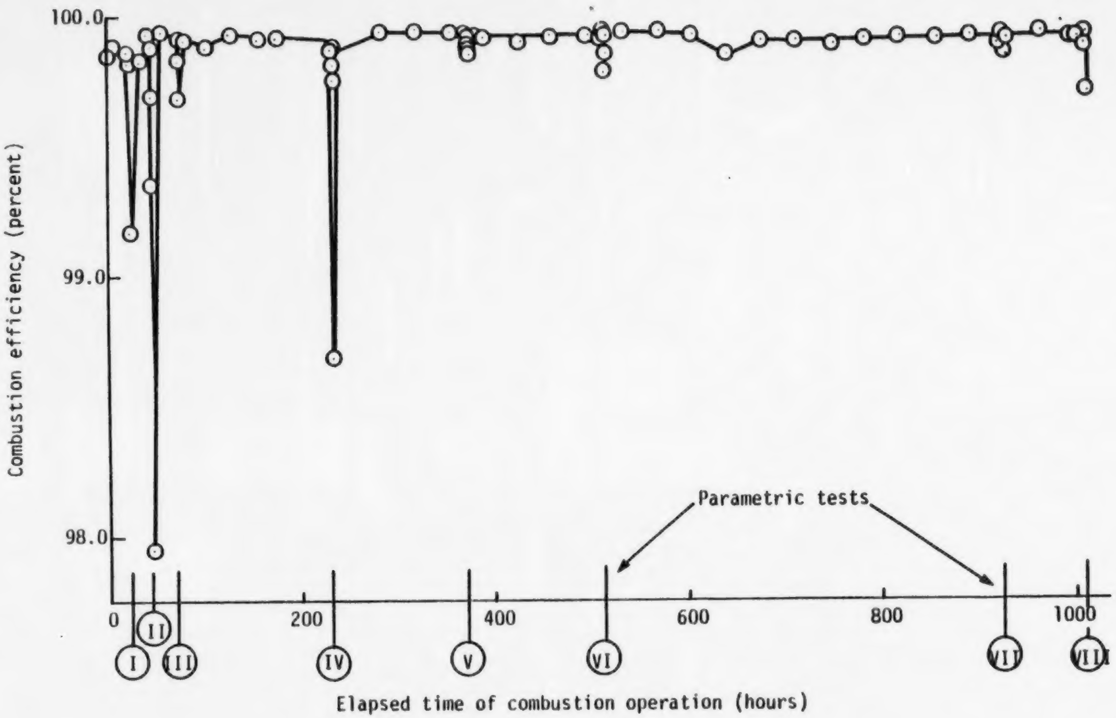

Figure 3-15. Durability test combustion efficiency performance.

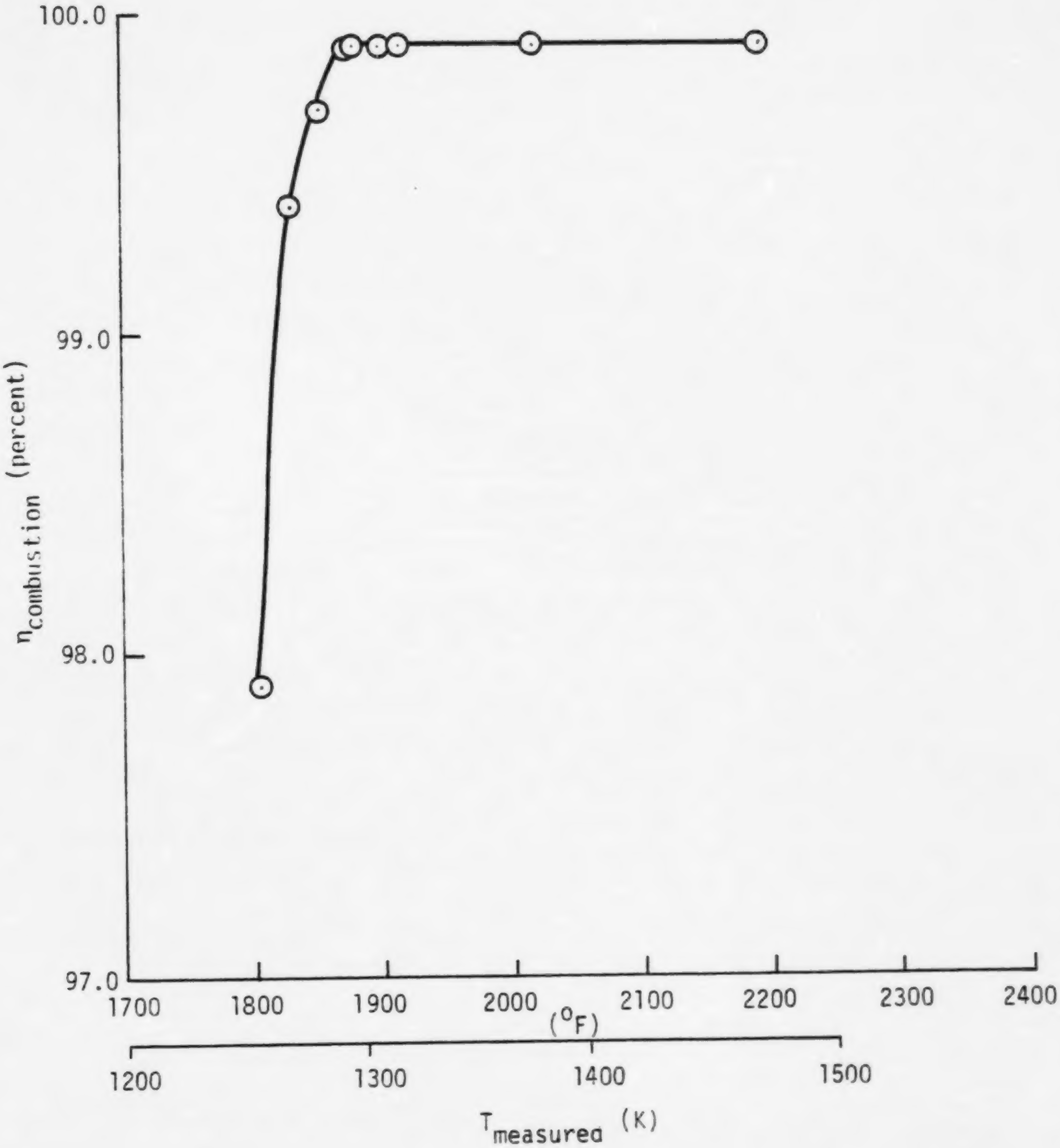

Figure 3-16. Parametric study -- effects on combustion efficiency.

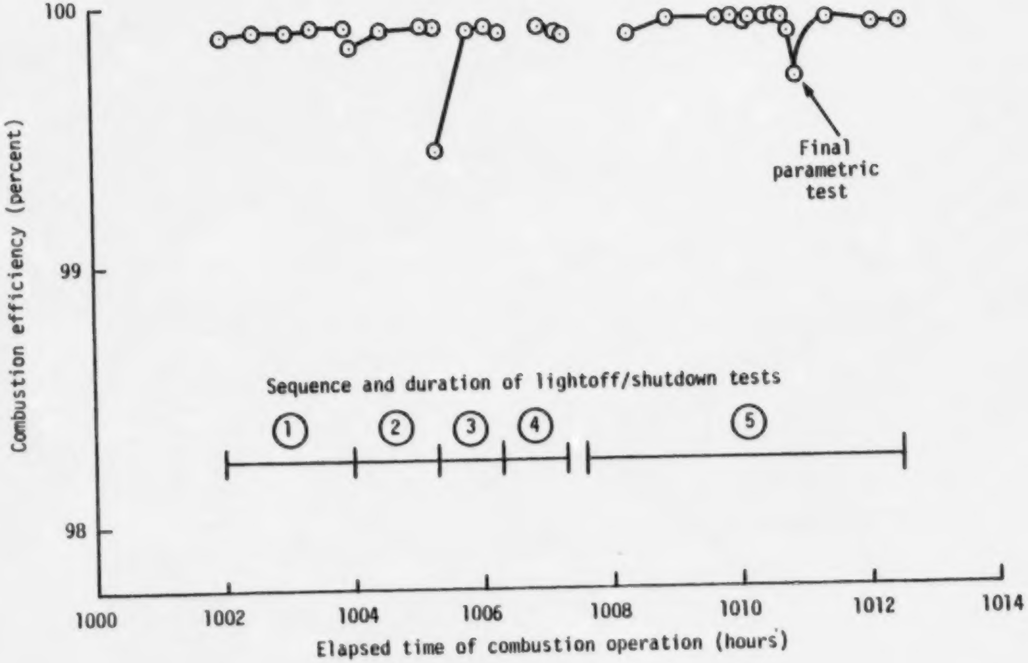

Figure 3-17. Thermal cycling performance.

were catalytic. Following each lightoff, temperature and emissions data were collected over a 1 to 2 hour period before shutdown. The reactor was allowed to cool for several hours following shutdown before the next lightoff. During the last cycle, a final parametric test was conducted to note any further changes in activity. Before the final shutdown, an attempt was made to switch to diesel fuel. The attempt was successful; however, the catalyst became inactive within about 8 minutes. The reason for this behavior appeared to be fuel preparation problems. Following the diesel test, the catalyst was returned to the previous condition, again on propane. A final inspection of the disassembled reactor revealed no further damage or change from the cyclic tests.

The results of the durability test were very successful in showing the long life capabilities of catalyst activities and materials. The TCT catalyst formulation currently appears to be the best available for monolithic catalysts operating at temperatures near 1700K, as would be required in advanced gas turbine systems.

REFERENCES FOR SECTION 3

3-1. Kesselring, J. P., et al., "Design Criteria for Stationary Source Catalytic Combustion Systems," EPA-600/7-79-181, NTIS-PB80-147317, August 1979.

3-2. Kesselring, J. P., Compiler, "Proceedings 4th Workshop on Catalytic Combustion," EPA-600/9-80-035, NTIS-PB81-176067, August 1980.

3-3. Kesselring, J. P., Compiler, "Proceedings: Fifth Workshop on Catalytic Combustion (San Antonio, TX, September 1981)," EPA-600/9-84-002, NTIS-PB84-145580, January 1984.

3-4. Alcock, C. B. and Hooper, G. W., "Thermodynamics of the Gaseous Oxides of the Platinum Group Metals," Proc. Roy. Soc., A254:551, 1960.

3-5. Hindin, S. G. and Pond, G. R., "Method for the Combustion of Carbonaceous Fuels Utilizing High Temperature Stable Catalysts," U.S. Patent 4,088,435, May 1978.

3-6. Heck, R. M., et al., "Durability Testing at One Atmosphere of Advanced Catalysts and Catalyst Supports for Automotive Gas Turbine Engine Combustors," NASA CR-135132, June 1977.

3-7. Tong, H., et al., "Development of High Temperature Durable Catalyst for Use in Catalytic Combustors for Advanced Automotive Gas Turbine Engines," NASA CR-165396, June 1981.

3-8. Lauder, A., "Stable Perovskite Catalysts," U.S. Patent 4,126,580, November 1978.

3-9. Chemical and Process Technology Encyclopedia. D. M. Considine, Editor-in-Chief, pp. 222, McGraw Hill Book Co., New York, 1974.

3-10. Stone, F. S., "The Significance for Oxide Catalysis of Electronic Properties and Structures," J. Solid State Chemistry, 12: 271, 1975.

3-11. Voorhoeve, R. J. H., Remeika, J. P., and Trimble, L. E., "Defect Chemistry and Catalysis in Oxidation and Reduction over Perovskite-Type Oxides," Annals of the N.Y. Academy of Sciences, 272: 3, 1976.

3-12. Cimino, A. and Indovina, V., J. Catalysis, 17: 54, 1970.

3-13. Ackerman, R. J. and Thorne, R. J., "Vaporization of Oxides," in Progress in Ceramic Science, Vol. 1, J. E. Burke, Editor, Pergamon Press, New York, 1961.

3-14. Caplan, D. and Cohen, H., "The Volatilization of Chromium Oxide," J. Electrochemical Soc., 108: 438, 1961.

3-15. Alcock, C. B. and Hooper, G. W., "Thermodynamics of the Gaseous Oxides of the Platinum-Group Metals," Proc. Roy. Soc., A254: 551, 1960.

3-16. Handbook of Materials and Techniques for Vacuum Devices, by W. H. Kohl, Reinhold Publishing Corporation, New York, 1967.

3-17. Open Cycle Coal Fired MHD: High Temperature Materials, Inorganic Materials Division, National Bureau of Standards, Quarterly Progress Report supported by ERDA-Fossil Energy, Contract No. E(49-13)-1230, March 1975.

3-18. Kingery, W. D., Bowen, H. K., and Uhlmann, D. R., Introduction to Ceramics, John Wiley and Sons, Inc., New York, 1976.

3-19. Levin, Ernest, et al., Phase Diagrams for Ceramists, compiled at the National Bureau of Standards, the American Ceramic Society, 1969.

3-20. Johnson, Jr., D. W., et al., "The Nature and Effects of Platinum in Perovskite Catalysts," J. Catalysis, 48: 87, 1977.

3-21. Welty, J. R., Wicks, C. E., and Wilson, R. E., "Unsteady State Conduction Charts," Fundamentals of Momentum, Heat and Mass Transfer, John Wiley, & Sons, New York, 1976. p. 303.

3-22. Holman, J. P., Heat Transfer, 4th Edition, McGraw Hill Book Company, New York, 1976, p. 112.

3-23. Coble, R. L. and Kingery, W. D., "Effect of Porosity on Thermal Stress Fracture," J. American Ceramic Society, 38: 33, 1955.

3-24. Hasselman, D. P. H., "Elastic Energy at Fracture and Surface Energy as a Design Criteria for Thermal Shock," J. American Ceramic Society, 46: 535, 1963.

3-25. Hasselman, D. P. H., "Unified Theory of Thermal Shock Fracture Initiation and Crack Propagation in Brittle Ceramics," J. American Ceramic Society, 52: 600, 1969.

3-26. Nakayama, J. and Ishizuka, M., "Experimental Evidence for Thermal Shock Damage Resistance," American Ceramic Society Bulletin 45: 666, 1966.

3-27. Tennery, V. J., "Thermal Shock Analysis of Ceramic Multi-Hundred Watt Spheres," MLM-2104, March 1974.

3-28. Kingery, W. D., Bowen, H. K., and Uhlmann, D. R., Introduction to Ceramics, 2nd Edition, Chapter 16, John Wiley and Sons, New York, 1976.

3-29. Kohl, W. H., Handbook of Materials and Techniques for Vacuum Devices, Reinhold Publishing Corp., New York, 1976.

3-30. Huminek, Jr., J., High Temperature Inorganic Coatings, Reinhold Publishing Corp., New York, 1963.

3-31. Kesselring, J. P., et al., "Catalytic Component and System Prototype Development," Acurex Draft Annual Report TR-79-38/EE under EPA Contract No. 68-02-3122, October 1979.

3-32. Kraft, E. H. and Copolla, J. A., "Thermo-Mechanical Properties of Sintered Alpha Silicon Carbide," Presented at 5th Army Materials Technology Conference, Ceramics for High Performance Applications -- II, Newport, Rhode Island, 1977.

3-33. Smith, J. T., "GTE Si_3N_4-Based Ceramics," Presented at Highway Vehicles Systems, Contractor's Coordination Meeting, April 1979, Dearborn, Michigan, April 1979.

3-34. "Ceramics Technology Readiness Development Program," Westinghouse Electric Corporation, FE-2786-38, developed under DOE Contract No. EF-77-COL-2786, November 1979.

3-35. Holcombe, C. E., et al., "Survey Study of Low Expanding, High Melting, Mixed Oxides," Oak Ridge Y-12 Plant, Report Y-1913, prepared for the U.S. Atomic Energy Commission, Contract W-7405, Eng. 26, February 1974.

3-36. Skaggs, S. R., "Zero and Low Coefficient of Thermal Expansion Polycrystalline Oxides," Los Alamos Scientific Laboratory, Report LA-6918-MS, prepared for ERDA, Contract W-7405, Eng. 36, September 1977.

3-37. Pentecost, J. L. and Cochran, J. K., "Low Expansion Ceramic Material for Catalytic Supports, "SAE publication No. 740198, February 1974.

3-38. Henry, J. L. and Thompson, G. G., "Thermal Expansion Match Between Molybdenum (TZM Alloy) and Aoxides of the Perovskite and Spinel Types," Ceramic Bulletin, 55: 282, 1976.

3-39. Donald, I. W. and McMillan, P. W., "Review Ceramic-Matrix Composites," J. Materials Sc., 11: 949, 1976.

3-40. Homeny, J. and Bradt, R. C., "Thermal Shock of Refractories," Paper Presented at Conference on Thermal Stresses in Materials and Structures in Severe Thermal Environments, VPI, Blacksburg, Virginia, March 1980.

3-41. Hockman, L. E., "Engineering Steel Film Reinforced Refractories," Presented at Annual Meeting, American Ceramic Society, May 1977.

3-42. Hasselman, D. P. H. and Singh, J. P., "Analysis of Thermal Stress Resistance of Microcracked Brittle Ceramics," Am. Ceram. Soc. Bulletin 58: 856, 1979.

3-43. Rossi, R. C., "Thermal Expansion of BeO-SiC Composites, J. Am. Ceram. Soc., 52: 290, 1969.

3-44. Claussen, N., Steel, J., and Pabst, R. F., "Effect of Induced Microcracking on the Fracture Toughness of Ceramics," Am. Ceram. Soc. Bulletin, 56: 559, 1977.

3-45. Hasselman, D. P. H., Becker, P. F., and Mazdiyasui, K. S., "Analysis of the Resistance of High-E, Low-E Brittle Composites to Failure by Thermal Shock," Z. Werkstofftech 11: 82, 1980.

3-46. Rossi, R. C., "Thermal Shock Resistant Ceramic Composites," Am. Ceram. So. Bulletin, 48: 736, 1969.

3-47. Kirchner, H. P. and Graver, R. M., "Chemical Strengthening of Polycrystalline Ceramics," J. Am. Ceram. Soc., 49: 330, 1966.

3-48. Pincus, A. G., "Critical Compilation of Ceramic Forming Methods," AF Contract No. 33(657)-10574, Report No. MT-63-12, September 1963.

3-49. Bagley, R. D., "Extrusion Method for Forming Thin Walled Honeycomb Structures," Corning Glass Works, U.S. Patent 3,790,654, February 1974.

3-50. Stack, T. N., "Corrugated Heat Transfer Exchangers," 3-M Company, U.S. Patent 3,198,248, Agusut 1965.

3-51. Dundsager, C. B., Turner, G. J., and Pentecost, J. L., "Thermoplastic Process for Catalyst Substrates," SAE Publication No. 760311, Detroit, Michigan, February 1976.

3-52. Clyde, R. A., "Supported Catalyst," U.S. Patent 3,998,758, December 1976.

SECTION 4

FUNDAMENTAL STUDIES

Following the early fundamental experimental work reported in Reference 4-1, additional studies were conducted under the catalytic combustion fundamentals task. This work focused on obtaining accurate surface kinetics data. Good heterogeneous chemical kinetics data are of prime importance in optimizing a catalytic combustion system design for fuel ignition and stable operation, high throughput characteristics, and compactness. Limited additional data were also collected under fuel NO_x studies on a platinum catalyst.

4.1 EXPERIMENTAL SETUP

The basic experimental facility and procedures have been described in detail in Reference 4-2. Reviewing briefly, combinations of one, two, or three cylinders of a given diameter were mounted in parallel within flow ducts of various cross sections. The cylinders were oriented in a plane normal to the flow duct axis. Figure 4-1 shows a plan view schematic of the two most commonly used configurations. The degree of flow blockage was designed to yield about 5 percent fuel conversion through sub-stoichiometric heterogeneous combustion. Mixing of the surface combustion products with the remaining unreacted flow occurred downstream of the cylinder surfaces. The objective was not to achieve complete combustion of the fuel, but rather to study the process by reacting a small portion of the flow. At this condition, gas phase ignition and homogeneous combustion were suppressed, yet sufficient product concentrations were available for accurate measurement.

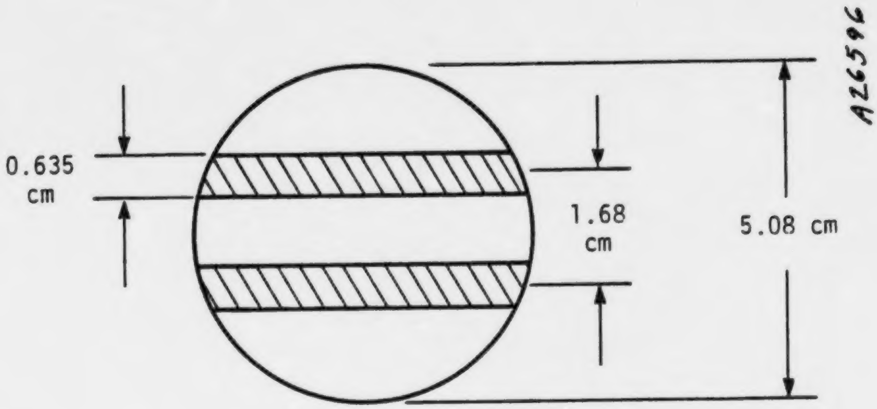
0.635 cm
1.68 cm
5.08 cm
A26596

1a. Large double cylinder configuration

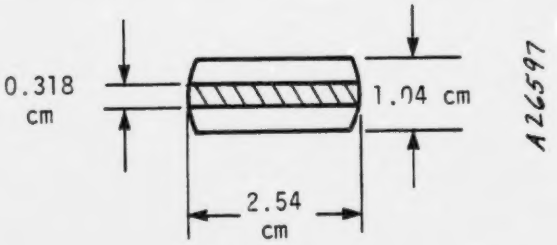
0.318 cm
1.04 cm
2.54 cm
A26597

1b. Small diameter single cylinder in approximately rectangular cross section duct

Figure 4-1. Common test configurations (flow direction normal to plane of page).

The alumina cylinders were obtained from Coors Porcelain Company in two diameters, 3.18×10^{-3}m and 6.35×10^{-3}m, and measured 5.08×10^{-2}m in length. Oxy-Catalyst, Inc. applied the γ-alumina washcoat, and platinum catalyst coatings of nominally 0.45 percent of cylinder weight were done at Acurex. The platinum loading was obtained by brushing an aqueous solution of chloroplatinic acid (H_2PtCl_6), fixing with hydrogen sulfide, and calcining at approximately 673K for 3 hours. The resulting catalyst surface was considered to be more representative of a prototype catalytic combustor than pure platinum filaments used in other studies (e.g., References 4-3 and 4-4). To allow for washcoat sintering prior to experimental data collection, the cylinders were held at approximately 1310K for 1 hour by fuel-lean surface combustion.

Sampling of major product species was done with a water cooled, low pressure (approximately 37.3 kPa), traversing probe downstream of the cylinders. Flow temperatures were measured with upstream and downstream thermocouples while surface temperatures were obtained by locating thermocouples within the hollow cylinders. Data were collected on methane (CH_4) and propane (C_3H_8) fuels with air as the oxidizer. Methane alone was used in screening and reaction characterization studies while kinetics data were obtained on both fuels.

4.2 REACTION CHARACTERIZATION

An early objective in the experimentation was to confirm the operational characterization of the cylinder in crossflow catalyst configuration. Another goal was to identify whether the dominant product from heterogeneous combustion of methane was carbon monoxide or carbon dioxide. This would identify the global oxidation mechanism for methane at a catalyst active site as either $CH_4 \rightarrow CO$ or $CH_4 \rightarrow CO_2$. Under fuel-lean steady state operation, reactants diffuse to the catalyst and react at active sites on and within the surface. The reaction rate increases with surface temperature until it is faster than the maximum inward diffusion rate of the lean reactant. Thus, mass transfer limitations begin to control the conversion rate of methane at about 1000K and of propane at about 625K. Under this diffusionally controlled heterogeneous process, the conversion of reactants to products occurs primarily at the surface, providing the freestream mixture remains below ignition temperatures.

The results of sample probe traverses dowhstream of the cylinder in crossflow configuration are discussed in References 4-1 and 4-2. The nominal test conditions for the reaction characterization studies consisted of a test section flow velocity of 6 m/s, reactant preheat temperature of 644K, and methane-air equivalence ratios ranging from fuel-rich at $\phi_{FA} = 1.25$ to fuel-lean at $\phi_{FA} = 0.67$.

Figure 4-2 reviews the results of one condition in which three 3.18 mm diameter cylinders were mounted within a test duct of 50.8 mm circular cross section. All gas phase concentration measurements presented here are on a dry volume basis. A considerable variation in gas phase concentrations was evident. For example, the profiles of CO and CO_2 measurements were very cyclical and indicated a clear definition between surface combustion products (sampled directly behind each cylinder) and the unreacted freestream. At measurement points located farther downstream, these sharp divisions became less pronounced as a result of cross-stream mixing.

The total amount of fuel conversion remained constant with distance, indicating that significant homogeneous processes were essentially absent and fuel was being consumed primarily at the catalytic surfaces. This behavior is confirmed in Figure 4-3 which shows enhanced unburned hydrocarbon (UHC) levels and decreasing concentrations of product species (CO and CO_2) with increasing downstream distance directly behind a catalyst cylinder. The most distant measurement points show that the CO and CO_2 concentrations are significantly diluted from the levels found immediately adjacent to the catalyst surface. The UHC levels are due to the unreacted methane in the freestream flow.

The data can also be studied with regard to relative amounts of CO and CO_2, shown plotted as a function of methane-air equivalence ratio in Figure 4-4. The ratio is small throughout the range of fuel-lean mixtures, indicating CO_2 to

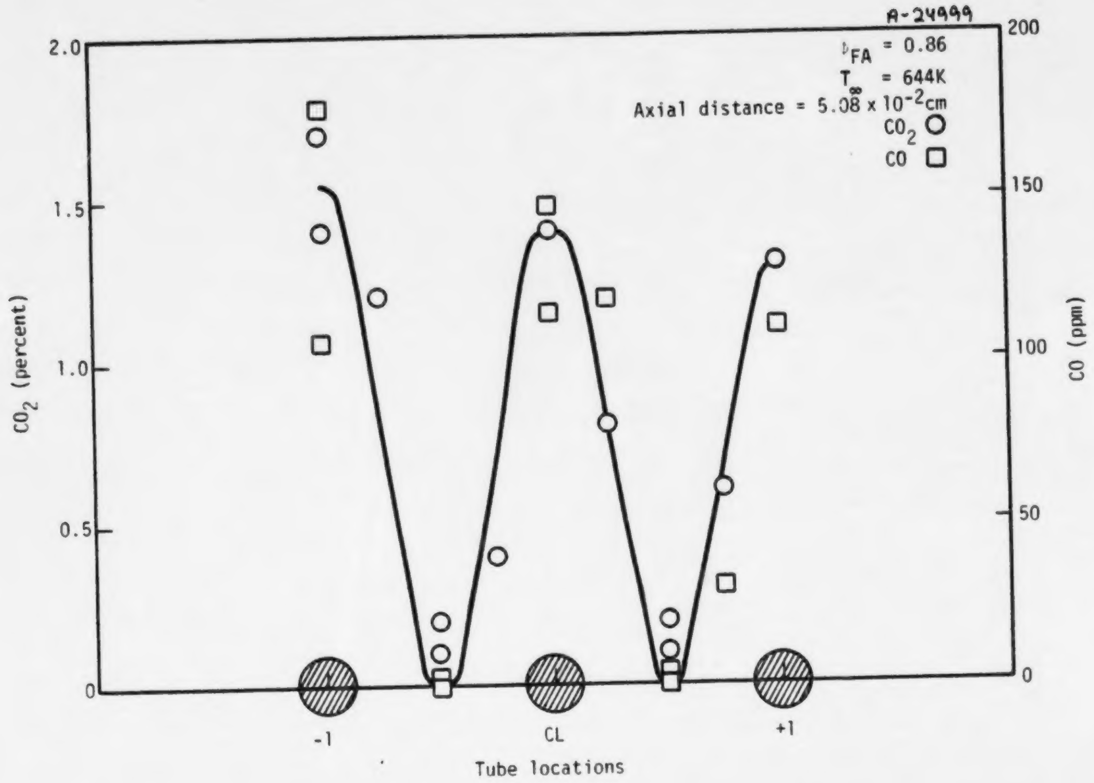

Figure 4-2. Radial distribution of CO_2 and CO concentrations at 5.08 x 10^{-2} cm for 3.18 mm tubes.

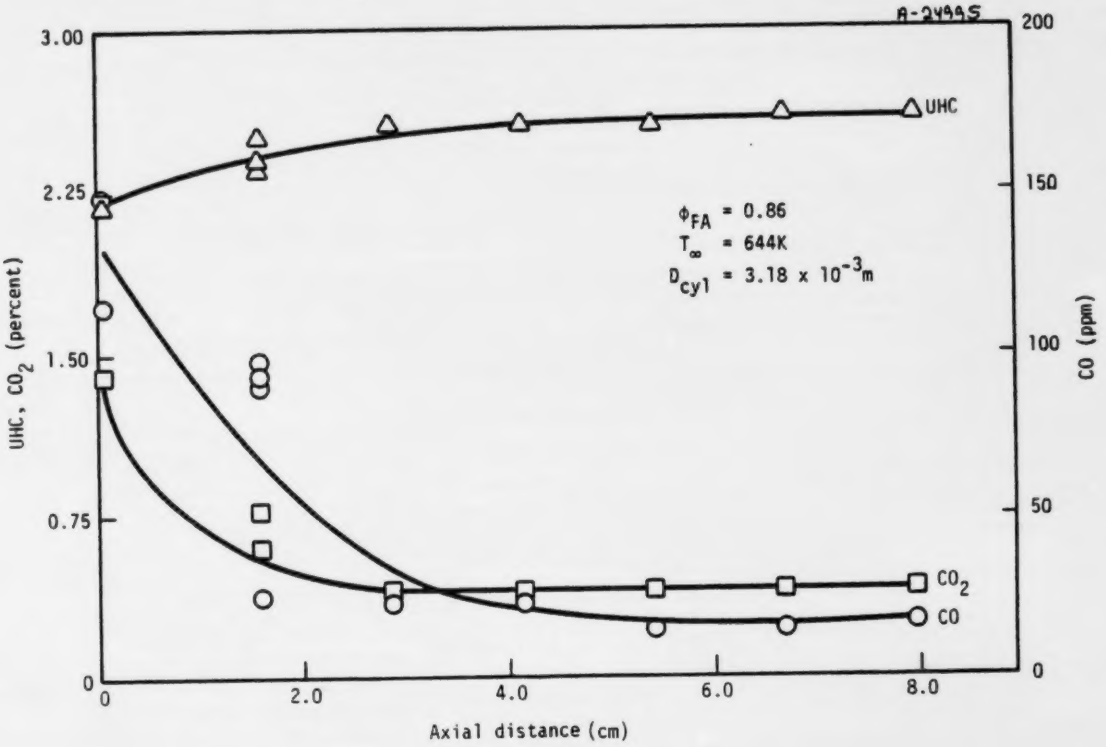

Figure 4-3. Species concentration measurements in the axial direction in line with catalyst tube.

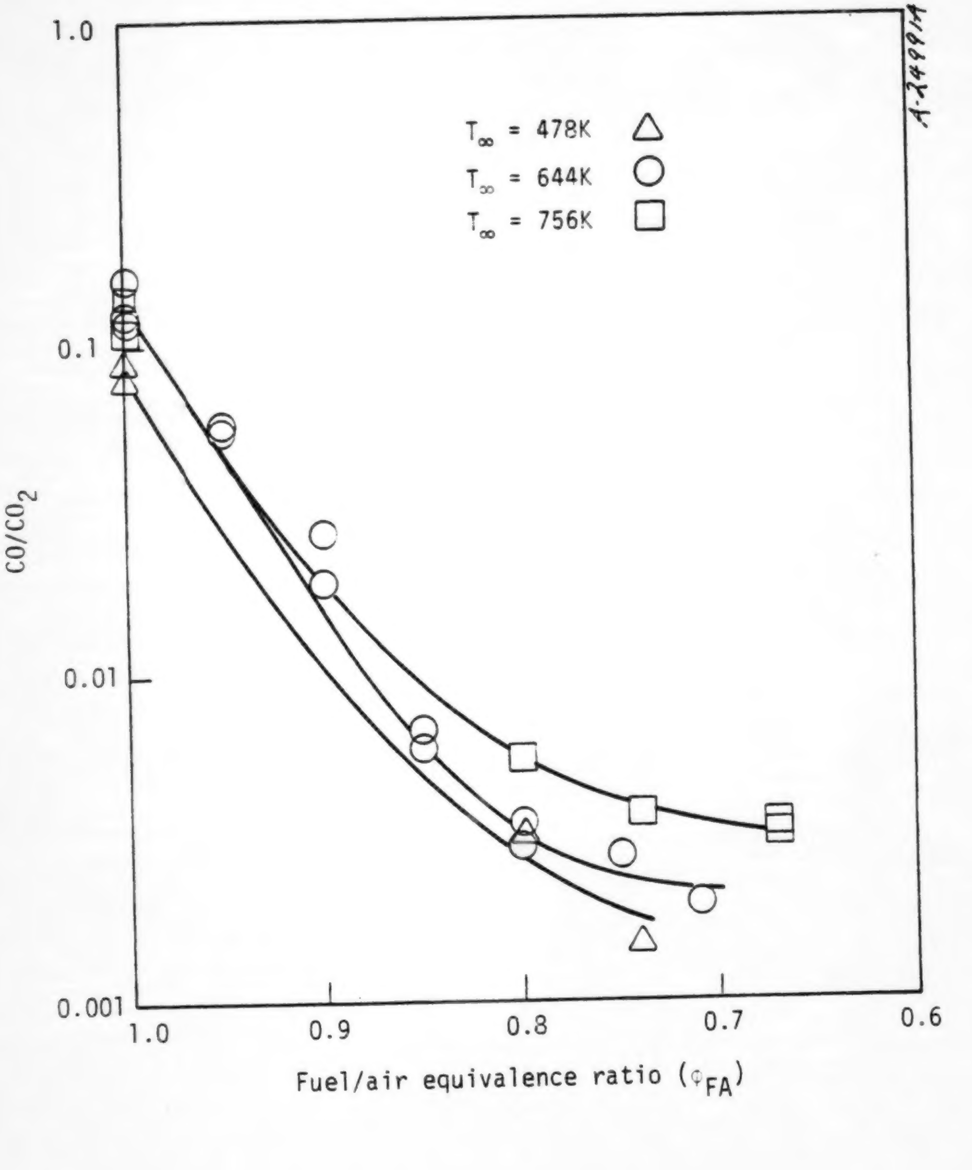

Figure 4-4. CO/CO$_2$ ratio for 6.35×10^{-3}m diameter platinum coated cylinders.

be the major product. This agrees with the investigations of Schwartz, et al. (Reference 4-5) and Anderson (Reference 4-6) which showed that in oxygen-rich systems, most hydrocarbons, including propane, convert into CO_2 and H_2O at the surface without forming CO. The CO/CO_2 ratio increases as the stoichiometric condition is approached from the fuel-lean side, reflecting an increased production of CO. Figure 4-4 also indicates that the reactant preheat temperature has a small effect on the relative amounts of CO and CO_2 as compared to the fuel/air equivalence ratio. It appears that the thermal environment in which the reaction occurs is influenced more by the reactant stoichiometry at the surface than by the reactant gas temperature.

Under the diffusionally controlled reaction, low levels of input fuel conversion to CO_2 (and CO) can be represented by:

$$\eta = \frac{\text{rate of fuel diffusion to surface}}{\text{total fuel flowrate}} \times 100$$

$$= \frac{\left(X_{CO_2} + X_{CO}\right)_{\text{products}}}{\left(X_{\text{fuel}}\right)_{\text{reactants}}} \times 100 \qquad (4\text{-}1)$$

A list of symbols appears at the end of Section 4. The diffusional process may be predicted through a heat transfer analogy (Reference 4-7). The applicable heat transfer model is Hilpert's (Reference 4-8) cylinder in crossflow correlation as modified by Morgan (Reference 4-9) for closed duct blockages and revised thermophysical property data. The correlation is given by:

$$Nu_f = 0.583(Re_f)^{0.471} \qquad (4\text{-}2)$$

Combining Equations (4-1) and (4-2) we find:

$$\eta \propto \frac{(Re_f)^{0.471}}{Re_f} = (Re_f)^{-0.529} \qquad (4\text{-}3)$$

Figure 4-5 shows measured methane conversion as a function of cylinder Reynolds number (total flowrate). The data are well described by the functional behavior of Equation (4-3), confirming the overall transfer process. The measured conversion is also plotted as a function of reactant stoichiometry in Figure 4-6. Only a weak dependence with stoichiometry (or surface temperature) is indicated. This again suggests the dominant role of mass transfer, especially in the near-stoichiometric higher surface temperature regime. Shown as the horizontal solid line in Figure 4-6 is the predicted methane conversion level based on Equation (4-1) with properties evaluated at the average of surface and freestream temperatures. As can be seen, the measured reaction rates are significantly increased over the model. However, since the freestream turbulence levels and velocity profiles are not well defined in the present data, their effects are not included in the correlations. Comings, et al. (Reference 4-10) found Nusselt number increases over baseline calculations of 26 to 45 percent at turbulence intensities of 2.7 to 8 percent, respectively. The high temperature difference between the cylinder surface and the freestream also enhances the Nussult number over that based on correlations of data under more modest temperatures. Recorrelations for large temperature differences have been presented by Douglas and Churchill (Reference 4-11) which result in about a 3 percent increase in the diffusional limit at the present experimental conditions. Morgan (Reference 4-9) reviewed the work of Churchill and Brier, Gosse, and others for loading factors to be used under high temperature differences. The recommended corrections give an increase of up to 6 percent in the mass transfer coefficient at the present conditions. Morgan cautioned, however, that more work was essential before the effects could be better quantified.

One additional source of combustion products which may lead to the higher than expected conversion level would be the existence of an otherwise undetected gas phase reaction zone. A small stagnation zone attached to the lee side of the cylinders could provide a region into which reactants could

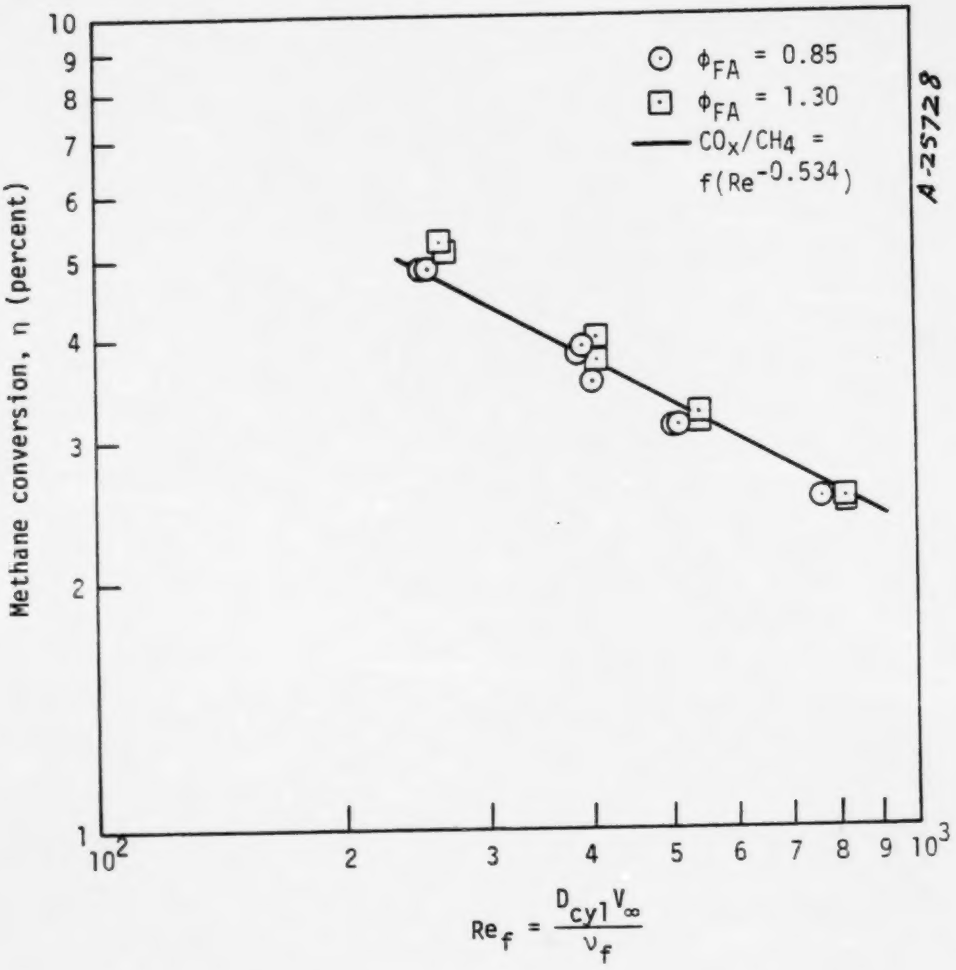

A-25728

Figure 4-5. CH_4 conversion to CO_2 + CO at variable throughput.

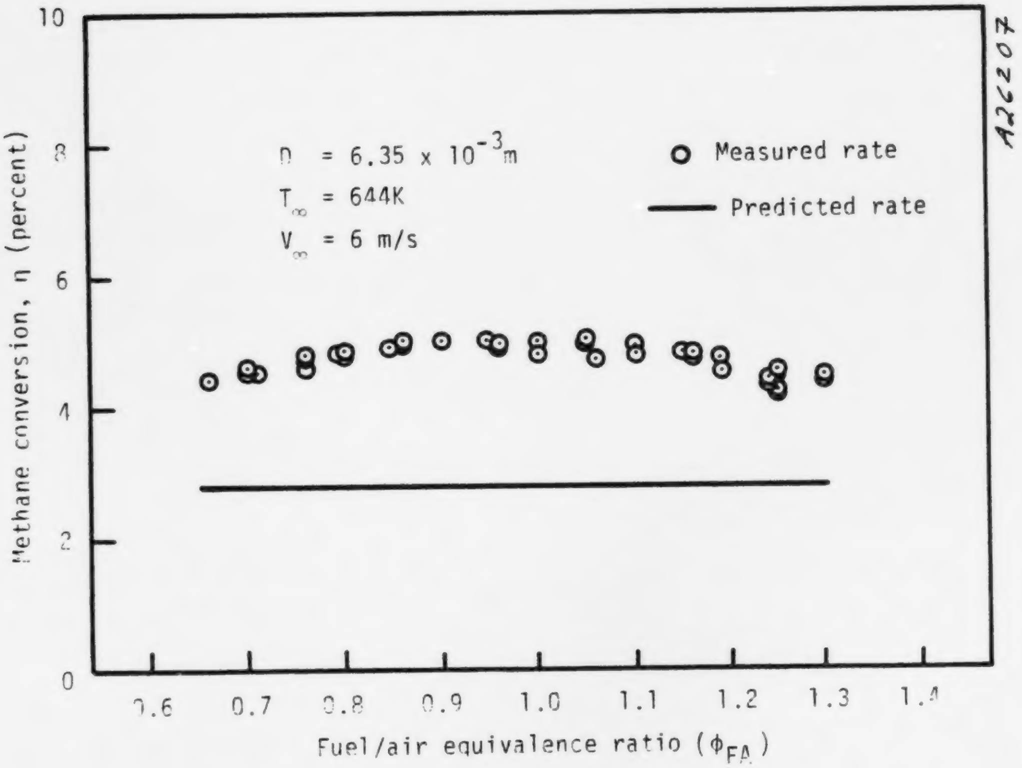

Figure 4-6. CH_4 conversion to CO, CO_2 as a function of stoichiometry.

circulate and be converted to products. In this situation, one might expect a higher proportion of CO formation due to the gas phase reaction mechanism. This concept is discussed further below.

4.3 HETEROGENEOUS KINETICS

To obtain global heterogeneous kinetic rate information on the platinum catalyst, the methane and propane reactions were studied at surface temperatures below 1000K and 625K, respectively. In these temperature ranges, the overall reaction rates were limited by chemical processes, and kinetic rates were directly observable. Control of the surface temperature was made possible by combusting a small amount of hydrogen on the catalyst. By adding hydrogen concentrations of 1.4 to 4.9 percent by volume in the reactant flow, the surface temperature could be varied between 465K and 1333K. Within this range, the hydrogen reaction remained diffusionally limited. Without the stability and control furnished by the hydrogen augmentation, the kinetically limited heat release rate, being insufficient to overcome losses, would lead to rapid extinguishment of the methane or propane reaction.

Experimental data were correlated with the first order Arrhenius rate equation:

$$\frac{RR}{C_\infty} = k = Ae^{-E/RT_w} \qquad (4\text{-}4)$$

The rate of fuel consumption, RR, was measured by product levels of CO_2 and CO which were corrected for background concentrations contained in the fuel and combustion air:

$$RR = (X_{CO} + X_{CO_2}) \frac{Q_T}{A_{cyl}} \frac{P}{T_{STP}R} \qquad (4\text{-}5)$$

The lean reactant (fuel) molar concentration, C_∞, is calculated with the freestream or inlet fuel mole fraction and the measured surface temperature:

$$C_\infty = X_{fuel} \frac{P}{T_w R} \tag{4-6}$$

In this analysis, it was assumed that the fraction of fuel converted to products, η, is small and that only a minimal amount of water vapor is produced. An uncertainty of less than 0.1 percent results when the measured species concentrations, taken on a dry basis, are considered equivalent to wet or actual species concentrations. Also, it was assumed that the total number of moles is conserved during reaction so that the measured mole fractions of CO and CO_2 combined are equal to the mole fraction of fuel consumed. At the existing conversion levels, the associated uncertainty is negligible.

To assess possible reaction mechanism effects due to the presence of hydrogen, the relative reactant concentrations were fixed while the test duct flow velocity was varied. The resulting variation in hydrogen diffusion rates and corresponding surface temperature behavior gave identical methane and propane kinetic data. In addition, no apparent effect on reaction mechanisms or kinetic information was seen as reactant volume concentrations were changed from 2.8 percent to 4.5 percent for methane and from 0.5 percent to 1.2 percent for propane.

Figures 4-7 and 4-8 show methane and propane data plotted using Equation (4-4) with the rate constant, k, versus the inverse of surface temperature, T_w. The slope of the plotted data gives the apparent activation energy, E. Since the freestream fuel concentration, C_∞, was used in the correlation, the apparent activation energy depends on the rate of lean reactant diffusion to the catalyst surface. In the higher temperature ranges, the increasing reaction rate approaches mass transport limitations, and the apparent activation energy is less than the actual value.

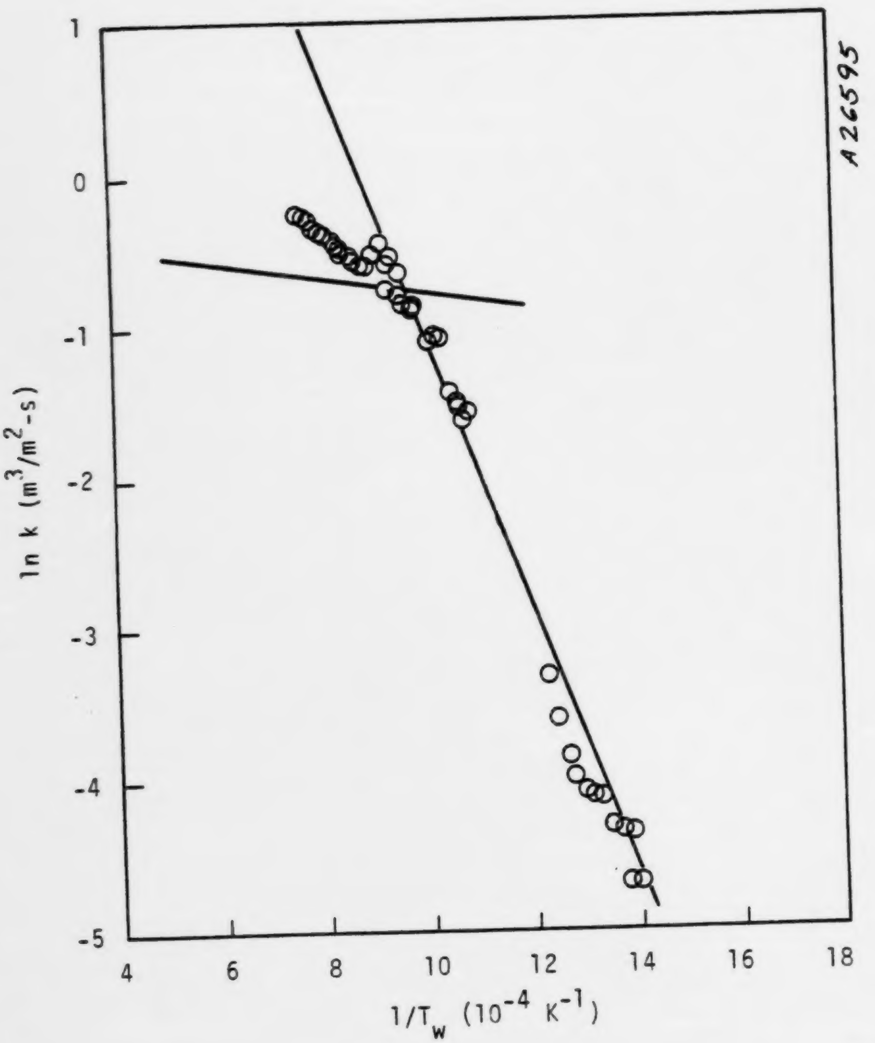

Figure 4-7. Heterogeneous kinetics, methane on platinum.

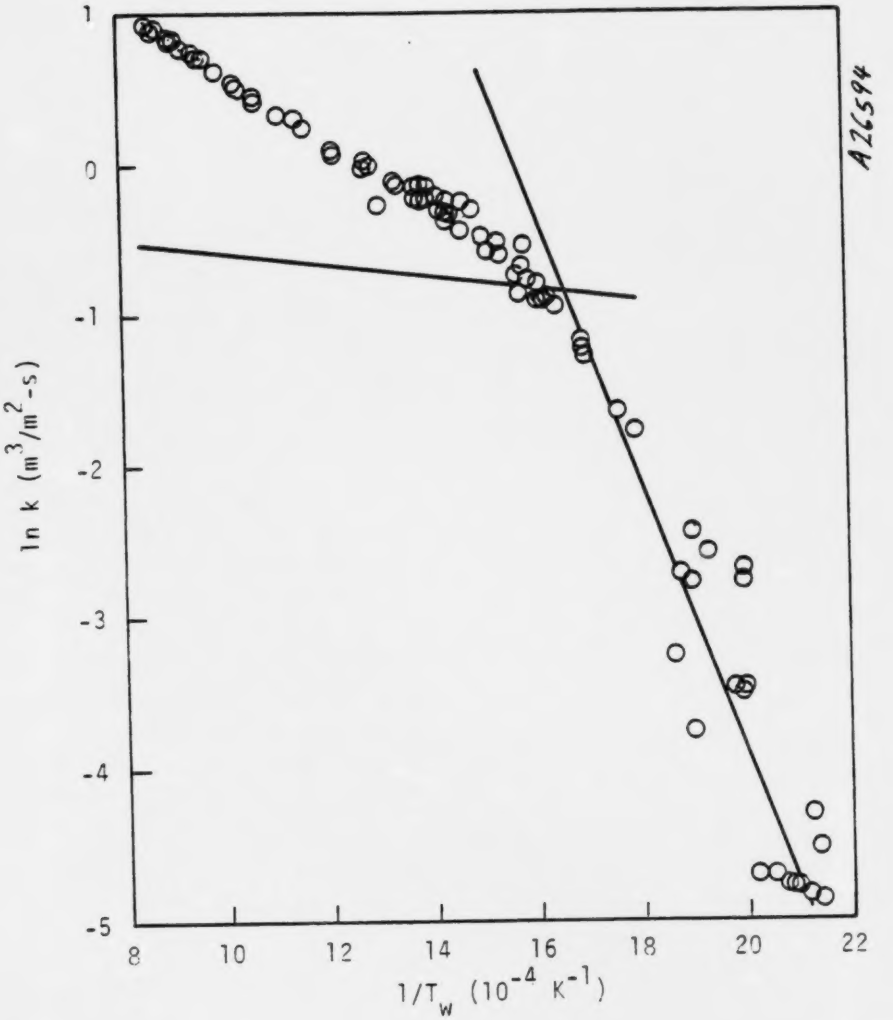

Figure 4-8. Heterogeneous kinetics, propane on platinum.

For the methane reaction shown in Figure 4-7, the effects of diffusional limitations are apparent above 1000K ($1/T_w < 10^{-4}$). The transition occurs at about 600K for propane, shown in Figure 4-8. Because of variations in the local Nusselt number around the cylinder circumference, transition to diffusional control is not as abrupt as expected, nor is it apparently complete in the temperature range studied. Data are plotted on Figure 4-7 for a single 3.18 mm cylinder.

The nearly horizontal line on Figure 4-7 which intersects the data in the 1000K range predicts the rate constant behavior with respect to full diffusional control for the cylinder. As in Figure 4-6, this is somewhat below the measured performance due to complexities in the diffusional process not fully accounted for in the calculated mass transfer coefficient. Again, the existence of a small stagnation region attached to the cylinder would result in such an underprediction. However, one would expect a higher proportion of CO formation, especially as the surface temperature and mixture adiabatic flame temperature are increased through the range shown. Figure 4-9 shows the ratio of CO to CO_2 plotted against the inverse surface temperature for the methane kinetics data for both a single 3.18 mm diameter cylinder and double 6.35 mm diameter cylinder. Recall that the surface temperature is controlled through variable amounts of additive hydrogen which also determines the mixture adiabatic flame temperature. Here the expected behavior is not clearly seen; indeed, the ratio appears to decrease with increasing temperature. However, if the data for the larger diameter cylinders (plotted as squares) are closely inspected above 1111K (below $1/T_W = 9 \times 10^{-4}\ K^{-1}$), an increasing trend in the CO to CO_2 ratio is evident. In this region, the absolute carbon monoxide concentration increased from 1.5 ppm to 6.3 ppm while the carbon dioxide levels changed from 1238 ppm to 1713 ppm. An analysis of this increase in carbon

A26592

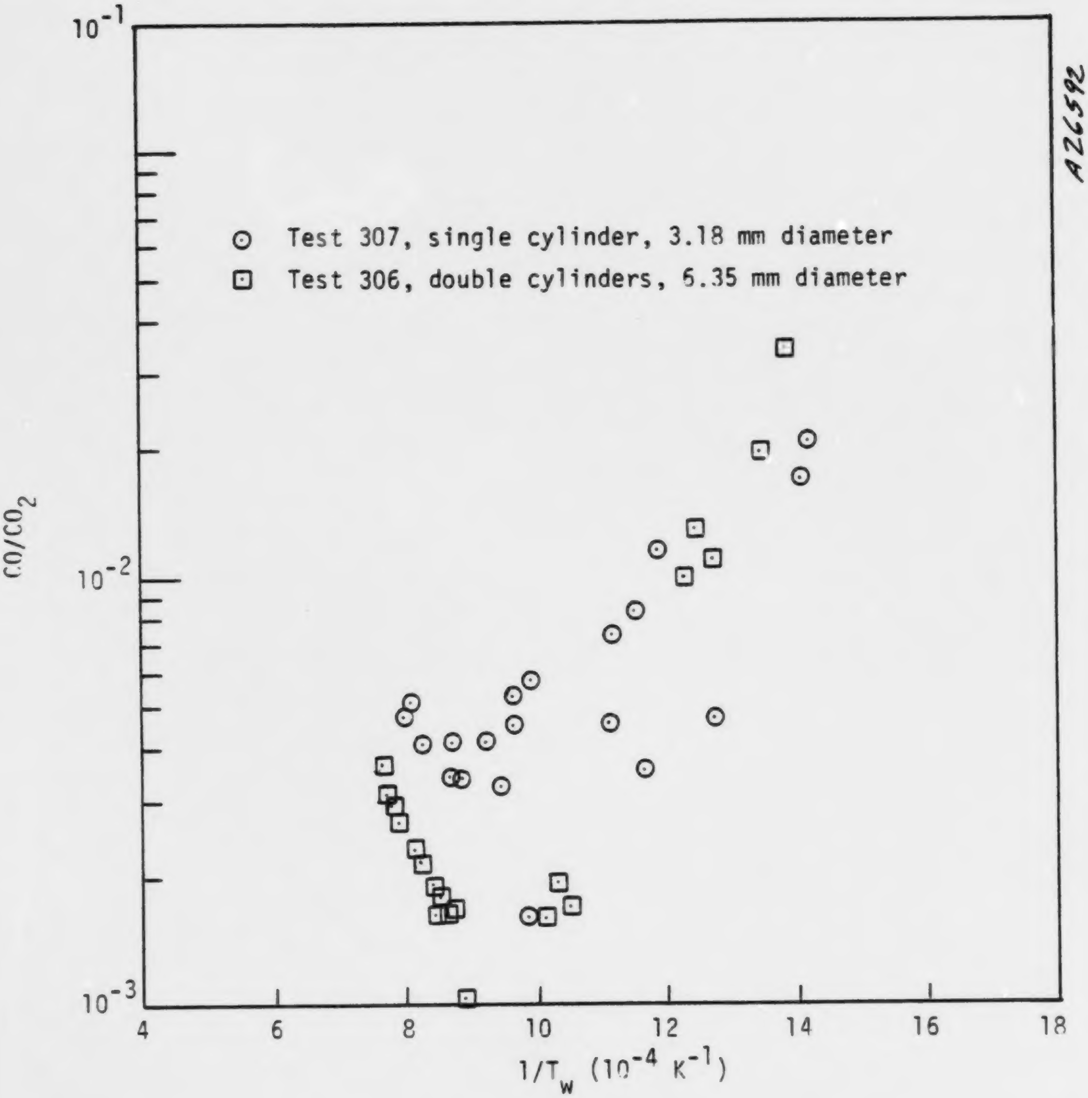

Figure 4-9. CO/CO_2 behavior with surface temperature for heterogeneous kinetics data, methane on platinum.

monoxide alone, however, is not sufficient to account for the reaction rate or rate constant increase over the predicted level.

The propane heterogeneous kinetics data in Figure 4-8 were obtained on a single 3.18 mm diameter cylinder only. In this case, the reaction makes the transition from a kinetically controlled surface process at about 600K. The calculated rate constant behavior for full diffusional control intersects the data at 600K and also significantly underpredicts the actual performance. Figure 4-10 shows even less of a trend in relative CO and CO_2 concentrations than was seen in Figure 4-9. The absolute concentrations of carbon monoxide varying between 0 and 10 ppm, also did not indicate a clear trend with temperature. This would tend to further contradict the presence of a small gas phase reaction in a stagnation or recirculation zone unless sufficient residence time, temperature, or the presence of hydrogen promoted full conversion to carbon dioxide.

In the low temperature kinetically controlled regime, the slope of the plotted data represents the true activation energy. A least squares linear fit was applied to both the methane and propane data and is indicated in Figures 4-7 and 4-8. The resulting kinetic parameters are summarized in Table 4-1 along with those reported by other workers. The values for activation energy, E, obtained in the present study show good agreement with the other entries. This term is most useful since it is widely applicable to various configurations and operational characteristics of a given catalyst providing the reaction mechanism remains unchanged. Table 4-1 indicates a wider range in the values of the pre-exponential factor, A, however. Unlike the activation energy, this parameter is dependent on individual catalyst characteristics such as geometry, active sites dispersion, and flow properties. The pre-exponential factor in this work is based on total catalyst cylinder geometric surface area presented to the reactant flow. Anderson, et al. (Reference 4-12) reported a pre-exponential factor based on bulk catalyst volume as 2.24×10^7 m^3/m^2-s. Trimm and Lam (Reference 4-13) studied

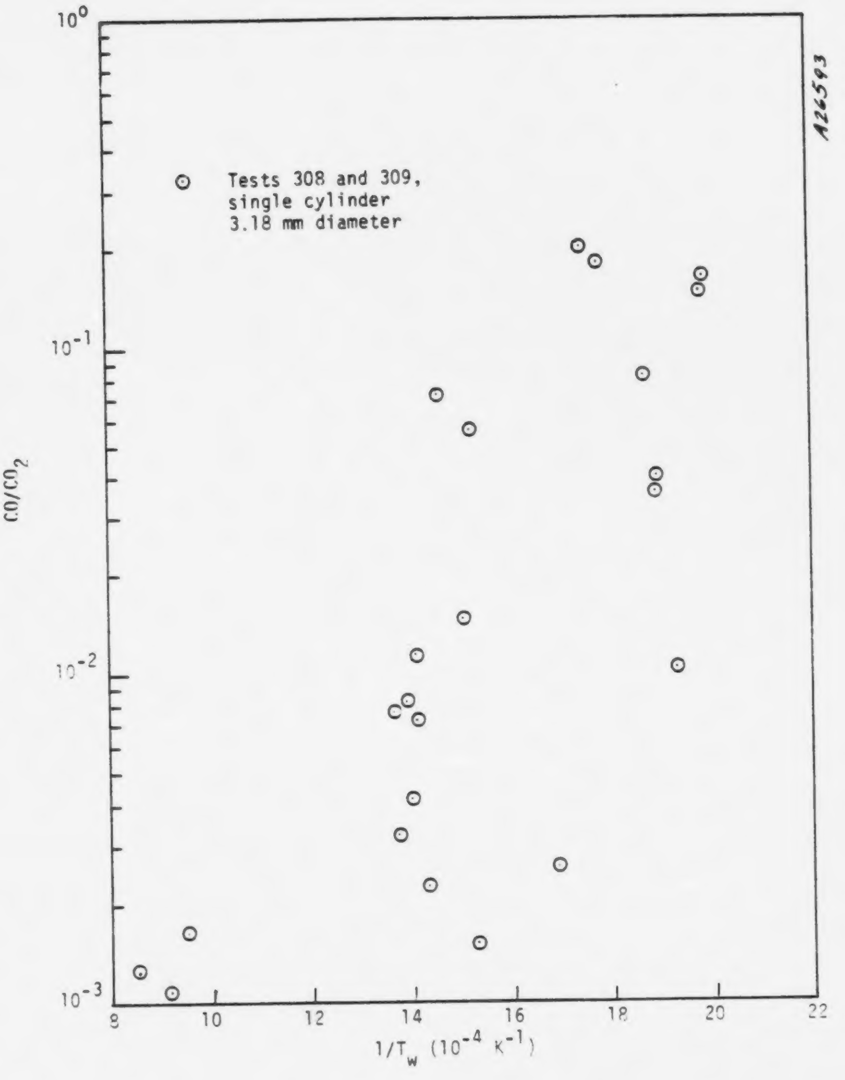

Figure 4-10. CO/CO_2 behavior with surface temperature for heterogeneous kinetics data, propane on platinum.

TABLE 4-1. HETEROGENEOUS KINETIC PARAMETERS

Reference	Fuel/Catalyst	Pre-exponential Factor, A $\left(\frac{m^3}{m^2\text{-s}}\right)$	Activation Energy, E $\left(\frac{J}{\text{kg-mole}}\right)$	$\left(\frac{\text{kcal}}{\text{mole}}\right)$
This work	CH_4/Pt on alumina, γ-alumina washcoat	3.27×10^3	7.54×10^7	18.0
Anderson, et al. (Ref. 4-12)	CH_4/Pt on γ-alumina washcoat	*	9.84×10^7	23.5
Trimm & Lam (Ref. 4-13)	CH_4/Pt on porous alumina fiber	*	8.58×10^7	20.5
Trimm & Lam (Ref. 4-13)	CH_4/Pt on porous alumina fiber	*	7.58×10^7	18.1
This work	C_3H_8/Pt on alumina, γ-alumina washcoat	1.19×10^6	7.42×10^7	17.7
Bracco, et al. (Ref. 4-14)	C_3H_8/Pt on cordierite, γ-alumina washcoat	1.09×10^7	7.37×10^7	17.6
Marteney (Ref. 4-15)	C_3H_8/Pt on ceramic honeycomb	8.00×10^{8}**	4.19×10^7	10
Hiam, et al. (Ref. 4-4)	C_3H_8/Pt wire filament, 99.99% purity	1.1×10^7	7.12×10^7	17.0

*See text

**Reported as 960 kg/m^2-s

methane combustion on a fiber pad burner and found pre-exponential factors of 1.03×10^5 kg-mole/m^2-s and 3.20×10^{-6} kg-mole/m^2-s, respectively, for porous and nonporous alumina pad fibers. Their results are based on platinum metal surface area determined by CO adsorption. Table 4-2 gives a comparison of rate constant temperature dependence for methane and propane derived from the present work.

TABLE 4-2. HETEROGENEOUS RATE CONSTANTS (this work)

T_w (K)	k_{CH_4} $\left(\frac{m^3}{m^2\text{-s}}\right)$	$k_{C_3H_8}$ $\left(\frac{m^3}{m^2\text{-s}}\right)$
500	4.34×10^{-5}	2.11×10^{-2}
1000	3.77×10^{-1}	1.58×10^{2}
1500	7.74×10	3.10×10^{3}

4.4 HETEROGENEOUS FUEL BOUND NITROGEN STUDY

A small amount of data over that reported in Reference 4-1 was collected under fuel bound nitrogen studies during the third year of the program.

Similar to the methane conversion studies illustrated in Figure 4-5, the platinum coated cylinder in crossflow configuration was utilized to determine the conversion behavior of ammonia dopant with variable crossflow velocity or Reynolds number. Ammonia was used to model fuel nitrogen compounds and was added at a rate of 1.3 percent by volume of fuel. Under fuel-lean (ϕ_{FA} = 0.85) and fuel-rich (ϕ_{FA} = 1.30) conditions, the test section velocity was varied to give a Reynolds number range of 250 to 800. The

Reynolds number was based on catalyst cylinder diameter (6.35 mm) and properties evaluated at the film temperature between the freestream (644K) and surface temperatures. Figure 4-11 shows that the percent of input ammonia converted to NO_x does not exhibit the same functional behavior as the methane process in Figure 4-5. Thus, the reaction mechanism governing the oxidation of ammonia dopant is more complex and may not be dominated by surface events. Additional processes which may be occurring include the reduction of formed NO to N_2 by the ammonia dopant remaining in the freestream at levels of about 1000 ppm. Since nitrogen (N_2) was not measured, this may also account for nitrogen species closures which were sometimes below 60 percent of input ammonia.

To assess the potential for the reduction of NO_x on the catalyst surface during fuel-rich combustion of methane, nitric oxide was used as a dopant, and the mixture was combusted over the platinum coated cylinders. At a reactant preheat temperature of 506K, the fuel/air equivalence ratio was varied from $\phi_{FA} = 0.95$ to $\phi_{FA} = 1.50$. The corresponding surface temperature of the platinum coated cylinders (0.635 cm diameter) ranged from 1390K to 1247K. A flow of NO was introduced to give a reactant stream concentration of 250 ppm. Compositional measurements downstream of the catalyst cylinders indicated that virtually all of the input NO was unchanged. There was, however, a slight increase in the measured NH_3 level to about 1.6 percent of the input NO at the richest condition. These data are not conclusive, and further work in both thermal and fuel NO_x areas is of interest.

4.5 CONCLUSIONS

The experimental technique has proven useful for studying the heterogeneous portion of catalytic combustion. In the higher temperature ranges of operation (near stoichiometric), the surface reaction rate on the cylinder in crossflow configuration is limited by lean reactant diffusion. In this regime, the combustion of methane was promoted to completion by the

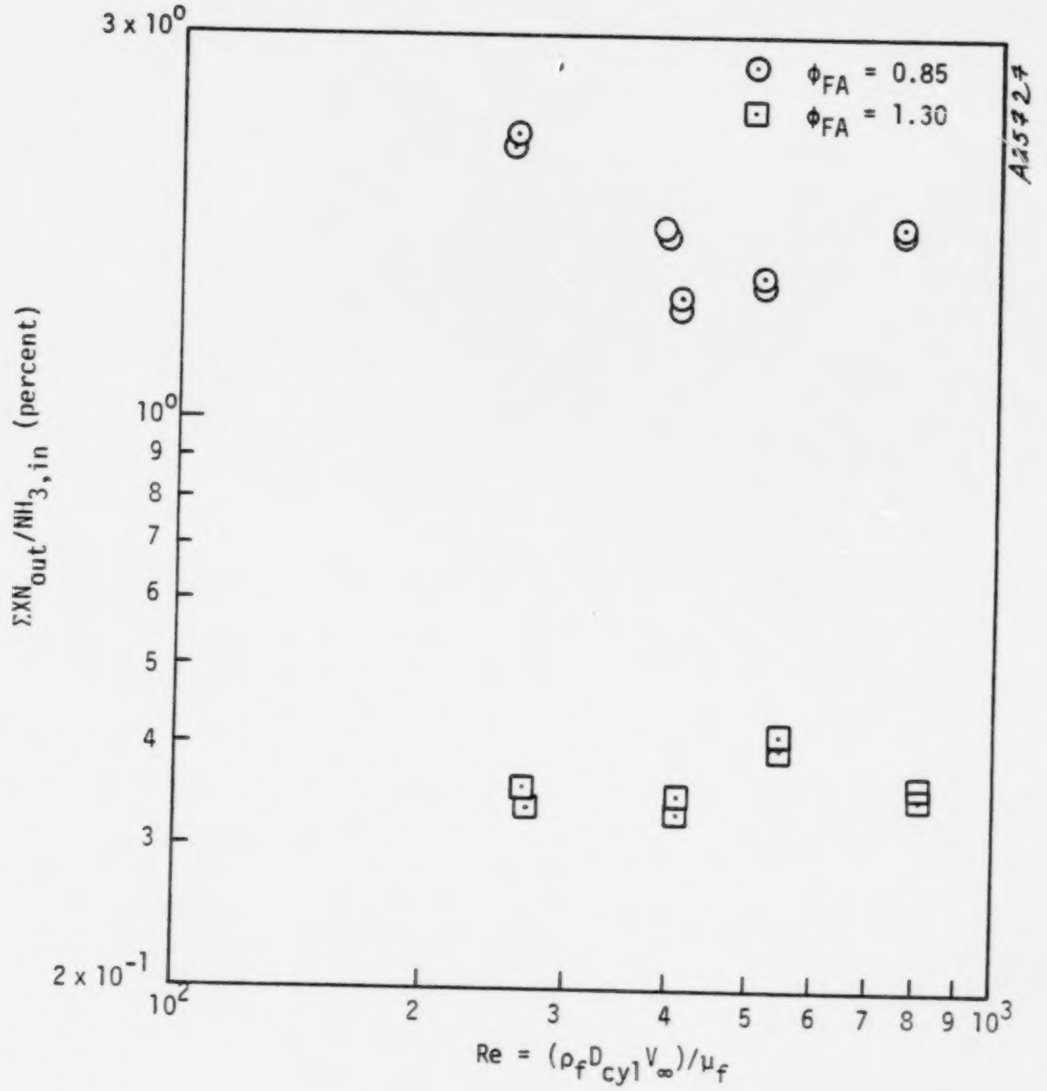

Figure 4-11. NH_3 conversion to NO at variable throughput.

catalyst with carbon dioxide as the major product. This data is most useful for understanding normal, steady state operation encountered in honeycomb monolith type catalysts. It will allow further optimization in the amount of surface area required for a specific energy release rate.

The measured conversion rates were significantly underpredicted by calculated lean reactant mass transfer limitations. This may be due to the use of a mass transfer coefficient which does not fully account for freestream turbulence levels or high surface temperatures. Regions of flow stagnation or recirculation, possibly attached to the cylinders, may also promote higher conversion rates. However, other data, including carbon monoxide formation behavior, are not clearly supportive of this concept.

Small amounts of hydrogen in the reactant flow gave precise catalyst surface temperature control over ranges in which methane and propane heterogeneous kinetics could be quantified. The experimentally measured activation energies were 7.54×10^7 J/kg-mole for methane and 7.42×10^7 J/kg-mole for propane. These values compare favorably with those reported by other workers. Also, the relative magnitudes agree with experience in which propane ignition occurs earlier and at a lower temperature and is more difficult to blow out than methane on a given catalyst. This surface reaction rate information is required for efficient design of catalyst entry regions. The Nusselt number (Sherwood number for mass transfer) is large in these or other zones where flow stagnation may occur, giving high mass transfer rates. Additionally, kinetic information is necessary to predict lightoff characteristics and maximum throughput capabilities before catalyst blowout.

LIST OF SYMBOLS

A	pre-exponential factor	m^3/m^2-s
A_{cyl}	catalytic cylinder surface area	m^2
C	molar concentration of reactant species	kg-mole/m^3
CL	flow duct centerline	
D_{cyl}	diameter of catalyst cylinder	m
E	activation energy	J/kg-mole
k	first order reaction rate constant	m^3/m^2-s
Nu	Nusselt number	
P	absolute pressure	Pa
Q_T	total volume flowrate	m^3/s
R	gas constant	8.314×10^3 J/kg-mole-K
RR	species reaction rate	kg/mole/m^2-s
Re	Reynolds number	
T	temperature	K
V_∞	freestream reactant flow velocity	m/s
X	mole fraction	
η	reactant conversion	%
ν	kinematic viscosity	m^2/s
ρ	density	kg/m^3
ϕ_{FA}	fuel/air equivalence ratio, $(F/A)_{actual}/(F/A)_{stoichiometric}$	

Subscripts

f	film temperature conditions
i	species
w	catalyst surface
STP	standard conditions
∞	freestream conditions

REFERENCES FOR SECTION 4

4-1. Snow, G. C., Krill, W. V., and Kendall, R. M., "Mechanisms and Kinetics in Catalytic Combustion," published in "Proceedings: Fifth Workshop on Catalytic Combustion (San Antonio, TX, September 1981)," EPA-600/9-84-002, NTIS-PB84-145580, pp. 105-133.

4-2. Snow, G. C., Chu, E. K., Krill, W. V., Kesselring, J. P., and Kendall, R. M., "Fundamental Studies in Catalytic Combustion," Paper No. WSS/CI-81-27, Western States Section/The Combustion Institute, 1981 Spring Meeting, Pullman, WA, 1981.

4-3. Rader, C. G. and Weller, S. W., "Ignition on Catalytic Wires: Kinetic Parameter Determination by the Heated-Wire Technique," AIChE J., Vol. 20, p. 515, 1974.

4-4. Hiam, L., Wise, H., and Chaikin, S., "Catalytic Oxidation of Hydrocarbons on Platinum," J. Catal., Vol. 10, pp. 272-276, 1968.

4-5. Schwartz, A., Holbrook, L. L., and Wise, H., "Catalytic Oxidation Studies with Platinum and Palladium," J. Catal., Vol. 21, pp. 199-207, 1971.

4-6. Anderson, D. N., "Preliminary Results from Screening Tests of Commercial Catalysts with Potential Use in Gas Turbine Combustors, Part I. Furnace Studies of Catalyst Activity," NASA TMX-73410, 1976.

4-7. Kays, W. M., Convective Heat and Mass Transfer, McGraw-Hill, New York, 1966.

4-8. Hilpert, R., "Warmeabgabe von geheizten Drahten und Rohren im Lufstrom," Forsch. Geb. Ingenieurw., Vol. 4, pp. 215-224, 1933.

4-9. Morgan, V. T., "The Overall Convective Heat Transfer from Smooth Circular Cylinders," Advances in Heat Transfer, Vol. 2, pp. 199-264, Academic Press, New York, 1975.

4-10. Comings, E. W., Clapp, J. T., and Taylor, J. F., "Air Turbulence and Transfer Processes. Flow Normal to Cylinders," Industrial and Engineering Chemistry, Vol. 40, pp. 1076-1082, 1948.

4-11. Douglas, W. J. M. and Churchill, S. W., "Recorrelation of Data for Convective Heat Transfer Between Gases and Single Cylinders with Large Temperature Differences," Chem. Eng. Progr., Symposium Series, Vol. 52, 18, pp. 23-28, 1956.

4-12. Anderson, R. B., Stein, K. C., Feenan, J. J., and Hofner, L. J. E., "Catalytic Oxidation of Methane," Ind. & Eng. Chem., Vol. 53, 10, pp. 809-812, 1961.

4-13. Trimm, D. L. and Lam, C. W., "The Combustion of Methane on Platinum-Alumina Fibre Catalysts -- I Kinetics and Mechanism," Chem. Eng. Sci., Vol. 35, pp. 1405-1413, 1980.

4-14. Bracco, F. V., Bruno, C., Yaw, Y., and Walsh, P. M., "Computed and Measured Emissions from the Catalytic Combustion of Propane/Air Mixtures," Proceedings Fourth Workshop on Catalytic Combustion, EPA-600/9-80-035, NTIS-PB81-176067, August 1980.

4-15. Marteney, P. J., "Determination of the Rate of Heterogeneous Reaction on Catalytic Surfaces," Proceedings: Third Workshop on Catalytic Combustion, EPA-600/7-79-038, NTIS-PB293 336, February 1979.

SECTION 5

FIRETUBE BOILER PROTOTYPE DEMONSTRATION

5.1 INTRODUCTION

The objective of the firetube boiler prototype demonstration was to demonstrate the fiber burner as a low NO_x burner for commercial boilers. The demonstration was to advance the technology to a point where a field demonstration of longer duration could be performed leading to commercialization. A prototype fiber burner was designed based on the results of tests performed during the second year of the program. Burners were fabricated, retrofitted into a commercial firetube boiler, and performance-tested over a range of conditions. A 1000-hour durability test was then conducted.

Compared with the as-received boiler burner, the fiber burner reduced NO_x 80 percent, operated at lower excess air levels (nominally 10 percent rather than 30 percent) without breakthrough of CO, increased boiler efficiency by approximately two percent, and was substantially quieter. The durability of the burner was shown by successful completion of the 1000-hour test, readying the system for field demonstration.

The firetube boiler selected and purchased for the demonstration was a York-Shipley 2.45×10^5 watt (25 horsepower) low pressure steam boiler with an input heat rate of 1106 MJ/hr (1,048,000 Btu/hr). Although the boiler could fire either gas or light oil, only gas firing was demonstrated since the fiber burner had not been tested on liquid fuels.

The fiber burner designed for the firetube boiler was approximately 0.31 m (12 inches) in diameter and 1.07 m (42 inches) long, occupying approximately 80 percent of the volume of the boiler first pass. The burner was fabricated over a perforated sheet support structure and cantilevered into the combustion chamber of the boiler. Figure 5-1 shows the burner before installation into the boiler.

Minimal changes to the boiler were required for fiber burner retrofit. Some minor changes were required for testing that would not be necessary for commercial systems.

Subscale testing of the fiber burner was conducted prior to testing in the firetube boiler. Two successful burners had been identified: the Chemo-Thermic Industries (CTI) burner, and the Johns-Manville (J-M) burner. Both burners were tested in the high pressure test facility in a water-walled configuration that modeled the first pass of a firetube boiler (Reference 5-1). The burners were cylindrical, closed on one end, and had length-to-diameter ratios similar to typical firetubes. The burner diameter allowed a 2.5 to 3.8 cm annulus between the burner and the 20.6 cm inside diameter combustion chamber wall.

5.1.1 Chemo-Thermic Industries Burners

Four CTI burners were fabricated and tested. The CTI burners were approximately 14 cm (5.5 inches) in diameter and 61 cm (24 inches) long, with a nominal heat release of 264 MJ/hr (250,000 Btu/hr). The burners were formed over a fine wire screen which remained an integral part of the burner. For testing, the burners were slipped over a support assembly and cantilevered inside the facility test sections. An inner burner tube formed an annulus to maintain high internal reactant velocities for flashback prevention. Figure 5-2 shows the subscale design.

The test matrix was designed to determine operating conditions for stable combustion on natural gas and to show performance characteristics of the burners. Surface temperatures and emissions were measured at stoichiometries ranging from 0 to 50 percent excess air and heat release rates per

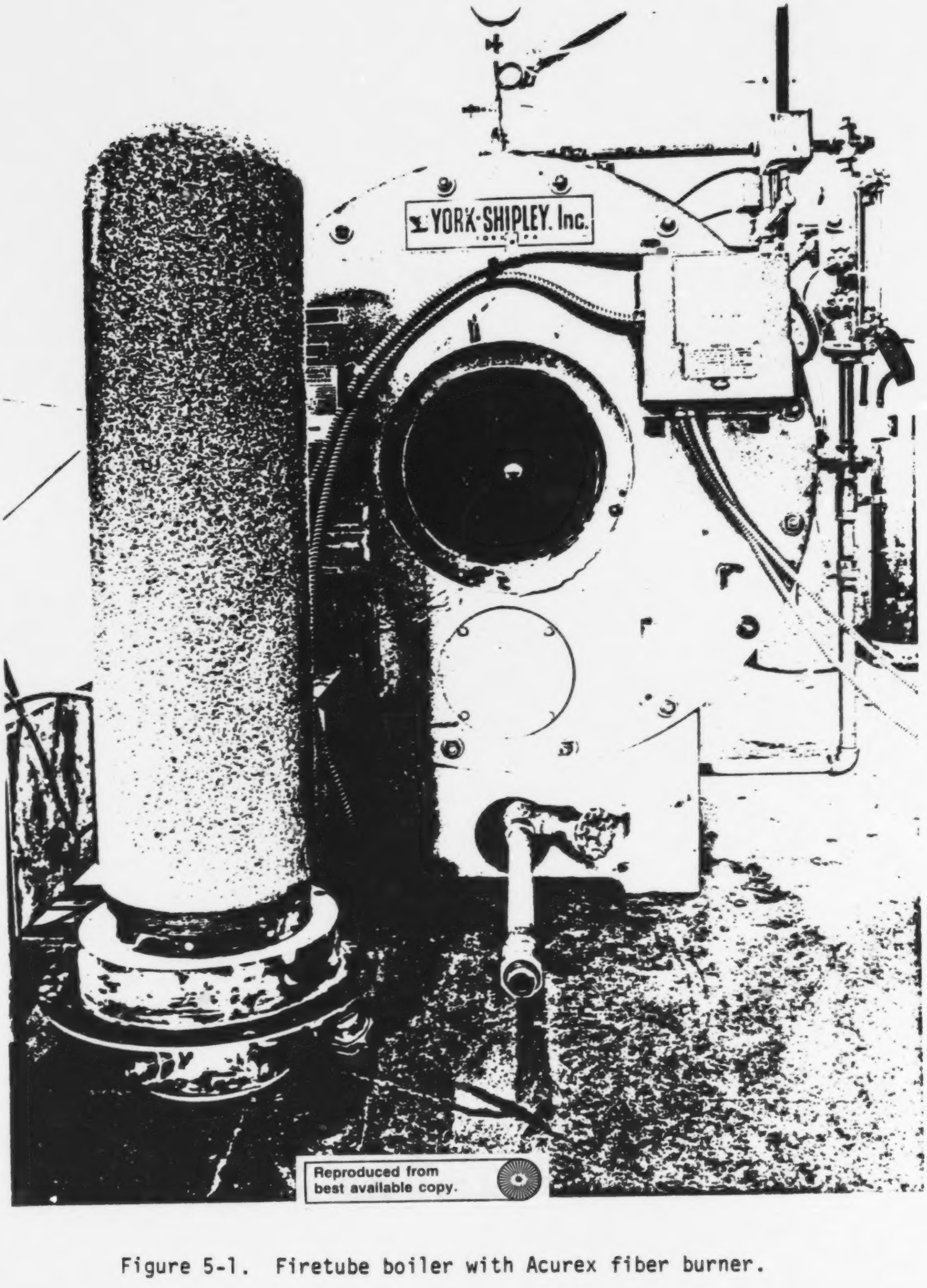
YORK-SHIPLEY, Inc.

Reproduced from
best available copy.

Figure 5-1. Firetube boiler with Acurex fiber burner.

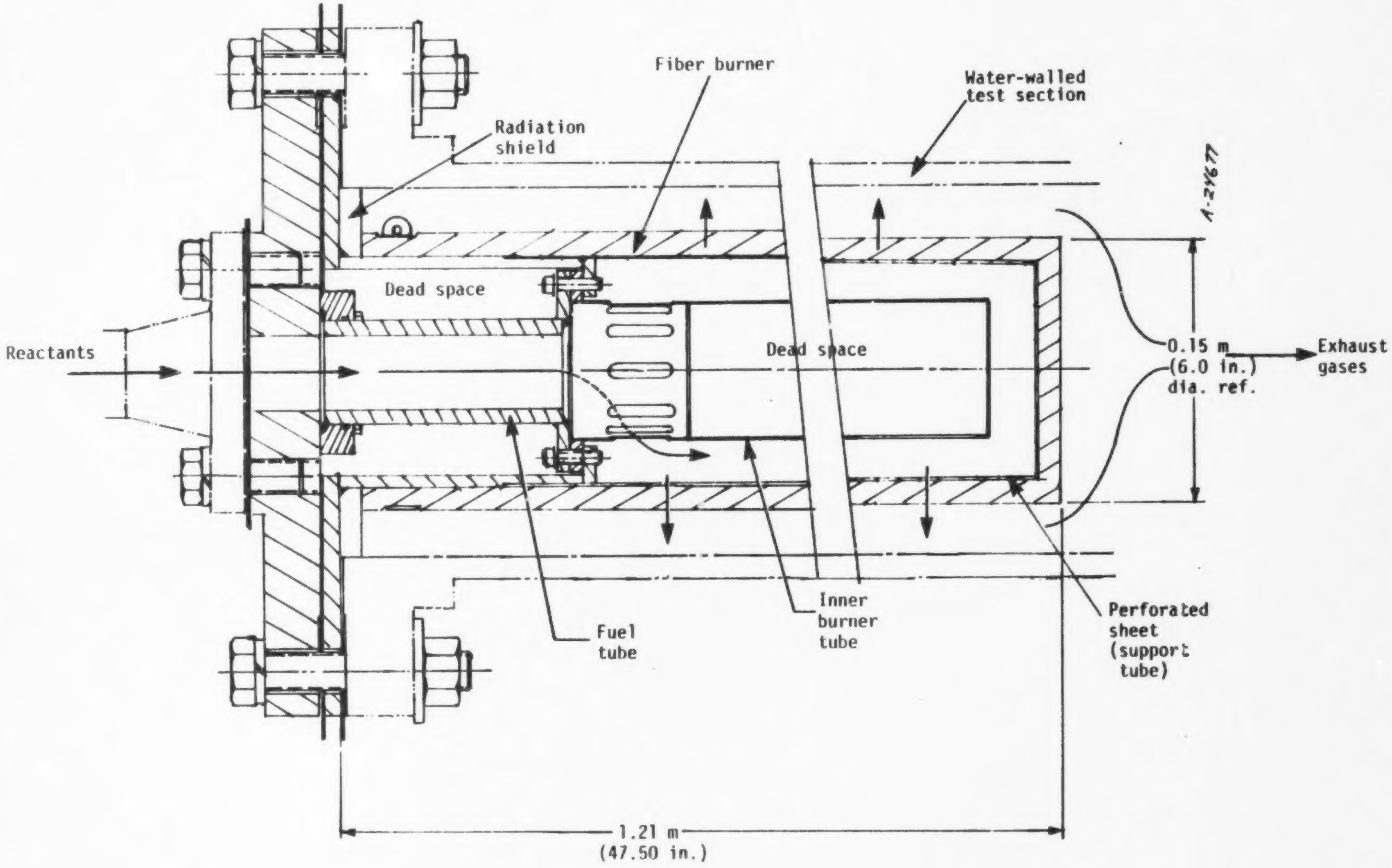
Fiber burner
Water-walled test section
Radiation shield
A-24677
Dead space
Reactants
Dead space
0.15 m (6.0 in.) dia. ref.
Exhaust gases
Fuel tube
Inner burner tube
Perforated sheet (support tube)
1.21 m (47.50 in.)

Figure 5-2. Subscale firetube boiler burner assembly.

unit area from 205,000 to 394,000 watts per m^2 (65,000 to 125,000 Btu/hr per ft^2) of burner surface area. The test data are shown in appendix Tables A-4 to A-7.

All four CTI burners operated stably over the entire range of test matrix conditions. Emissions performance varied, however, with higher NO_x for CTI 1 and 2 than for CTI 3 and 4. For example, NO_x at 10 percent excess air and 252,000 watts/m^2 (80,000 Btu/hr-ft^2) was 35 ppmv for CTI 1 and 2, and about 20 ppmv for CTI 3 and 4. The NO_x emissions from CTI 3 and 4 were similar to those in tests conducted on smaller CTI burners for other projects. CO and UHC emissions were substantially the same for all burners. The data from tests conducted on the CTI burners are shown in Figures 5-3 through 5-6.

The difference in NO_x emissions for the four burners was probably due to the burner curing method, which affects its uniformity. The first two burners were not completely cured, leaving high pressure drop areas in the fiber matrix. The nonuniform fiber matrix allowed high velocity gases to pass through some regions of the burner and burn downstream, causing high thermal NO_x. To avoid this problem, CTI 3 and 4 were cured with an improved method, resulting in lower NO_x emissions during operation.

5.1.2 Johns-Manville Burner

Johns-Manville fabricated a 0.15 m (6 inch) diameter by 1.07 m (42 inch) long burner for testing under the same conditions and in the same test facility as the CTI burners. Throughout the tests, the J-M burner was stable with NO_x, CO, and HC emissions similar to those of CTI 3 and 4.

In addition to the parametric tests, the J-M burner was tested for 100 hours to show the durability potential of the burner. No performance or visible physical degradation occurred during the extended test, nor in parametric tests repeated at the end of the 100 hours. The data are shown in Tables A-8 and A-9. Figures 5-7 and 5-8 show burner emissions for the

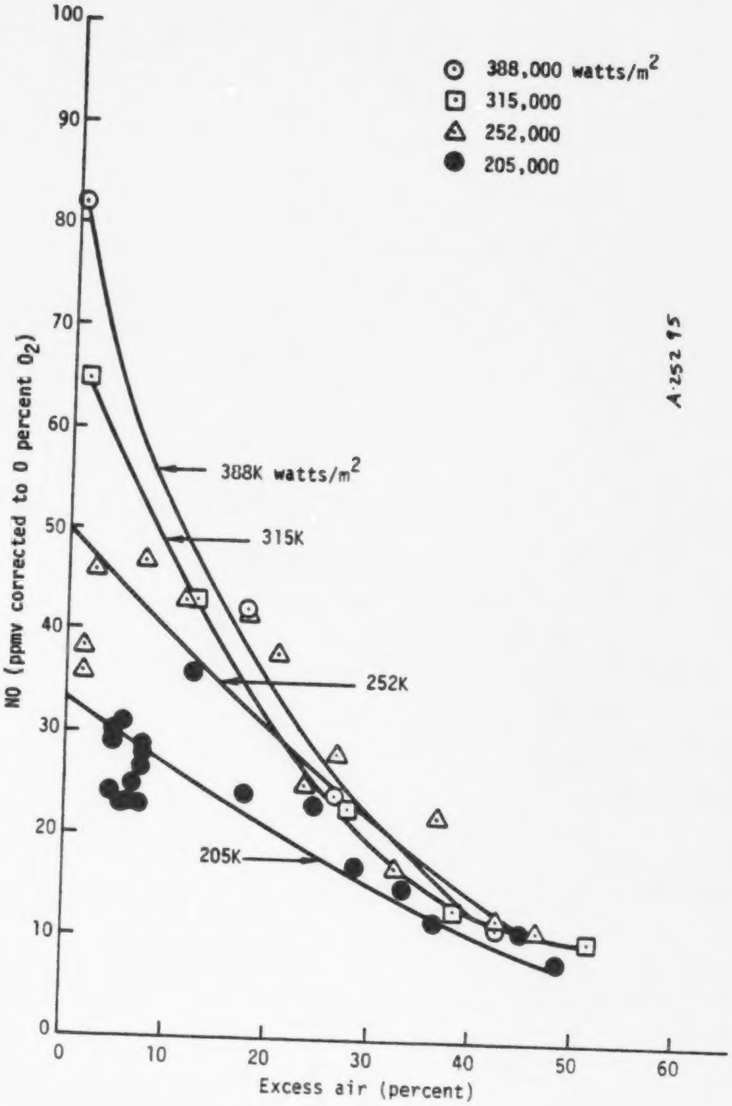

A·252 95

Figure 5-3. CTI 1 NO_x emissions.

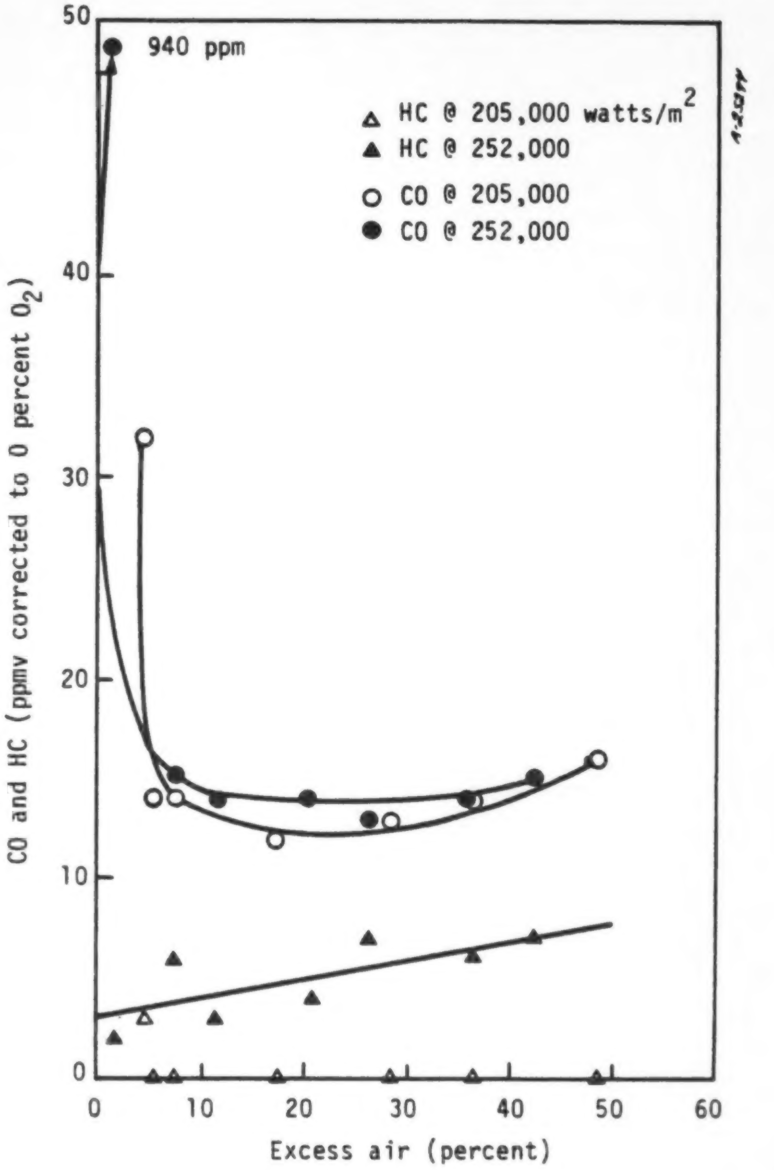

Figure 5-4. CTI 1 CO and HC emissions.

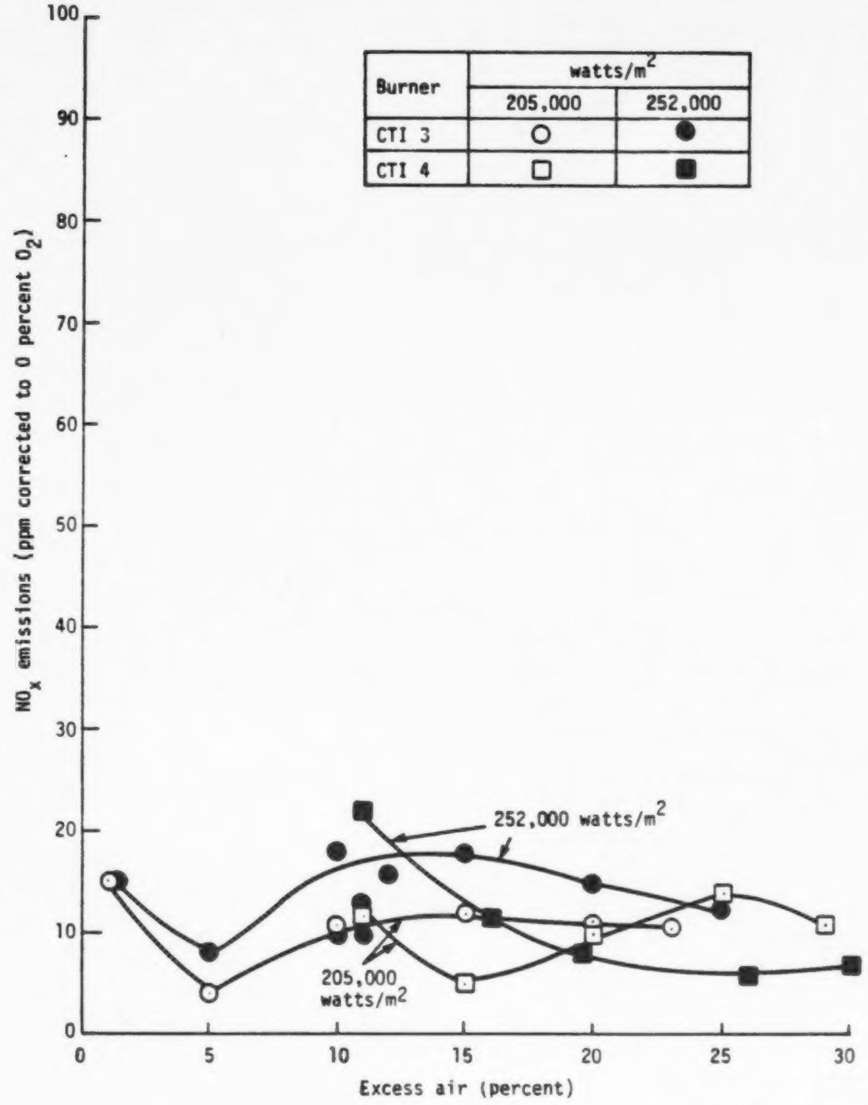

Figure 5-5. CTI 3 and 4 -- NO_x emissions.

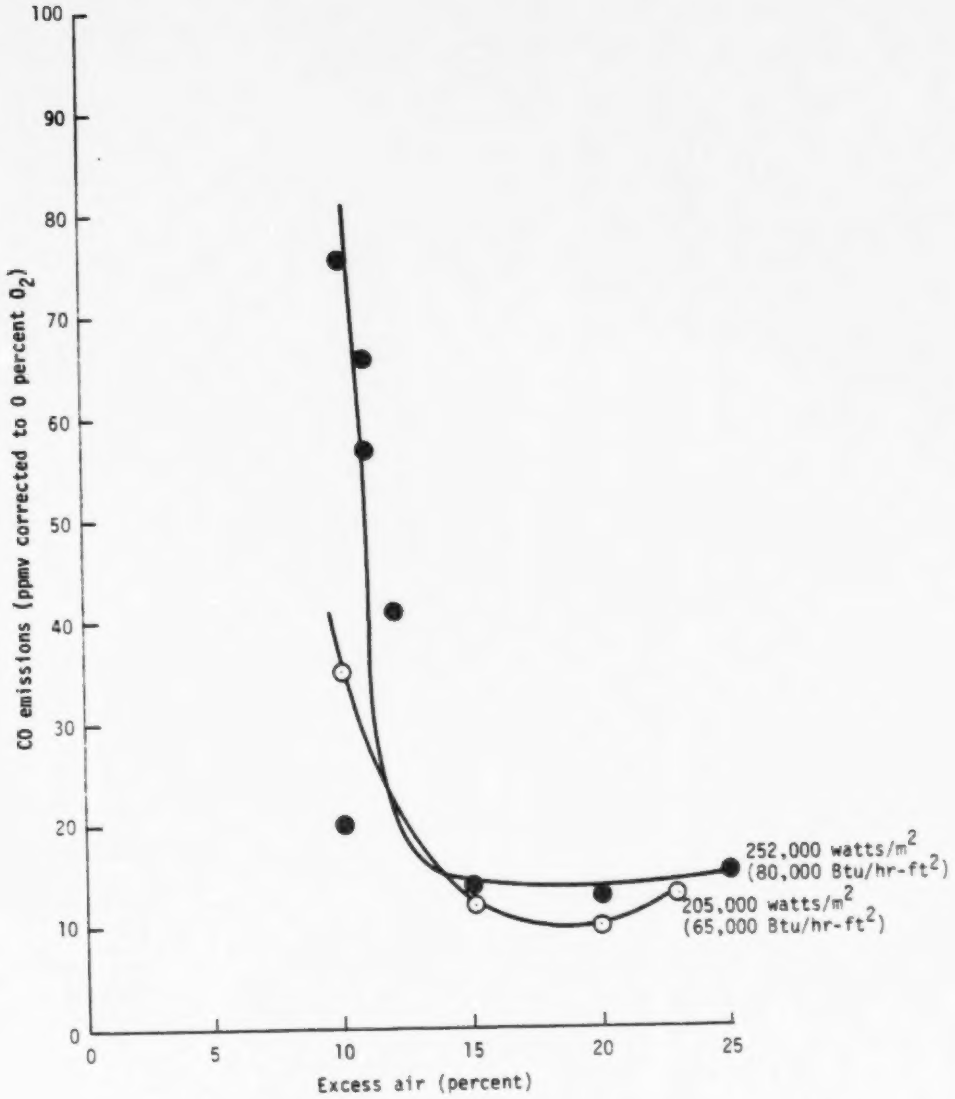

Figure 5-6. CTI 3 CO emissions.

A·25398

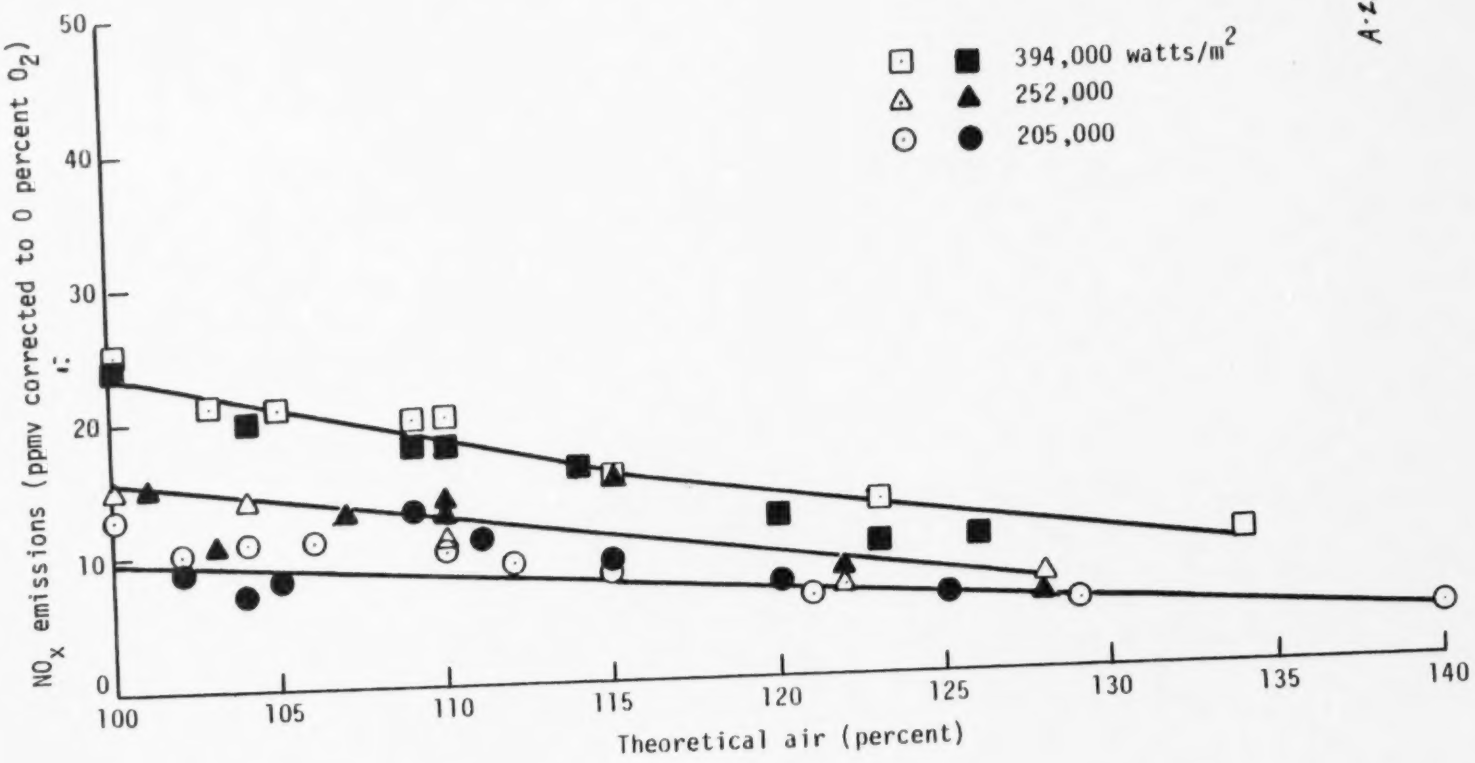

Figure 5-7. J-M burner NO_x emissions.

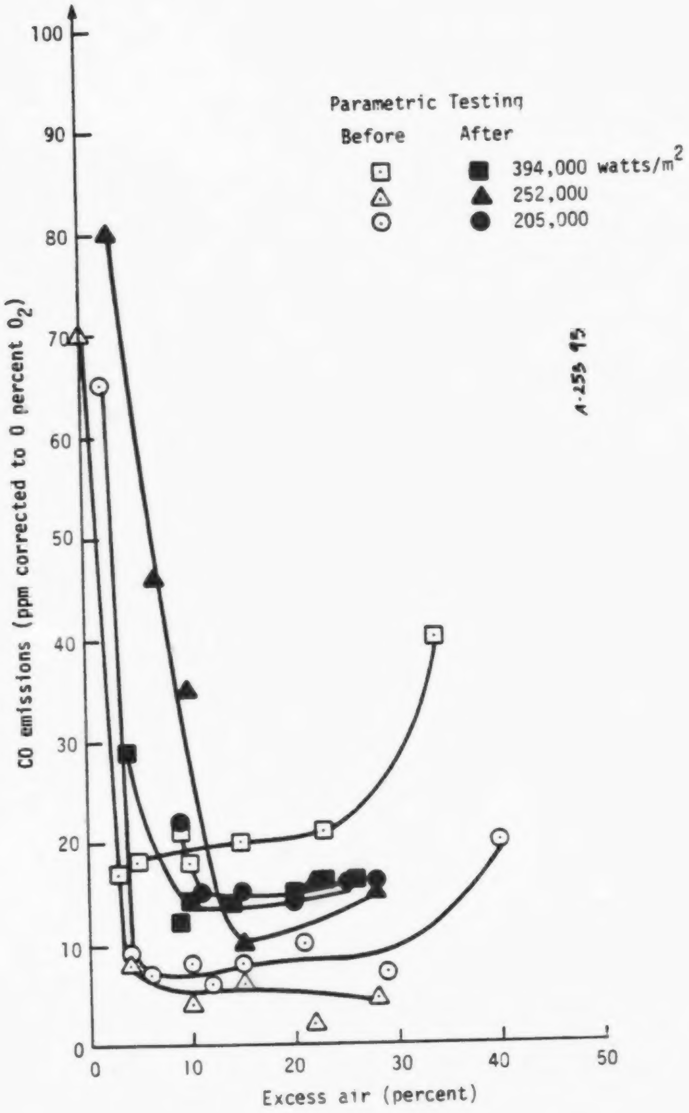

Figure 5-8. J-M burner CO emissions.

parametric tests before and after the 100-hour test, and Figures 5-9 and 5-10 show data trends during the 100-hour test.

The tests conducted on the Chemo-Thermic and Johns-Manville burners indicated that both burners had potential for commercial firetube boiler retrofit and were acceptable for testing in the prototype demonstration phase of the program. The NO_x emissions were below 20 ppm, burner performance was stable over the range of test conditions, and the 100-hour test showed the potential for long burner life. The discrepancy in NO_x emissions between the first two CTI burners and the last two tested indicated that burner uniformity can affect performance. Therefore, uniform burners had to be fabricated for best results in the prototype demonstration.

5.2 PROTOTYPE SYSTEM DESIGN

In a commercial firetube boiler, the fiber burner must operate safely and continuously and with low emissions with a unit efficiency equal to or better than that of the boiler with the conventional burner. Initial testing had shown that to achieve acceptable operation, the burner should have a uniform flow distribution through the fiber material with no potential for flashback.

For a fiber burner/boiler system that can be readily commercialized and marketed, the burner must be designed to require as few changes to the existing boiler as possible.

5.2.1 Design Method

To meet the stated criteria, several design features must be addressed. The method for achieving the burner design is described in the following sections.

5.2.1.1 Burner Surface Area

In the earlier development work, fiber burners had been found to operate with low emissions and high efficiency at 315,000 watts per m^2

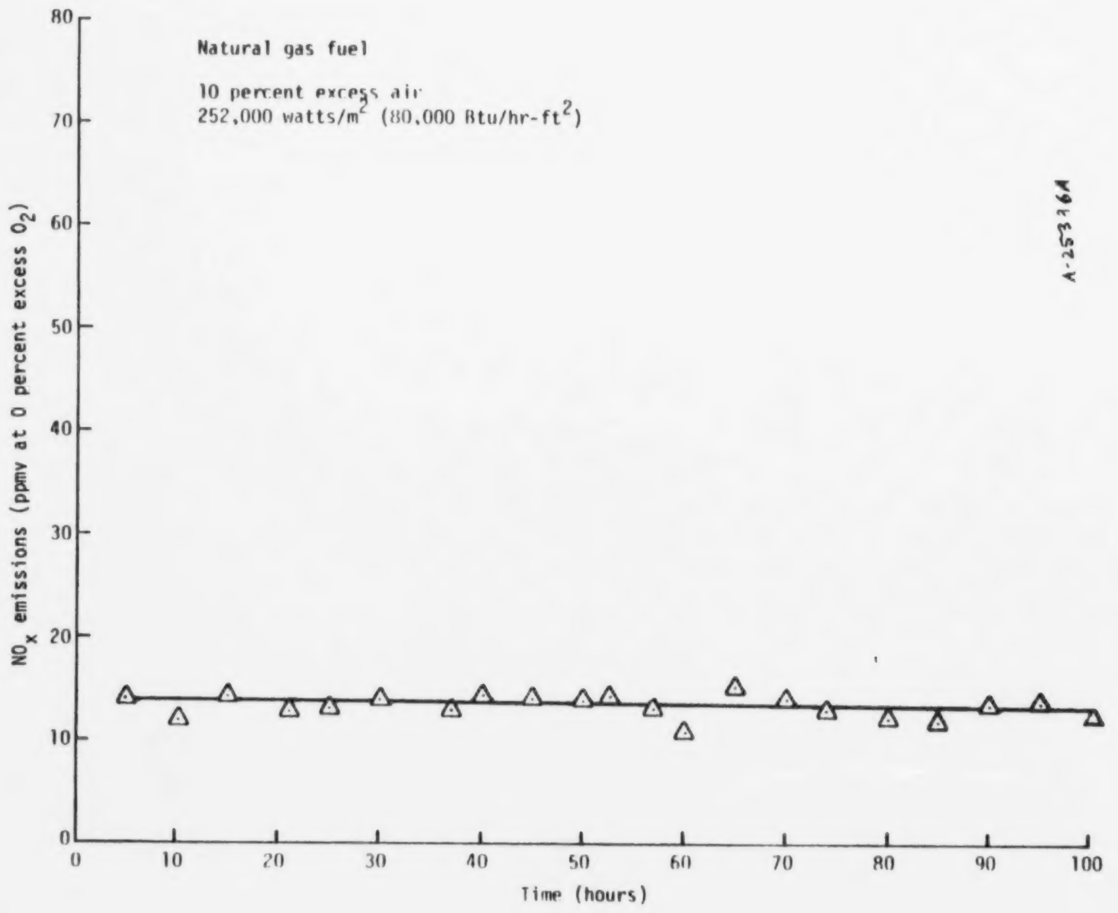

Figure 5-9. J-M burner 100-hour test NO$_x$ emissions.

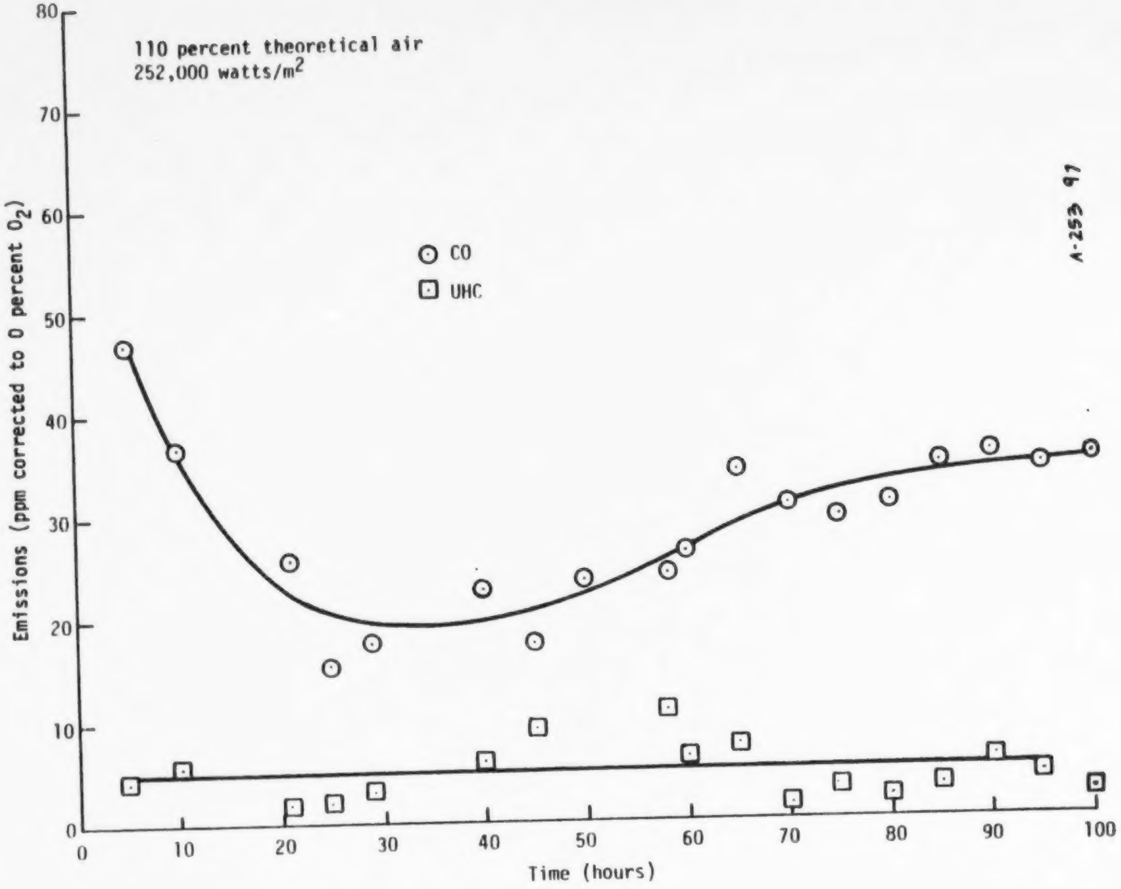

Figure 5-10. J-M burner 100-hour test CO and UHC emissions.

(100,000 Btu per hour per square foot) of burner surface. Therefore, burner surface area is determined by this optimum heat flux and the boiler heat rate according to the following equation:

$$\text{Surface area} = \text{Boiler rating} \div \text{Burner heat flux} \qquad (5\text{-}1)$$

5.2.1.2 Burner Shape

The firetube boiler burner is a cylinder closed on one end. While the surface area of the cylinder is set by the above equation, the length-to-diameter ratio depends on several factors:

- Combustion chamber size. The burner will have an L/D similar to that of the combustion chamber to achieve a sufficient burner surface area required by most boiler designs.
- Heat transfer. For uniform heat transfer, the burner must be designed with a high radiation shape factor between burner and firetube wall.
- Annulus width. The annulus between burner and firetube wall must be wide enough to accommodate the igniter and the flame sensor. A width of 3.8 cm (1.5 inches) is acceptable.
- Fabrication and handling. Handling during fabrication, curing, and installation must be considered. Because the fiber burner is somewhat fragile, handling must not be overly difficult. Special tools for handling and installing the burners are required.
- Structural strength. To cantilever the burner into the combustion chamber, the length-to-diameter ratio should not be greater than 15. The deflection should be less than 1 cm (0.4 inches), according to the following equation:

$$\delta = \frac{wl^4}{8EI} \qquad (5\text{-}2)$$

where w = material density
l = length
E = modulus of elasticity
I = moment of inertia of area
δ = deflection

5.2.1.3 Burner Support Design

a. Material

The burner support consists of the screen which supports the fiber layer and its attachment ring to the front boiler wall. The following criteria are used in the design. The material for the burner support screen is selected after considering the following:

- Thickness. The support screen must be thick to maximize structural strength, yet thin to minimize weight. The proper thickness can be devised by use of Equation (5-2) and the expression for the moment of inertia of a hollow cylinder with end cap:

$$I = \frac{\pi l(1 - f)w}{4}\left[(2rt - t^2)^2 + (2rt - t^2)l\right] + \pi r^2(1 - f)wt\left[\frac{r_2}{4} + l^2)\right] \qquad (5\text{-}3)$$

  where t is the support screen thickness, r is the cylinder outer radius, and f is the fraction of screen open area. Calculations for various thicknesses for a given length, radius, and material can be used to determine whether deflections are within 1 cm.

- Corrosion resistance. Since the burner slurry is mildly corrosive, a corrosion-resistant material should be used to prevent rusting. Stainless steel and epoxy- or zinc-coated carbon steel are acceptable.

- Perforations. The perforations in the screen should be small to prevent fibers from slipping through during forming. Also, small perforations help to maximize local velocity of gases which helps prevent flashback. The perforations should be close together to ensure good fiber packing. Materials that have been found acceptable include 16 to 18 wire mesh and perforated plate with 1.6 mm holes on 2.38 mm staggered centers.

b. Flashback Prevention

The burner system was designed to prevent flashback and minimize the volume of premixed fuel and air by:

- Blocking heat conduction into reactant stream. Heat conduction paths must be avoided in the burner design. Paths that are unavoidable should be insulated.
- Eliminating hot spots. A high radiation shape factor, smooth surface with no corners, and uniform burner thickness all help to prevent hot spots.
- Minimizing internal volume. A center body was designed to prevent buildup of combustibles inside the burner.
- Maximizing internal velocity. Small cross-sectional flow areas inside the burner were designed to keep the reactant gas velocity above the flame speed of the mixture.

c. Structural Strength

The design must allow for the burner to support itself, cantilevered into the firetube combustion chamber. To assure sufficient strength, the following should be considered:

- Length-to-diameter ratio -- should not be greater than 15
- Support material -- should be sufficiently stiff and strong
- Burner system deflection -- should be negligible

d. Leak Prevention

Preventing leaks of unburned gases minimizes unburned hydrocarbon and carbon monoxide emissions. In addition, no NO_x is formed as a result of blue flames issuing from leak holes. To prevent leaks, the burner system was designed to incorporate the following:

- Burner/support interface. The burner screen and internal filler and support structure are designed as a single unit to avoid connections that are difficult to seal. The burner is fabricated with an internal structure that remains as an integral part of the burner to further eliminate sealing needs.
- No joints, corners. The fiber matrix may not fully cover a sharp corner, and joints require sealing. Eliminating these reduces the possibility of leaks.
- Uniform fiber matrix thickness. Uniform thickness assures even flow distribution and eliminates the potential for breakthrough of CO and hydrocarbons.

e. Fabrication

The fiber burner must be able to be handled during fabrication and curing. Since the burner is fragile and contact should be avoided, a tool or handle should be used on the burner support.

5.2.1.4 Fiber Burner/Firetube Boiler Integration

Installation of the fiber burner into the firetube boiler required consideration of the following:

- Blower. Experience with the fiber burner has shown the pressure drop across the burner to be between 50 and 249 Pa (0.2 to 1 inch of water). Therefore, the blower may remain in place if it can provide more than approximately 373 Pa (1.5 inches of water). If not, then a new blower must be specified.

- Interface design. The existing burner flange and refractory ring may require alteration for burner mounting.
- Target ring. For boilers with first pass internals, they may be removed to allow a longer length burner.
- Installation tool. A tool should be designed to install the burner with minimum handling and to ensure the burner is centered in the combustion chamber.
- Igniter. The igniter may require redesign to extend sufficiently far into the firetube to reach the fiber surface.
- Back boiler plate. Increased insulation may be needed to reduce the back plate skin temperature, thereby reducing radiation losses.
- Gas train. For laboratory testing, the gas flow must be measured. Since the flowmeter introduces a large pressure drop, the natural gas must be at a higher pressure than that for which the conventional boiler was designed. Therefore, the original valves and regulators on the boiler gas train may have to be replaced with higher pressure parts. Note that changes to the gas train should not be required in field installations.
- Instrumentation. To provide test data, the boiler was instrumented with thermocouples, pressure taps, and an emissions probe.

5.2.2 Prototype Burner Description

Two burner systems were designed and tested for prototype demonstration in the York-Shipley boiler, one using the Johns-Manville burner and the other using Chemo-Thermic burners (subsequently purchased by Acurex).

5.2.2.1 The Fiber Burner

Table 5-1 lists the design specifications of Acurex and Johns-Manville burners. The J-M burner was tested first, and based on these tests, design

TABLE 5-1. FIBER BURNER SPECIFICATIONS

	Johns-Manville Burner	Acurex Burner
• Surface area	1.08 m^2 (11.6 ft^2)	1.07 m^2 (11.5 ft^2)
• Specific heat release rate at 100% load	285,000 watts/m^2 (90,350 Btu/hr-ft^2)	287,000 watts/m^2 (91,000 Btu/hr-ft^2)
• Burner dimensions	0.34 m dia by 0.91 m long (13.5 by 36 inches)	0.30 m dia by 1.07 m long (12 inches by 42 inches)
• Fiber matrix thickness	19.1 mm (0.75 inch)	12.7 mm (0.5 inch)
• End design	Flat	Rounded
• Burner screen	Not integrated with fiber matrix	Integrated with fiber matrix
• Screen material	20 gage stainless steel perforated sheet. 1.6 mm dia holes on 2.9 mm staggered centers, 41% open area	20 gage stainless steel perforated sheet. 2.0 mm dia holes, 11.5 holes per cm^2, 36.2% open area
• Blower	New blower	Original blower

changes were made to the Acurex burner including decreasing the burner diameter to allow more room for the igniter and increasing burner length to maintain high surface area. In addition, J-M burners are formed with no integral support screen, while Acurex burners are fabricated over a screen which becomes a permanent part of the burner. Since J-M burners had high CO and HC emissions, which could indicate leaks, treating the screen as an integral part of the burner provides less opportunity for leaking. Figure 5-11 shows the J-M burner for comparison to Figure 5-1.

Both screen materials performed satisfactorily. Each was selected to meet the requirements as discussed in the previous section, but material availability impacted the specific material selected.

5.2.2.2 The Burner System

Both Acurex and Johns-Manville burner systems were designed with a similar internal filler and support structure. The internal body was added to the structure following fabrication and resulted in gas path leaks in both burner systems as discussed in Section 5.3. The burner design with the Johns-Manville material is shown in Figure 5-12. The Acurex design is similar, but with shortened refractory ring and support ring to accommodate the larger burner. The J-M burner required a larger blower while the Acurex burner operated with the original boiler blower.

The blower air mixes with gas injected into four ports downstream of the blower. The premixed gas and air enter the burner and pass through the slots of the filler tube. The gases travel along the annulus, pass through the fiber matrix, and combust at the outer surface of the fiber layer. The fiber matrix is supported by a perforated metal cylinder. The center body, or filler tube, reduces the cross-sectional flow area to keep the gas and air mixture velocity well above the flame speed.

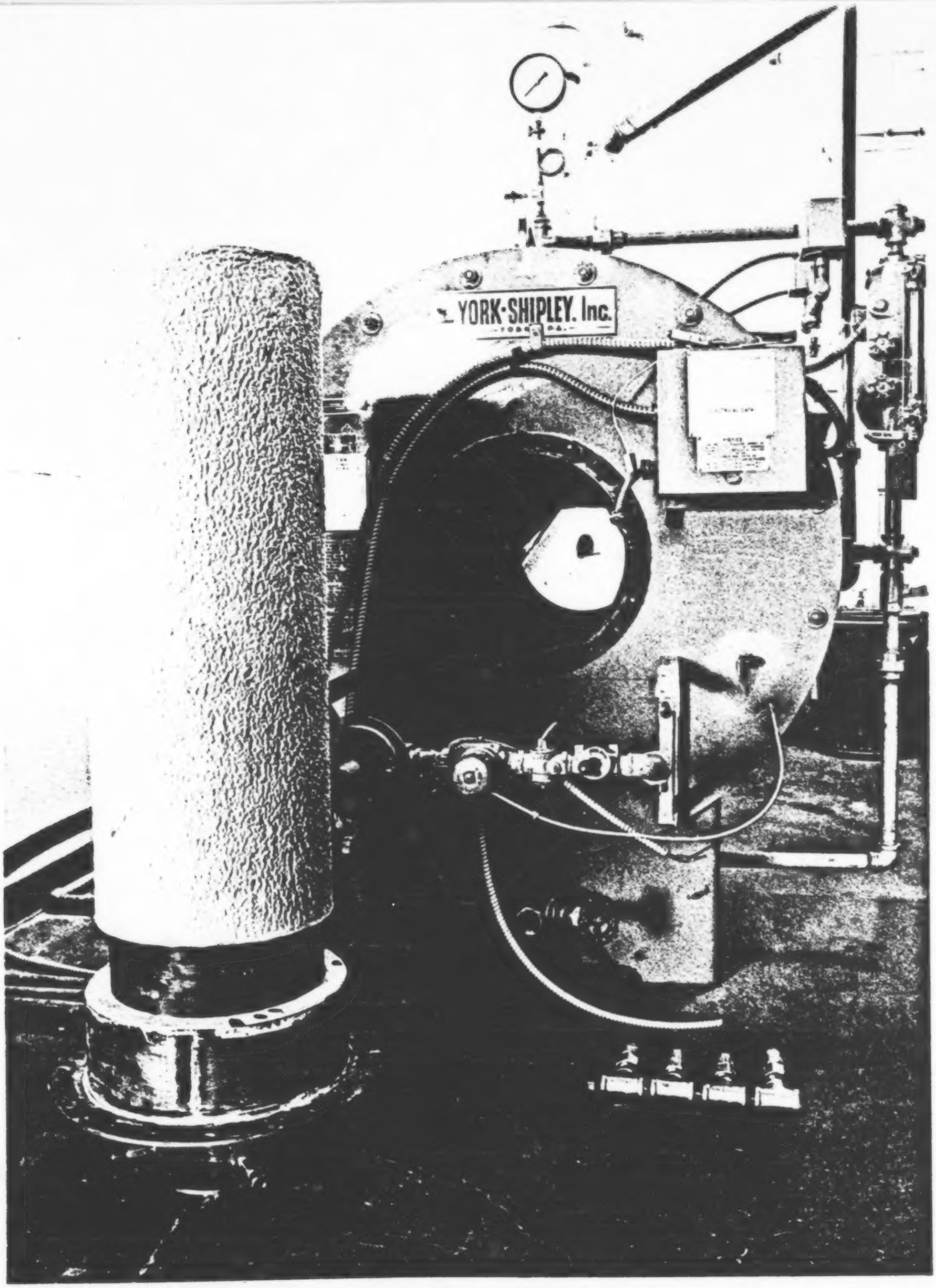
YORK-SHIPLEY, Inc.

Reproduced from
best available copy.

Figure 5-11. Firetube boiler with J-M burner.

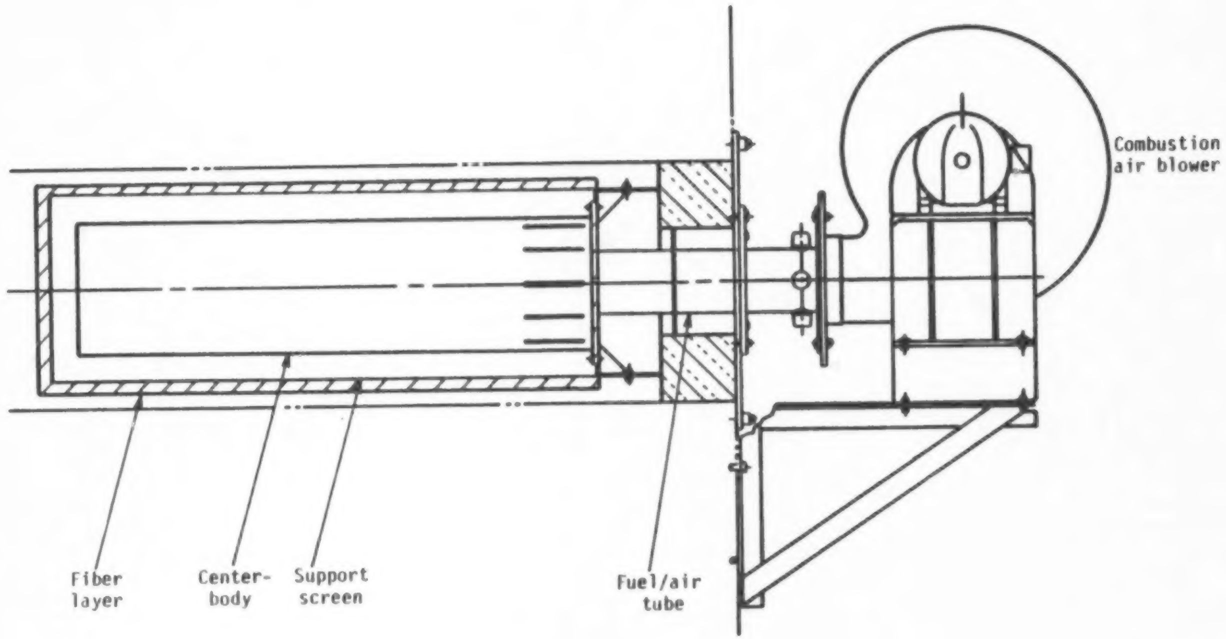
Combustion air blower
Fiber layer
Center-body
Support screen
Fuel/air tube

Figure 5-12. Firetube boiler fiber burner assembly.

5.2.2.3 Retrofit Hardware

The retrofit requirements for the Johns-Manville fiber burner and the Acurex fiber burner were somewhat different. The following sections briefly describe each design.

Blower

Since the pressure drop of the Johns-Manville burner was 747 to 995 Pa (3 to 4 inches of water) compared to about 249 Pa (1 inch) for the conventional burner, a larger blower was needed for combustion air. The Acurex burner had a pressure drop similar to the conventional burner and could use the original blower.

Interface Design

Hardware downstream of the blower included a gas mixing spool with four gas injectors aligned perpendicularly to the flow stream. The same spool was used for both J-M and Acurex burners and was bolted to the front boiler plate. The plate also supported the refractory ring which was modified to take up less space and provide instrumentation ports. The original refractory ring provided flame anchoring for the conventional burner with a conical form, which was not needed for the fiber burners. Since the Acurex burner was 15.2 cm (6 inches) longer than the J-M burner, the refractory ring was shortened.

Also bolted to the front plate of the refractory plug and cantilevered inside the boiler was the burner support spool. The burner slipped over the spool, and the burner collar bolted to the cylindrical spool. Inside the burner was the filler tube used to reduce the internal volume.

Igniter

To reach the burner surface with the pilot for ignition, a spark plug with a 46 cm (18 inch) extension was used. The spark plug was placed in a

46 cm long tube through which the pilot gas flowed and ignited at the spark. The igniter was the same for both burners and was wired and plumbed into the original boiler pilot system.

Installation System

A system was built to install the fiber burners in the boiler without contacting the firetube walls (that could potentially damage the burners). The installation system supported the burner system from the inside, and was mounted on wheels. The burner could then be rolled into the firetube chamber, centered, and bolted into place. The installation system was then disconnected from the burner and removed.

5.2.2.4 Test Hardware

Precise gas measurements were needed for boiler testing, and flow controls required a higher gas pressure than supplied with the conventional boiler system. Therefore, for all boiler testing (including the conventional burner testing), the pressure regulators and solenoid valves which were rated at inches of water pressure were replaced with parts rated at several pounds per square inch pressure. The commercial fiber burner system would not require these modifications.

Five thermocouples were welded to the firetube wall at approximately 25.4 cm (10 inch) intervals along the bottom of the firetube. Measurements were:

- Gas temperature at the viewport at the boiler back end
- Steam temperature at the steam outlet of the boiler
- Gas temperature at the entrance to the second pass, out of view of the fiber burner
- Flue gas temperature at the exit of the boiler
- Ambient temperature

Two pressure taps, one situated downstream of the blower and the other at the flue gas exit, were used to measure gas side pressure drop through the boiler. An exhaust gas sampling probe was installed at the flue gas exit from the boiler, and CO_2, O_2, CO, HC, and NO_x measurements were made.

5.3 TEST RESULTS

The boiler was tested on natural gas with the conventional gas burner (original), the Johns-Manville fiber burner, and the Acurex fiber burner over a range of load conditions and excess air levels. The load conditions were 50, 68, 80, 100, and 120 percent of full input load (1106 MJ/hr), and stoichiometry was varied from 0 to 50 percent excess air. The Acurex fiber burner was then selected for a 1000-hour durability test conducted at 15 percent excess air and 100 percent load.

Of the three burners tested, the Acurex burner had the lowest NO_x emissions while maintaining low CO and UHC emissions. A comparison of the three burners' results is shown in Table 5-2. Nominal operating conditions are defined as the highest boiler load (up to the design heat rate) and the lowest excess air level achievable before CO breakthrough. As shown, the Acurex burner had the lowest nominal excess air level of the three burners, at 10 percent. The Acurex burner also had the highest boiler efficiency (82.6 percent) as a result of both the low excess air level and a lower flue temperature. The complete data are given in Tables A-10 to A-12.

NO_x emissions for the three burners at 80 percent load are shown in Figure 5-13. The Acurex and J-M fiber burners are very similar; both reduce NO_x approximately 80 percent compared with the conventional burner. Figures 5-14 and 5-15 show the NO_x emissions versus excess air of the J-M and Acurex fiber burners, respectively, at various boiler loads, each in comparison with the conventional burner NO_x emissions. The Acurex burner was tested at loads higher than the boiler rating, but the NO_x emissions remained less than 25 ppmv.

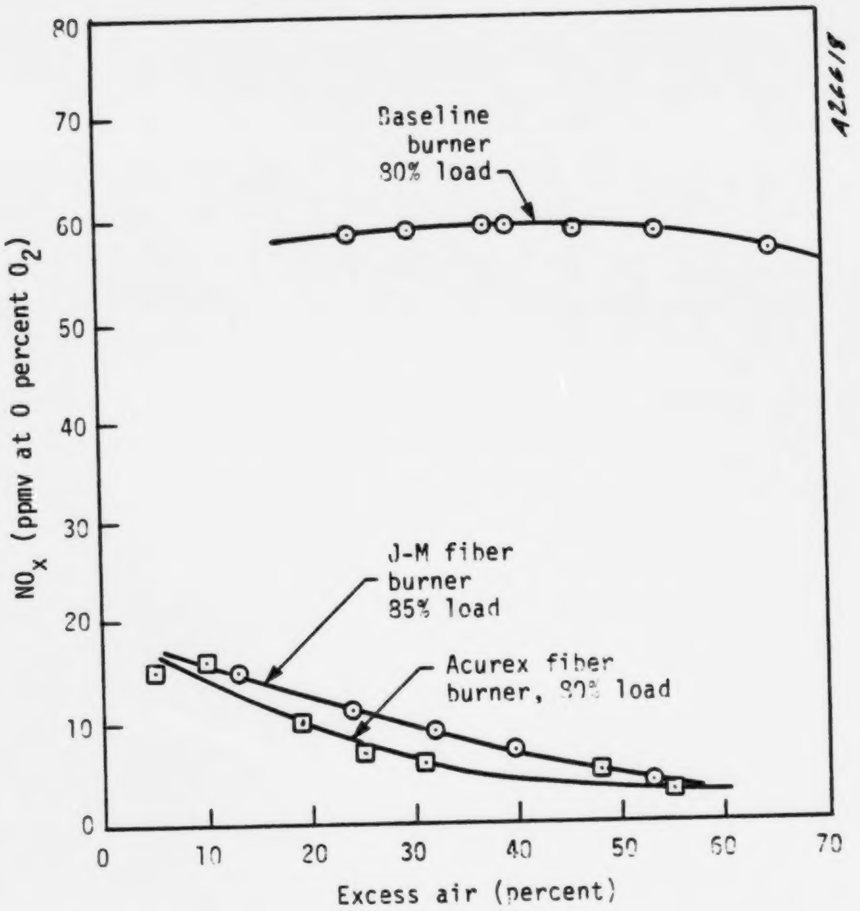

Figure 5-13. Firetube boiler NO$_x$ emissions.

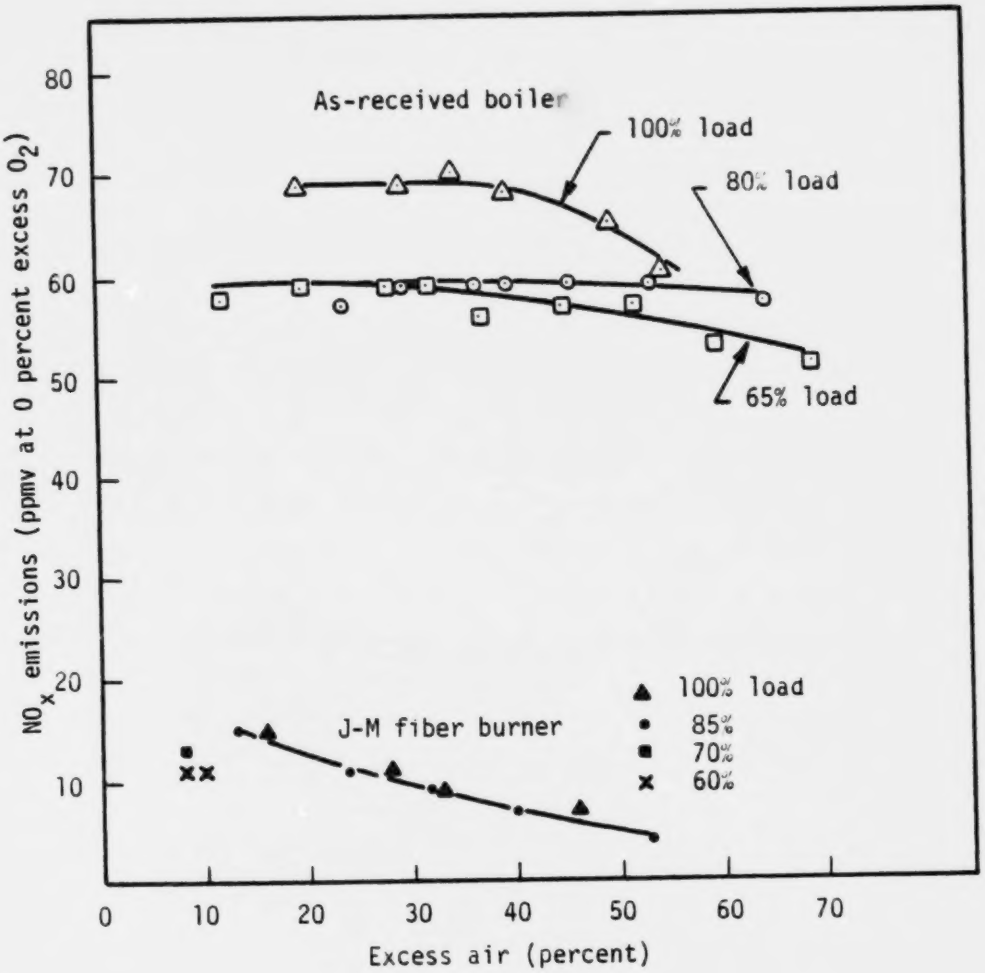

Figure 5-14. Firetube boiler with J-M burner NO$_x$ emissions at various boiler loads.

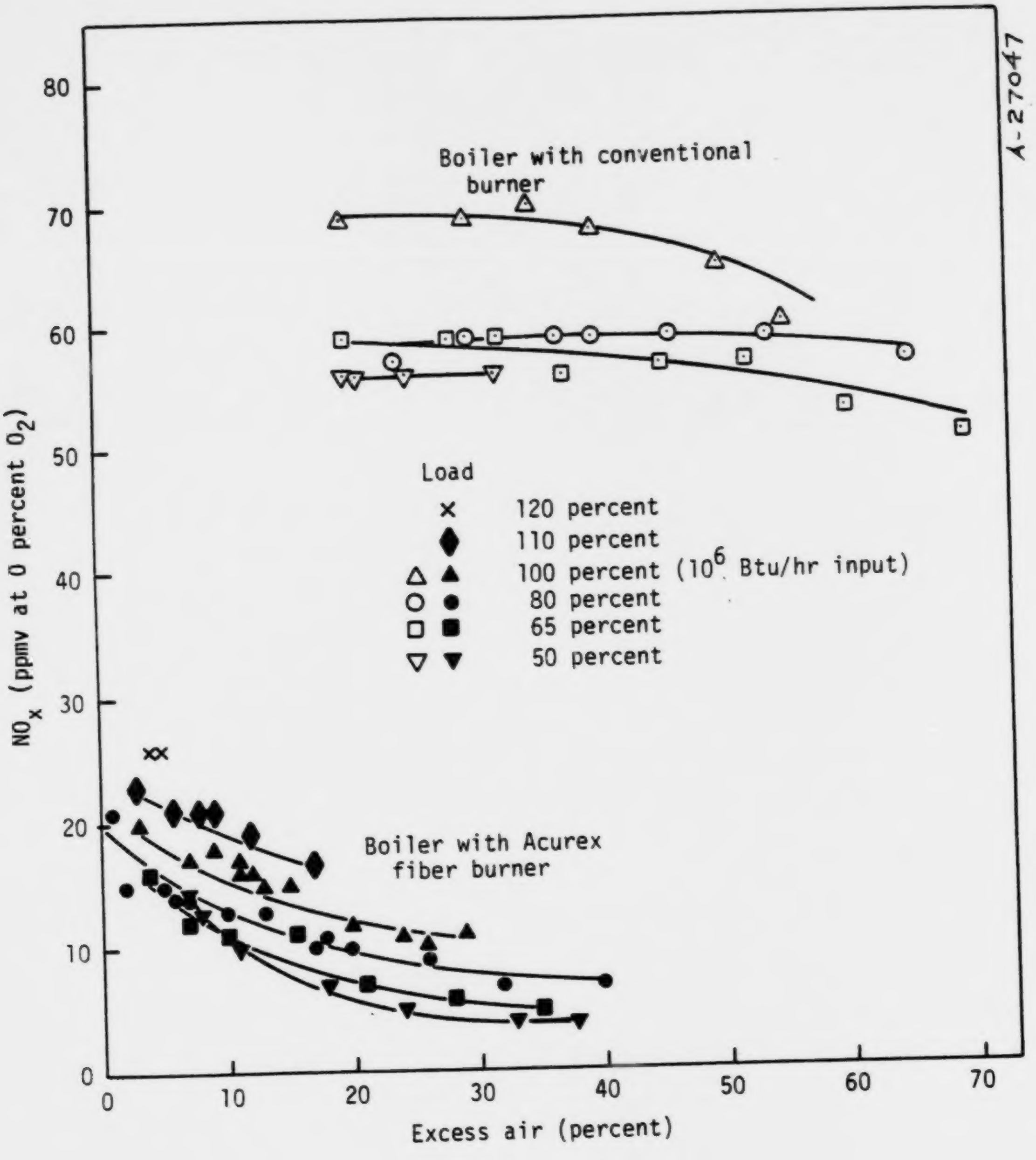

Figure 5-15. Firetube boiler with Acurex burner NO_x emissions at various boiler loads.

TABLE 5-2. BURNER PERFORMANCE DATA

	Conventional Burner	Johns-Manville fiber burner	Acurex fiber burner
● Nominal operating conditions			
- Percent full load	100	100	100
- Excess air, percent	30	15	10
● At nominal operating conditions			
- Emissions, ppmv at zero percent excess air			
NO_x	69	15	17
CO	31	40	22
UHC	~10	150	22
● Efficiency, percent, by ASME Heat Loss Method	80.9	81.8	82.6
● Pressure drop, Pa (inches of water)	149 (0.6)	1045 (4.2)	246 (0.99)

Figure 5-16 shows the carbon monoxide emissions for the three burners. The curves clearly show the point where CO begins to break through. The Acurex fiber burner can operate as low as 10 percent excess air before breakthrough, whereas the Johns-Manville burner has breakthrough at about 15 percent excess air, and the conventional burner at 30 percent excess air. Operating close to stoichiometric conditions is desirable from a boiler efficiency standpoint.

Figure 5-17 shows the unburned hydrocarbon emissions versus excess air at full load. The conventional burner results indicate UHC breakthrough at 15 percent excess air whereas the Acurex fiber burner has low UHC emissions very close to stoichiometric. The high UHC levels of the J-M burner indicate a leak in the burner seal.

Boiler efficiency (Figure 5-18) was calculated by the ASME Heat Loss Method in which the losses are primarily at the stack. At nominal operating conditions, the Acurex fiber burner increased boiler efficiency 1 to 2 percent over the conventional boiler. This efficiency improvement translates to a $682 savings per year (1982 dollars) for this 245,000 watt boiler at full load, operating 80 percent of the time. At loads higher than rated capacity, the Acurex fiber burner demonstrated the ability to maintain efficiency comparable to that with the conventional burner operating at one-third lower load.

The fiber burner increased the back boiler plate skin temperature from 450K (350°F) to about 644K (700°F) in an area local to the end of the first boiler pass. This temperature increase causes minor energy losses due to convection and radiation. York-Shipley engineers, however, are confident that increasing the back plate insulation thickness would drop the temperature and decrease the energy losses.

The parametric tests showed that using retrofit fiber burners can reduce NO_x by 80 percent or more over the conventional burner. Furthermore, the Acurex fiber burner appears attractive over the Johns-Manville burner due to:

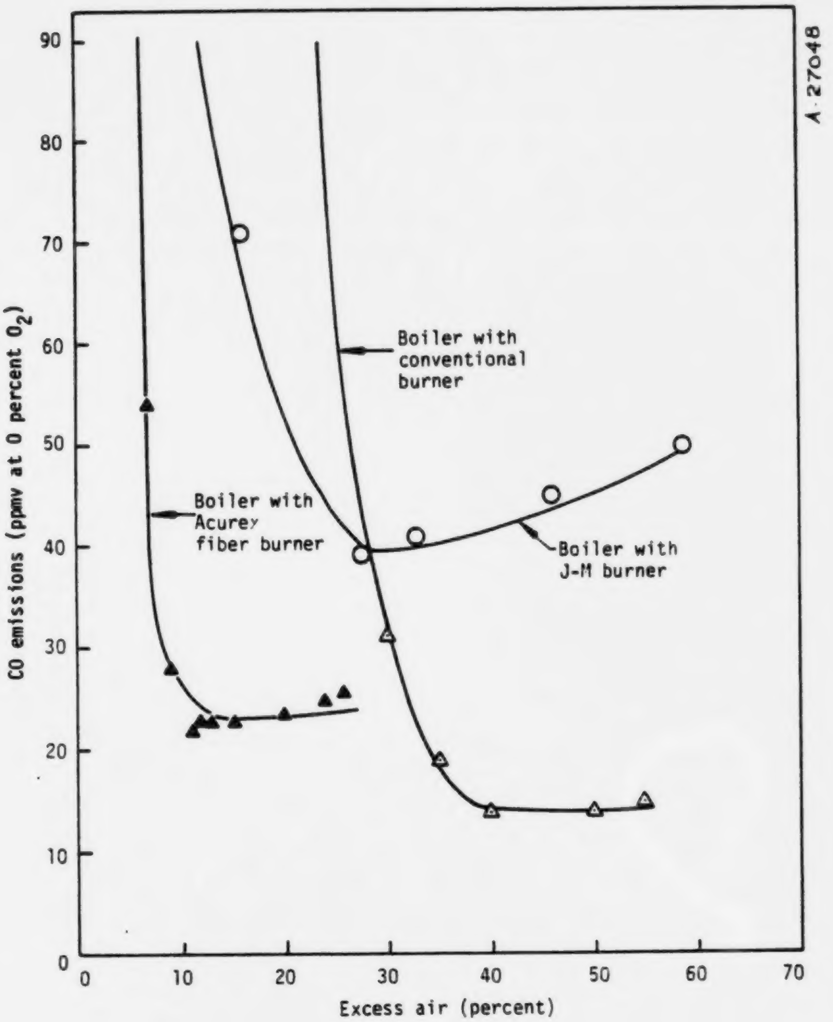

Figure 5-16. Firetube boiler CO emissions versus excess air at 100 percent boiler load.

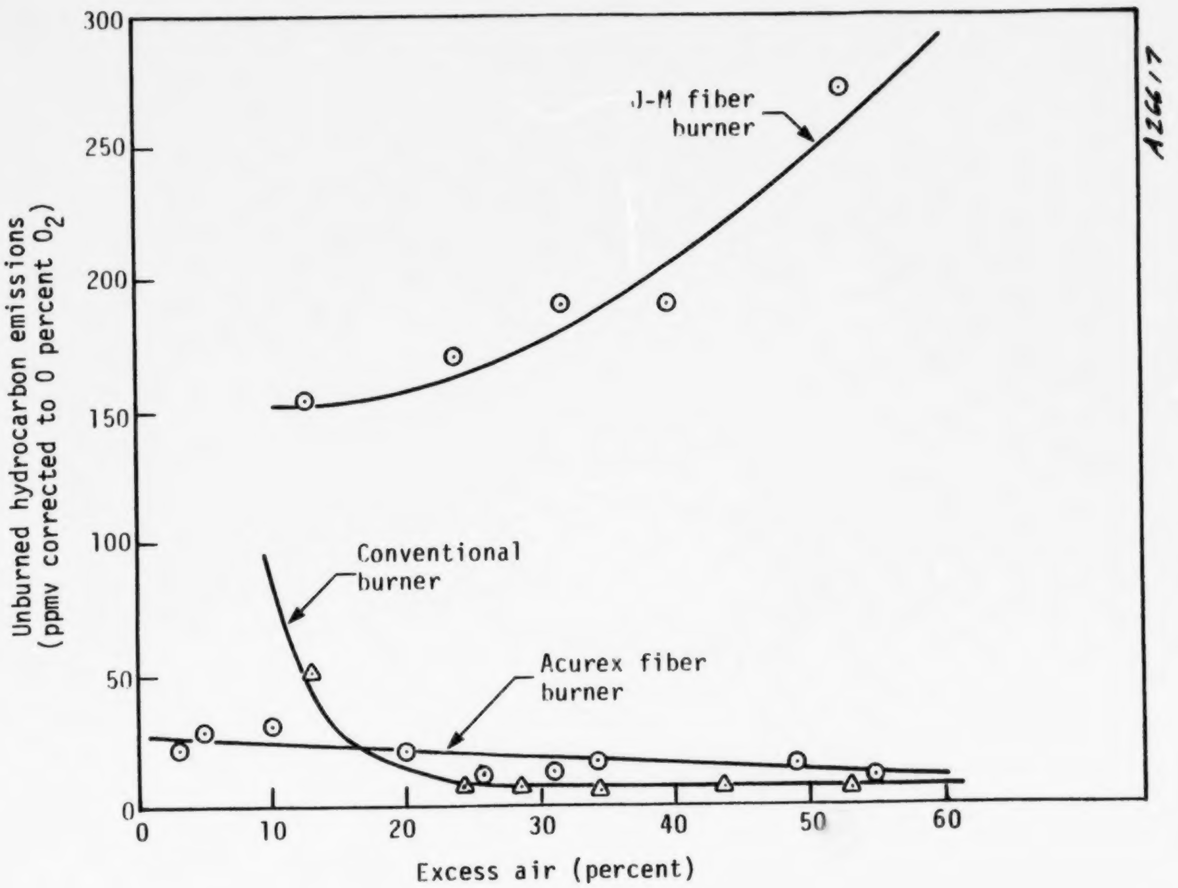

Figure 5-17. Firetube boiler UHC emissions at 100 percent boiler load.

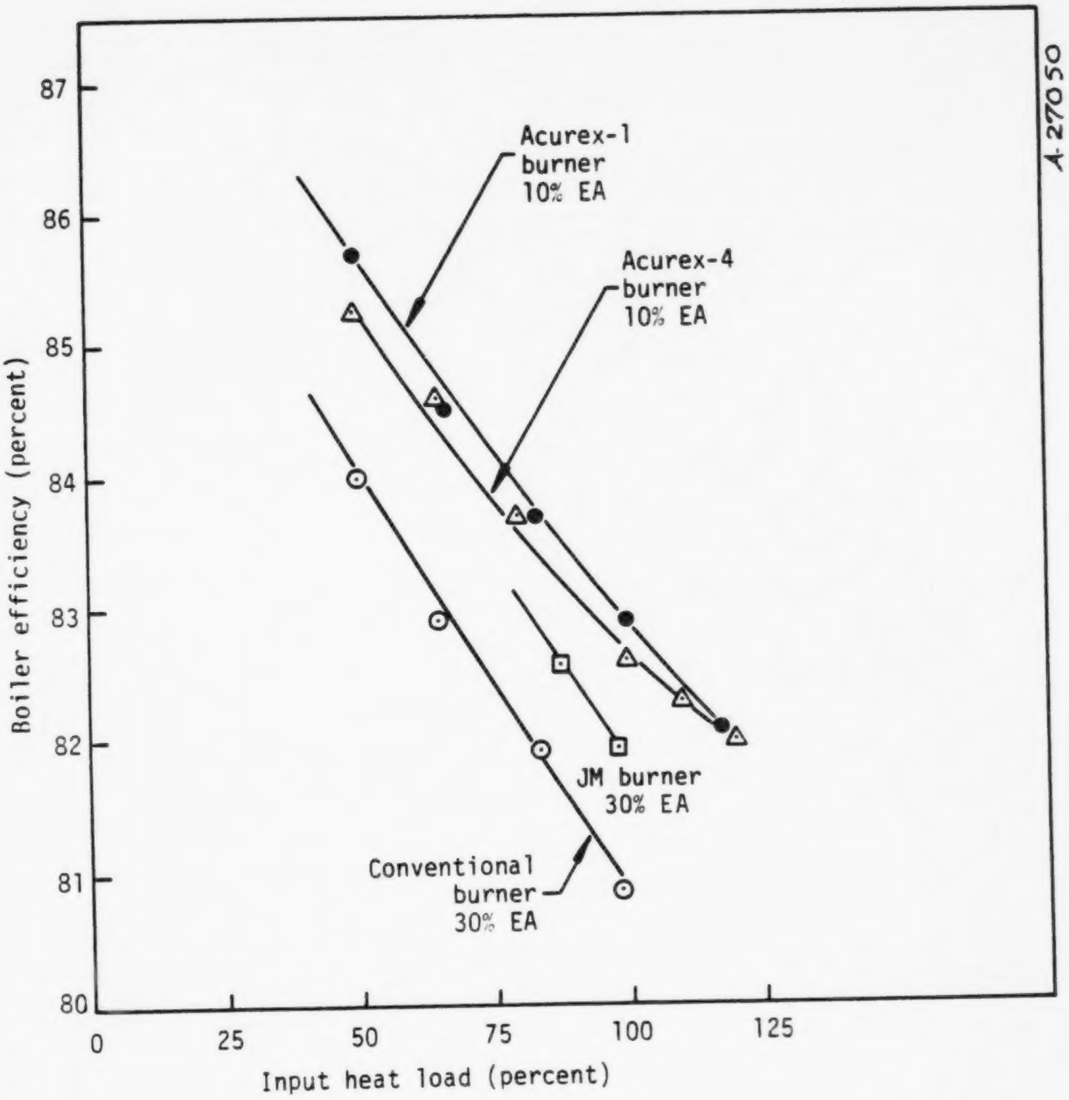

Figure 5-18. Firetube boiler efficiency versus heat load.

- Lower pressure drop
- Better opportunity to seal burner and support, since screen is integral part of burner
- Greater design flexibility (size and shape)
- No evidence of failure as with J-M burner (rupture in burner end cap)

Therefore, of the three burners tested, the Acurex fiber burner was considered the best performing burner and was selected for the 1000-hour durability test.

During the durability test, the boiler was run for a total of 1020 hours and had 14 on/off cycles. Most of the testing was done at conditions of 100 percent load and 15 percent excess air.

As shown in Figure 5-19, NO_x and CO emissions remained steady throughout the test at 13 ppmv and 29 ppmv corrected to zero percent excess air. Boiler efficiency was constant at just over 82 percent. The unburned hydrocarbons, however, slowly increased throughout the test. UHC were initially 23 ppmv, and rose to 166 ppmv after 1020 hours. Boiler front end emissions probing indicated that the cause of the increasing UHC emissions was an imperfect seal at the burner collar which slip-fit over the cylindrical support structure. The sealing material held a seal only to about 533K (500°F), and as the test continued the material slowly burned away, leaving passages through which unburned fuel could escape.

The front end probing was done with a stainless steel tube inserted through a port in the refractory plate. Emissions were measured at intervals of 2.5 cm (1 inch) from the front boiler plate. As shown in Figure 5-20, high UHC levels (hundreds of ppmv) were encountered near the collar/support structure seal. The emissions decreased to 5 ppmv as the probe was moved in along the side of the burner, indicating that true burner emissions were much lower than those measured in the stack.

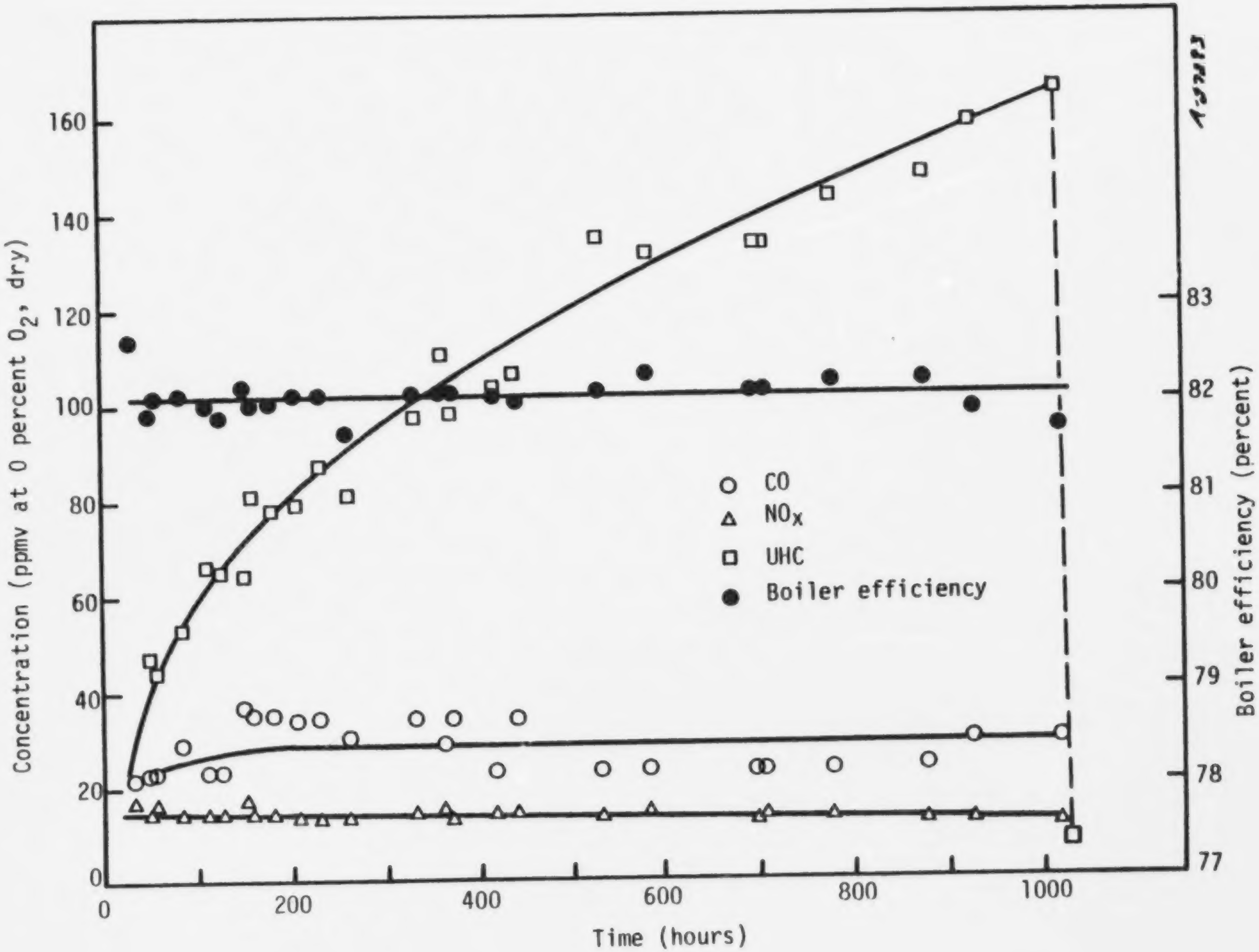

Figure 5-19. Firetube boiler durability test emissions and efficiency.

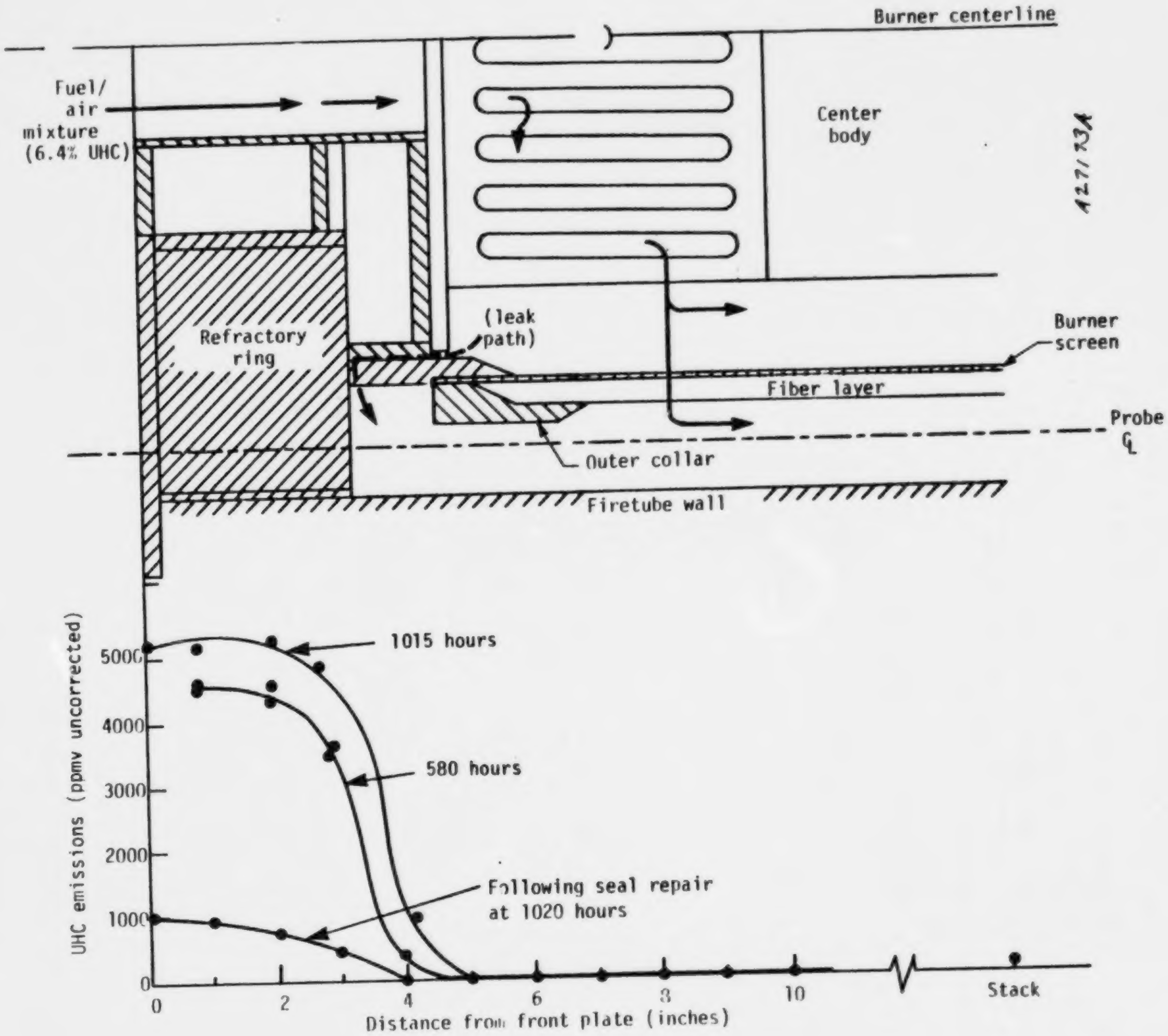

Figure 5-20. UHC emissions versus distance from front boiler plate.

Following the durability test, the burner was removed for inspection, and the seal at the front flange repaired. The burner was then reinserted and test data were obtained giving the lower hydrocarbon emissions of Figure 5-20. The leak was apparently reduced but not totally gas tight. Even with the partial leak indicated, stack gas concentrations were reduced to 10 ppm hydrocarbons, as indicated in Figure 5-19.

The unburned gases escaping at the collar probably were pushed against the cold firetube wall and allowed to pass through unreacted. At the end of the first pass, the gases were then mixed together, resulting in the high UHC levels in the stack. A flanged connection or a solid unit without flanges would solve this leak problem. UHC emissions should then be at the expected level of about 5 ppm.

Following 1020 hours of testing, inspection of the burner revealed several areas where partial degradation had occurred. The closed end of the cylinder had a spotted appearance as shown in Figure 5-21, apparently caused by local sintering of fibers at the surface. This area of the burner viewed the insulated boiler back wall, running at temperatures of 811K (1000°F) or more. This hot surface effectively limited radiation transfer away from the burner end and caused the fiber surface temperature to correspondingly operate at higher levels than would be experienced by more active cooling (such as toward the firetube wall). As time of operation progressed, the higher fiber surface temperatures caused local degradation of the material by sintering. The sintered material, however, did not apparently cause any negative effects on performance or emissions. Burner designs incorporating an inactive cylinder end may be more appropriate for dry-back boiler applications.

The material on the cylindrical surfaces, however, appeared very similar to its original condition with a uniformly gray, smooth surface. Two localized areas of the surface were changed, however. At the aft end of the cylinder on one side, erosion of the fibers by the gas stream apparently occurred. This whitish appearing area can be seen in Figure 5-22. Fibers were also

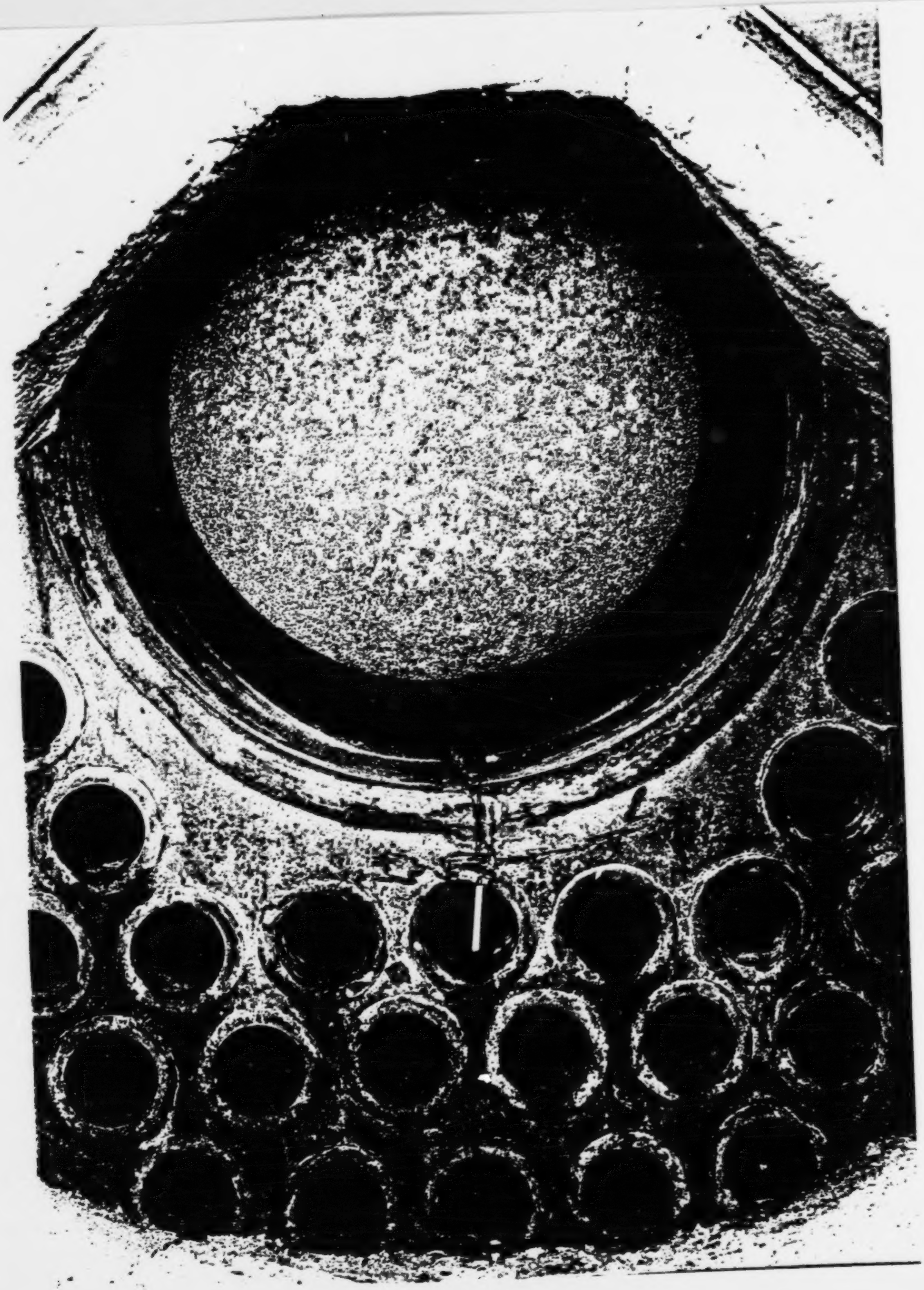

Reproduced from
best available copy.

Figure 5-21. Fiber burner end following 1020-hour durability test.

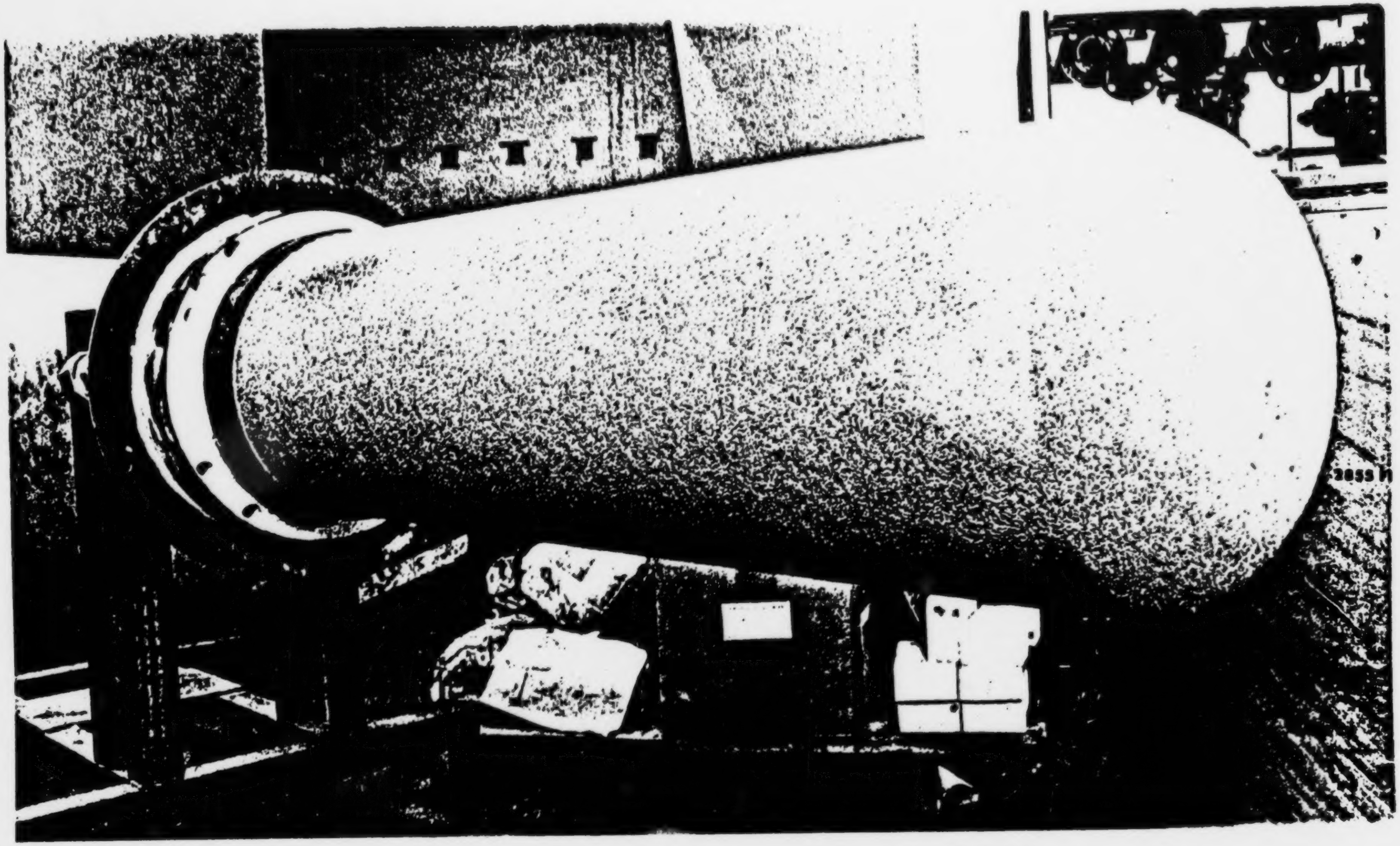

Figure 5-22. Fiber burner following 1020-hour durability test.

found deposited on the aft end of the boiler. The quantity was not significant, however, and should not cause limitations in the burner life. Closer centering of the burner within the firetube may be required to alleviate the problem.

Also, toward the burner front end (at the support collar), several cracks in the fiber layer were apparent. These cracks may have resulted from thermal expansion of the collar during operation or from handling. Future design and installation would require consideration of these features.

The demonstration of the prototype firetube boiler showed that the Acurex burner, with a 90 percent reduction in NO_x, is indeed a low NO_x system. Furthermore, as the burner reduces NO_x, CO and UHC emissions are also low, allowing lower excess air operation and increased boiler efficiency. The burner was retrofitted into a commercial firetube boiler, demonstrating that it can be used in commercial systems. The fiber burner operated successfully for 1000 hours, making the next step toward commercialization a field demonstration of longer duration.

REFERENCE FOR SECTION 5

5-1. Merrick, E. B., et al., "Development of a Low NO_x Burner for Gas-Fired Firetube Boilers," Proceedings of the 1981 International Gas Research Conference, pp. 964-974, published by Government Institutes, Inc., Rockville, MD, February 1982.

SECTION 6

WATERTUBE BOILER

6.1 INTRODUCTION

A radiative catalyst/watertube boiler has been developed as a prototype to small industrial sized boilers. The operating criteria for this system were to demonstrate near-stoichiometric combustion of gaseous and distillate fuels with controlled catalyst surface temperatures, to achieve less than 20 ppmv of thermal NO_x at 110 percent theoretical air with an overall combustion efficiency greater than 99.9 percent, and to yield low fuel NO_x emissions by staged combustion in a rich/lean configuration.

A representation of the system concept is shown in Figure 6-1. A stoichiometric fuel/air mixture is fed to the radiant section which contains a close-packed array of catalyst-coated ceramic tubes and watertubes. The tubes are arranged in either a nonconcentric or concentric fashion as shown in Figure 6-2. The mixture is partially combusted on the catalyst surface which is kept at a temperature of 1256K to 1589K (1800°F to 2400°F) by radiation heat transfer to the watertubes. The combustion products, air, and remaining unburned fuel from the radiant section are passed to a downstream catalytic adiabatic combustor to complete the combustion reactions. In the case of staged combustion for fuel NO_x control with high nitrogen content fuels, secondary air is injected prior to the adiabatic combustor. A final convective section extracts energy from the fully combusted gases. Both catalyst sections operate well below the maximum use temperature of the catalyst substrate materials -- the radiative section by radiative cooling and the adiabatic section by dilution of the fuel/air mixture with exhaust products from the radiative section.

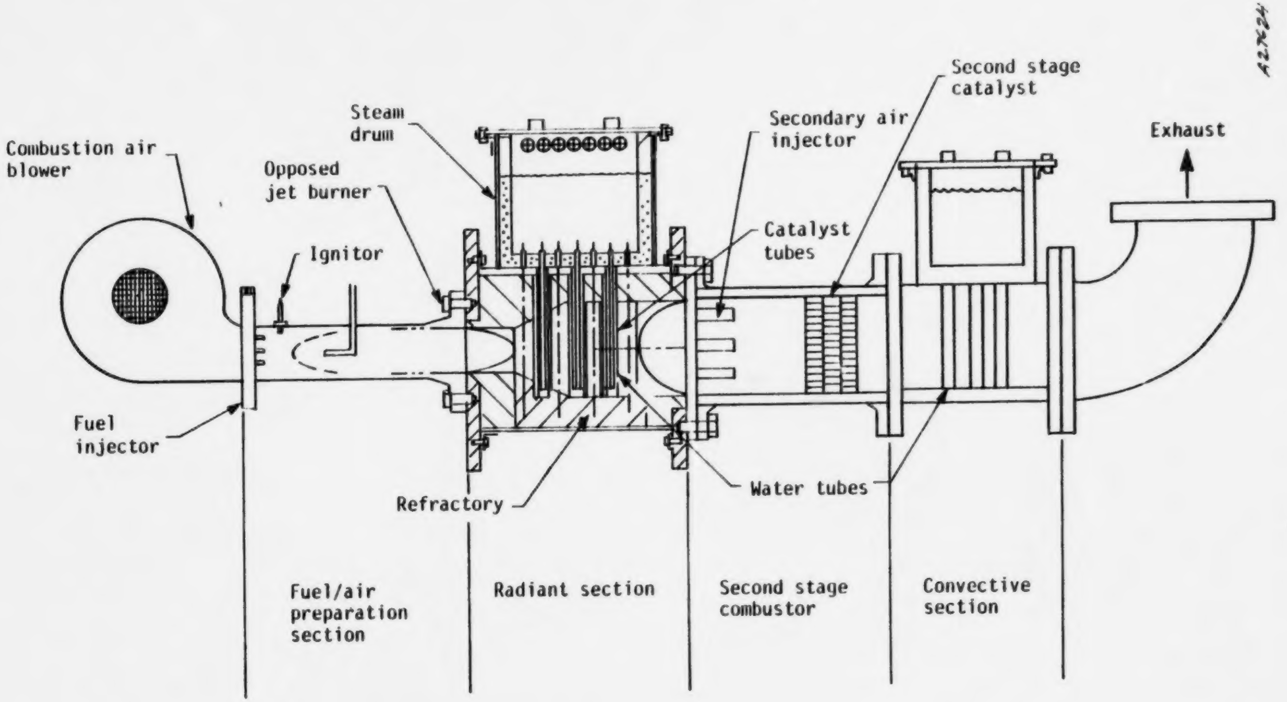
A2K24
Combustion air blower
Steam drum
Opposed jet burner
Ignitor
Secondary air injector
Second stage catalyst
Exhaust
Catalyst tubes
Fuel injector
Refractory
Water tubes
Fuel/air preparation section
Radiant section
Second stage combustor
Convective section

Figure 6-1. Catalytic watertube boiler schematic.

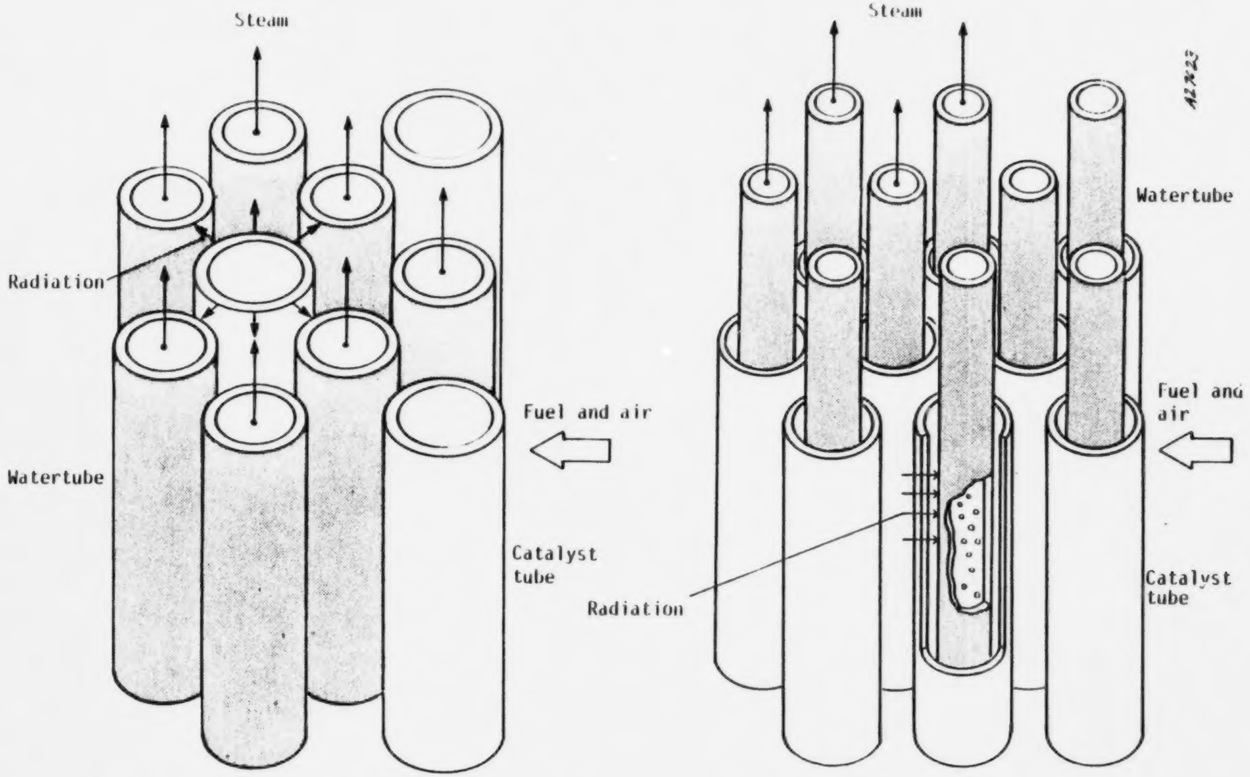
Steam
Radiation
Watertube
Fuel and air
Catalyst tube
Steam
Watertube
Fuel and air
Catalyst tube
Radiation
A2K23

A. Nonconcentric tubes

B. Concentric tubes

Figure 6-2. Catalytic watertube boiler radiant section tube arrangements.

The development of the catalytic watertube boiler system has been conducted through testing of a series of radiant section designs. The various designs tested are shown in Table 6-1. The systems have been scaled from 211 MJ/hr (200,000 Btu/hr) to 1055 MJ/hr (1×10^6 Btu/hr) design heat inputs. In addition to the scaling of heat rates, the two different watertube/catalyst tube arrangements have been tested. Tests of systems 1, 2, and 3 were reported in References 6-1 to 6-3.

Early testing at a subscale heat release rate of 211 MJ/hr (Reference 6-1) used a nonconcentric radiant section arrangement with catalyst tubes spatially separate from watertubes. Thermal NO_x emissions were very low, never exceeding 2 ppmv, and radiant section efficiency (excluding downstream adiabatic combustion and convective heat exchange) was 37 percent. As expected, combustion efficiency for the radiant section alone did not meet the 99.9 percent goal. In addition, the exposed watertube surfaces provided the potential for fouling when operated with distillate or residual fuel oils.

To permit operation with liquid fuels and improve combustion efficiency, a concentric tube design was developed. In this arrangement, the watertube is located within the catalyst tube, separated by a small air gap. Thermal energy generated on the catalyst tube outside surface is transferred by conduction to its inner surface and by radiation across the air gap to the watertube. Early tests of the concentric watertube/catalyst arrangement resulted in a combustion efficiency of 93 percent. However, increases in combustor operating temperature due to increased gas phase reactions surrounding the tubes caused fracturing of the ceramic catalyst tubes. This problem was resolved by using high strength, high thermal conductivity silicon carbide tubes.

Several concentric tube radiant section geometries were tested for combustion efficiency and thermal NO_x emissions. Results for a graded, concentric tube arrangement were reported in Reference 6-2. Excessive flameholding off the front cylinder rows in the graded design produced moderate levels of thermal NO_x (30 to 55 ppmv for 115 to 100 percent theoretical air, respectively). The flameholding became more severe with

TABLE 6-1. HISTORICAL DEVELOPMENT OF CATALYTIC WATERTUBE BOILER

System Number	Design Features	Boiler Capacity MJ/hr (Btu/hr)	Substrate/Catalyst	Fuels Tested	Major Experimental Results
1	• Nonconcentric tubes • 1.3 cm (1/2 inch) OD catalyst tubes and watertubes • Water-cooled, no steam generation	211 (2×10^5)	• Coors alumina/Acurex noble metal • Coors alumina/cobalt oxide	Natural gas, propane	• 37 percent combustion efficiency • 2 ppm NO_x
2	• Concentric tubes • 1.9 cm (0.75 inch) OD catalyst tubes, 0.95 cm (0.375 inch) OD watertubes • Water-cooled, no steam generation	211 (2×10^5)	• McDanel Refractory alumina/UOP noble metal • Coors alumina/Acurex noble metal	Natural gas, propane	• 93 percent combustion efficiency • <10 ppm NO_x • Severe tube cracking • Flameholding
3	• Concentric tubes • 1.9 cm (0.75 inch) OD catalyst tubes, 0.95 cm (0.375 inch) OD watertubes • Water-cooled, no steam generation	264 to 475 (2.5×10^5 to 4.5×10^5)	• Norton silicon carbide/chromium oxide	Natural gas, diesel fuel	• 99.9 percent combustion efficiency • <20 ppm NO_x • Flameholding and combustion along the walls • Catalyst tube cracking
4	• Concentric tubes • 3.8 cm (1.5 inch) OD catalyst tubes, 2.2 cm (0.875 inch) OD watertubes • Natural circulation steam boiler	1055 (1×10^6)	• Norton silicon carbide/nickel oxide • Norton silicon carbide/chromium oxide	Natural gas	• >99 percent combustion efficiency • 30 ppm NO_x • Catalyst tube cracking
5	• Nonconcentric tubes • 2.5 cm (1.0 inch) OD catalyst tubes, 2.2 cm (0.875 inch) OD watertubes • Natural circulation steam boiler	1055 (1×10^6)	• Bolt Technical Ceramic alumina/UOP noble metal	Natural gas	• 85-98 percent combustion efficiency • 30-120 ppm NO_x at 20 percent excess air • Some tube fracturing

increased throughout and preheat temperature, resulting in tube surface temperatures in excess of 1922K (3000°F).

In the later phases of development, work continued on establishing a concentric combustor section geometry which operated with lower catalyst tube surface temperatures and thermal NO_x emissions. A nongraded tube geometry (compared with the graded tube geometry in Figure 6-3) was tested under operating conditions similar to the graded tube geometry. A comparison of thermal NO_x data in Figure 6-4 indicated a two-fold reduction between 80 and 130 percent theoretical air. At 110 percent theoretical air and 264 MJ/hr (250,000 Btu/hr) heat release rate, values of thermal NO_x averaged less than 20 ppmv. The data are described in detail in Section 6.1.1. Since this nongraded tube design met the desired objectives more closely than other designs tested, data gained from its testing during the third year was used to design a scaled up concentric tube unit.

The scaleup design of the concentric radiant section, however, resulted in greater catalyst tube thermal stresses and significant failures of the silicon carbide tubes. In addition, gas phase reactions promoted by the design resulted in gas temperatures that were higher than catalyst surface operating temperatures, thus over-temperaturing the materials and increasing thermal NO_x emissions. Since material requirements of the concentric design appeared to be beyond the capabilities of available ceramics, and since NO_x emissions only marginally met the program goal of less than 20 ppm at 10 percent excess air, the nonconcentric design became the focus for final development. Therefore, in the final year of the program, a 1055-MJ/hr system with a nonconcentric radiant tube section was designed and operated as a demonstration unit. The remaining problem of condensation of vaporized distillate fuels on exposed watertubes remains to be evaluated, although:

- Higher boiler steam pressures would increase watertube surface temperatures to near or above the fuel dew point
- Increasing combustion air preheat would lessen the tendency for fuel condensation

Section 6-2 describes the detailed procedure developed and used for the design of the 1055-MJ/hr catalytic watertube boilers. Since this

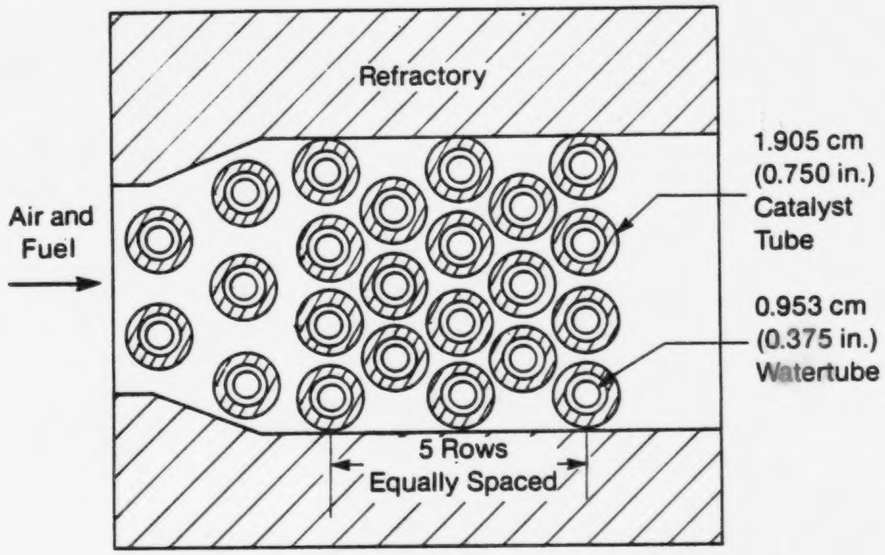
Refractory
1.905 cm
(0.750 in.)
Catalyst
Tube
Air and
Fuel
0.953 cm
(0.375 in.)
Watertube
5 Rows
Equally Spaced

a. Graded tube spacing

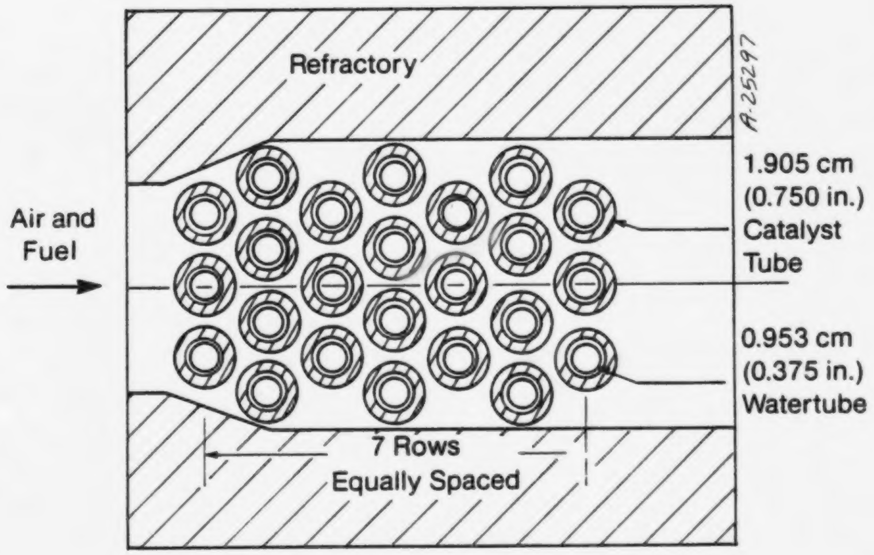
Refractory
A-25297
1.905 cm
(0.750 in.)
Catalyst
Tube
Air and
Fuel
0.953 cm
(0.375 in.)
Watertube
7 Rows
Equally Spaced

b. Nongraded tube spacing

Figure 6-3. Graded and nongraded radiant section geometries.

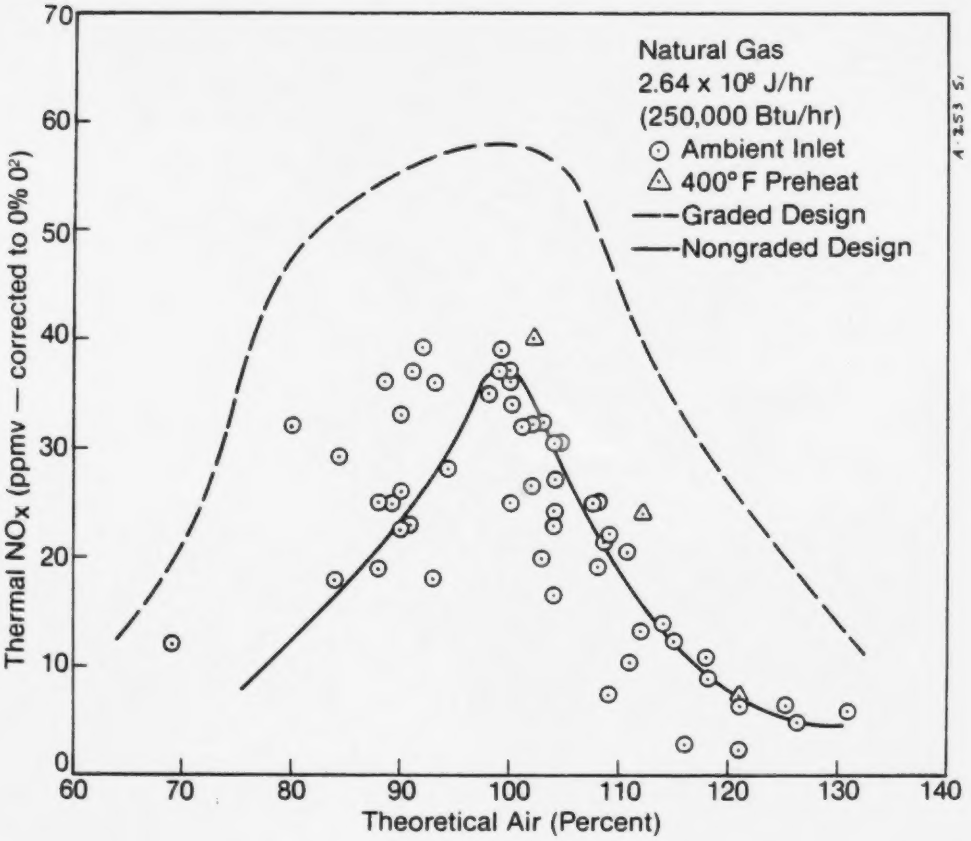

Figure 6-4. Graded and nongraded watertube system thermal NO$_x$ comparison.

procedure relies on data obtained in previous subscale tests of the radiant section, detailed test data for subscale tests not presented in prior documents are also presented. The performance of the 1055-MJ/hr systems is presented in Sections 6.3 and 6.4. The needs for further development based on these results are presented in Section 7.

6.1.1 Subscale Concentric Tube Radiant Section Results

To quantify thermal NO_x emissions for the nongraded, concentric tube design, initial tests were conducted with natural gas. Fuel NO_x control was also investigated by doping natural gas with 0.50 weight percent ammonia to simulate high nitrogen content fuels. Performance on distillate fuel was also achieved by operating with combustion air preheat to vaporize the No. 2 diesel fuel.

A two weight percent chromium oxide (Cr_2O_3) catalyst was used on the 11.4-cm (4.5-inch) long, 1.905-cm (0.75-inch) diameter silicon carbide tubes. This catalyst displays long life and acceptable activity at the encountered 1478K to 1589K (2200°F to 2400°F) tube surface operating temperatures. Noble metals were not used as catalyst materials since they rapidly vaporize at temperatures above 1589K (2400°F) (Reference 6-2).

To ensure high combustion efficiency with a limited catalyst surface area, some degree of gas phase fuel burnout at controlled temperatures is desirable. However, high temperature gas phase combustion in regions with uncooled surfaces contributes to thermal NO_x production. Some gas phase combustion was visually observed in the open regions between the refractory liner and the steel outer casing that probably contributed significantly to the scatter in thermal NO_x data for the nongraded geometry. NO_x data at 477K (400°F) preheat are also shown in Figure 6-4. The higher preheat value intensifies the combustion along the walls, resulting in slightly increased values of thermal NO_x.

The high, scattered values of thermal NO_x between 80 and 100 percent theoretical air in Figure 6-4 resulted from flameholding near the section inlet region (test data are shown in Table A-13). This is evident from a comparison of temperature profiles for lean and rich combustion in Figures 6-5 and 6-6. At 105 to 120 percent theoretical air at ambient (80°F) inlet temperatures (Figure 6-5), front row cylinder temperatures were between 366K and 394K (200°F and 250°F) and velocities between tubes were 19.8 to 22.9 m/s (65 to 75 fps). The second row raises the temperature from 977K to 1255K (1300°F to 1800°F), varying with adiabatic flame temperature and velocity (at constant fuel input). The temperature rises to 1477K (2200°F) on the center rows and drops to 1366K (2000°F) on the sixth row as the remaining fuel is consumed. Under rich conditions, as inlet velocities are lowered (at constant fuel input) to approximately 16.8 m/s (~55 fps), the front row tubes light off, and the surrounding gas phase combustion intensifies. This is illustrated in Figure 6-6, showing front row temperatures of 1005K to 1561K (1350°F to 2350°F). By operating with front row velocities greater than 21.3 m/s (70 fps), this condition of gas phase combustion can be eliminated.

Throughput testing was performed to identify operating limits for the nongraded configuration. Figure 6-7 compares temperature profiles taken adjacent to the SiC tubes for 264, 369, and 445 MJ/hr (250,000, 350,000, and 422,000 Btu/hr) heat release rates at 100 percent theoretical air. As surface velocity increased with increasing throughput, tube temperatures in the front rows decreased, and downstream tube and exhaust temperatures increased. At greater than 110 percent theoretical air for a heat release rate of 445 MJ/hr (422,000 Btu/hr), breakthrough began to occur. Corresponding velocities between the tubes on the first and second rows were 35.1 m/s and 25.9 m/s (115 and 85 fps), representing an upper limit for this boiler geometry.

The reduction in surface temperature with increased throughput corresponded to a similar decline in watertube energy removal efficiency, shown in Figure 6-8. Here, the energy removed by the watertubes is compared with previous data for the graded concentric and nonconcentric designs. The high energy removal efficiency of the concentric, graded design is the result of high tube surface temperatures (greater than 1923K) caused by in-bed gas phase reactions that were not evident with the nongraded design. The decline in watertube energy removal efficiency with increased throughput for the

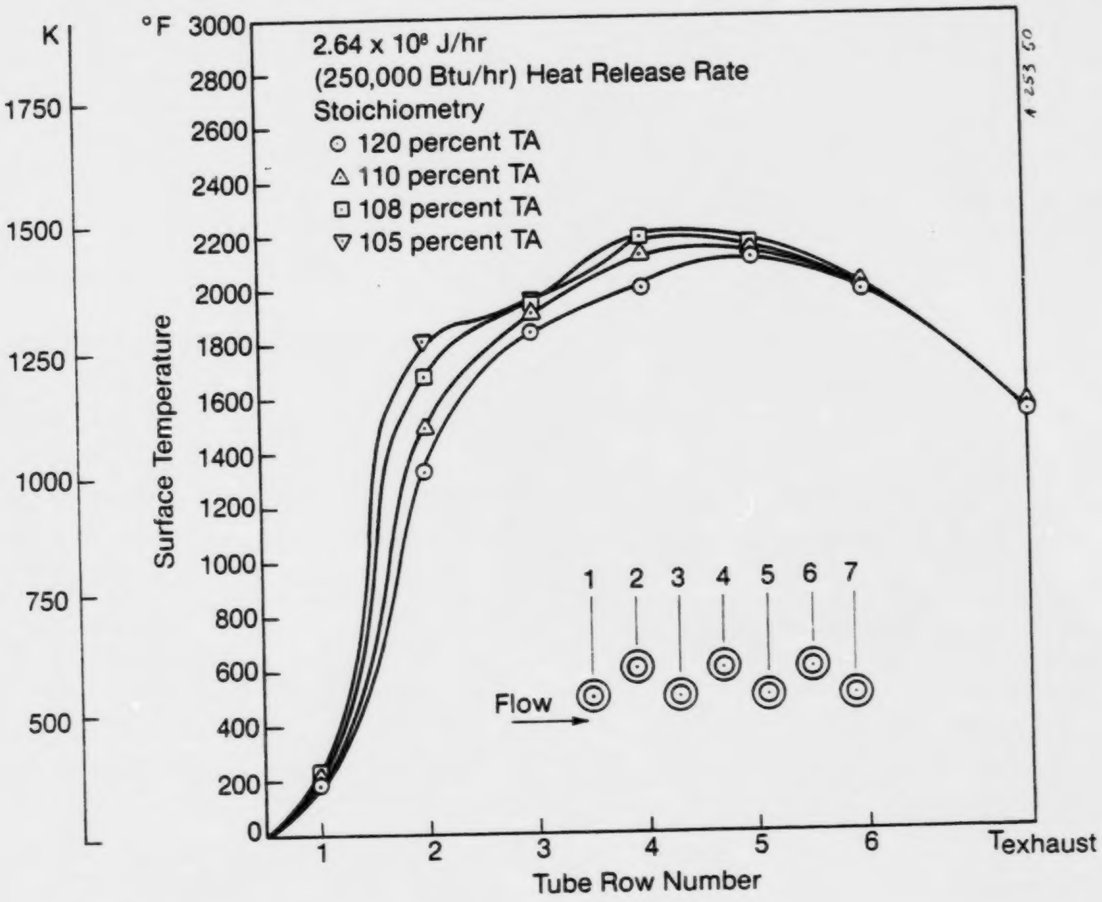

Figure 6-5. Tube temperature profile for lean combustion at 264 MJ/hr (250,000 Btu/hr).

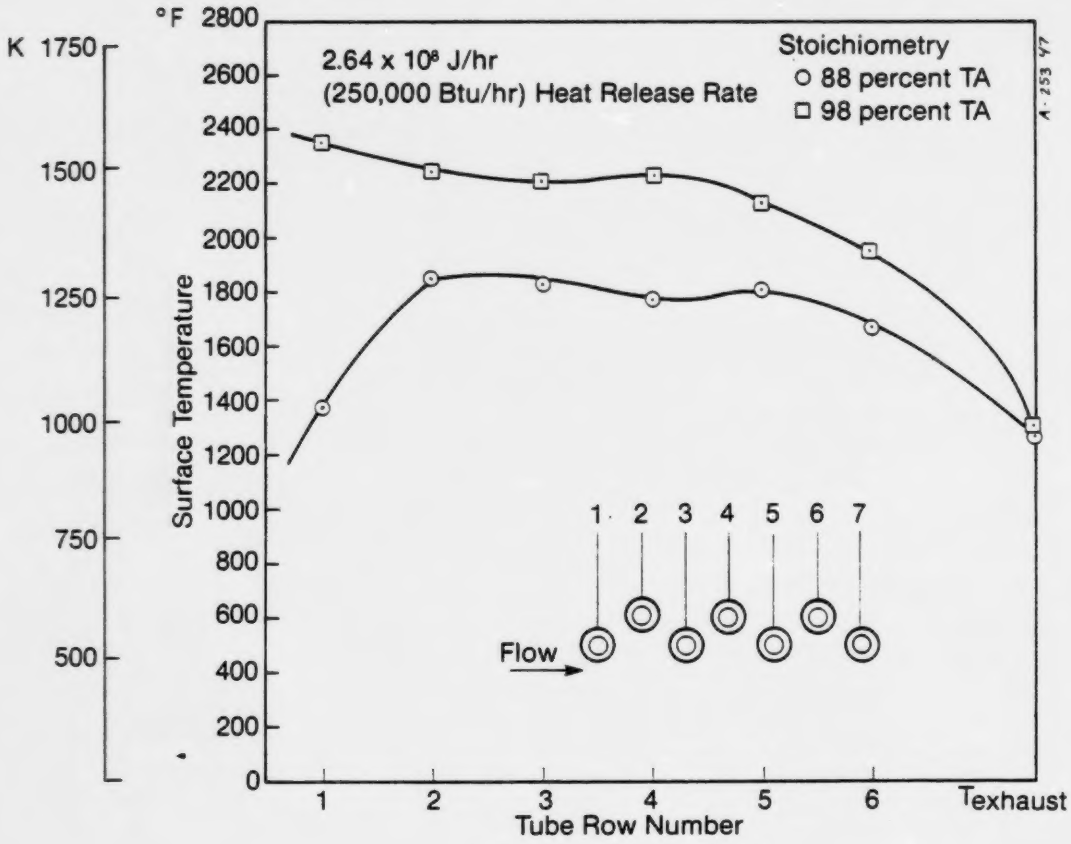

Figure 6-6. Tube temperature profile for rich combustion at 264 MJ/hr (250,000 Btu/hr).

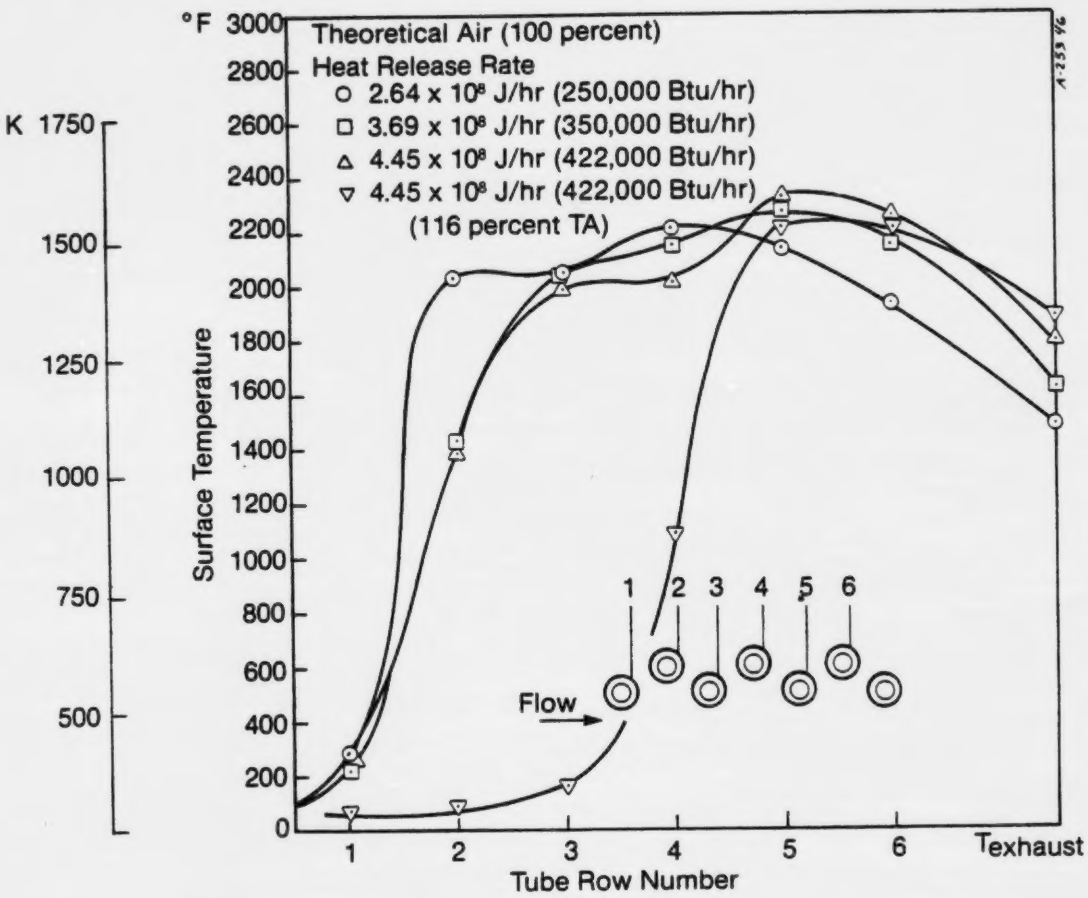

Figure 6-7. Tube surface temperature profile for variable throughput testing.

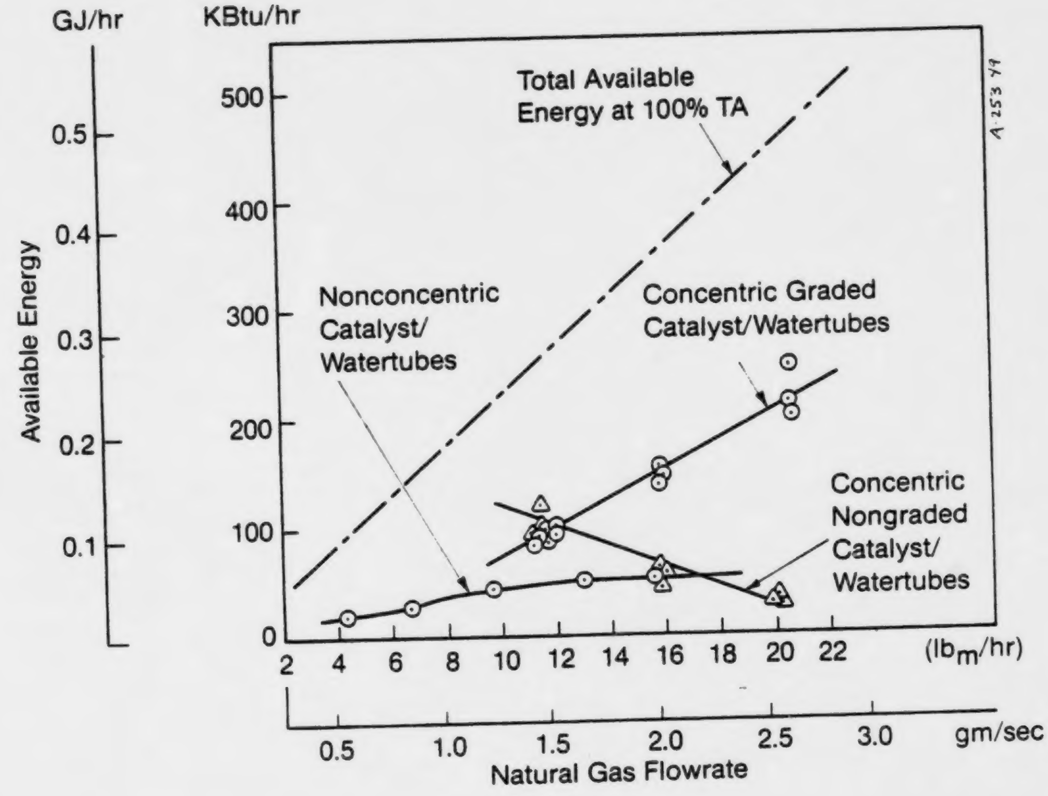

Figure 6-8. Radiant section energy transfer to watertubes.

nongraded design results in a greater energy loss to the exhaust. The optimum energy removal efficiency for this design is near 264 MJ/hr (250,000 Btu/hr) heat release rate where tube surface temperatures are uniform over the test section length.

Lean combustion efficiency for the nongraded combustor design averaged greater than 99.9 percent. The value was influenced by gas phase combustion along the walls. Values of CO and UHC averaged between 20 and 100 ppmv. Reduction of these values is achievable with modifications to the boiler geometry or by addition of a monolithic reactor downstream for secondary fuel burnout.

Conversion of fuel nitrogen was investigated by doping natural gas with 0.5 weight percent ammonia. Minimum conversions on the rich side are desirable for two-stage combustion as a means of controlling fuel-NO_x formation. Data were taken at 264 MJ/hr (250,000 Btu/hr). Fuel nitrogen conversion characteristics are summarized in Table A-14 and displayed in Figure 6-9. High total yields of NH_3, NO_x, and HCN on the rich side are similar to data of previous flameholder tests (Reference 6-3). A minimum yield of 70 percent conversion (NH_3, NO_x, and HCN) occurred at approximately 75 percent theoretical air. Fuel nitrogen conversion to NO_x ranged from 40 to 50 percent between 70 and 95 percent theoretical air and was the major contributor to total NO_x. Elimination of uncontrolled gas phase combustion regions should reduce total fuel nitrogen conversion.

Testing was also performed with diesel fuel at 264 MJ/hr (250,000 Btu/hr) heat release rate with a 617K (650°F) inlet preheat temperature. This inlet temperature caused increased gas phase combustion along the walls and produced high values of thermal NO_x, as shown in Table A-13. High surface temperatures also caused structural damage to the refractory walls, therefore, testing was subsequently terminated. Post-test inspection revealed 8 out of the 24 SiC tubes fractured near the base. All of these tubes were located in the high temperature regions at the inlet and along the walls. Eliminating high temperature regions caused by inlet flameholding and gas phase combustion along the refractory walls was expected to eliminate this problem.

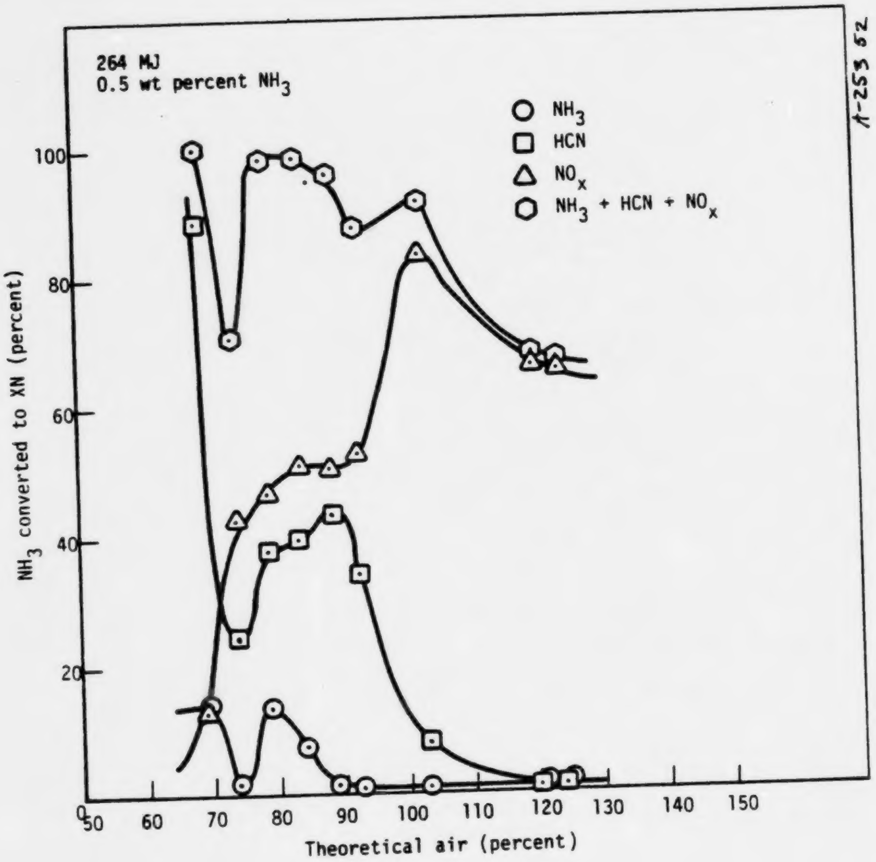

Figure 6-9. Radiant section fuel nitrogen conversion.

The results reported above with the nongraded design established a twofold reduction in thermal NO_x over the previous graded tube design. Throughput testing established nearly a 2:1 turndown ratio for the nongraded tube design without the requirement of inlet preheat. Additional thermal NO_x reduction is possible by eliminating flameholding at the inlet and gas burning along the refractory walls. The former can be eliminated by operating at higher throughputs. Gas burning along the walls can be eliminated by decreasing the surface area/volume ratio and by moving catalyst tubes closer to the refractory walls.

To further advance the concept of catalytic combustion for watertube boilers, it is important to demonstrate a functional prototype complete with ignition, steam generation, and system controls. Since most small to medium size watertube boilers are used in industrial applications, a scaleup should be intermediate between the subscale systems and small industrial sized boilers. It was also desirable to limit the scaleup boiler size so that it could be tested in the existing test facility which offered appropriate instrumentation, control, and data acquisition capabilities. The final design should demonstrate low NO_x emissions and incorporate changes that address problem areas defined in the subscale tests. To satisfy these objectives and constraints, two versions of a 1055 MJ/hr (10^6 Btu/hr) catalytic watertube boiler were developed as intermediate scaleups to small industrial-sized boilers. These versions addressed both concentric and nonconcentric radiant section designs. The scaleup consisted of designing and integrating the radiant combustor, fuel-air preparation section, the watertube and steamdrum system, controls, and downstream adiabatic combustor and secondary air injector components. The design procedure for each of these components is discussed in the following section. Although the nonconcentric tube design became the main program focus, the procedure for design of both radiant section arrangements is addressed in Section 6.2.

6.2 SYSTEM DESIGN PROCEDURE

The design procedure for each of the components of the catalytic watertube boiler is summarized in Table 6-2. Many aspects of the final design

TABLE 6-2. WATERTUBE BOILER DESIGN PROCEDURE

Component	Design Procedures
1. Radiant combustor • Catalyst tube arrangement	1. Initial selection of catalyst tube diameter 2. Determine number of tubes by transfer unit analysis 3. Use heat and mass transfer calculations to determine tube size and spacing 4. Determine catalyst tube steady state operating temperature
• Catalyst tube thickness	1. Determine factors of safety for thermal fracture due to radial and circumferential stresses
• Combustor geometry	1. Determine radiant combustor cross-sectional dimensions, length, and shape 2. Select refractories
• Catalyst materials	1. Select materials (based on prior data)
2. Fuel/air preparation section	1. Size fuel injector 2. Size opposed jet igniter 3. Establish cross sectional areas and configurations from flow velocity requirements
3. Watertubes and steam drum	1. Predict circulation capabilities of selected watertube size 2. Establish construction details 3. Select drum shape and establish capacity
4. Boiler controls • Steam side	1. Select steam drum level control 2. Locate steam traps 3. Provide pressure relief
• Combustion side	1. Fuel/air mixture control 2. Select ignition timing
5. Second stage combustor	1. Establish catalyst operating conditions 2. Select catalyst configuration and materials 3. Secondary air injector design
6. Convective section	1. Predict required tube surface area 2. Interface with radiant section steam system

are determined by fluid dynamic and heat transfer predictions. These calculational methods are summarized below. Due to the complexity of the system, however, the design procedure also relies on data obtained from subscale tests to establish certain design constraints. These experimental conditions are also specified in the following design procedure.

The sizes of all boiler components are determined once the system firing rate is specified. In the sections that follow, the specific design procedures and the resulting configuration for the 1055 MJ/hr (1 million Btu/hr) boilers tested under this program are described. This firing rate was selected as being compatible with existing test facilities, allowing a firing range of 525 to 1320 MJ/hr, and of sufficient size to be similar in construction to full size boilers.

6.2.1 Radiant Section

In the radiant section, premixed fuel and air react on a catalyst tube surface. The catalyst tube, in turn, heats up and radiates to the cooler watertubes. The process is shown schematically in Figure 6-2. To control the rate of chemical reaction and rate of radiant heat transfer to the watertubes, the spacing of the catalyst tubes and watertubes is selected to allow the catalyst tubes to operate within a temperature of 1256K to 1589K (1800°F to 2400°F), dependent upon catalyst material temperature limits and catalyst activity. It is desired to select a temperature range in which chemical reactions will occur on the catalyst surface and at a diffusion-limited rate. Operating at a diffusion-limited rate provides two advantages: 1) it reduces the chance of gas phase reactions occurring in the reactants around the tubes and 2) it allows the design to be more simply modelled by using conventional heat and mass transfer correlations for sizing of the system.

6.2.1.1 Catalyst Tube Arrangement

The first step in radiant section design is an initial consideration of catalyst ceramic tube diameter. The final tube size will be dependent on heat transfer considerations presented below. Ideally, the tube diameter would be in the range of 5.8 to 8.9 cm (2.0 to 3.5 inches) such that it would be compatible with tube sizes in existing watertube boiler designs. Since this diameter would result in an unrealistically small number of tubes in a boiler radiant section of 1055 MJ/hr (as described in the following subsection), however, and since the production of these diameters in most ceramics represents an extension of current ceramic technology, tube diameters of 2.2 to 3.2 cm (0.88 to 1.25 inches) were used for the scaleup configurations. The number of tubes required for the given diameter (i.e., total surface area) is then specified by a transfer unit analysis.

The geometric size of the radiant combustor is established, in part, by the catalyst surface area required for a percentage of fuel burnout by heterogeneous combustion. The remaining percentage of fuel is consumed by catalytic combustion in the adiabatic section and by homogeneous gas phase reactions (at controlled temperatures to minimize thermal NO_x formation). The catalyst surface area required is based on results from subscale tests and determined analytically with a heat-mass transfer analogy that specifies the number of transfer units (NTU) required for a percentage of fuel combustion by heterogeneous surface combustion. The heat-mass transfer analogy is valid when $L_e \approx 1$, boundary conditions are identical, and flow is subsonic. The second assumption becomes an approximation for a catalyst surface with radiative cooling.

For flow past a single tube, an energy balance around the tube yields:

$$\dot{m}c_p \Delta T = -h\pi dl(T - T_w) \qquad (6\text{-}1)$$

where πdl is the surface area of a single tube, h is the convective heat transfer coefficient, m is the mass flux in the streamtube passing the tube, T is the freestream temperature, T_w is the tube surface temperature, and ΔT is the change in bulk mean temperature due to a single tube. Integrating this equation over multiple tubes N_t in series (assuming an infinitesimal temperature difference between successive tubes),

$$\dot{m}c_p \ln \frac{T_o - T_w}{T_i - T_w} = -h\pi dl \cdot N_t \qquad (6\text{-}2)$$

In Equation 6-2, one transfer unit defines the number of tubes required for the temperature to reach 1 - 1/e (63.2 percent) of the final value. Two transfer units (equivalent to time constants) correspond to a temperature 86.5 percent of the final value, etc. To achieve sufficient fuel conversion for proper inlet conditions to the adiabatic combustor, at least 50 percent of final temperature must be achieved. This allows sufficient energy to be extracted via the watertubes such that the adiabatic flame temperature of the products from the first stage is within temperature limitations of the adiabatic combustor catalyst materials (below 1600K). Therefore, approximately one transfer unit is required. This criterion was borne out by temperatures measured in subscale tests. Using these temperatures and inserting known values into Equation 6-2, it was determined that the subscale design at optimum performance (369 MJ/hr, 350,000 Btu/hr heat release rate) corresponded to approximately one transfer unit. The one transfer unit criterion was thus applied to subsequent designs.

From Equation 6-2 for one transfer unit,

$$\ln \frac{T_o - T_w}{T_i - T_w} = -1 \qquad (6\text{-}3)$$

Therefore, the number of tubes, N_t, for one transfer unit is:

$$N_t = \frac{\dot{m}c_p}{\bar{h}\pi d l} \qquad (6\text{-}4)$$

By using the definitions of

$$Re = \frac{\dot{m}/A_s \cdot d}{\mu} \quad \text{Reynolds Number} \qquad (6\text{-}5)$$

$$Nu = \frac{hd}{k} \quad \text{Nusselt Number} \qquad (6\text{-}6)$$

$$Pr = \frac{c_p\mu}{k} \quad \text{Prandtl Number} \qquad (6\text{-}7)$$

and defining a pseudo tube hydraulic diameter per unit length of flow section as

$$D_{h_t} = \frac{4A_s}{\pi dT} \qquad (6\text{-}8)$$

and substituting 6-5 through 6-8 into 6-4, the following expression is obtained for the number of tubes per transfer unit:

$$N_t = \frac{Re \cdot D_{h_t} \cdot Pr}{4Nu} \qquad (6\text{-}9)$$

The mass transfer analogy of this expression is

$$N_t = \frac{Re \cdot D_{h_t} \cdot Sc}{4Sh} \qquad (6\text{-}10)$$

- The Colburn relation for forced convection over a staggered tube bundle arrangement defines the Nusselt Number as:

$$Nu = 0.33(Re)^{0.6}(Pr)^{0.33} \quad , \qquad (6\text{-}11)$$

and by heat-mass transfer analogy, the Sherwood Number as

$$Sh = 0.33(Re)^{0.6}(Sc)^{0.33} \qquad (6\text{-}12)$$

To solve Equation 6-9 using Equation 6-11, the outside diameter of the catalyst tube support along with the tube length and spacing (to calculate Re) must be specified.

The main criterion for establishing the catalyst tube diameter is that the radiation view factor from the catalyst tube to the watertube should be in the range of 0.75 to 1.0 (the values used in subscale designs) to achieve the proper catalyst surface temperatures. The expected catalyst temperature can then be predicted by an energy balance method described below. Adjustments to the tube diameter and spacing may be required to achieve a specific temperature requirement.

As mentioned, a 3.8-cm (1.5-inch) OD tube was selected for the concentric system described in Section 6.3. A tube length of 20.3 cm and spacing (distance between adjacent tube surfaces) of 3.2 mm were initially used to calculate a need for thirty-one 3.8-cm OD tubes for the 1055 MJ/hr boiler radiant section. For the nonconcentric design, tube specifications were 2.2-cm (0.88-inch) diameter by 25.4-cm length. The spacing between catalyst and watertubes was 1.26 cm, resulting in 40 tubes to achieve one transfer unit. The tube spacing and length are used in subsequent calculations to fully specify the tube arrangement. These dimensions are then verified for compatibility with the resulting section geometry.

These tube spacing and length parameters also specify the flow velocities within the radiant section that determine the heat and mass transfer rates between the reactant stream and catalyst tube via Equations 6-11 and 6-12. In the graded tube configuration, combustion performance of the tube bank has been experimentally found to be sensitive to variations in throughput. Therefore, transfer rates to tubes established in subscale tests have been maintained in larger scale designs.

To further verify that tube spacing is appropriate, the expression for the Nusselt Number from Equation 6-6 can be substituted into Equation 6-11 and solved for the heat transfer coefficient

$$h = K \frac{V^{0.6}}{d^{0.4}} \qquad (6\text{-}13)$$

where $K = 0.33k^{0.67}c_p{}^{0.33}/\mu^{0.27}$ with gas properties evaluated at a temperature between the wall and bulk gas temperatures. Taking K as a constant, this equation indicates that to maintain identical heat and mass transfer coefficients as tube diameters are increased, the flowrate per unit area (tube spacing x number of spaces between tubes x tube length) must also increase, but by a lesser amount. For catalyst tubes of fixed length, this means that the tube spacing must become closer as larger tubes are used. Values of velocity in the range of 18.3 to 33.5 m/s (60 to 100 fps) are generally acceptable.

The above analysis assumes heat transfer to a single tube in crossflow. For a staggered tube arrangement, however, this transfer coefficient,

$$h = C\left(\frac{V_\infty d}{\mu}\right)^n Pr^{1/3}\left(\frac{k}{d}\right), \qquad (6\text{-}14)$$

would apply to the tenth row of a tube bank that is ten rows deep (Reference 6-4). For rows upstream of the tenth row, a correction factor to h is given in Table 6-3.

Table 6-3. CORRECTION FACTORS FOR HEAT TRANSFER COEFFICIENTS IN STAGGERED TUBE ARRANGEMENTS

Row	1	2	3	4	5	6	7	8	9	10
Factor	0.68	0.75	0.83	0.89	0.92	0.95	0.97	0.98	0.99	1.0

In nonconcentric tube radiant section designs, the more conservative first row heat transfer coefficient has been used to establish tube numbers and tube spacing.

Note that for a specified number of tubes in a given row of the combustor, the tube spacing and tube length can be adjusted to achieve the proper transfer coefficients. As will be discussed, the optimum configuration in the present design is a combustor with a square cross-sectional area. This geometry minimizes the surface area for a given firing rate and hence, minimizes system heat losses. Establishing an acceptable relationship between tube spacing and height may require an iterative procedure to satisfy both heat transfer and spatial requirements.

The heat transfer analysis used for a cylinder in crossflow can also be utilized to predict the catalyst tube steady-state operating temperature which provides a specification for catalyst materials. The analysis also provides a technique for determining the number of catalyst tubes per row and hence the number of tube rows in the radiant section. The energy balance around a catalyst cylinder is:

$$k_m \Delta H_c X_b = h(T_w - T_b) + F\sigma\varepsilon\alpha(T_w{}^4 - T_s{}^4) \qquad (6\text{-}15)$$

where the term on the left side of the equation is the heat released by the catalyst tube due to chemical reaction, the first term on the right side is the heat transfer by convection from the catalyst tube wall to the bulk gas stream, and the second term is the heat transfer by radiation from the catalyst tube wall to watertubes at a given sink temperature. The view factor for the concentric tube design is obtained analytically for two concentric cylinders such as by the equations of Reference 6-5. For the nonconcentric tube designs, the view factor is more complex, and an analytical calculation for two parallel cylinders is combined with Hottel's graphical crossed-string method (Reference 6-6) to obtain an approximate value where catalyst tubes and watertubes may be of different diameters and configuration. The catalyst tube emissivity ε and watertube absorptivity α were assumed as 0.4 and 0.8, respectively.

The concentration of fuel in the bulk gas stream, X_b, is computed as:

$$N_t = -\ln\,(1 - f)\,\frac{\dot{m}}{k\pi dT} \qquad (6\text{-}16)$$

$$f = 1 - \frac{X_b}{X_{b_o}} \qquad (6\text{-}17)$$

based on the number of tubes the gas passes over. The calculation can be done on an incremental basis in order to determine catalyst tube temperatures along the direction of gas flow. A first cut analysis is made assuming that the bulk gas temperature, T_b, is constant at its initial value T_{b_o}.

To solve for the change in bulk gas temperature, the following relationship applies:

$$\dot{m}c_p \frac{dT_b}{dN_t} = \pi d l h(T_w - T_b) - \pi d l_{wt}(T_b - T_{wt})\frac{dN_{wt}}{dN_c} \qquad (6\text{-}18)$$

The change in bulk temperature in the direction of gas flow through the tube rows can be computed by integrating Equation (6-18). The change in the number of watertubes with respect to the number of catalyst tubes, dN_{wt}/dN_c, is assumed constant for a given tube arrangement. The catalyst tube wall temperatures determined from the first order analysis are used to determine bulk temperature at each tube row. The new bulk temperatures are then used in Equation 6-14 to recalculate the catalyst tube temperature. This iterative procedure is followed until all computations result in negligible changes in tube temperature and bulk gas temperature. The heat transfer coefficient for gas flowing around the watertube, h_{wt}, is computed by the correlation given in Equation 6-14.

An analysis was performed to determine how well the model correlated with the data obtained from the first watertube boiler design. Results indicated that the temperature predicted was high by about 20 percent and could be corrected by lowering the mass transfer coefficient by a factor of approximately 1.8. As a result, calculations for the scaleup designs used a mass transfer coefficient corrected by this factor.

An example of catalyst tube temperature calculations for various nonconcentric tube arrangements with various tube sizes and tube spacings follows. An inlet temperature of 672K (750°F) was selected to predict maximum tube temperatures likely to be encountered, and a gas velocity (between tubes) of 18.3 m/s (60 ft/sec) was used. The various configurations selected are tabulated in Table 6-4. The number of tubes was based on 63 percent fuel conversion (1 NTU). The width and height of the systems were made equal for symmetry. The temperature of the first row of catalyst tubes was found to be 1422K to 1478K (2100°F to 2200°F) for all of these configurations.

The fifth configuration was selected for the 1055 MJ/hr nonconcentric radiant section tested in this program since it provides a low length to height (or width) ratio and keeps the height at less than 25.4 cm (10 inches) to reduce transition difficulties from an 11.4-cm inlet pipe.

6.2.1.2 Catalyst Tube Thickness

Due to variations in convective heat transfer coefficients in the circumferential direction for a cylinder in crossflow and to heat flows across

Table 6-4. Predicted Tube Temperatures for Various Watertube Configurations

No.	Catalyst Tube Diam, cm (in.)	Watertube Diam, cm (in.)	Number of Catalyst Tubes per Row	Tube Spacing, cm (in.)	Section Width & Height, cm (in.)	Number of Tubes for 1 NTU	First Row Tube Temp K (°F)	Radiant Section Length, m (in.)
1	2.2 (0.875)	2.2 (0.875)	3	0.95 (0.375)	19.1 (7-1/2)	54	1472 (2190)	1.11 (43-3/4)
2	2.2 (0.875)	2.2 (0.875)	4	0.64 (0.250)	22.9 (9)	45	1445 (2141)	0.66 (25-7/8)
3	2.2 (0.875)	2.2 (0.875)	5	0.48 (0.188)	27.0 (10-5/8)	39	1428 (2110)	0.44 (15-15/16)
4	2.5 (1.0)	2.2 (0.875)	3	0.95 (0.375)	20.0 (7-7/8)	48	1468 (2183)	1.04 (40-3/4)
5	2.5 (1.0)	2.2 (0.875)	4	0.64 (0.250)	24.1 (9-1/2)	40	1444 (2139)	0.57 (22-5/8)
6	2.5 (1.0)	2.2 (0.875)	5	0.48 (0.188)	28.6 (11-1/4)	34	1428 (2111)	0.37 (14-11/16)
7	5.1 (1.25)	2.2 (0.875)	3	0.80 (0.313)	21.0 (8-1/4)	39	1464 (2176)	0.88 (34-9/16)
8	5.1 (1.25)	2.2 (0.875)	4	0.48 (0.188)	25.4 (10)	33	1443 (2137)	0.54 (21-7/16)
9	5.1 (1.25)	2.2 (0.875)	5	0.32 (0.125)	30.2 (11-7/8)	28	1430 (2114)	0.34 (13-1/4)
10	3.8 (1.5)	2.2 (0.875)	3	0.80 (0.313)	22.9 (9)	33	1463 (2174)	0.81 (31-13/16)
11	3.8 (1.5)	2.2 (0.875)	4	0.48 (0.188)	27.9 (11)	27	1445 (2141)	0.46 (18-3/16)
12	3.8 (1.5)	2.2 (0.875)	5	0.32 (0.125)	33.3 (13-1/8)	23	1434 (2121)	0.31 (12-1/8)

the tube walls in the concentric configuration, combined stresses due to temperature gradients can be established within the material during startup, shutdown and steady-state operation. These temperature gradients result in radial and hoop stresses that determine the required cross-sectional area or tube thickness for a ceramic material of given strength.

For the nonconcentric tube design, catalyst tube thickness is selected primarily based on availability or manufacturability. Radial temperature gradients are generally small due to heat flowing away from the outer (catalyst) surface rather than to the inside. Circumferential gradients due to differences in heat transfer around the tube are alleviated by radiant exchange within the inside of the tube. Therefore, stress analysis is generally not required for the nonconcentric arrangement, and catalyst tube material property specifications are less stringent.

For the concentric tube design, the radiative component of Equation 6-15 can be used as the heat flow radially across the tube material. The heat transfer is then used with Fourier's Law for heat conduction through a hollow cylinder:

$$q = kA \frac{T_i - T_o}{r_o - r_i} \qquad (6\text{-}19)$$

to predict the temperature difference $T_i - T_o$ within the material. Temperature differences of 60K to 130K have been found typical of most concentric tube configurations.

Roark and Young (Reference 6-7) derived formulas for calculating the tension and compression of a hollow cylinder with inner surface at uniform temperature T and outer surface at uniform temperature T + ΔT. These equations are:

Outer Surface -- Compression

$$\sigma_c = \frac{-\Delta T \alpha_t E}{2(1 - v)\ \ln(r_o/r_i)} \left(1 - \frac{2r_i^2}{r_o^2 - r_i^2} \ln r_o/r_i\right) \qquad (6\text{-}20)$$

Inner Surface -- Tension

$$\sigma_t = \frac{-\Delta T \alpha_t E}{2(1 - \nu)\ln(r_o/r_i)} \left(1 - \frac{2r_o^2}{r_o^2 - r_i^2} \ln r_o/r_i\right) \qquad (6\text{-}20)$$

where σ = stress (psi)
ΔT = temperature difference (°C)
α_t = thermal expansion coefficient (1/°C)
E = modulus of elasticity (psi)
ν = Poisson's ratio (≈0.25 for ceramics)
r_o = outer radius
r_i = inner radius

Fracturing of a ceramic tube will occur if the stresses exceed the compressive or tensile strengths of the material. As indicated, compression and tension vary with the temperature gradient across the wall, configuration (ratio of outside to inside tube radii), and material properties (thermal expansion coefficient and modulus of elasticity) which in turn vary with operating temperature. In addition, both compressive strength and tensile strength decrease with increasing temperature. A comparison of tensile strengths at combustion temperatures for alumina and silicon carbide ceramics is shown in Figure 6-10. Note the higher strength of the SiC, which was the original impetus for use of the material in the concentric design. For design purposes, a factor of safety between developed stress at steady state and fracture strength of at least 2.5 is recommended.

The above procedure for determining required tube thickness to prevent failure by radial temperature profiles in concentric tube systems contains the inherent assumption of uniform outer and inner surface temperatures and heat flux. This is an idealized assumption for the close-packed, cross flow tube banks. Additional circumferential temperature gradients can be established due to variations in transfer coefficients from the freestream to the tube in the circumferential direction. The result of these gradients is combined stresses within the tube materials that require a finite difference analysis for resolution. That analysis has not been performed under this program, but the effects of such stress have been evaluated experimentally as discussed in Section 6.3. Similar types of analyses can also be performed for transient

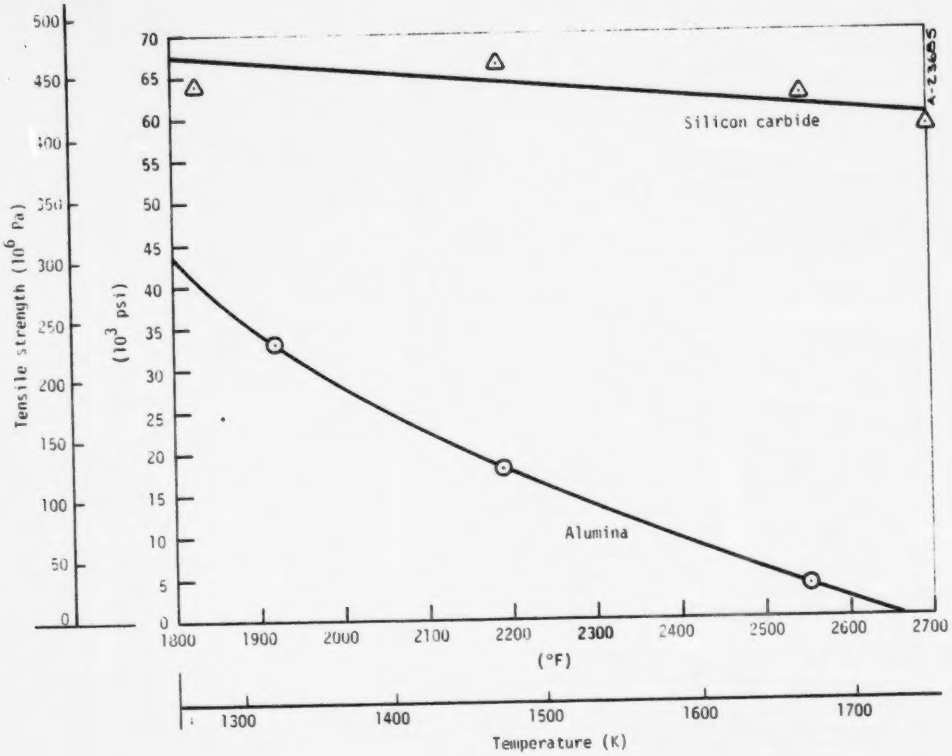

Figure 6-10. Ceramic tensile strength comparison.

temperature gradients at lightoff and shutdown. The temperature gradients expected and the relatively high strengths of the ceramic materials at lower temperatures did not warrant further analysis in this investigation, however.

6.2.1.3 Combustor Geometry

Having established the number and dimensional requirements of the ceramic catalyst tubes and the required tube spacing, the final tube arrangement and combustor dimensions can be specified. Although exact specifications are not currently known for all conditions and configurations, it is generally desirable to have 5 to 7 tube rows in the flow direction of the concentric tube system to achieve sufficient combustion. Additional rows are required in nonconcentric designs with 10 rows being used in the latest design. Also, a staggered tube arrangement is preferred. A square cross-sectional area provides the least system heat loss and is easier to interface with an upstream circular fuel-air preparation section. These general guidelines allow the internal dimensions of the radiant combustor to be established.

The outer dimensions of the combustor are dependent on insulation thickness between the inner wall and outer wall. A dense castable refractory or firebrick is used to form the internal flow chamber because of the high flow velocities encountered and the potential for erosion of lower density materials. Multiple layer insulations can be utilized if outer dimensions must be minimized. In addition to the above requirements, the tube arrangement and cast refractory allow transition from square to round cross-section and expansion at the inlet end of the radiant section.

6.2.1.4 Catalyst Materials

As stated in Reference 6-2, silicon carbide became the preferred catalyst support material for the concentric tube design due to its high strength and thermal conductivity at combustion temperatures. Various SiC fabrication methods and material formulations are available. In this program, two materials were tested:

1. Norton Co. Crystar CS101 (30 percent porosity)
2. Kyocera International, Inc. SC-400 (40 percent porosity)

Both were special formulations with low free silica content and specified porosity. The Norton material experienced some thermal fraction as described in Section 6.3.

The adherence of a catalyst to silicon carbide is difficult to maintain due to the low surface area of dense SiC and the apparent lack of affinity between catalyst compounds and the substrate. The high porosity was specified to enhance catalyst adhesion. No washcoat was used in the coating process, and an aqueous solution was applied by dipping, drying, and calcining. Data from catalyst screening tests developed throughout the program provided the criteria for catalyst selection. Selections were based primarily on operating temperatures and desired fuel nitrogen conversion characteristics. Catalyst materials were either nickel or chromium oxide at a loading of 1 to 4 weight percent. In some tests, platinum was added to make a mixed metal oxide/noble metal catalyst. Chromium oxide exhibited higher activity in the temperature range tested, but lacked the ability to achieve low fuel nitrogen conversion under rich conditions. For high nitrogen fuels, nickel oxide was deemed the most appropriate catalyst.

In the nonconcentric tube radiant section tests, alumina was used as the catalyst support. The two materials tested were:

1. Coors Porcelain Company AD-998 (fully dense)
2. Bolt Technical Ceramics BTC ML80-P 80 percent alumina, 12 percent porosity, 1 μm pore diameter)

Neither material was totally acceptable for the application.

Due to the lower catalyst surface temperatures of the designed nonconcentric systems, platinum catalysts were used in all tests. Alumina-based washcoats were used on these tubes to provide sufficient catalyst adhesion and dispersion. The test results are described in Section 6.4.

6.2.2 Fuel/Air Preparation Section

The fuel/air preparation section shown in Figure 6-1 consists of the combustion air blower, fuel injector, opposed jet igniter, and mixing duct. In the reported experiments, all system components in series were tested to determine total pressure drop. Therefore, a blower was not specifically sized for the system. Pressure drop data was taken for the radiant combustor, however, that provides an initial design condition. A doubling of the measured values of 8910 to 14,900 Pa (3-5 in H_2O) could be used to roughly estimate the total boiler air pressure requirement.

The fuel injector used for the 1055-MJ/hr boiler was capable of both gaseous and distillate fuel injection into the combustion air. The injector flange supported three gas fuel tubes used to introduce gas coflow with the air stream. The gas fuel tubes were sized such that gas and air velocities at the injection point were approximately equal at the nominal 80 percent firing rate. A single air-atomizing Spraying Systems 1/8-JJ nozzle with 0.30-radian (15 degree) solid spray angle was mounted at the center of the injector for liquid fuel introduction. All fuel and atomizing air streams were supplied through taps in the flange.

The fuel-air mixture must be maintained at a velocity above the flame speed of the mixture to avoid flashback from the combustor and flameholding on the fuel injector. Although flamespeeds for a variety of fuel-air mixtures at varying pressures, temperatures, and stoichiometries are difficult to obtain, a minimum flow velocity of 6.1 m/s (20 fps) has been found to be an acceptable design criterion for all conditions encountered in the watertube boiler entrance region. Therefore, the mixing section diameter should be selected such that the 6.1 m/s velocity is maintained at the lowest design firing rate. Tests of concentric tube radiant combustors have shown turndown capabilities of approximately 3:1 without experiencing NO_x emission levels above 20 ppm or combustion efficiency below 99.9 percent. Nonconcentric designs enjoy even greater turndown (6:1) although combustibles passing to the second stage adiabatic combustor may increase at very low or very high loads.

The fuel/air preparation section also contains a gas-fired jet and spark plug for raising the catalyst tubes to their lightoff temperature. In operation, gas is introduced to the jet at approximately half-load flow conditions. The jet tube is sized such that the injection velocity is approximately 20 times that of the opposed-flowing air stream. In large flow ducts, multiple jets may be required for stability. All gas jets must be aligned within 0.035 radians (2 degrees) of the airflow direction. The gas jet establishes a flow stagnation region that is ignited by the spark plug to maintain a standing flame. Fuel is then introduced at the main fuel injector to reach a catalyst tube temperature of approximately 1144K (1600°F) where catalytic reactions are self-sustaining. The opposed jet gas is then shut off, blowing out the jet flame to support catalytic combustion only.

The mixing section length is related to the ability of the fuel injector to provide a uniform distribution across the duct and the spatial requirements of the opposed jet flame and spark plug. A mixing length (from injector to catalyst tubes) to diameter ratio of 6 was found adequate for most systems.

An expansion from the circular cross-sectional area of the inlet to the larger square cross-sectional area of the radiant section is required. In the concentric design, a gradual expansion region was incorporated within the first three rows of catalyst tubes in the 1055 MJ/hr radiant section. The gradual expansion helps to prevent flameholding by reducing the tendency for recirculation. Open areas within each tube row in the expansion section maintain velocities between tubes consistent with those in the main combustion section. In the nonconcentric design, a rapid expansion was used with no apparent adverse flameholding.

6.2.3 Watertube/Steam Drum System

The operating conditions for the 1055-MJ/hr watertube/steam drum system are:

- Production of saturated atmospheric pressure steam
- Naturally circulating water/steam cycle

These conditions are related to watertube boilers in the small industrial sizes -- relatively low pressure boilers without superheat. The majority of these units are steam producers (rather than hot water) and operate wholly by natural circulation.

For the radiant combustor designs adopted in this program, solid ceramic tubes that slide over the watertubes were used rather than axially-split tubes that would be capable of clamshelling around the watertubes. The clamshell arrangement involves a more complex tube end support design and probably no greater ease in tube installation for small boiler sizes. However, the one piece tube requires a concentric watertube configuration since watertubes welded at both ends would provide no means for catalyst tube installation. In such a system, the downcomer tubes are situated inside the steam riser tubes, both of which are surrounded by the catalyst tube in the combustor section (Figure 6-11).

The watertube sizes are constrained by the selected catalyst tube size. For both 1055-MJ/hr systems tested in this program, a watertube OD of 19 mm (0.75 in.) was used. This size allowed a radiation view factor of approximately 0.75 between catalyst and watertubes, resulting in catalyst tube temperatures of 1256K to 1589K (1800°F to 2400°F). In larger boiler designs, watertube sizes of 51 to 64 cm (typical of existing boilers) would be more appropriate.

In addition to being constrained in size by the catalyst tube, the cross-sectional areas of the concentric downcomer and riser tubes must be large enough to provide proper circulation. Excess surface friction and other fluid losses retard water and water-steam flow and do not allow tube heat input to be carried away fast enough. The result is called departure from nucleate boiling (DNB) and represents the onset of film boiling. This results in rapid increases in watertube metal temperatures that may cause eventual failure. The critical heat flux required for DNB also increases with increasing steam pressure up to the critical pressure. As a result, low pressure boilers are the most susceptible to film boiling when operating in a naturally circulating cycle. To avoid DNB, experimental data on critical heat flux in two-phase flow was reviewed. However, considerable uncertainty exists in extrapolating existing data to the unique concentric tube geometry at the expected operating conditions. As a result, the natural circulation of a single watertube model was tested in the laboratory.

A diagram of the single watertube test fixture is shown in Figure 6-12. A radiant heat flux equivalent to that produced by surrounding catalyst tubes

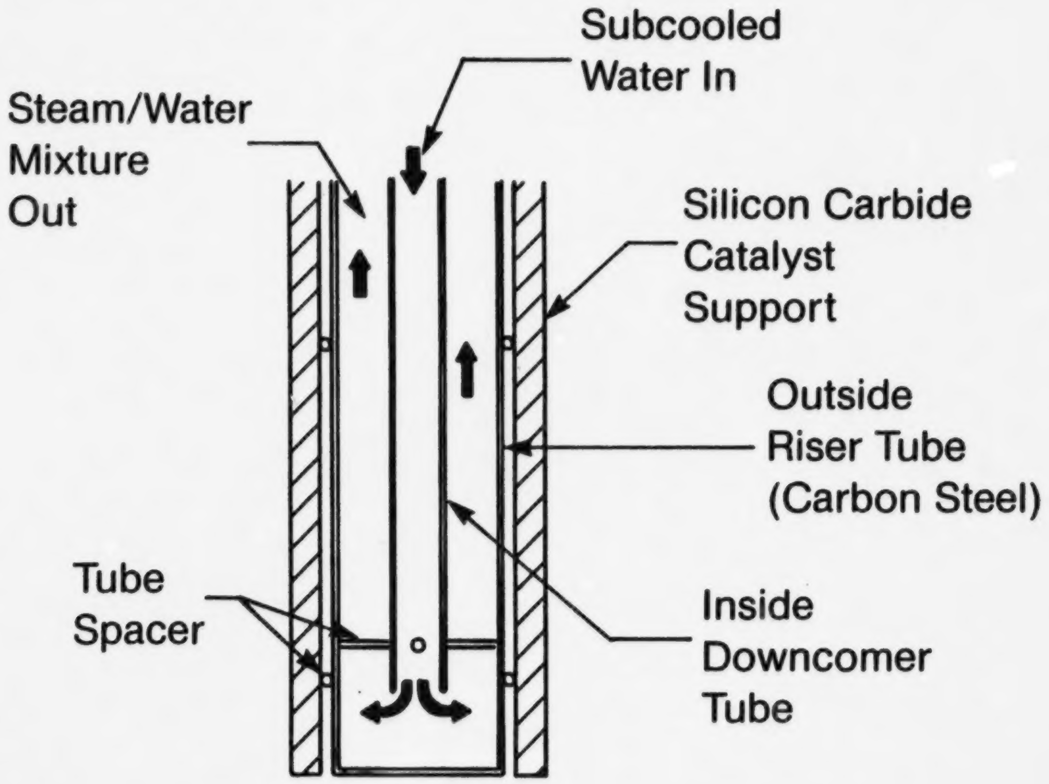
Subcooled
Water In
Steam/Water
Mixture
Out
Silicon Carbide
Catalyst
Support
Outside
Riser Tube
(Carbon Steel)
Tube
Spacer
Inside
Downcomer
Tube

Figure 6-11. Concentric watertube arrangement.

was simulated with a pair of electric clamshell heaters placed around the watertube. At full power, a heater wall temperature of 1492K (2135°F) provided a heat flux of approximately 205,000 W/m^2 (65,000 Btu/hr-ft^2) to the outside watertube surface. The absorption of this heat in the annulus (riser) produces a water-steam mixture of lower density than water in the center tube (downcomer). This difference in density provides the force available for natural circulation. Subcooled water (due to the cooler makeup water) flows from the steam drum in the downcomer and returns as a mixture of saturated water and steam in the riser. An internal baffle arrangement in the fixture of Figure 6-12 separated the steam and water for venting of steam from the top of the vessel and also prevented entrainment of steam to the downcomer. Room temperature makeup water was added at the side of the steam drum. The tube surface temperature was measured at the top and bottom with attached chromel-alumel thermocouples. Excess tube surface temperatures during operation are an indication of undesirable film boiling.

At a full heater input of 10 MJ/hr (950 Btu/hr), the 205,000 W/m^2 flux was delivered to the 130 cm^2 (0.14 ft^2) surface area of the watertube. During steady-state operation, 4.2 kg/hr (9.3 lb/hr) of steam were generated, resulting in close agreement with the energy input to the heater. A maximum tube surface temperature of 387K (236°F) under full load conditions indicated the absence of film boiling.

These tests verified proper circulation for the 1055 MJ/hr boiler at up to 205,000 W/m^2. At the highest boiler load, the maximum expected heat flux from the catalyst tubes was expected to be as great as 250,000 W/m^2. The ability of the tube design to provide natural circulation at this heat rate was confirmed in later testing.

For boilers of larger size with more typical watertube diameters, the predictability of circulation characteristics should be improved due to the greater quantity of data available. Also, as steam pressure and tube size increase, steam circulation improves. Establishing design criteria for the concentric tube system over a range of conditions has not been conducted under this program, however. In nonconcentric radiant combustor designs, it may also be possible to design the watertube circulation in a more conventional way. Since the catalyst tubes are independent of the watertubes, a straight

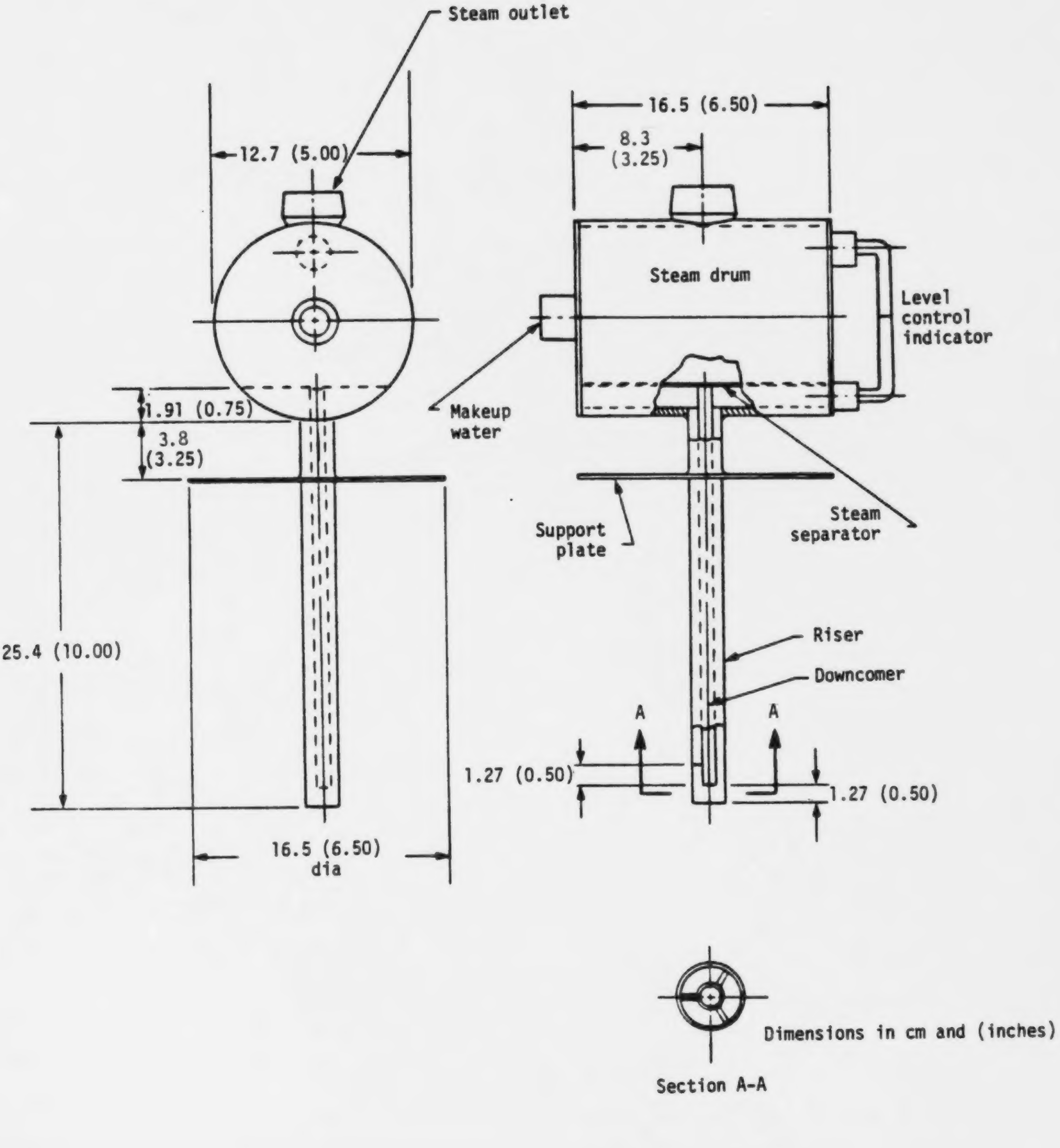
Steam outlet
12.7 (5.00)
16.5 (6.50)
8.3
(3.25)
Steam drum
Level
control
indicator
Makeup
water
1.91 (0.75)
3.8
(3.25)
25.4 (10.00)
Support
plate
Steam
separator
Riser
Downcomer
A
A
1.27 (0.50)
1.27 (0.50)
16.5 (6.50)
dia
Dimensions in cm and (inches)
Section A-A

Figure 6-12. Concentric watertube test fixture.

through flow from mud drum to steam drum is possible. In small boilers, however, it may be difficult to design sufficient space to install catalyst tubes between the welded watertube bank.

The riser tubes in the 1055 MJ/hr boiler were 19.1-mm (0.75-inch) carbon/steel tubing welded or screwed to the bottom of the steam drum. The downcomers were 9.3 mm (0.375 inch) carbon steel welded to the bottom of the inside steam drum liner.

The small combustor dimensions and tube sizes of the 1055 MJ/hr boiler dictated the use of a rectangular steam drum. As boiler size increases, a circular drum with bent tubes would be more appropriate. Certainly, as steam pressure increases, a more circular drum would be required. Steam drum capacity was selected such that a sufficient water head would exist on the watertube bank to provide circulation between high and low level cutoff points. The drum was fabricated of carbon steel with a steam outlet area of 10.2 cm (4 inch) diameter to maintain steam velocities below 45 m/s (150 fps) at full load. Additional drum fittings for automatic level control, water inlet, drain, traps, and pressure relief were included.

6.2.4 Boiler Controls

Since extensive testing of the radiant combustor has occurred in an existing experimental flow facility, development of combustion and steam controls for the boiler has been limited. As mentioned, steam drum level control was provided (Mercoid Type 123 level switch and solenoid valve) as were steam traps and pressure relief valves. Additional low level alarms and other steam controls would be required for stand-alone boilers. Ignition sequencing and control of combustion conditions has also been performed manually, relying on temperature and exhaust composition measurement for system control. Complete boiler systems will require automatic ignition sequencing and jet flame and catalyst sensing for flame safety. Ultraviolet flame sensors are appropriate for opposed jet sensing; however, catalyst temperature sensing would require thermocouple or flame ion sensing. Fuel-air mixture control at varying load is also of importance. Existing boiler techniques for reactant stream control should prove acceptable.

6.2.5 Second Stage Combustor

A second stage combustor may be required in catalytic watertube boilers of two types:

1. A radiant combustor with either concentric or nonconcentric tubes requiring a downstream combustor to burn out unreacted hydrocarbons from the radiant section
2. A boiler operating on high-nitrogen content fuel, operated in a rich-lean staged configuration for NO_x control

In the first case, no additional fuel or air injection is required and the second stage provides as much as half of the total heat release. In the second case, secondary air is injected between stages to bring rich combustion products from the radiant combustor up to normal excess air levels, providing 10 percent or more of the total heat release. The design of this second stage catalyst is similar for the two cases.

When low concentrations of hydrocarbons must be oxidized in either of cases 1 or 2, the catalyst would operate at or slightly above the radiant combustor exit gas temperature. Catalyst temperatures are not expected to exceed 1256K (1800°F), and a high activity, low velocity design is required. Although definitive design information is not currently available, a noble metal catalyst on a small cell (nominally 3 mm diameter) support is suggested. Frontal area should be sized to limit velocities to around 12.2 m/s (40 fps). A length of 7.6 to 10.2 cm (3 to 4 inches) should be sufficient. Automotive cleanup catalyst compositions available from existing manufacturer formulations may be appropriate.

Requirements for a catalyst providing more significant percentages of the total heat release are stricter. Operating temperature is dependent on the radiant combustor inlet stoichiometry and quantity of energy extracted and may reach temperatures as high as 1811K (2800°F) at low values of first stage theoretical air. This combustion temperature can be predicted via adiabatic flame calculations accounting for the reactant stream enthalpy removed in the radiant combustor steam. For operating temperatures below 1478K, noble metal catalysts are required. At higher temperatures, metal oxide or mixed oxide/noble metal formulations are appropriate. The need for a high heat release rate can also benefit from a graded cell configuration. A length of 7.6 cm (3 inches) and catalyst inlet velocity not greater than 24.4 m/s (80 fps) are recommended.

The second stage combustor for fuel NO_x control also requires a secondary air injector. One concept developed during this program utilizes the multiple tube injector arrangement shown in Figure 6-13. Seven tubes inject air at a velocity equal to that of the mainstream at the nominal flow condition (80 percent of full load). The nozzles are sharp edged to avoid recirculation regions in the hot combustion products that could potentially result in flame-holding.

6.2.6 Convective Section

The final boiler convective section can be designed according to current practice, selecting the required tube surface area for an expected inlet gas temperature of 1367K to 1589K (2000°F to 2400°F). Either a straight-through or concentric tube arrangement could be used, the design dictated by interfaces and similarity to the radiant combustor steam system. The convective section could contain its own steam drum as shown in Figure 6-1 or be combined with that of the radiant section.

The system design procedure for the 1055 MJ/hr boiler has been described. The resulting configurations and test data for the two radiant section designs are described in the following sections. In addition, downstream boiler sections were designed (although not tested) for the nonconcentric system described in Section 6.4. Test data obtained on these boiler units have allowed additional refinement of design procedures and details.

6.3 CONCENTRIC TUBE RADIANT SECTION

6.3.1 System Description

The tube arrangement, flow section, and steam drum design for the 1055 MJ/hr concentric radiant section are shown in Figures 6-14 and 6-15. The tube bank includes thirty-one 3.8-cm diameter silicon carbide tubes mounted within a 20.3-cm square cross section. The first three rows of tubes are mounted within a gradual transition built into the cast refractory to allow

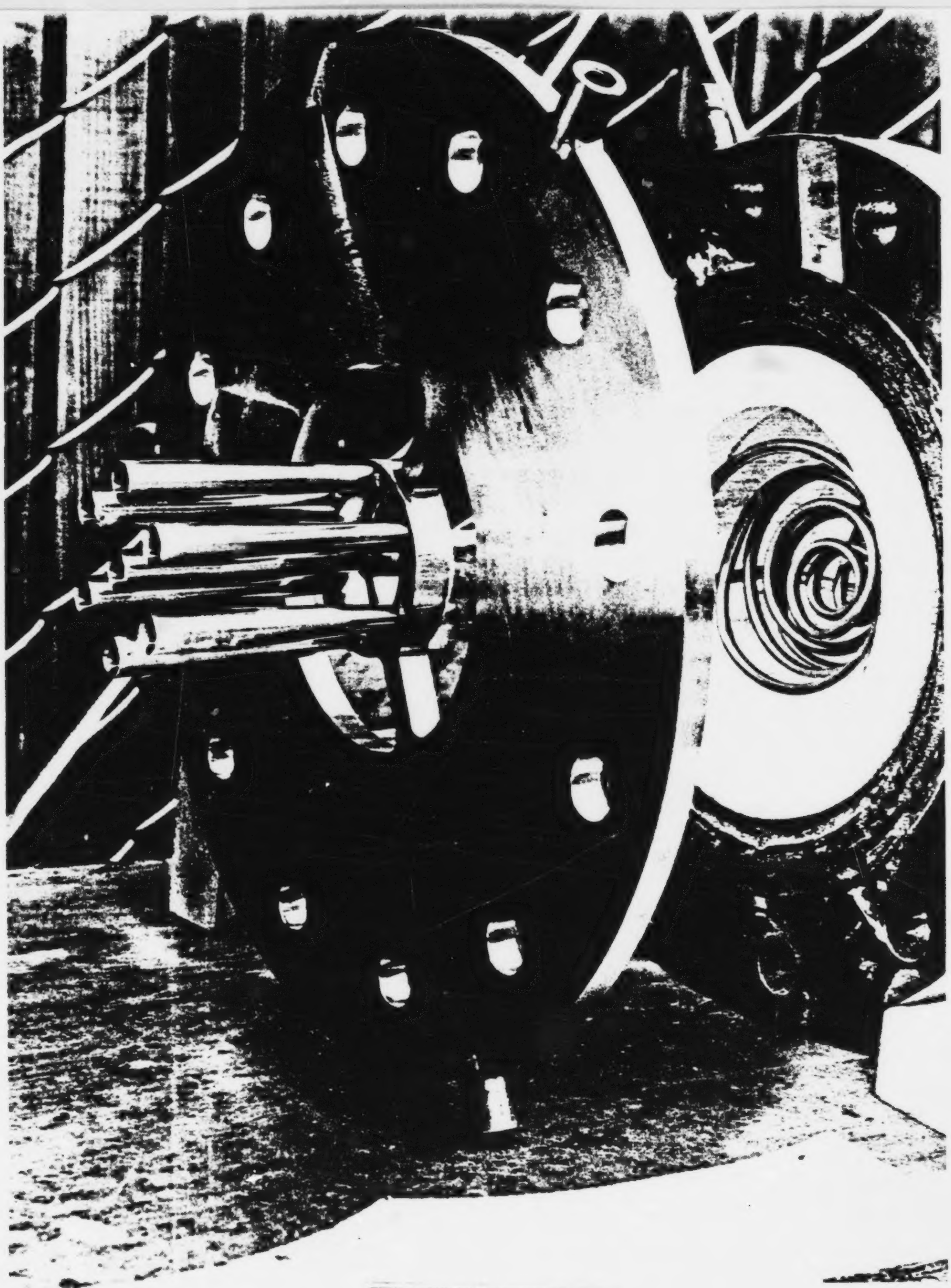

Reproduced from
best available copy.

Figure 6-13. Secondary air injector.

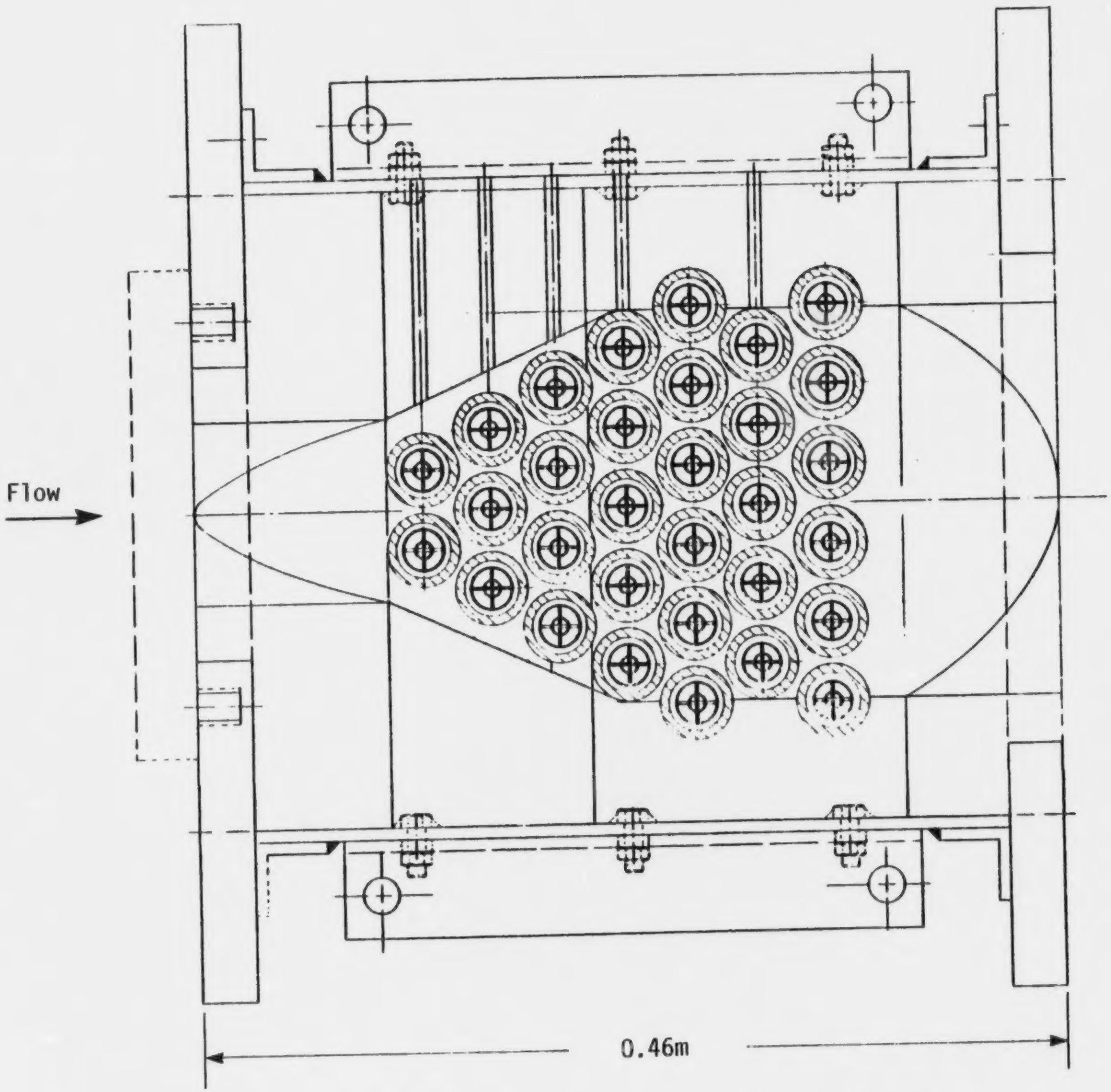

Figure 6-14. 1055 MJ/hr radiant section tube arrangement.

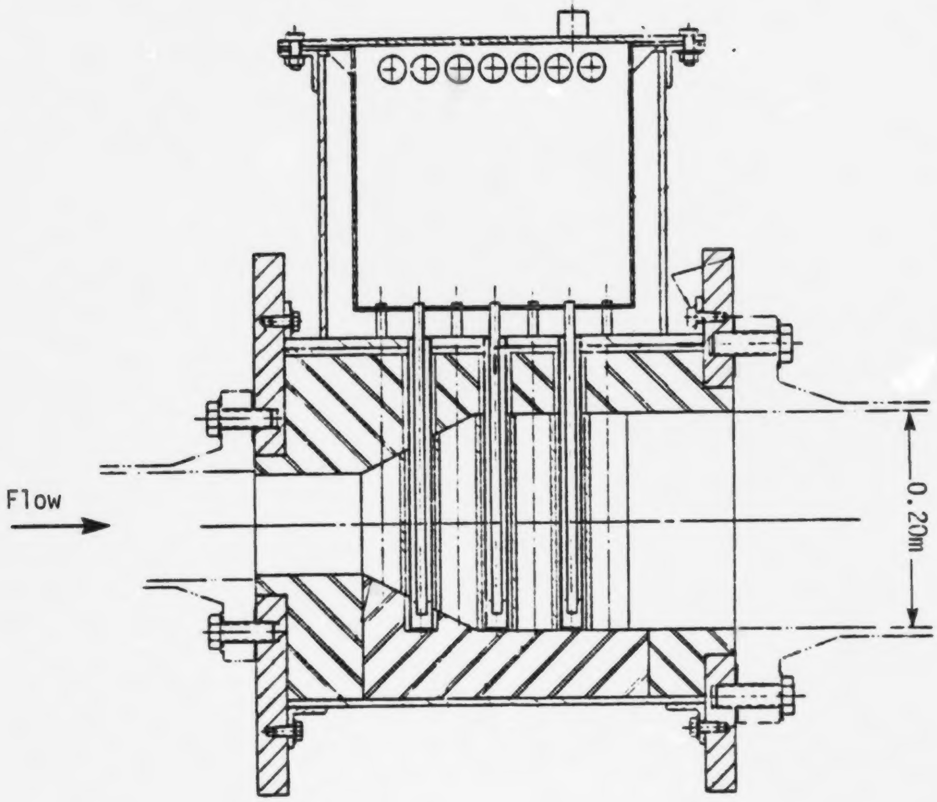

Figure 6-15. 1055 MJ/hr radiant section side view.

gentle expansion of the reactant stream. Gas phase combustion along the refractory walls is minimized by placement of silicon carbide catalyst tubes partially recessed within the walls. Seven tube rows were established in the flow direction to achieve near-complete combustion. Spacing between catalyst tubes is 3.2 mm. An air gap of 3.2 mm is maintained between catalyst and watertubes by wire standoffs welded to the sides of the watertubes. Catalyst tubes are inserted into the radiant section through a removable bottom plate.

The steam drum is rectangular and contains an inner liner that supports the downcomers of the concentric steam tubes. The steam/water mixture flows from the outer drum passage to the liner where steam separates and exits through the top plate. Steam pressure was limited to below 1×10^5 Pa (15 psig).

6.3.2 Test Results

Initial firing of the concentric tube 1055 MJ/hr radiant section at a heat release rate of 844 MJ/hr (800,000 Btu/hr) indicated the need for a multiple arrangement of opposed jets for acceptable stability at lightoff. The mixing section was subsequently modified to include three jets at the same axial location. Thus a greater quantity of fuel could be injected at the jets while maintaining velocities below 122 m/s (400 fps). Overlap of the jet boundaries significantly increased stability at the desired operating conditions (420 MJ/hr heat release rate).

The instability of the jet was also apparently responsible for fracturing of some of the catalyst tubes. The porous silicon carbide was coated with a nickel oxide catalyst that required a somewhat higher surface temperature to light off than previous chromia catalysts tested at a smaller scale. Repeated shocks during lightoff appeared to rattle some of the tubes sufficiently to cause their fracture. To avoid further problems, the more active chromium oxide catalyst with platinum added was used in subsequent tests to facilitate lightoff.

Initial testing of the system on natural gas at 844 MJ/hr showed promising results despite the limited nature of the data. The catalyst tube bank appeared very uniform and stable. Natural circulation of water and steam through the concentric watertubes was excellent, and preliminary calculations indicated approximately 30 to 40 percent of the incoming energy used to raise steam. Thermal NO_x emissions were also improved over the former system, peaking at approximately 30 ppm at near-stoichiometric conditions.

With the chromium oxide/platinum catalyst, some additional difficulties in achieving lightoff were encountered. Therefore, air preheat to 700K (800°F) was used to provide acceptable startups. Thermal NO_x data were generated between 100 and 140 percent theoretical air with natural gas at nominal heat release rates of 791, 1055, and 1319 MJ/hr (0.75, 1.0, and 1.25 x 10^6 Btu/hr). Figure 6-16 presents this data at both ambient and 533K (500°F) preheat air inlet temperatures. Operation on ambient air was achieved by turning off the preheat once the combustor section was operating and stable. The dashed curve in the figure indicates values of thermal NO_x from previous subscale tests with natural gas at 264 MJ/hr. As can be seen, the scaleup to 1055 MJ/hr lowered the peak value of thermal NO_x at 100 percent theoretical air to 26 ppmv (at 1097 MJ/hr and ambient inlet temperatures) and flattened the leanside NO_x curve. Values of thermal NO_x at 110 percent theoretical air without preheat and at the design condition were nearly identical with values from the subscale tests. The data also indicated a 20 to 25 percent reduction in thermal NO_x values by eliminating the 533K preheat temperature at similar firing rates. At the same inlet preheat temperature, increasing throughput caused a slight increase in the values of thermal NO_x. The upswing in the curve for 1304 MJ/hr heat release rate and ambient inlet temperature at greater than 120 percent theoretical air probably indicates the beginning of breakthrough and the initiation of a greater fraction of homogeneous gas phase combustion reactions downstream of the combustor tube bank.

Corresponding CO and UHC data are tabulated in Table A-15 for the data in Figure 6-16. These low values translate to combustion efficiencies greater than 99.99 percent. Energy removal efficiency in the combustor section was also calculated by time-averaging the water makeup to evaluate the steam rate. With 533K preheat, energy removal by the watertubes was between 30 and 40 percent. These values were similar to the subscale tests which demonstrated approximately 40 percent energy removal without preheat at 264 MJ/hr firing rate.

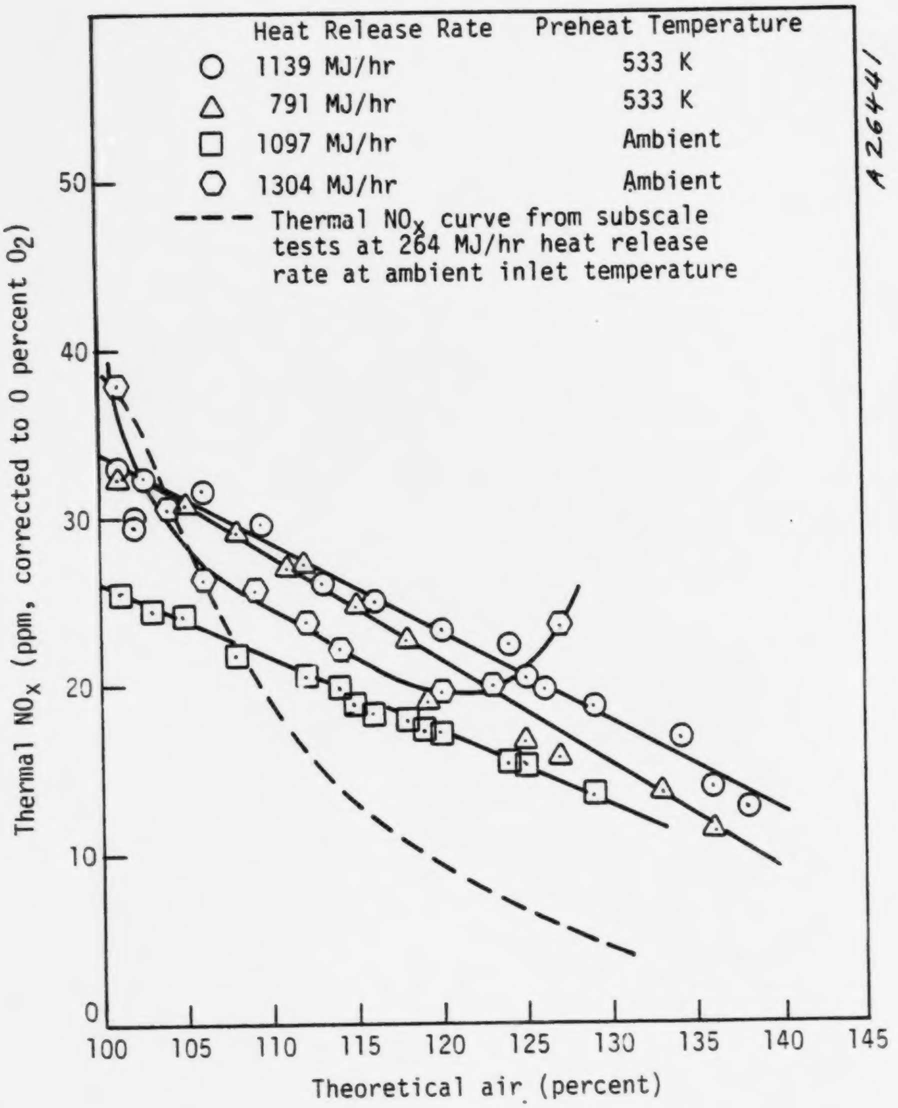

A26441

Figure 6-16. Concentric tube thermal NO$_x$ data for the 1055 MJ/hr watertube boiler radiant section.

Testing was terminated after approximately 8 hours due to fracturing of the silicon carbide tubes. Similar stress cracks on tubes in the final four rows of the combustor section indicated a common mode of failure, and thermal stress calculations were performed to define the failure mode. Although exact modeling of the stresses is difficult, simplified analyses indicated the likelihood of fracture as the result of stresses caused by a combination of circumferential and longitudinal temperature gradients, and not radial temperature gradients that caused failures in early subscale tests. Circumferential temperature gradients result from localized differences in heat and mass transfer coefficients around a cylinder in crossflow. These temperature gradients are enhanced by the close spacing of the silicon carbide tubes in the concentric tube arrangement. Longitudinal (axial) gradients may have resulted from preferential flow along the top of the combustor section where a somewhat greater open area was apparent, or uneven fuel/air mixing or catalyst application from top to bottom of the ceramic tubes.

Simple tests were conducted to evaluate the effects of circumferential and longitudinal stresses. A longitudinal piece of SiC cut from one side of a tube and a short section or ring of SiC tube were heated in localized areas. Despite heating one-half of the longitudinal piece to incandescence while the other half remained cool, this severe longitudinal temperature gradient did not cause a fracture. However, when one-half of the ring piece was heated to incandescence, the resulting circumferential temperature gradient repeatedly caused fracturing with the same pattern as experienced in the boiler section tests.

An approximate analytical model was used to determine if the thermal stresses from a circumferential temperature gradient become more severe with increasing tube size (that would be required in larger scale designs). The model assumed a cylinder with the front or forward section at temperature T_1 and rear section at temperature T_2. The resulting stress was found to be proportional to t/r where t is the tube thickness and r is the inside tube radius. This means that for a constant tube thickness, the critical stress decreases as the tube radius increases. Silicon carbide tubes can, therefore, be used with larger watertube diameters during scaleup without developing excessive stresses due to size alone.

Several solutions to the problem of SiC tube fracture with the concentric tube arrangement are possible:

- Stress relief -- Sawcutting a slot the length of each SiC tube to eliminate nonlocal circumferential stresses
- Tube thickness -- Reducing the tube wall thicknesses to decrease the stress from a given temperature gradient
- Tube material -- A stronger tube material may withstand the thermal stresses that result with the existing tube configuration
- Temperature control -- Reduce the overall temperature within the combustor. This helps decrease the severity of the temperature gradient for a single tube.

To complete verification of circumferential temperature gradients on tube durability, a final watertube/silicon carbide tube arrangement was established (as shown in Figure 6-17) and tested. The eight exposed watertubes in the latter rows of the combustor reduce localized heat transfer between tubes and quench gas phase combustion reactions, lowering the overall combustor temperature. The effects of the localized temperature reduction on SiC tube performance, exposed watertube performance, and hydrocarbon and CO emissions were subsequently determined. In addition, a single SiC tube with a longitudinal sawcut was placed in the rear row where performance could be compared with full-circumference tubes. Also in the rear row, one SiC tube obtained from Kyocera was added for performance comparison with the Crystar tubes from Norton.

Testing of the modified arrangement was conducted at 775 to 1319 MJ/hr (735,000 to 1,250,000 Btu/hr). Lightoff was somewhat more difficult due to the exposed watertubes, requiring preheat to 533K. The data are given in Table A-16. The NO_x emissions data have also been plotted for test points

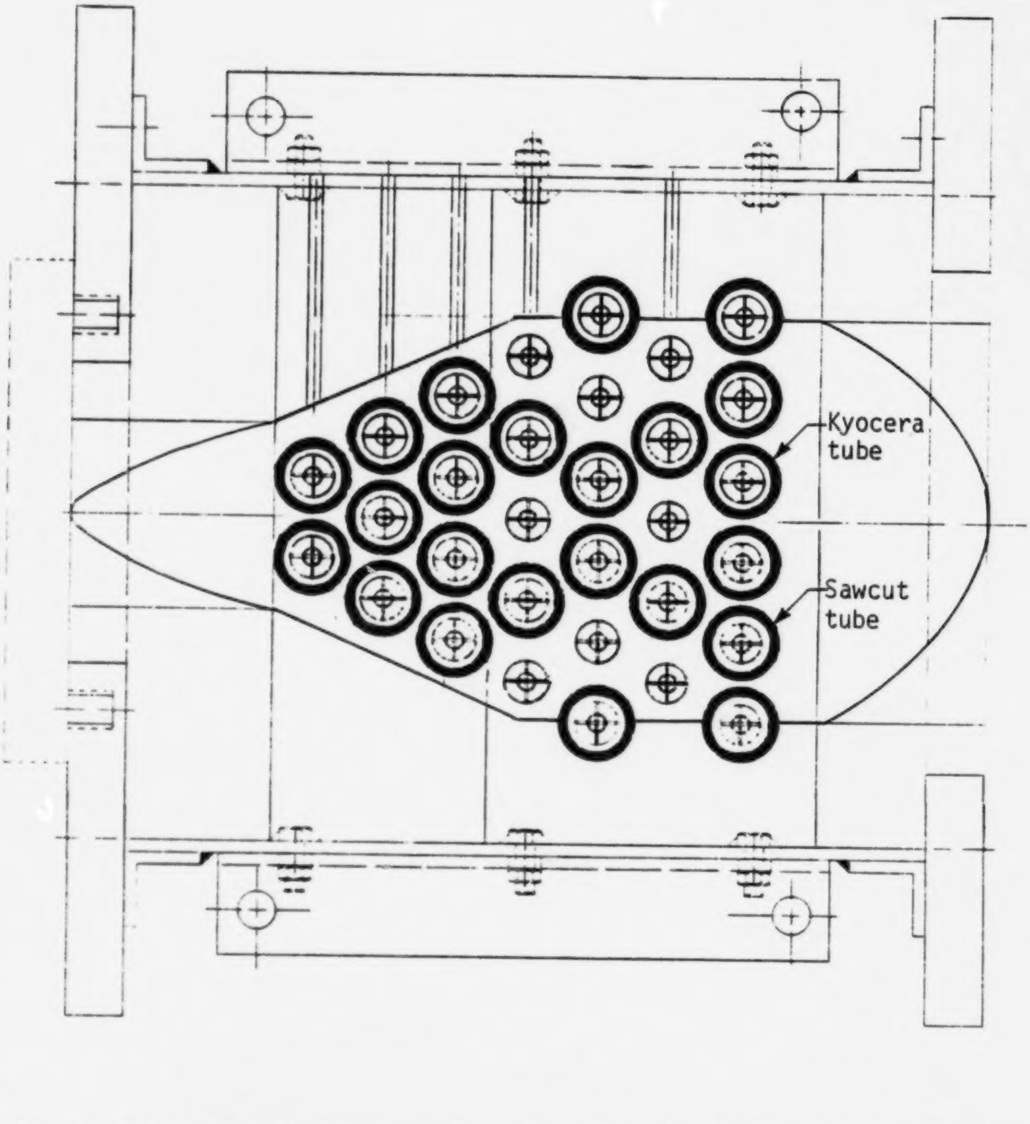
Kyocera tube
Sawcut tube

Figure 6-17. Modified concentric tube watertube boiler radiant section.

with and without preheat in Figures 6-18 and 6-19. In general, thermal NO_x emissions were somewhat lower than those of the totally concentric tests due to greater cooling effects of the exposed watertubes. At the 1055 MJ/hr design firing rate, emissions of 5 ppm were achieved without preheat. These very low NO_x levels were also typical of the nonconcentric tube design tested in the program.

Following the first 5 hours of testing, the tube bank was inspected from both inlet and outlet ends. Two tubes in the inlet transition region and two tubes in the back row (one being the sawcut Norton tube) were fractured. The sawcut tube fractured despite its ability to relieve circumferential stresses by thermal growth around the tube circumference. Invisible fractures may have been induced by the machining process which subsequently resulted in failure. No additional fracturing was observed during the remaining 3 days of testing. Following disassembly of the section, a hairline fracture was observed in the Kyocera tube. None of the other Norton tubes at the center of the tube bank were fractured, however.

Verification that tube failures occurred primarily due to circumferential stresses presented a major obstacle to achieving a durable system with the concentric tube arrangement. The close spacing between ceramic tubes results in high local heat transfer and stresses beyond the strength of the silicon carbide material. The close spacing, however, is required to minimize thermal NO_x production within the system. The modified concentric tube arrangement allowed wider tube spacing without increasing NO_x by direct gas cooling with exposed watertubes. Other approaches to reducing stress (tube slotting, reduction of wall thickness, and identification of stronger materials) require additional material development and have not been pursued in this program.

The final watertube boiler design incorporated a nonconcentric tube arrangement with separate catalyst tubes and watertubes. This arrangement was expected to have the greatest probability of success for very low NO_x with clean fuels in watertube boilers. The ability to combust liquid fuels remains unknown, however. These tests are described in the following section.

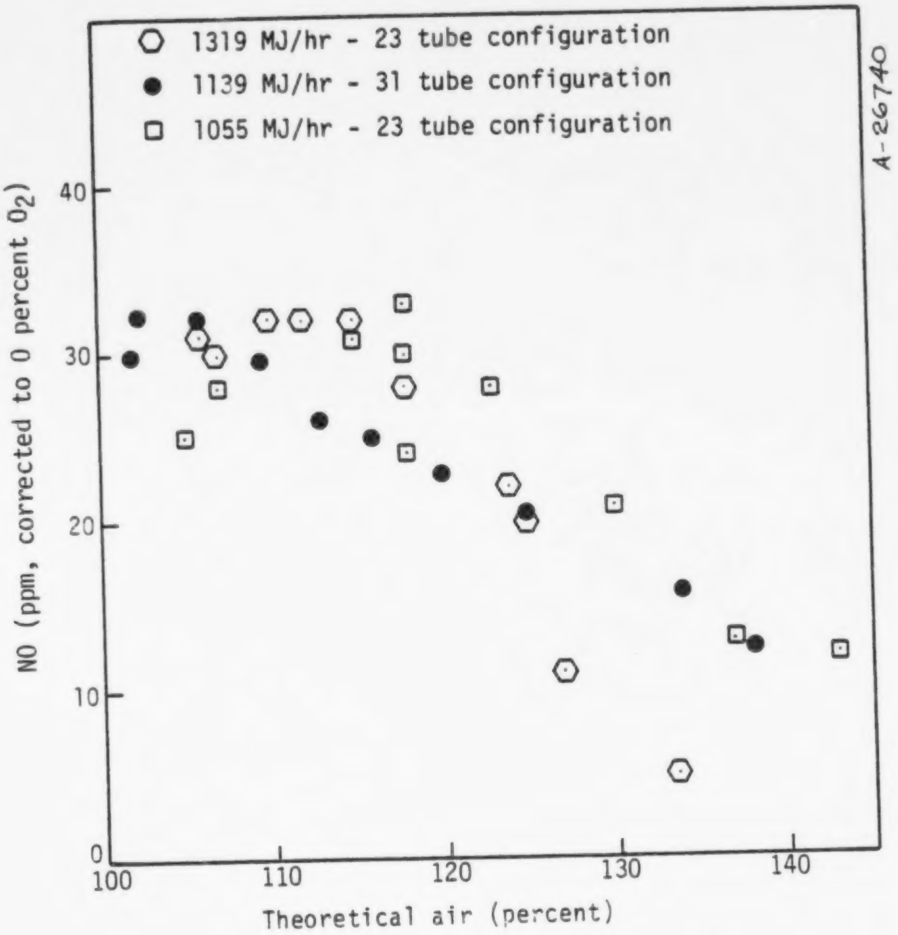

Figure 6-18. Concentric watertube boiler radiant section NO_x emissions with preheat.

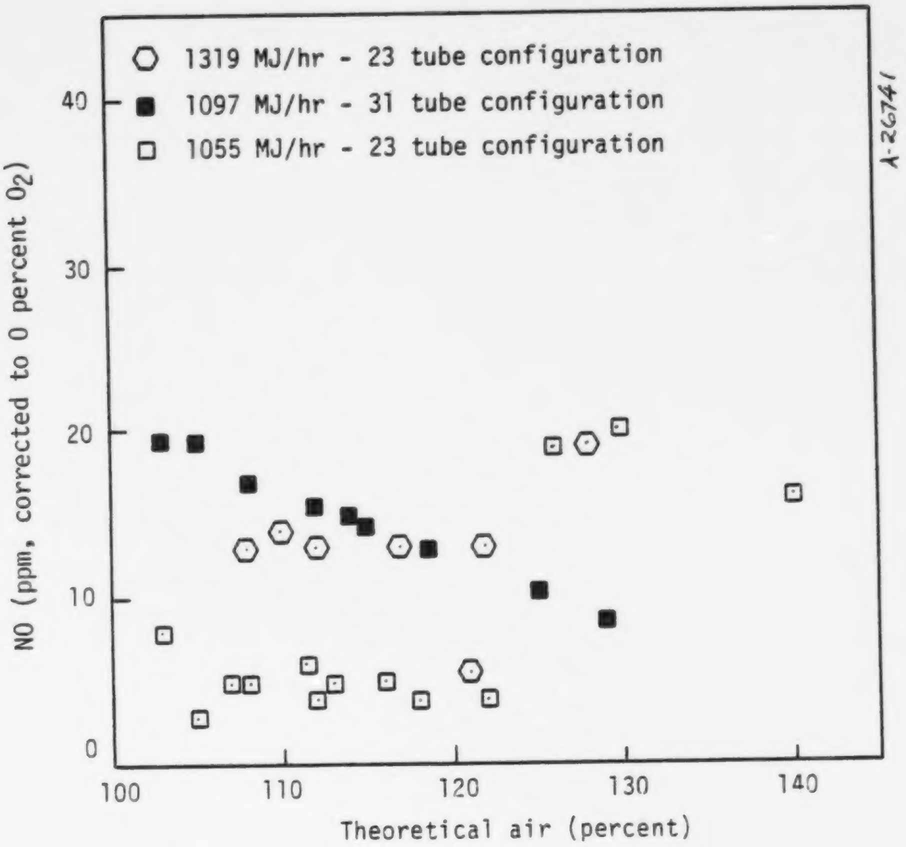

Figure 6-19. Concentric watertube boiler radiant section NO_x emissions without preheat.

6.4 NONCONCENTRIC TUBE BOILER

6.4.1 System Description

The integrated nonconcentric watertube boiler system is shown in Figure 6-20. This system has a modular design to provide flexibility in testing of sections either together or separately. The configurations of the radiant, adiabatic, and convective sections are discussed below.

6.4.1.1 Radiant Section

The radiant section assembly is shown in Figure 6-21 and details of the radiant section top and bottom plates are shown in Figure 6-22. The top plate separates the radiant section combustion zone from the steam drum above. the smaller holes in the upper plate support the catalyst tubes (by insert pins), and the larger holes support the watertube risers. The watertube risers have 2.22 cm (0.875 inch) outer diameters. Six watertubes surround one catalyst tube. Ten rows of 2.5 cm diameter catalyst tubes (four per row) make up the radiant combustion zone. The front row of catalyst tubes differs from other rows in that this row has only three catalyst tubes (the fourth catalyst tube would have been in an inactive flow region and was thus replaced with a watertube). The overall size of the flow channel is 24.1 cm (9.50 inches) square and 78.7 cm (31 inches) in length.

The bottom plate contains larger holes for removal of catalyst tubes (through the bottom of the section) and ten thermocouple parts for gas phase temperature measurements. The bottom plate and channel sidewalls are insulated with fibrous insulation and castable refractory.

The boiler downcomer tubes are welded to a trough which forms the steam drum liner (see Figure 6-21). The unit is inserted at the top of the drum and covered with a lid. Various parts of the lid are used for steam outlet, water level control, boiler feedwater, water temperature measurement, and pressure relief. The lid for the steam drum is bolted in place and suspends the drum liner from a machined gap between the lid and the top edge of the steam drum shell. All plates are carbon steel (except for the catalyst insert pins) and continuous-welded.

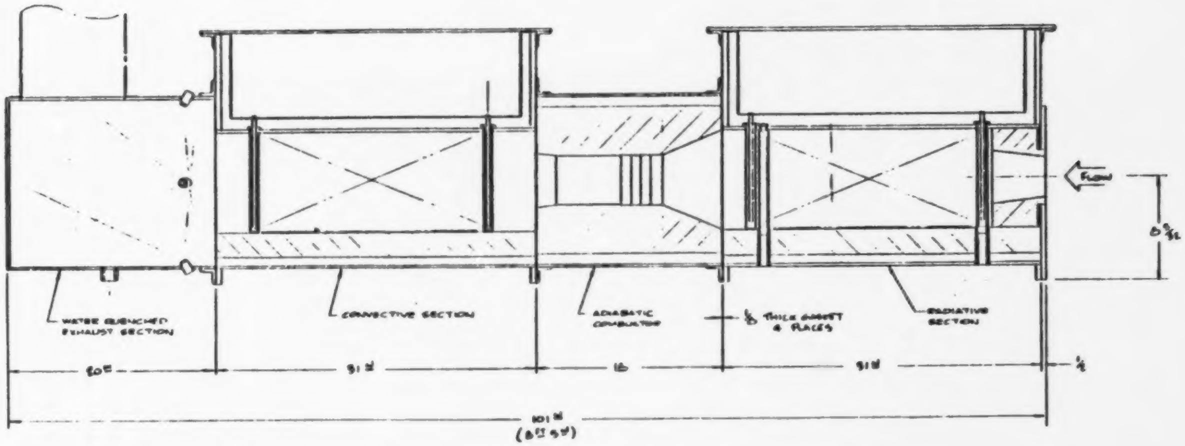
FLOW
6
WATER QUENCHED EXHAUST SECTION
CONVECTIVE SECTION
ADIABATIC COMBUSTOR
1/8 THICK GASKET 4 PLACES
RADIATIVE SECTION
16

Reproduced from
best available copy.

Figure 6-20. Catalytic watertube boiler system.

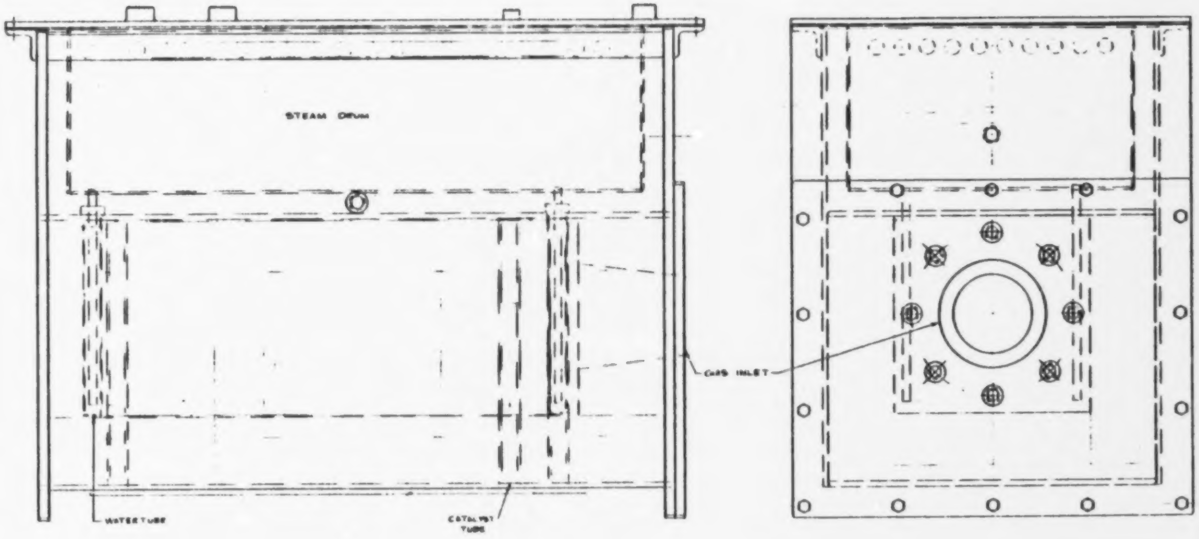
STEAM DRUM
WATERTUBE
CATALYST TUBE
GAS INLET

Figure 6-21. Radiative section assembly.

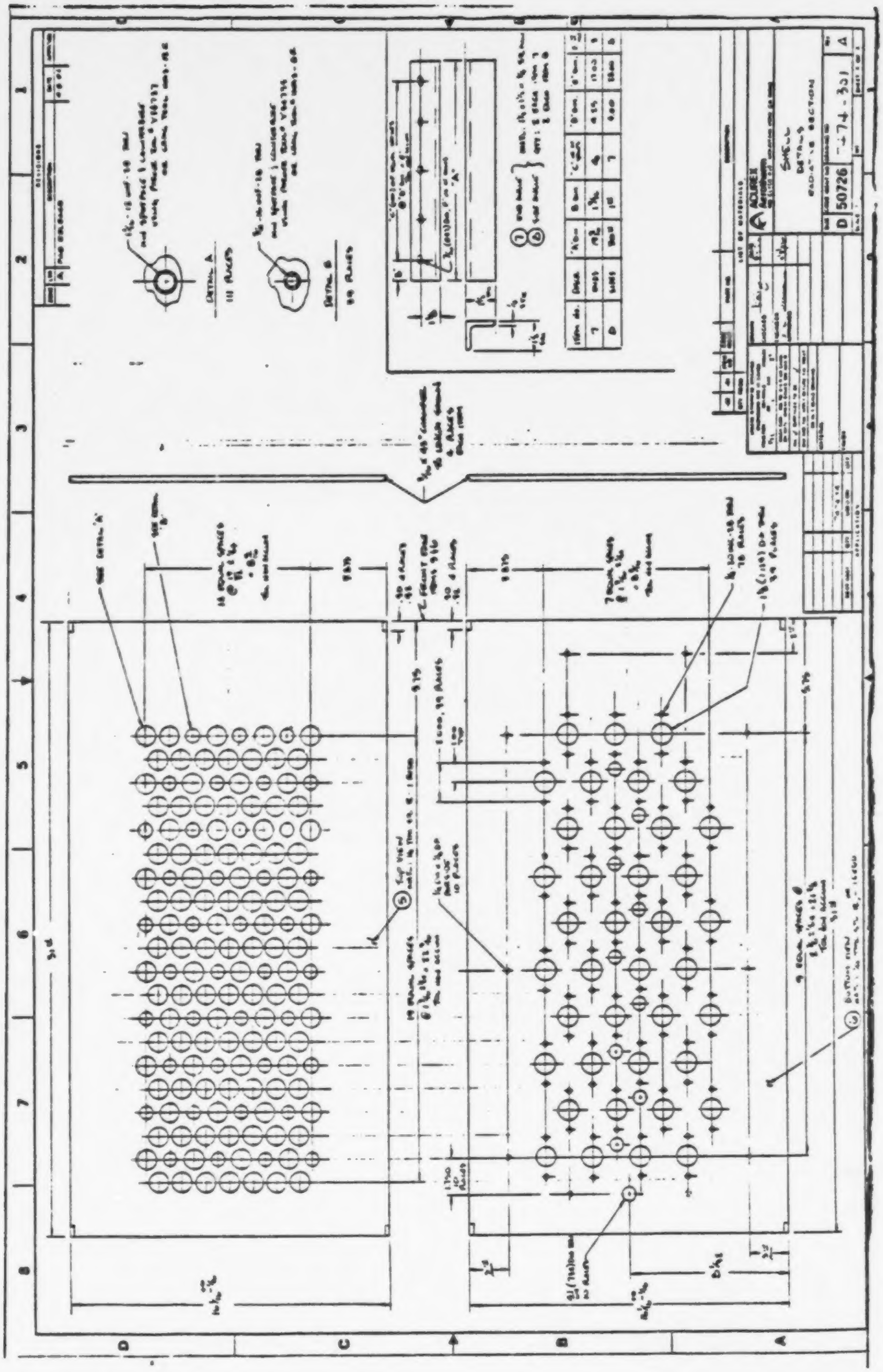

Figure 6-22. Shell details, watertube boiler.

The gas inlet to the radiant section (see Figure 6-20) is constructed of castable refractory and anchored to a cover plate. This provides a transition in the flow area from the circular mixing section via a 0.122 radian (7-degree) half-angle expanding cone. The flow area at the exit of the cone matches the area of flow between the tubes. The cover plate seals the radiant section (using a square array of bolt holes) and allows connection to the flanged mixing section duct. The inlet duct is an 11.4-cm (4.5-inch) pipe.

6.4.1.2 Adiabatic Section

The shell for the adiabatic section was constructed of carbon steel top, bottom, and side wall plates. The gas path was lined with castable refractory backed by fibrous insulation, both of similar materials to those of the radiant section. The combustion gas path formed by the refractory was square for easy transition from the radiant section. The flow area for the monolith was nominally 12.07 cm (4.75 inches) square. The 0.393 radian (22.5 degree) (from centerline) angle for the converging section at the inlet of the catalyst was selected to minimize pressure loss through the transition.

6.4.1.3 Convective Section

The convective section was of similar design to the radiant section but contained no catalyst tubes. The watertube arrangement was represented by the hole pattern in the upper plate (Figure 6-23). The gas path was also approximately 24.1 cm (9.5 inches) square and 78.7 cm (31 inches) in length. Similarity in construction between the radiant and convective sections was maintained to reduce construction costs, but commercial applications may demand varying the designs to optimize construction for different operating conditions.

6.4.1.4 Water-Quenched Exhaust Section

The water-quenched exhaust section could be used to cool gases exiting from any of the various hot gas sections shown in Figure 6-20. Four spray nozzles were used to atomize water for rapid mixing and cooling of hot gases.

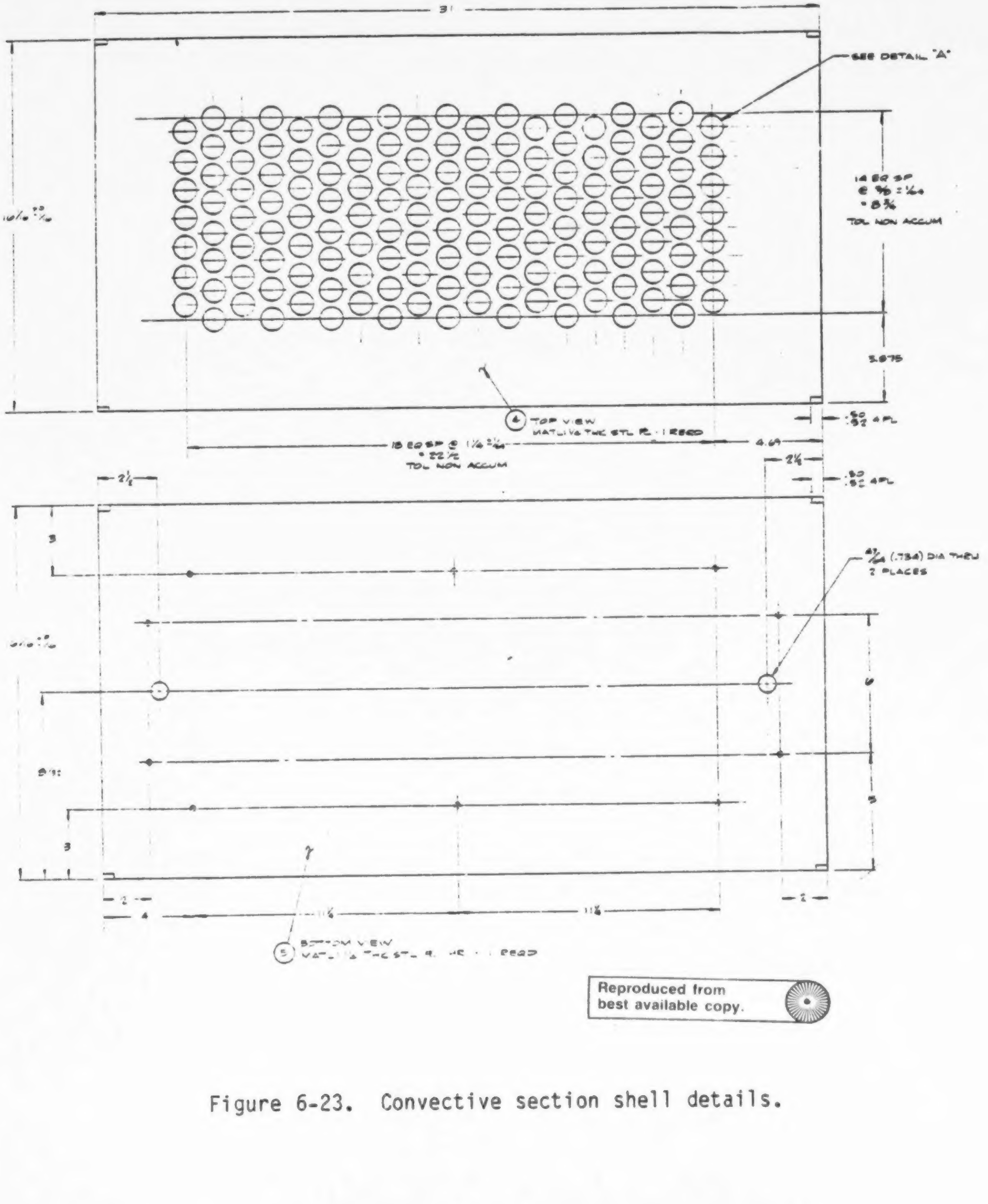
31
SEE DETAIL "A"
14 EQ SP @ 9/16 ± 1/64 = 8 3/4 TOL NON ACCUM
3.875
.50 .52 4 PL
④ TOP VIEW MAT'L 1/4 THK STL PL · 1 REQD
18 EQ SP @ 1 1/4 ± 1/64 = 22 1/2 TOL NON ACCUM
4.69
2 1/8
.50 .52 4 PL
47/64 (.734) DIA THRU 2 PLACES
3
6
5
3
2
4
11 1/4
11 1/4
2
⑤ BOTTOM VIEW

Reproduced from
best available copy.

Figure 6-23. Convective section shell details.

A photograph of the radiant section, mixing section, and exhaust section ready for testing is shown in Figure 6-24.

6.4.2 Test Results

Experimental objectives were to determine the operating characteristics and emissions performance of the nonconcentric watertube boiler. In the later stages of the program, only the radiant section could be tested. The test procedure included checkout of the radiant section and auxiliary equipment.

Operation of the boiler and test facility auxiliary equipment was checked during the curing cycle of the radiant section castable refractory. The refractory was cured with electrically preheated air, attaining 700K to 756K (800°F to 900°F) temperatures at the boiler inlet by the end of the cycle. The preheated air provided an opportunity to check gas thermocouples and pressure gauges as well as the boiler water feed and exhaust water quench systems.

The operation of the opposed jet was subsequently checked to identify a stable operating point to preheat the catalyst tubes to near 1256K (1800°F) for the initiation of catalytic combustion. This test was performed before installation of the catalyst tubes. Use of the opposed jet also provided an opportunity to test the water circulation system at higher gas temperatures.

Nine test points were run at air preheat conditions of 339K (150°F). One point was identified that provided a reasonable amount of stability with a jet to mainstream velocity ratio of 18, jet stoichiometry of 16 percent theoretical air, and air only in the mainstream. The mainstream air was also preheated to 589K (600°F) with the test point still found to be stable. This point was thus used for all subsequent operation of the opposed jet.

After opposed jet tests, the catalyst tubes were installed in the radiant section for two lightoff attempts: (1) lightoff with preheat only, and (2) lightoff with preheat and the opposed jet. In the preheated air lightoff tests, peak catalyst tube surface temperatures of 644K to 700K (700°F to 800°F) were achieved, and fuel was injected at two stoichiometries, 100 and 170 percent theoretical air. Catalyst lightoff was not achieved, however.

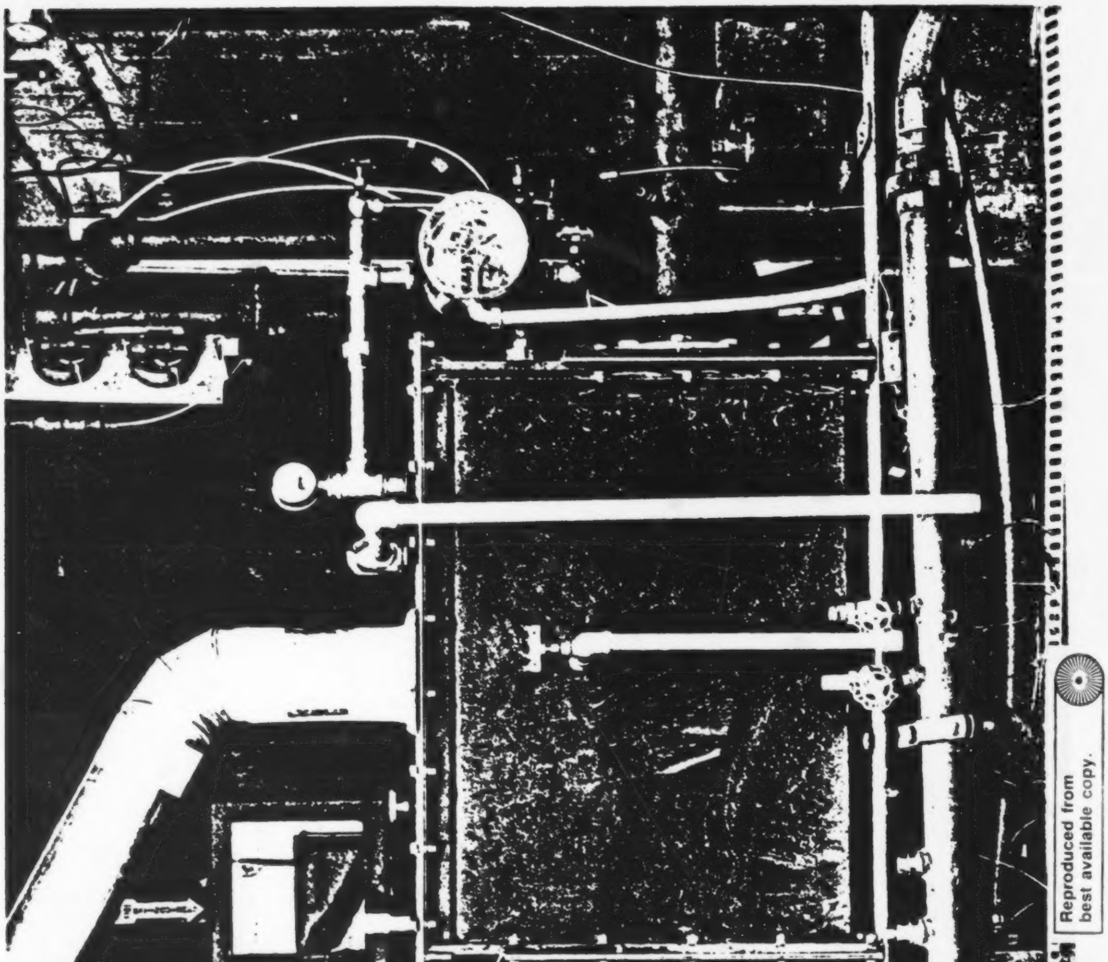

Reproduced from
best available copy.

Figure 6-24. Watertube boiler radiant section test setup.

With the opposed jet, a catalyst surface temperature of 967K (1700°F) was achieved. The opposed jet was then shut off and the mainstream fuel switched on. Due to difficulties in sustaining lightoff at these conditions, preheated air (588K to 644K) was used with the opposed jet to increase the temperature of the catalyst tubes. The front rows of the catalyst tubes were easily lit off and achieved surface temperatures of 1478K (2200°F). Combustion was sustained during these conditions with a near-stoichiometric mixture of fuel and air in the mainstream.

During testing, catalyst surface temperatures and gas temperatures in the radiant section were monitored at a 5-second data rate. A sheathed thermocouple (R-type) was attached to the surface of one catalyst tube in every other row. These thermocouples were located at the center of the tube length at the stagnation point. Ten additional thermocouples (K-type) were used to monitor gas temperatures behind each row of catalyst tubes. Pressure drop across the radiant section tube bed was measured with a magnehelic gauge. Emissions of carbon dioxide, oxygen, unburned hydrocarbons, carbon monoxide, and NO_x were also monitored.

An evaluation of the radiant section performance relative to design conditions was performed based on 7 hours of testing. A list of test points for which full emissions data were taken is given in Table A-17. Corresponding catalyst surface and gas temperatures are given in Table A-18 according to their order along the flowpath.

Combustion efficiency and NO_x emissions are shown in Figures 6-25 and 6-26, respectively. In both figures, data are plotted for input heat rates of 720 MJ/hr (683,000 Btu/hr) (with 667 to 703K preheat) and 962 MJ/hr (912,000 Btu/hr) with variable preheat and theoretical air.

At the low firing rate, combustion efficiency ranged from 85 to 99 percent and appeared to peak at around 140 percent theoretical air. NO_x emissions increased as excess air decreased toward stoichiometric conditions, resulting in emissions as high as 130 ppm (corrected to 0 percent O_2) at 118 percent theoretical air. These high combustion efficiencies and high NO_x emissions were not expected based on system design. Flameholding is suspected to be responsible for this performance, and is discussed below.

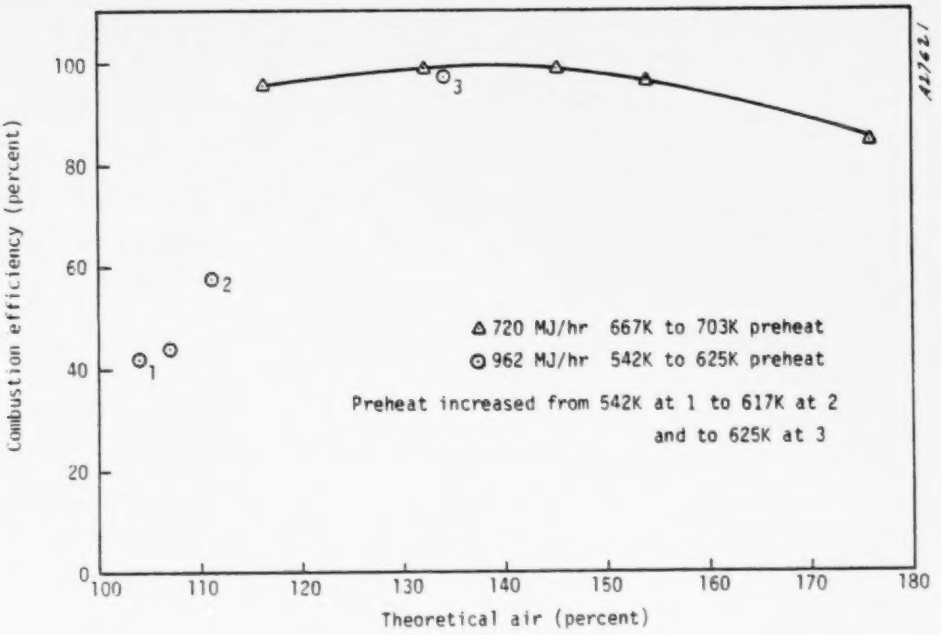

Figure 6-25. Watertube boiler combustion efficiency.

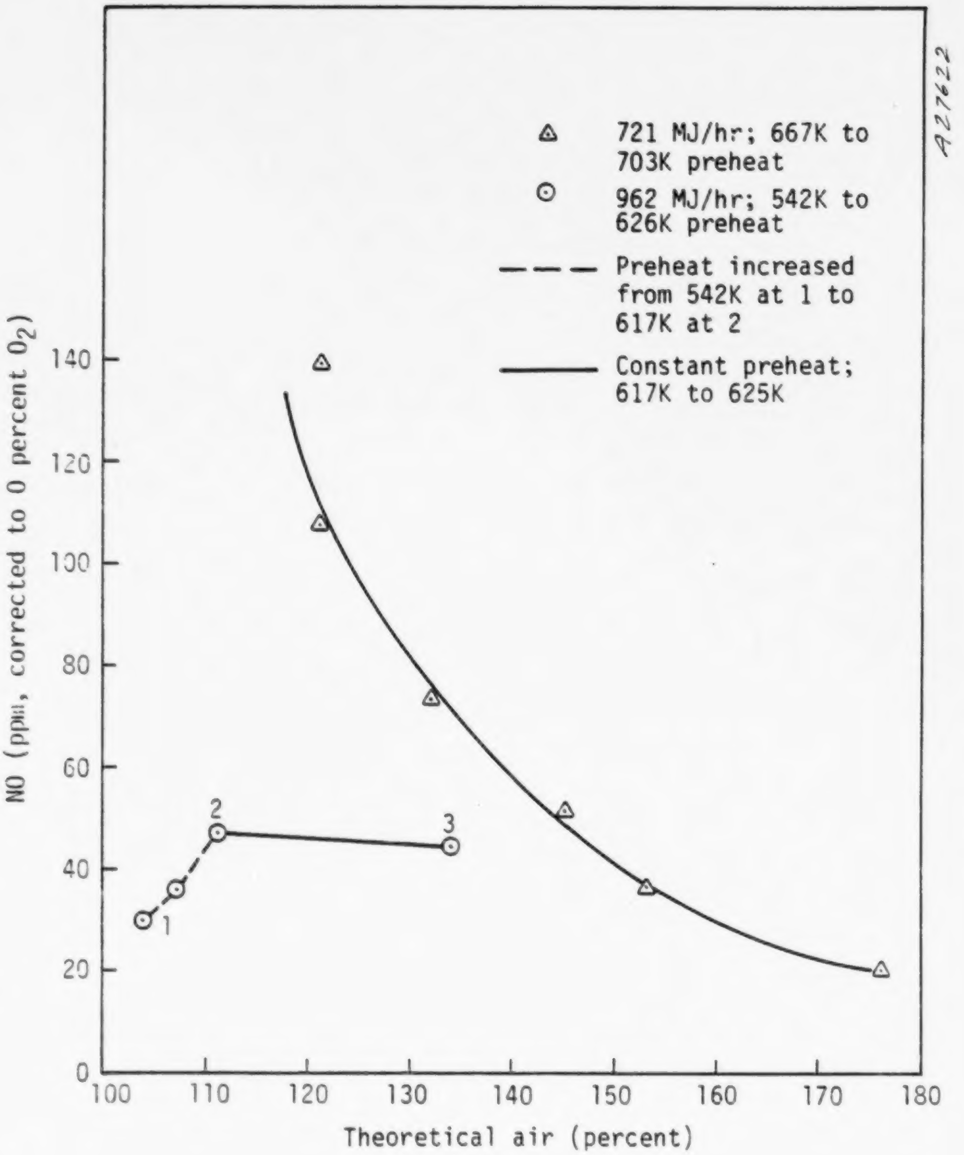

Figure 6-26. Watertube boiler NO_x emissions.

At the higher firing rate, preheat was varied to determine the effects of inlet temperature, but variations in stoichiometry also occurred. The results indicate strong effects of preheat and stoichiometry on the radiant section combustion performance. When preheat was reduced to around 542K (515°F) with 104 percent theoretical air, combustion efficiency was as low as 40 percent. With preheat increased to 617K, combustion efficiency increased to 60 percent at 111 percent theoretical air. Finally, with 625K preheat (almost constant) and theoretical air increased to 134 percent, combustion efficiency increased to 98.5 percent. NO_x emissions ranged from 30 to 47 ppm. The lower NO_x emissions appear due to a reduction in flameholding.

The presence of flameholding was noted by comparing measured temperatures of the catalyst tubes and gases in the immediate tube vicinity. Figure 6-27 shows these temperatures for two selected data points at the 720 MJ/hr and 962 MJ/hr firing rates. Temperatures for other data points in Table A-18 are comparable to those plotted. Flameholding is noted by gas temperatures in the first row in excess of catalyst tube temperatures, indicating that burning is taking place in the gas phase. Following the first three rows of catalyst tubes, a rapid drop in gas and catalyst tube temperatures was noted, indicating that little additional combustion takes place, and the balance of tube rows are primarily removing heat from the hot gases.

Some additional data indicated that flameholding could be eliminated such that catalytic reactions would predominate (as was intended in the design). Figure 6-28 illustrates the lack of gas phase reactions at a lowered preheat of 506K (450°F), a heat input of 962 MJ/hr, and 105 percent theoretical air. Catalyst tube temperatures exceeded gas temperatures at all corresponding locations. Also, the catalyst tube temperature profile is closer to that expected for catalytic reactions alone. The low preheat also lowered front tube temperatures and increased back row tube temperatures. Emissions data were not available to compute combustion efficiency or corrected NO_x emissions at this data point.

Catalyst tubes were inspected after 7 hours of testing. Several tubes in the first two rows were found to have cracked. Also, the first three rows of tubes suffered from a loss of catalyst, probably due to the high temperatures caused by flameholding. Catalyst tubes beyond the third row

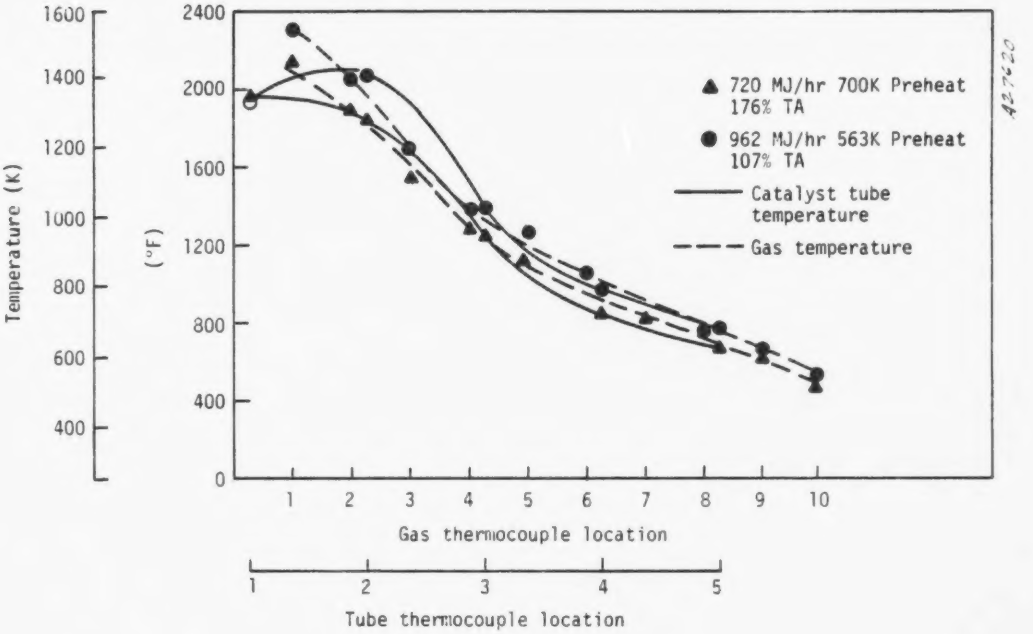

Figure 6-27. Catalyst tube and gas temperatures.

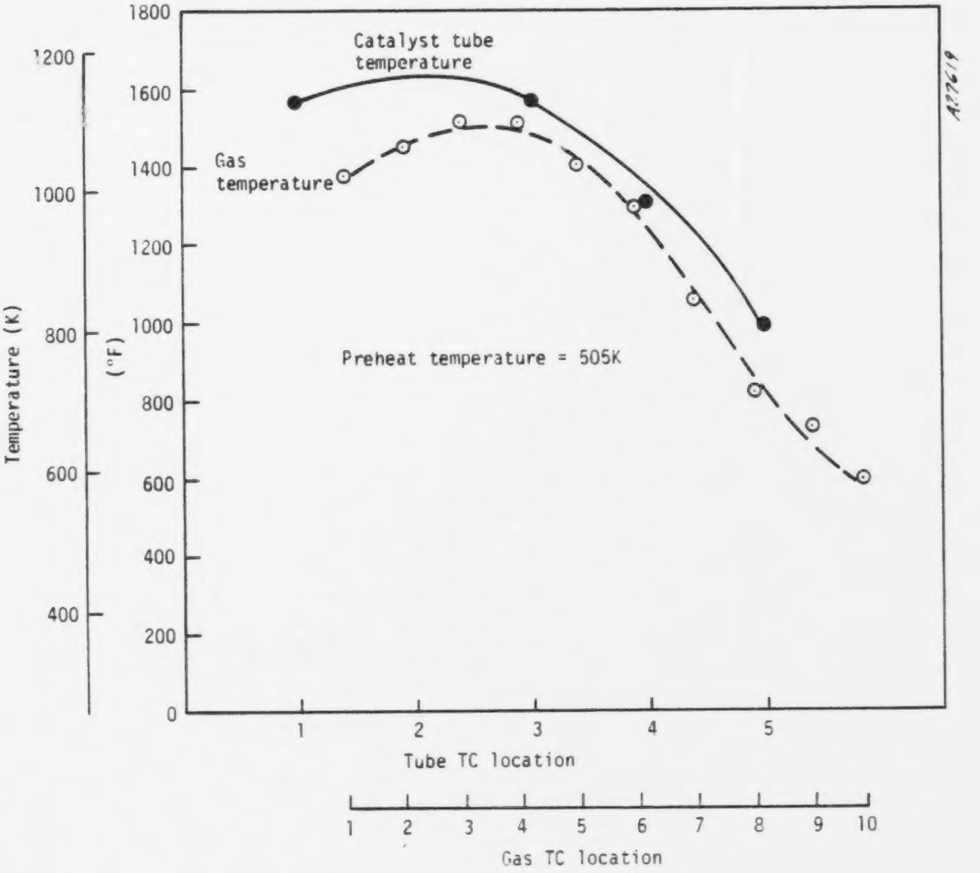

Figure 6-28. Catalyst tube and gas temperatures at low preheat.

showed little change from their original appearance. The tube cracks are expected to be a result of surrounding gas temperatures being higher than expected from system design. Thermal and mechanical shocks imposed by the opposed jet system during lightoffs of the system may also have contributed to tube cracking.

The limited testing of the watertube boiler radiant section indicated that operating conditions could be achieved that supported predominantly catalytic reactions with combustion efficiencies comparable to those expected from design analysis. However, high preheat temperatures were required for startup of the system which tended to support gas phase reactions within the tube bank. Operation at the design conditions without preheat should achieve the expected low NO_x emissions with combustion efficiencies near 50 percent. Additional testing is required to map performance over a range of parameters to determine acceptability of the radiant section. Resulting modifications could then be implemented for testing of the complete boiler system. Additional discussion of the recommended approach is provided in Section 7.

LIST OF SYMBOLS

English

A	Area
C	Constant
c_p	Specific heat at constant pressure
d	Diameter
D_h	Hydraulic diameter
E	Modulus of elasticity
F	View factor
h	Heat transfer coefficient
H_c	Enthalpy
k	Thermal conductivity
K	Constant
l	Tube length
ln	Natural logarithm
m	Mass flowrate
N	Number
Nu	Nusselt number
Pr	Prandtl number
q	Heat transfer
r	Radius
Re	Reynolds number
Sc	Schmidt number
Sh	Sherwood number
T	Temperature
v	Poisson's ratio
V	Velocity
X	Fuel mass fraction

Subscripts

b	Bulk gas
c	Catalyst
f	Flow
i	Inner or initial
o	Outer or final
s	Watertube surface
t	Tube
w	Wall
wt	Watertubes
∞	Free stream

Greek

α	Absorptivity
α_t	Coefficient of thermal expansion
ε	Emissivity
μ	Absolute viscosity
σ	Stefan-Boltzmann constant
σ_c	Tensile stress
σ_t	Compressive stress

REFERENCES FOR SECTION 6

6-1. Kesselring, J. P. et al., "Design Criteria for Stationary Source Catalytic Combustion Systems," EPA-600/7-79-181, NTIS-PB80-147317, August 1979.

6-2. Krill, W. V., et al., "Prototype Catalytic Systems," published in "Proceedings Fourth Workshop on Catalytic Combustion (Cincinnati, OH, May 1980)," EPA-600/9-80-035, NTIS-PB81-176067, August 1980, pp. 302-321.

6-3. Friedman, M. A., et al., "Development of a Catalytic/Radiative Watertube Boiler," published in "Proceedings: Fifth Workshop on Catalytic Combustion (San Antonio, TX, September 1981)," EPA-600/9-84-002, NTIS-PB84-145580, January 1984, pp. 333-352

6-4. Holman, J. P., Heat Transfer, McGraw-Hill Book Company, 1972.

6-5. Sparrow, E. M. and R. D. Cess, Radiation Heat Transfer, Hemisphere Publishing Corporation, 1978.

6-6. Siegel, R. and J. R. Howell, Thermal Radiation Heat Transfer, Hemisphere Publishing Corporation, 1981.

6-7. Roark, R. J. and W. C. Young, Formulas for Stress and Strain, McGraw-Hill Book Co., 1975.

SECTION 7

REQUIREMENTS FOR FUTURE DEVELOPMENT

7.1 STATUS OF RELATED RESEARCH PROGRAMS

Research, development, and demonstration programs in catalytic combustion technology that are closely related to the goals of the program described here have been conducted by several other investigators. All of these programs have focused on the application of honeycomb catalytic combustors to stationary gas turbine engines.

Work is being conducted by Westinghouse Electric Corporation and Engelhard Minerals and Chemicals Corporation under both in-house and Electric Power Research Institute support on the application of catalytic combustion to power turbines. Rig tests on catalyst elements of 0.36m (14-inches) diameter have been conducted in steady-state operation. Extremely low NO_x emissions were noted with No. 2 oil as fuel. Additional development tests were found to be required to improve fuel-air distribution approaching the catalyst. Work remaining included demonstration of startup and transient operation, improving performance, and durability verification.

A Japanese program conducted by the Central Research Institute of Electric Power Industry has been concerned with the development and evaluation of catalysts, a determination of optimum operating conditions for combustibility and flue gas composition, and development of a model catalytic combustor. The last stage of the program is to develop a prototype low NO_x catalytic combustor for a high temperature gas turbine.

The characteristics of catalytic combustion under both atmospheric pressure and pressurized conditions were investigated using in-house manufactured catalysts. A part of the catalytic combustion tests under pressurized conditions was sponsored by the Agency of Industrial Science and Technology of the Ministry of International Trade and Industry.

Results of the test program showed that thermal NO_x formation was reduced to less than 20 ppm at 1273K to 1773K at 0.101 to 0.808 MPa pressure, and complete catalytic combustion was achieved at 1373K to 1773K at 0.101 to 0.808 MPa pressure. The volumetric heat release rate increased as the combustion temperature, fuel flowrate, and combustion pressure were raised, and more than 1300×10^6 kcal/hr-m^3-cat was obtained at 1773K at 0.808 MPa.

Gulf Research and Development Company has developed a process to utilize flue gas from underground combustion enhanced oil recovery projects to provide some of the energy necessary for air compression while incinerating air pollutants. Flue gas enters a two-stage catalytic combustor at an elevated temperature, where it is burned at a controlled rate and expanded through a power turbine which drives an air compressor. Both the chemical energy and the potential energy of the pressurized gas are used to maximize the useful work extracted. Despite the low heat value of the flue gas, no supplemental fuel is required for catalytic combustion.

Data from small scale high pressure combustor tests using flue gas from an active combustion project illustrated the anticipated system performance in the prototype turbine. It was found that substoichiometric catalytic combustion fulfills the constant heat release and constant mass flow requirements of a gas turbine. Unburned hydrocarbon emissions from substoichiometric combustion were determined according to a combustion hierarchy with methane, an acceptable emission, the least likely to be totally burned. Carbon monoxide emissions can be controlled with proprietary catalyst formulations. Nitrogen oxide emissions ranged from 2 to 10 ppm.

The results of these related research programs are compatible with the results obtained under the program reported here. Clearly, further development work is required, as is discussed in the following section.

7.2 REQUIRED FURTHER DEVELOPMENT FOR SYSTEM IMPLEMENTATION

There have been three primary industrial combustion systems addressed in this program: the gas turbine combustor, the firetube boiler, and the watertube boiler. The catalytic combustors for each of these systems have obtained various levels of development, as reported in Sections 2, 5, and 6, and require different levels of effort for completion of demonstration. Clearly, different technical and marketing strategies to achieve commercialization are also needed for these widely diverse applications. The developmental requirements for each of these systems are described in the following discussion.

7.2.1 Gas Turbine

The gas turbine combustor tested under this program with its 1055 MJ/hr firing rate would be appropriate for a small engine of approximately 75 kW size. The combustor has been shown capable of cycling through startup and shutdown cycles for operation with both gaseous and distillate fuels. The next step in the development would be to integrate the combustor with a small engine, probably in the range of 50 to 300 kW. Testing at that scale would show additional combustor design criteria required for durable operation in the machine environment.

The monolithic catalyst configuration operating at high throughputs will continue to be the preferred catalyst arrangement. Although substrate materials compatible with current turbine inlet temperatures are suitable for these applications and are expected to have acceptable life, an extension to higher operating temperatures by increasing turbine inlet temperatures or by requirements for a larger percentage of dilution air would require further ceramic development. There is also room for catalyst coating improvement for existing catalyst material combinations.

Application of the combustor to small engines should require minimal additional development, and a working machine could be available within a 1-year time period. Successful small engine demonstration would allow extension to larger engines in progressive steps to the more demanding system constraints of the multiple-megawatt machines used for stationary power generation.

7.2.2 Firetube Boiler

Of the three systems tested in this program, the fiber burner in the firetube boiler has been brought closest to implementation as a commercial product. The successful 1000-hour durability demonstration has shown that the burner can be retrofit and perform suitably in a commercial firetube boiler.

The extension of this technology to the gas-fired industrial firetube boiler will require several further activities. First, fabrication of the burner in larger sizes must be addressed to meet the minimum boiler size of about 10,000 MJ per hour (200 hp). One-piece burner fabrication at these sizes appears impractical, and multisection burners are envisioned. Burner mounting and installation will also require development for these size boilers.

Although the existing burner materials appear sufficiently durable, advantages could be derived from less fragile fiber surfaces and surfaces that are capable of operation at higher temperatures without sintering. Other fiber material and fabrication procedures require investigation and testing to verify their improvements in performance.

Finally, since dual-fuel capabilities have been desirable in many previous firetube boiler applications, an investigation of operating the fiber burner on distillate fuels should be conducted. Although handling a premixed fuel and air mixture is difficult and probably requires sufficient air preheat to maintain a large fraction of the fuel oil in vaporized form, early tests of fiber materials have shown promise for combusting these mixtures. Primary development appears to be in the area of fuel handling rather than burner performance.

To ultimately achieve commercialization of an industrial firetube boiler with fiber burner, demonstrations of up to 5000 hours are required, representing an acceptable life to the user. These tests should be conducted in an industrial environment where it is feasible to provide representative test conditions.

The application of the fiber burner to commercial firetube boilers could be achieved with only small efforts beyond those of this program. For application to the more numerous industrial boiler applications, a development time of approximately 2 years is envisioned. Completion of these activities would then lead to extended applications to the largest firetube boilers.

7.2.3 Watertube Boiler

The catalytic watertube boiler represents the greatest departure from conventional system design of the three systems developed. Therefore, development of the system has required extensive work on system components, particularly the radiant section, in addition to containment of the catalyst itself. The nonconcentric tube radiant section of the 1055 MJ/hr boiler demonstrated in the program has shown promise for operation with very low NO_x emissions.

Since the full boiler system, including adiabatic combustor and convective section has not been tested to date, this effort is required to complete system demonstration. Tests would be conducted to verify low NO_x and high combustion efficiency and catalyst and boiler component durability. Additional catalyst tube coating durability may require attention although available materials appear sufficiently durable for the 1450K temperature requirement of the nonconcentric design. Monolithic catalyst development activities similar to those for the gas turbine application (although at lower throughputs) are anticipated for achieving acceptable operation to 1700K (2600°F) in the adiabatic combustor. Optimum monolithic catalyst configurations should also be addressed.

Since a large number of industrial watertube boilers are fired on oil (or dual-fueled), the possibility of firing fuel oils in the nonconcentric radiant section should be investigated. As with the fiber burner in the firetube boiler, premixed, prevaporized fuel streams may be required. The potential for watertube fouling by distillate and heavier fuels at varying levels of air preheat require investigation.

Following initial testing with liquid fuels, durability should be further investigated via 1000-hour demonstration testing. A final test of nitrogen containing fuels in an air-staged arrangement should also be performed.

The additional testing and development for each of the three combustion systems should provide sufficient demonstration of the technology for manufacturer implementation in existing or new product lines. Continuing market analysis is required to develop commercialization plans and marketing strategies. These activities are best performed by manufacturers of gas turbine and boiler systems and can be most easily achieved by their intimate involvement in the development process.

APPENDIX A

TEST DATA

TABLE A-1. EPA-084 DATA SUMMARY

Test Point	Fuel (scfm)	Air (scfm)	Fuel (lbm/hr)	Air (lbm/hr)	TA* (%)	Space Velocity (hr^{-1})	Temp Inlet (°F)	Temp tile front (°F)	Temp tile (°F)	Temp tile rear (°F)	CO (ppm)	NO (ppm)	HC (ppm)	Q (Btu/hr)	Comments
48	0.072	1.165	0.182	5.24	170	53,300	80	125	290	350	10	2.4	1	4,000	Blue flame
49		1.096		4.93	160	50,326	80	175	600	1200	7.5	3.8	1		
51		1.028		4.63	150	47,397	81	275	780	1510	7.5	5.6	1		
52		0.959		4.32	140	44,423	82	400	1100	1875	7.5	12.5	0		
53		0.891		4.01	130	41,494	82	475	1275	1980	10	19.0	0		
55		0.822		3.70	120	38,520	84	550	1525	2050	15	34	0		
56		0.788		3.55	115	37,055	84	600	1660	2090	10	48	0		
57		0.761		3.42	111	35,892	84	625	1750	2110	12.5	59	0		Incandescent flashback
59		0.740		3.33	108	34,987	87	1700	1200	1090	42	36	27		
26	0.045	0.728	0.114	3.28	170	33,307	76	250	700	1360	2.5	4.9	2	2,500	Blue flame
27		0.685		3.08	160	31,454	76	310	860	1600	2.5	6.1	2		
28		0.643		2.89	150	29,644	76	400	1060	1710	2.5	8.8	2		
29		0.560		2.52	140	26,068	77	525	1390	1840	2.5	15	2		
34		0.557		2.51	130	25,939	78	1160	1650	1490	125	6.2	50		Incandescent flashback
35		0.514		2.31	120	24,086	82	1450	1050	875	25	20	7		
41	0.031	0.502	0.077	2.26	170	22,966	79	450	1010	1680	10	5.5	5	1,700	Blue flame
42		0.472		2.12	160	21,673	79	500	1160	1750	10	7.0	4		
43		0.443		1.99	150	20,424	79	570	1380	1780	10	9.7	4		
45		0.413		1.86	140	19,131	80	1000	1560	1500	245	8.5	75		Incandescent flashback
46		0.384		1.73	130	17,881	83	1350	1000	880	35	21.5	10		
37	0.018	0.291	0.045	1.31	170	13,314	80	1150	790	650	15	8.8	6	1,000	Unstable, flashback occurs
38	0.018	0.274	0.045	1.23	160	13,141	81	1125	760	650	12.5	15	6	1,000	
76	0.25	3.40	0.63	15.3	143	157,270	90	2425	1940	1780	7.5	8	1	13,860	
77		3.16		14.2	133	146,929	91	2500	1980	1825	7.5	14	1		
78		3.05		13.7	128	142,190	92	2520	2000	1850	7.5	19	1		
79		2.95		13.3	124	137,881	94	2575	2010	1860	7.5	30	1		
80		2.67		12.0	112	125,816	96	2650	2040	1890	10	54	1		
57	0.24	3.54	0.60	15.9	155	162,872	83	2360	1900	1700	7.5	5.7	1	13,305	Maximum throughput test
58	0.27	4.37	0.68	19.7	170	199,927	83	2290	1890	1690	10	3.1	5	15,000	
60	0.36	5.76	0.91	25.9	168	263,694	82	2310	1950	1750	7.5	3.5	2	20,000	
62	0.45	7.07	1.14	31.8	165	324,020	82	2360	2025	1810	7.5	3.9	1	25,000	
64	0.54	8.43	1.36	37.9	164	386,497	81	2310	2050	1810	7.5	4.0	2	30,000	
65	0.63	9.60	1.59	43.2	160	440,788	81	2350	2090	1850	7.5	4.5	1	35,000	
66	0.72	10.96	1.82	49.3	160	503,265	81	2310	2090	1850	10	4.7	1	40,000	
67	0.81	12.18	2.05	54.8	158	559,710	80	2260	2100	1840	12.5	5.0	0	45,000	
68	0.92	13.66	2.32	61.5	156	628,219	79	2250	2110	1860	12.5	5.5	0	51,000	

*Stoichiometry determined by exhaust O_2 measurements

TABLE A-2. EPA-085 DATA SUMMARY

Test point	Fuel (scfm)	Air (scfm)	Fuel (lbm/hr)	Air (lbm/hr)	TA (%)	Space velocity (hr^{-1})	Temp inlet (°F)	Upstream temp (°F)	Tile temp (°F)	Downstream temp (°F)	CO (ppm)	NO (ppm)	HC (ppm)	Q (Btu/hr)
2	0.018	0.291	0.045	1.31	170	15,772	72	1175	910	690	102.5	9.5	40	1,000
3	0.018	0.291	0.045	1.31	170	15,772	73	1175	910	690	47.5	11	20	1,000
5	0.031	0.502	0.077	2.26	170	27,205	70	425	1050	1660	7.5	5.5	2	1,700
6		0.472		2.12	160	25,674		500	1190	1850		7.4	2	
7		0.436		1.96	148	23,836		750	1350	1900		11.5	1	
9		0.410		1.85	139	22,509		1010	1650	1490	--	--	--	
13		0.407		1.83	138	22,356		--	--	--	95	10	75	
15	0.045	0.728	0.114	3.28	170	39,455	72	390	860	1625	7.5	5.7	1	2,500
16		0.685		3.08	160	37,260	72	425	975	1790	7.5	7.4		
17		0.634		2.85	148	34,658	73	525	1160	1990	7.5	12		
18		0.582		2.62	136	32,003	73	640	1310	2025	10	18.5		
21		0.556		2.50	130	30,676	77	950	1510	1400	55	15	60	
23	0.072	1.165	0.182	5.24	170	63,139	73	225	550	940	10	4.6	9	4,000
24		1.096		4.93	160	59,617	73	275	650	1200		6.6	3	
25		1.00		4.50	146	54,717	74	400	1010	1900		12.5	1	
26		0.93		4.19	136	51,144	74	490	1150	2090		18.5	1	
27		0.88		3.96	128	48,592	75	550	1275	2200		30	2	
28		0.82		3.69	120	45,530	75	625	1380	2260		46	2	
29		0.788		3.55	115	43,896	75	700	1450	2290	12.5	62	3	
30		0.753		3.39	110	42,109	75	810	1500	2350	12.5	69	4	
31		0.747		3.36	109	41,803	79	1710	1400	1075	85	37	42	
34	0.25	3.57	0.63	16.07	150	194,980	81	2490	2280	1860	7.5	12.5	0	13,860
35		3.81		17.14	160	207,230	81	2470	2250	1850		7.4		
36		3.33		14.99	140	182,730	83	2550	2325	1890		15		
37		3.09		13.90	130	170,480	86	2620	2360	1910	10	28		
38		2.86		12.87	120	158,740	90	2610	2360	1890		33		
39		2.62		11.79	110	146,490	92	2660	2390	1900		44		
44*	0.24	3.66	0.60	16.47	160	199,064	78	2360	2050	1950	12.5	3.2	1	13,305
45	0.27	4.37	0.68	19.66	170	236,835	78	2320	2040	1925	7.4	2.3		15,000
46	0.36	5.83	0.91	26.24	170	315,950	77	2340	2100	1950	10	2.6		20,000
47	0.451	7.30	1.14	32.85	170	395,627	77	2350	2140	1950		2.4		25,000
48	0.54	8.74	1.36	39.33	170	473,670	76	2320	2140	1910		2.6		30,000
49	0.63	10.20	1.59	45.90	170	552,786	76	2300	2175	1900		2.8		35,000
50	0.722	11.41	1.82	51.35	166	619,242	76	2350	2240	1975	12.5	3.1		40,000
51	0.812	12.68	2.05	57.06	164	688,660	75	2350	2240	1800	10	3.5		45,000

*Second tile

TABLE A-3. EPA-086 AND EPA-087 DATA SUMMARIES

Catalyst	Test point	TA (%)	SV (1/hr)	$\dot{m}_{fuel}$ (lb/hr)	$\dot{m}_{air}$ (lb/hr)	T_{front} (°F)	T_{back} (°F)	Velocity (ft/sec)	Q (Btu/hr)	Comments
EPA-086	1	186	87,450	1.71	54.7	1300	1500	6.2	37,620	Shut down, gasket blown out
	2	145	88,760	2.19	54.7	2000	2000	6.3	48,180	
	3	144	76,490	1.92	47.4	2000	2000	5.3	42,240	
	4	158	88,280	2.02	54.7	2000	2000	6.3	44,440	
	5	158	88,280	2.02	54.7	2000	2000	6.3	44,440	
	6	142	93,590	2.24	57.9	2000	2000	6.6	49,280	
	7	126	92,690	2.62	56.5	2240	2220	6.6	57,640	Small cracks appear near thermocouple
	8	126	94,900	2.67	57.9	2200	2200	6.7	58,740	Cracks increasing
	9	131	90,900	2.47	55.6	2200	2240	6.4	54,340	
	10	138	91,310	2.37	56.1	2200	2210	6.5	52,140	
	11	133	94,000	2.34	53.4	2200	2200	6.7	51,480	Does not stay lit
	12	103	90,490	3.07	54.3	2370	2400	6.4	67,540	Does not stay lit, flashback
EPA-086 and 087	13	164	76,880	1.94	54.7	2100	2000	6.2	42,680	Fine cracks
	14	183	76,580	1.74	54.7	2000	1900	6.2	38,280	Increasing cracks and fractures
	15	183	76,580	1.74	54.7	2000	1900	6.2	38,280	|
	16	178	76,700	1.79	54.7	2000	1950	6.2	39,380	|
	17	178	76,700	1.79	54.7	2020	1950	6.2	39,380	

TABLE A-4. FIRETUBE BOILER BURNER (CTI 1) TEST DATA SUMMARY

Test point	TA (%)	Specific heat release (Btu/hr-ft^2)	Heat release (Btu/hr)	Velocity (ft/sec)	$\dot{m}_{air}$ (lbm/hr)	$\dot{m}_{fuel}$ (lbm/hr)	ΔP_{burner} in.H_2O	T_{burner} max (°F)	T_{burner} avg (°F)	NO_x (ppm)	CO (ppm)	UHC (ppm)	$T_{exhaust}$ (°F)
0001	137							2140	2003				1746
0002	142	122,200	366,600	0.55	416	16.7	0.30	2147	2001	11	--	--	1707
0003	126	123,000	369,000	0.50	372	16.8	0.35	2080	2002	24	--	--	1812
0004	117	123,700	371,900	0.47	348	16.9	0.34	2092	2028	42	--	--	1846
0005	100	123,600	370,800	0.41	299	16.9	0.40	2183	2097	82	--	--	1973
0006	98	123,300	369,900	0.40	292	16.8	0.42	2252	2121	77	--	--	2007
0007	151	99,000	297,100	0.47	359	13.5	0.30	2023	1943	10	--	--	1674
0008	138	99,000	297,000	0.43	321	13.5	0.30	1989	1931	13	--	--	1726
0009	127	99,000	297,000	0.40	302	13.5	0.35	2006	1942	23	--	--	1810
010	112	98,800	296,500	0.36	268	13.5	0.40	2044	1974	43	--	--	1886
011	107	98,100	294,300	0.34	253	13.4	0.42	2106	2023	59	--	--	1933
012	101	98,200	294,500	0.32	240	13.4	0.42	2148	2040	65	--	--	1956
013	97	98,000	294,000	0.31	230	13.4	0.42	2182	2034	59	--	--	1987
014	146	78,900	236,800	0.37	278	10.8	0.30	1969	1873	11	--	2	1686
015	132	78,500	235,500	0.33	249	10.7	0.32	1969	1880	17	--	1	1780
016	123	79,900	239,800	0.32	236	10.9	0.35	1987	1902	25	--	0	1834
017	117	79,300	238,000	0.30	224	10.8	0.35	2022	1933	42	--	0	1899
018	102	79,300	237,900	0.26	195	10.8	0.37	2115	1966	46	--	0	2030
019	101	78,300	234,900	0.26	192	10.7	0.37	2107	1956	38	--	0	2032
020	97	77,700	233,100	0.25	181	10.6	0.37	2081	1940	32	--	0	1982
021	144	64,600	193,900	0.31	223	8.8	0.25	1936	1836	11	--	0	1657
022	133	64,600	193,700	0.27	206	8.8	0.25	1951	1842	15	--	0	1982
023	124	64,600	193,700	0.26	193	8.8	0.25	1968	1863	23	--	0	1799
024	112	64,200	192,600	0.23	174	8.8	0.30	2012	1908	36	--	0	1890
025	104	64,400	193,200	0.22	162	8.8	0.30	2096	1949	29	--	1	1966
026	98	64,500	193,500	0.21	153	8.8	0.35	2063	1905	29	--	1	1976
027	97	64,700	194,000	0.21	153	8.8	0.35	2044	1895	31	--	1	1969
028	107	63,800	191,400	0.22	164.0	8.7	0.32	2095	1938	27	--	0	1918
029	104	64,800	194,300	0.22	163.3	8.8	0.32	2095	1940	24	--	1	1906
030	105	65,100	195,400	0.22	169.6	8.9	0.32	2090	1932	23	--	1	1889
031	106	65,142	195,400	0.23	166.5	8.9	0.32	2091	1930	23	--	0	1926
032	106	65,000	195,100	0.22	166.7	8.9	0.32	2095	1932	23	--	56	1970
033	107	64,600	193,900	0.22	166.1	8.8	0.32	2095	1933	23	--	0	1972
034	106	64,800	194,400	0.22	165.8	8.8	0.32	2107	1947	25	--	0	1962
035	107	64,400	193,200	0.22	166.5	8.8	0.32	2114	1955	28	--	0	1949

(continued)

TABLE A-4. CONCLUDED

Test point	TA (%)	Specific heat release (Btu/hr-ft^2)	Heat release (Btu/hr)	Velocity (ft/sec)	$\dot{m}_{air}$ (lbm/hr)	$\dot{m}_{fuel}$ (lbm/hr)	ΔP_{burner} in.H_2O	$T_{burner\ max}$ (°F)	$T_{burner\ avg}$ (°F)	NO_x (ppm)	CO (ppm)	UHC (ppm)	$T_{exhaust}$ (°F)
036	104	65,500	196,400	0.22	164.4	8.9	0.30	2113	1965	30	32	3	1870
037	105	65,600	196,700	0.23	166.7	8.9	0.30	2050	1930	31	14	0	1861
038	107	64,300	193,000	0.22	165.8	8.8	0.30	2013	1896	--	14	0	1818
039	107	64,100	192,400	0.22	164.7	8.7	0.30	2025	1910	29	14	0	1844
040	117	64,000	192,000	0.24	179.9	8.7	0.30	1988	1874	24	12	0	1812
041	128	64,000	192,000	0.26	196.7	8.7	0.30	1948	1839	17	13	0	1748
042	136	64,000	191,900	0.28	208.6	8.7	0.30	1926	1823	12	14	0	1684
043	148	63,500	190,400	0.30	224.9	8.7	0.30	1900	1802	8	16	0	1630
044	101	78,700	236,200	0.26	191.5	10.7	0.35	2142	1978	36	940	2	1928
045	98	78,600	235,700	0.25	185.5	10.7	0.35	2107	1948	39	1.5%	3	1925
046	111	78,600	235,900	0.28	209.5	10.7	0.35	2095	1977	43	14	3	1890
047	120	79,100	237,300	0.31	227.9	10.8	0.33	2066	1934	38	14	4	1853
048	136	77,500	223,400	0.31	252.5	10.6	--	2012	1906	22	14	6	1768
050	142	77,500	232,500	0.35	263.6	10.6	0.25	1981	1888	12	15	7	1669
051	126	77,200	231,500	0.31	233.3	10.5	0.30	2021	1918	28	13	7	1809
052	107	76,900	230,500	0.27	198.8	10.5	0.32	2126	2003	47	15	6	1901

TABLE A-5. FIRETUBE BOILER BURNER (CTI 2) TEST DATA SUMMARY

Test No.	TA (%)	Specific heat release (Btu/hr-ft^2)	Heat release (Btu/hr)	Velocity (ft/sec)	$\dot{m}_{air}$ (lbm/hr)	$\dot{m}_{fuel}$ (lbm/hr)	ΔP burner (inches H_2O)	T_{burner} max (°F)	T_{burner} avg (°F)	NO_x (ppm)	CO (ppm)	UHC (ppm)
002	106	66,000	200,000	0.23	163.3	9.4	--	1986	1916	25	60	0
003	110	64,400	193,100	0.23	166.6	8.8	--	1936	1891	26	22	0
004	105	63,800	191,500	0.22	160.6	8.7	--	1981	1916	22	101	0
005	100	63,800	191,400	0.20	150.1	8.7	--	1978	1895	27	3400	0
006	122	64,300	192,800	0.26	195.6	8.2	--	1942	1876	18	18	0
007	117	64,400	193,100	0.25	186.2	8.8	--	1949	1882	24	18	0
008	130	64,200	196,700	0.27	206.7	8.8	--	1933	1867	12	17	0
009	138	64,000	192,200	0.29	218.6	8.7	--	1973	1860	8	18	0
010	126	65,200	195,600	0.29	216.3	8.9	0.90	2031	1847	14	10	0
011	122	65,000	195,000	0.28	207.3	8.8	0.11	2046	1808	18	12	0
012	108	65,000	195,100	0.25	189.7	8.8	0.14	2080	1885	32	8	0
013	105	65,200	195,700	0.24	180.4	8.9	--	2091	1896	32	18	0
014	100	65,400	196,300	0.24	174.3	8.9	0.15	2100	911	32	1132	0
015	106	65,100	195,000	0.24	177.9	8.9	0.18	2100	1894	29	113	0
016	139	78,500	235,600	0.38	291.6	10.7	--	2088	1889	10	0	0
017	126	79,400	238,300	0.36	268.3	10.8	--	2114	1915	19	0	0
018	117	80,400	241,300	0.32	235.8	11.0	0.15	2150	1947	41	23	3
019	110	79,500	238,500	0.30	223.6	10.8	0.16	2178	1970	50	23	0
020	104	80,000	240,160	0.29	215.6	10.9	0.17	2209	2003	49	74	0
021	104	79,700	239,100	0.28	206.4	10.9	0.18	2176	1967	50	3345	0
022	112	79,400	238,200	0.31	229.2	10.8	0.16	2179	1980	49	32	0
024	112	99,700	299,200	0.35	262.2	13.6	0.14	2229	2013	45	18	4
025	106	99,600	298,700	0.33	244.6	13.5	0.16	2259	2038	55	23	3
026	119	99,000	296,900	0.37	275.2	13.5	0.14	2210	1996	35	13	2
027	113	98,800	296,400	0.35	257.4	13.5	0.16	2226	2011	47	12	2
028	112	122,300	366,800	0.42	308.5	16.7	0.16	2315	2080	58	13	3
029	110	124,700	374,000	0.42	306.7	17.0	0.17	2336	2098	68	18	2
030	107	125,400	376,300	0.40	292.2	17.1	0.17	2352	2113	71	18	1
031	108	123,500	370,600	0.40	297.5	16.8	0.18	2342	2106	71	12	1
033	114	123,100	369,200	0.42	306.6	16.8	0.15	2318	2082	58	15	1

TABLE A-6. FIRETUBE BOILER: CHEMO-THERMIC 3 -- PARAMETRIC TESTING

Test point	TA (%)	Specific heat release (Btu/hr-ft^2)	Heat release (Btu/hr)	Velocity (ft/sec)	$\dot{m}_{air}$ (lbm/hr)	$\dot{m}_{nat\ gas}$ (lbm/hr)	ΔP_{burner} (in. H_2O)	$T_{burner\ avg}$ (°F)	T_{exh} (°F)	NO_x (ppm)	CO (ppm)	UHC (ppm)	O_2 (%)	Comments
001	123	65,700	197,200	0.21	156.8	9.0	0.32	1678	1505	11	13	24	4.4	Natural gas at
002	120	64,600	193,800	0.20	149.3	8.8	0.32	1702	1529	11	10	7	3.8	65,000 Btu/hr-ft^2
003	115	64,900	194,700	0.19	139.3	8.9	0.32	1718	1537	12	12	6	3.0	
004	110	65,800	197,400	0.19	138.3	9.0	0.32	1742	1546	11	35	4	2.1	
005	105	65,100	195,200	0.19	134.0	8.9	0.32	1749	1522	4	601	8	1.2	
006	102	65,800	197,300	0.18	130.9	9.0	0.32	1806	1522	15	3147	9	0.48	
007	125	80,400	241,300	0.26	193.4	11.0	0.34	1711	1563	13	15	4	4.5	Natural gas at
008	120	79,800	239,300	0.26	189.2	10.9	0.34	1727	1570	15	13	4	3.9	80,000 Btu/hr-ft^2
009	115	80,300	240,800	0.25	186.2	11.0	0.36	1758	1591	18	14	4	3.0	
010	110	79,700	239,200	0.24	173.0	10.9	0.36	1776	1608	18	19	3	2.1	
011	105	79,200	237,700	0.24	171.5	10.8	0.36	1811	1611	8	469	4	1.0	
012	102	79,200	237,600	0.23	165.3	10.8	0.36	1823	1591	15	1819	4	0.51	
013	110	79,800	239,500	0.23	165.9	10.9	0.34			11	146	3	2.15	Steady state at
014	112	80,000	239,900	0.23	167.3	10.9	0.34			16	41	2	2.4	80,000 Btu/hr-ft^2
015	111	79,600	238,800	0.23	170.2	10.9	0.34			13	57	2	2.2	
016	110	79,800	239,500	0.23	165.9	10.9	0.34			10	76	4	2.1	
017	111	80,000	240,000	0.22	162.2	10.9	0.34			10	61	6	2.2	
018	110	80,000		0.22	35 scfm	4.3 scfm	0.34				0.22%	2	2.0	
019	115	80,000		0.22							102	0	3.1	

TABLE A-7. FIRETUBE BOILER: CHEMO-THERMIC 4

Test point	TA (by O_2) (%)	Specific heat release (Btu/hr-ft^2)	Heat release (Btu/hr)	Velocity (ft/sec)	$\dot{m}_{air}$ (lbm/hr)	$\dot{m}_{nat\ gas}$ (lbm/hr)	ΔP_{burner} (in. H_2O)	$T_{burner\ avg}$ (°F)	T_{exh} (°F)	NO_x (ppm)	CO (ppm)	UHC (ppm)	O_2 (%)	Comments
001	129	64,100	192,300	0.20	144.8	8.7	0.22	1764	1681	11	66	--	5.1	Natural gas at 64,000 Btu/hr-ft^2
002	125	64,000	192,000	0.18	134.0	8.7	0.24	1802	1675	14	75	--	4.6	
003	119	64,000	172,100	0.18	128.0	8.7	0.24	1818	1668	10	126	--	3.7	
004	115	64,100	192,300	0.17	125.8	8.7	0.24	1832	1666	5	503	--	3.0	
005	111	64,000	192,000	0.17	118.4	8.7	0.24	1856	1659	12	3325	--	2.2	
006	136	78,600	235,900	0.26	190.2	10.7	0.28	1820	1747	4	278	--	6.0	Natural gas at 80,000 Btu/hr-ft^2
007	130	79,500	238,600	0.25	183.4	10.8	0.28	1841	1774	7	279	--	5.3	
008	126	79,300	237,900	0.24	177.3	10.8	0.28	1854	1771	6	358	--	4.7	
009	119	79,300	238,000	0.23	166.8	10.8	0.28	1886	1784	8	416	--	3.8	
010	116	78,900	236,700	0.22	160.1	10.8	0.28	1904	1778	12	705	--	3.1	
011	110	78,800	236,300	0.21	149.9	10.7	0.30	1932	1744	22	3292	--	2.1	

TABLE A-8. J-M FIRETUBE BOILER BURNER PARAMETRIC TESTING (INITIAL)

Test Pt.	TA (%)	Specific heat release (Btu/hr-ft^2)	Heat release (Btu/hr)	Velocity (ft/sec)	$\dot{m}_{air}$ (lbm/hr)	$\dot{m}_{natural\ gas}$ (lbm/hr)	ΔP_{burner} (in. H_2O)	$T_{burner\ avg}$ (°F)	$T_{exhaust}$ (°F)	NO_x (ppm)	CO (ppm)	UHC (ppm)	Comments
0001	140	65,800	374,600	0.26	368.4	17.0	--	1957	1206	4	20	3	Natural gas at 65,000 Btu/hr-ft^2
0002	129	65,400	372,200	0.24	331.6	16.9	--	1935	1240	5	7	3	
0003	121	65,600	373,300	0.22	312.6	17.0	--	1925	1215	6	10	0	
0004	115	65,800	374,600	0.21	293.8	17.0	--	1940	1232	8	8	0	
0005	112	65,200	371,100	0.20	281.0	16.9	--	1973	1220	9	6	0	
0006	110	65,800	374,800	0.20	274.3	17.0	--	1999	1237	10	8	0	
0007	106	64,400	366,500	0.19	268.6	16.7	--	2002	1245	11	7	0	
0008	104	65,500	372,700	0.19	266.4	16.9	--	2023	1269	11	9	0	
0009	102	65,300	371,900	0.18	253.7	16.9	--	2048	1279	10	65	0	
0010	100	65,300	372,000	0.18	250.8	16.9	--	2062	1290	13	288	--	
0011	122	79,300	451,600	0.27	385.2	20.5	--	2051	1226	7	2	0	80,000 Btu/hr-ft^2
0012	128	79,800	454,300	0.29	402.1	20.7	--	2035	1230	7	4	0	
0013	115	79,400	452,200	0.26	361.3	20.6	--	2062	1249	9	6	0	
0014	110	79,600	453,500	0.25	344.2	20.6	--	2082	1265	11	4	0	
0015	104	79,400	452,100	0.24	327.4	20.6	--	2113	1280	14	8	0	
0016	100	80,000	455,300	0.23	311.2	20.7	--	2166	1309	15	70	0	
0017	134	123,900	705,500	0.43	599.1	32.1	6	2196	1365	10	40	12	125,000 Btu/hr-ft^2 UHC and CO not accurate
0018	123	125,000	711,500	0.39	548.5	32.3	6	2229	1368	13	21	11	
0019	109	123,700	704,300	0.35	488.3	32.0	6	2287	1396	20	21	12	
0020	115	125,300	713,300	0.38	527.4	32.4	6	2215	1388	15	20	11	
0021	105	125,100	712,200	0.35	483.7	32.4	6	2302	1416	21	18	10	
0022	100	124,800	710,900	0.35	475.1	32.3	6	2353	1450	25	749	7	
0023	110	124,700	710,300	0.37	515.5	32.3	6	2310	1446	20	18	11	
0024	103	124,600	709,200	0.34	466.8	32.2	6	2347	1470	21	17	8	

TABLE A-9. J-M FIRETUBE BOILER BURNER PARAMETRIC TESTING (AFTER 100 HOURS)

Test Pt.	TA (%)	Specific heat release (Btu/hr-ft^2)	Heat release (Btu/hr)	Velocity (ft/sec)	$\dot{m}_{air}$ (lbm/hr)	$\dot{m}_{natural\ gas}$ (lbm/hr)	ΔP_{burner} (in. H_2O)	$T_{burner\ avg}$ (°F)	$T_{exhaust}$ (°F)	NO_x (ppm)	CO (corrected) (ppm)	UHC (ppm)	Comments
0093	110	80,200	456,600	0.23	318	20.8	4	2104	1157	14	35	1	80,000 Btu/hr-ft^2
0094	107	80,500	458,500	0.22	307	20.8	4	2103	1155	13	46	0	
0095	103	79,400	451,900	0.21	292	20.5	4	2115	1161	11	80	0	
0096	101	79,500	452,700	0.21	280	20.6	4	2131	1152	15	445	0	
0097	110	79,500	452,800	0.22	305	20.6	4	2071	1135	13	14	0	
0098	115	79,200	450,800	0.23	321	20.4	4	2058	1145	15	10	0	
0099	128	80,400	457,900	0.27	374	20.8	4	2051	1150	6	15	0	
0100	122	80,200	456,400	0.26	362	20.8	4	2055	1153	8	16	0	
0102	111	64,600	367,700	0.19	267	16.7	3.5	1981	1092	11	15	3	65,000 Btu/hr-ft^2
0103	104	65,400	372,200	0.18	250	16.9	3.5	2013	1176	7	144	2	
0104	102	65,400	372,500	0.19	261	16.9	3.5	2034	1194	9	307	2	
0105	109	64,200	365,600	0.19	259	16.6	3.5	1998	1105	13	22	3	
0106	105	66,100	376,400	0.19	257	17.1	3.5	2021	1106	8	111	3	
0107	115	65,600	373,500	0.20	279	17.0	3.5	1982	1105	9	15	2	
0108	125	64,300	366,100	0.21	294	16.6	3.5	1977	1057	6	16	3	
0109	120	65,100	370,900	0.21	285	16.9	3.5	1987	1064	6	14	2	
0110	128	65,100	370,900	0.22	305	16.9	3.5	1984	1067	6	16	3	
0111	123	124,600	709,200	0.41	569	32.2	6	2234	1374	10	16	2	125,000 Btu/hr-ft^2
0112	126	124,800	710,400	0.41	569	32.3	6	2210	1374	10	16	1	
0113	120	124,200	707,000	0.40	557	32.1	6	2247	1390	12	15	2	
0114	114	124,400	708,100	0.38	527	32.2	6	2270	1395	16	14	2	
0115	110	125,300	713,300	0.37	512	32.4	6	2289	1407	18	14	2	
0116	109	--	--	--	--	--	6	2280	1421	18	12	2	
0117	100	124,600	709,400	0.35	477	32.2	6	2361	1416	24	3400	3	
0118	104	124,500	709,100	0.35	482	32.2	6	2295	1460	20	29	2	

TABLE A-10. FIRETUBE BOILER BASELINE DATA

Test No.	IA (%)	Specific heat release (Btu/hr-ft^2)	Heat release (Btu/hr)	$T_{firebox}$ exhaust (°F)	T_{flue} (°F)	T_{steam} (°F)	P_{boiler} (psi)	ΔP blower-viewport (in. wg)	Steam flow (gpm)	O_2 (%)	CO_2 (%)	Corrected to 0% O_2 NO_x (ppm)	UHC (ppm)	CO (ppm)	Comments
1	Rich	61,000	676,000	1760	351	233	6.5	0	0.99	1.8	10.0	55	770	11,000	Testing on natural gas at 65% of input capacity
2	112			1782	368	236	7.5		0.95	2.4	10.7	58	20	737	
3	120			1757	377	234	7.5		0.99	3.7	10.0	59	15	16	
4	128			1722	384	234	7.0		1.08	5.0	9.2	59	12	13	
5	132			1704	388	236	7.5		1.08	5.8	8.8	59	8	14	
6	137			1690	391	236	7.5		0.99	6.1	8.5	56	27	14	
7	145			1662	395	233	6.5		1.02	6.7	8.0	57	30	12	
8	152			1647	401	235	7.5		0.94	7.5	7.6	57	32	11	
9	160			1620	405	235	7.0		0.93	8.3	7.2	53	25	12	
10	169			1595	406	235	6.5		1.04	9.0	6.8	51	18	14	
11	181			1567	410	233	6.5	0.5	0.99	9.8	6.4	48	8	21	
12	191			1537	416	232	6.0	0.7	0.97	10.5	6.0	38	10	107	
13	101			1502	421	233	6.5	0.7	0.90	11.4	5.6	14	35	225	
14	Lean			1467	423	231	6.0	0.8	0.90	12.0	5.2	5	190	800	
15	Lean			1405	422	231	5.0	0.4	0.96	12.8	4.6	1	10,000	1,800	
R3	119			1745	377	233	7.5	0	0.95	3.4	10.0	58	24	2,182	
1	Rich	93,000	1,038,000	1908	431	232	6.5	0	1.33	2.4	10.0	61	646	10,775	100% of input capacity
2	114			1926	447	235	7.5	0	1.30	2.7	10.3	61	139	6,476	
3	120			1923	462	235	8.0	0.6	1.37	3.9	10.0	69	5	1,346	
4	130			1905	470	236	8.0	0.6	1.44	5.4	9.4	69	3	31	
5	135			1894	470	237	8.0	0.8	1.49	6.0	9.1	70	3	19	
6	140			1870	470	235	8.0	0.8	1.45	6.6	8.8	68	3	14	
7	150			1840	468	235	8.0	0.8	1.40	7.6	8.3	65	4	14	
8	155			1803	460	237	7.5	1.0	1.56	8.3	8.0	60	3	15	
1	Rich	77,000	854,000	1830	403	236	7.5	0	1.28	3.4	9.4	50	340	8,730	80% of input capacity
2	113			1842	406	236	8.0		1.25	3.6	9.6	52	52	3,890	
3	124			1840	417	236	8.0		1.20	4.4	9.4	57	6	380	
4	130			1823	423	236	8.0		1.25	5.2	8.9	59	5	15	
5	137			1805	427	236	8.0		1.27	6.0	8.5	59	6	14	
6	140			1796	430	238	8.0		1.25	6.4	8.3	59	6	13	
7	146			1792	429	236	8.0		1.20	7.0	8.0	59	5	11	
8	154			1760	434	235	8.0		1.24	7.8	7.5	59	5	11	
9	165			1715	430	235	8.0	0.6	1.30	8.8	7.1	57	5	12	
1	Rich	47,000	525,000	1645	317	328	8.5	0	0.73	2.4	10.4	51	420	6,920	50% of input capacity
2	Rich			1656	318	232	6.5		0.85	2.2	10.7	52	124	4,155	
3	112			1662	325	233	7.0		0.81	2.4	10.7	53	11	646	
4	116			1667	329	231	6.0		0.83	3.2	10.4	54	2	57	
5	119			1660	332	235	6.5		0.88	3.7	10.1	56	2	13	
6	121			1653	332	233	7.0		0.84	3.9	9.9	56	2	12	
7	125			1635	336	235	7.0		0.81	4.6	9.5	56	3	13	
8	132			1618	339	232	6.0		0.80	5.6	9.0	56	3	12	

TABLE A-11. JOHNS-MANVILLE FIBER BURNER TEST DATA

Test No.	Rating (%)	IA (%)	Specific Heat Release (Btu/hr-ft^2)	Heat Release (Btu/hr)	$T_{firetube\ exhaust}$ (°F)	T_{flue} (°F)	T_{steam} (°F)	P_{boiler} (psig)	$\Delta P_{blower\ exhaust}$ (in. of water)	O_2 (%)	CO_2 (%)	NO_x (ppm)	UHC (ppm)	CO (ppm)	Comments
1	97	107	88,000	1,017,000	1612	361	214	0	2.8	1.6	9.0	24	270	3.7%	Rich
2		107			1568	347			2.6	1.55	8.1	19	625	5.8%	
3		107			1638	366			3.2	1.6	9.8	23	237	2.8%	
4		128			1698	415	215		4.2	5.0	9.2	11	184	39	
5		116			1721	408	215		4.2	3.25	10.4	15	153	71	
6		110			1738	405	214		3.7	2.4	11.0	16	150	378	
7		133			1706	431	215		4.1	6.0	8.9	9	198	41	
8		146			1740	445			4.3	7.2	8.1	7	235	45	
9		159			1783	465			4.4	8.5	7.4	4	224	50	
10		110			1614	344	214		3.4	2.0	6.1	3	[illegible]37	8.3%	Rich
1	85	Rich	77,000	894,000	1575	339	214	0	2.3	---	9.5	24	250	2.7%	Rich
2		113			1680	380	215			2.9	10.6	15	155	103	
3		132			1646	400	214			5.6	9.0	9	190	54	
4		124			1660	396	215		3.8	4.6	9.6	11	171	51	
5		140			1657	417			3.7	6.7	8.4	7	188	43	
6		153			1700	434			3.6	8.0	7.7	4	271	64	
1	70	Rich	63,000	729,000	1444	310	214	0	2.5	1.4	9.4	18	380	3.2%	Rich
2					1450	314				1.4	9.6	18	380	3.0%	
3					1483	322				1.6	10.1	16.5	350	1.9%	
4		108			1541	339				1.6	11.1	13	370	1307	
1	61	108	55,000	640,000	1492	310	179	0	2.5	1.5	11.2	11	164	600	
3		110			1510	320	180			2.2	11.0	11	150	133	

TABLE A-12. ACUREX FIBER BURNER PARAMETRIC TEST SUMMARY

Test No.	Load rating (%)	Excess air (%)	Heat release (Btu/hr)	Specific heat release (Btu/hr-ft^2)	Emissions (corrected to 0% O_2) O_2 (%)	CO_2 (%)	NO_x (ppm)	UHC (ppm)	CO (ppm)	Firetube wall K_1 (°F)	K_{10} (°F)	K_7 (°F)	K_8 (°F)	K_9 (°F)	View-port K_6 (°F)	2nd pass gas K_2 (°F)	Flue K_3 (°F)	ΔP Fire-side K_3 (in. H_2O)	Efficiency (%)
56	120	5	1,258,000	114,000	1.0	11.4	26	49	106	262	264	423	321	335	2088	1540	496	1.4	82.0
57	120	4	1,258,000	114,000	0.8	11.6	26	42	240	261	263	428	321	334	2086	1524	494	1.4	
50	110	17	1,152,000	105,000	3.2	10.1	17	35	24	254	254	397	308	313	2008	1470	485	1.4	
51		12			2.3	10.7	19	45	23	261	258	420	315	335	2017	1450	482	1.17	
52		9			1.8	11.1	21	40	33	260	259	426	314	339	2017	1453	476	1.15	82.3
53		3			0.7	11.7	23	40	517	264	261	434	321	340	2023	1464	469	1.08	
54		8			1.6	11.1	21	38	33	262	260	426	316	340	2017	1446	477	1.16	
55		6			1.3	11.2	21	36	48	263	262	429	317	341	2018	1454	475	1.16	
38	100	20	1,049,400	95,400	3.8	10.0	12	18	24	255	251	398	299	321	1966	1445	478	1.14	
39		15			3.0	10.5	15	25	23	257	255	408	306	324	1961	1426	466	1.07	
40		11			2.2	10.8	17	22	22	258	256	416	312	324	1972	1430	460	0.99	82.6
41		3			0.6	11.8	20	26	310	260	260	426	314	329	1995	1470	448	0.93	
42		9			1.6	11.1	18	25	28	260	258	420	312	328	1977	1418	454	1.01	
43		24			4.1	9.6	11	23	25	255	254	396	301	320	1967	1434	477	1.15	
44		26			4.6	9.3	10	22	26	254	249	380	298	296	1960	1480	486	1.30	
45		29			4.8	9.2	11	20	26	252	248	378	300	298	1961	1470	486	1.28	
46		11			2.1	10.8	16	26	22	259	257	416	312	328	1970	1425	461	0.99	
47		12			2.4	10.7	16	26	23	259	256	416	312	327	1973	1410	460	0.99	
48		13			2.5	10.7	15	37	23	260	256	411	309	330	1958	1404	458	0.99	
49		7			1.3	11.3	17	38	54	263	260	421	314	334	1973	1410	449	1.02	
5	80	5	855,600	77,800	1.2	11.8	15	11	63	255	255	315	298	320	1875	1465	401	0.65	
6		2			0.6	12.0	15	11	215	256	253	313	299	316	1892	1440	401	0.62	
7		10			2.3	11.0	13	11	22	256	252	310	297	315	1894	1496	412	0.73	
8		13			2.9	10.7	13	14	23	254	254	303	293	313	1892	1475	419	0.78	
9		17			3.5	10.3	10	12	24	253	250	296	292	310	1870	1475	426	0.83	
10		26			4.6	9.6	9	13	26	250	246	288	286	302	1835	1456	436	0.85	
11		32			5.8	9.0	7	14	27	245	245	282	280	295	1872	1462	450	0.95	
12		40			6.5	8.5	7	13	29	242	242	276	274	288	1880	1462	456	1.0	
14		2			0.5	11.9	15	14	153	257	252	314	300	318	1898	1462	408	0.79	
15		18			3.5	10.1	11	13	12	255	250	296	294	308	1878	1428	424	--	
16		20			3.7	10.0	10	17	12	255	251	298	295	309	1880	1456	421	0.78	
17		6			1.4	11.4	14	19	53	257	253	315	304	316	1892	1394	407	0.65	
18		2			0.3	11.9	21	13	3070	256	252	315	300	313	1885	1363	395	0.60-	
19		5			0.8	11.5	15	12	63	257	256	315	302	317	1888	1385	401	0.65	
20		7			1.4	11.2	14	12	32	257	255	315	303	317	1891	1403	405	0.68	
28		10			1.8	11.0	13	22	28	257	253	312	302	316	1894	1418	406	0.70	
29		10			1.82	11.0	13	21	22	256	254	313	303	316	1894	1432	409	0.70	
37		10			1.95	11.0	13	--	28	255	252	313	300	314	1891	1375	405	--	83.7

(continued)

TABLE A-12. CONCLUDED

Test No.	Load rating (%)	Excess air (%)	Heat release (Btu/hr)	Specific heat release (Btu/hr-ft^2)	Emissions (corrected to 0% O_2)					Firetube wall					View-port	2nd pass gas	Flue	ΔP Fire-side	Efficiency (%)
					O_2 (%)	CO_2 (%)	NO_x (ppm)	UHC (ppm)	CO (ppm)	K_1 (°F)	K_{10} (°F)	K_7 (°F)	K_8 (°F)	K_9 (°F)	K_6 (°F)	K_2 (°F)	K_3 (°F)	K_3 (in. H_2O)	
21	65	35	682,000	62,000	5.7	8.6	5	6	14	244	244	278	276	286	1794	1435	402	0.6	
22		28			5.0	9.1	6	7	13	248	246	280	278	291	1780	1421	389	0.55	
23		21			3.8	9.8	7	7	12	250	248	287	281	297	1773	1322	378	0.5	
24		15			2.4	10.6	11	16	18	253	250	294	287	302	1768	1280	364	0.4	
25		7			1.4	11.3	12	10	27	253	252	297	288	305	1769	1289	358	0.35	
26		10			2.0	10.9	11	16	17	254	250	296	289	306	1768	1287	361	0.4	84.6
27		4			1.8	11.6	16	14	366	254	252	296	287	306	1770	1300	354	0.35	
30	50	11	525,400	48,000	2.1	10.8	10	10	22	242	250	286	280	291	1652	1246	328	0.15	85.3
31		8			1.5	11.2	13	--	870	242	251	286	279	291	1635	1246	306	0.13	
32		18			3.0	10.1	7	--	18	241	252	285	280	286	1641	1218	319	0.2	
33		24			4.0	9.6	5	--	13	240	250	280	278	285	1649	1203	329	0.2	
34		33			5.3	8.9	4	--	14	243	250	275	274	280	1661	1198	340	0.25	
35		7			1.4	11.2	14	--	1800	--	--	--	--	--	--	--	--	0.12	
36		38			5.7	8.5	4	--	14	245	246	272	272	279	1668	1197	346	0.3	

TABLE A-13. SUBSCALE CONCENTRIC WATERTUBE SECTION TEST DATA

Test I.D. No	Heat release rate (Btu/hr)	TA (%)	Fuel flow (lbm/hr)	Air flow (lbm/hr)	Upstream bed temp (°F)	Down-stream bed temp (°F)	$T_{exhaust}$ (°F)	$T_{air+fuel}$ in (°F)	T_{water} in (avg) (°F)	T_{water} out (avg) (°F)	Q_{water} tubes (Btu/hr)	$Q_{exhaust}$ (Btu/hr)	Combustion η (%)	Heat balance closure (%)	ΔP (inches water)	NO (ppm)	CO (ppm)	UHC (ppm)	CO_2 (% vol)	O_2 (% vol)	Comments
0009	241,580	121	11.2	246.4	1333	1988	1534	107	94	150	80,830	94,620	99.88	74.4	--	2	350	44	9.6	4.1	Lean side thermal NO_x data at 250,000 Btu/hr
0010	241,580	116	11.2	232.6	1490	2003	1544	104	99	161	89,490	90,165	99.62	76.4	--	2	675	250	10.2	3.1	
0011	241,580	109	11.2	219.6	1687	2006	1545	101	103	165	89,490	85,670	99.73	74.4	--	7	590	180	11.0	1.8	
0012	241,580	104	11.2	210.1	1805	2000	1541	103	103	167	92,380	81,910	99.87	73.9	--	16	400	70	11.5	1.0	
0013	239,430	100	11.1	196.8	1890	1989	1547	101	105	169	92,380	82,370	99.92	74.7	--	30	350	30	12.0	0.0	
0021	243,740	103	11.3	196.6	1855	1984	1433	101	101	167	95,265	70,840	99.95	69.8	5.0	32	126	37	11.8	0.6	
0022	243,740	100	11.3	192.3	1852	2005	1455	99	105	173	98,155	70,730	99.87	73.0	5.0	36	420	70	11.9	0.0	
0027	245,900	101	11.4	189.3	1726	2041	1473	97	126	184	83,720	70,840	99.95	64.5	4.2	32	200	15	11.8	0.2	
0028	245,900	107	11.4	199.5	1692	2024	1463	97	127	188	88,050	73,810	99.97	67.5	5.0	24	65	20	11.0	1.5	
0029	245,900	104	11.4	197.6	1727	2025	1466	97	127	190	90,940	73,310	99.97	68.4	5.0	27	65	22	11.4	1.0	
0030	245,900	114	11.4	211.9	1603	2006	1468	97	133	193	86,610	70,430	99.95	68.8	5.0	17	80	31	10.3	2.75	
0031	243,740	114	11.3	217.0	1551	2004	1465	97	137	196	85,165	80,015	99.90	69.5	5.0	13.5	123	70	10.3	2.75	
0032	243,740	120	11.3	203.0	1632	2014	1456	98	136	199	90,935	74,560	99.94	69.6	5.0	19.0	98	44	10.1	3.0	
0033	243,740	111	11.3	207.0	1397	2015	--	--	--	--	--	--	99.92	--	5.5	10.0	130	60	10.7	2.1	
0034	243,740	121	11.3	240.0	1160	1990	--	--	--	--	--	--	99.92	--	5.5	7.5	90	54	9.6	4.0	
0035	241,580	109	11.2	179.0	1067	1991	1404	88	74	134	86,610	63,950	99.84	64.1	5.0	21	145	145	10.8	1.9	
0036	243,740	108	11.3	170.8	1087	2011	1408	86	79	133	77,945	64,210	99.88	60.0	5.0	24	118	128	10.9	1.65	
0037	245,900	102	11.4	168.5	1937	2005	1402	87	89	141	75,060	60,445	99.97	56.7	5.0	32	95	20	11.6	0.5	
0038	245,900	100	11.4	166.0	1949	2004	1331	87	91	142	73,620	58,650	99.95	55.4	5.0	37	170	23	11.9	0.15	
0045	243,740	118	11.3	206.9	1446	1920	1459	111	123	160	66,400	75,710	99.95	60.0	5.5	10	135	21	9.9	3.5	
0046	243,740	111	11.3	194.3	1832	1931	1456	110	124	174	72,170	71,230	99.97	60.7	5.0	20	43	25	10.8	2.2	
0047	243,740	104	11.3	186.2	1993	1946	1452	110	122	173	73,615	68,220	99.97	59.9	5.0	27	55	19	11.4	1.0	
0048	241,580	100	11.2	174.0	2065	1940	1447	110	119	169	72,170	63,830	99.93	58.0	5.0	34	290	20	11.9	0.0	
0053	241,580	102	11.2	181.0	1838	1975	1465	103	111	158	67,840	64,690	99.99	56.5	3.5	22.5	3020	750	9.9	0.0	
0054	241,580	104	11.2	182.7	1897	1972	1441	104	109	156	67,880	66,500	99.99	57.3	3.0	19	4000	890	9.0	0.0	
0055	241,580	112	11.2	198.3	1664	1988	1457	102	103	150	67,840	72,730	99.98	59.9	4.0	37	2020	590	10.6	0.0	
0056	241,580	121	11.2	213.3	1293	1990	1412	101	108	143	50,520	75,200	99.97	53.7	4.5	37	550	35	11.8	0.0	
0057	245,900	131	11.4	227.9	1156	1967	1498	98	110	135	36,085	86,130	99.98	51.3	5.0	32	45	6	11.9	0.4	
0072	241,580	121	11.2	202.8	1298	1882	1563	85	118	160	60,625	74,600	99.65	57.9	5.0	22.5	30	9	11.4	1.06	
0073	243,740	120	11.3	200.6	--	--	--	--	--	--	--	--	--	--	6.0	13	40	11	10.5	2.5	
0074	243,740	125	11.3	202.4	1311	1908	1482	102	147	182	50,520	75,645	97.22	54.9	6.5	6.5	40	13	9.5	4.0	
0075	243,740	126	11.3	200.1	1250	1908	1471	105	144	149	72,700	74,870	98.94	62.5	6.5	6.0	18	11	8.8	5.4	

Reproduced from
best available copy.

TABLE A-13. CONTINUED

Test I.D. No.	Heat release rate (Btu/hr)	IA (%)	Fuel flow (lbm/hr)	Air flow (lbm/hr)	Up-stream bed temp (°F)	Down-stream bed temp (°F)	$T_{exhaust}$ (°F)	$T_{air+fuel}$ in (°F)	T_{water} in (avg) (°F)	T_{water} out (avg) (°F)	Q_{water} tubes (Btu/hr)	$Q_{exhaust}$ (Btu/hr)	Combustion η (%)	Heat balance closure (%)	ΔP (inches water)	NO (ppmv)	CO (ppmv)	UHC (ppmv)	CO_2 (% vol)	O_2 (% vol)	Comments
0008	245,900	99	11.4	196.4	2028	1930	1405	103	96	156	86,610	73,660	99.18	67.4	--	39	2050	550	11.5	0.12	Rich combustion thermal NO_x data at 250,000 Btu/hr
0014	239,430	93	11.1	187.9	1893	2012	1579	100	105	167	89,490	73,110	99.33	70.1	--	36	2390	290	11.3	0.0	
0015	239,430	86	11.1	173.4	1751	2032	1580	97	105	153	68,285	70,590	97.67	61.5	--	36	6110	1200	9.7	0.0	
0016	237,270	92	11.0	188.1	1468	1653	1525	96	103	136	47,635	73,150	97.06	54.2	--	39	8960	920	8.4	0.0	
2023	245,900	90	11.4	177.5	1775	1989	1501	97	109	161	75,060	68,110	99.08	60.4	3.5	26	2400	510	10.5	0.0	
0024	245,900	91	11.4	179.1	1749	1986	1507	97	109	160	73,615	69,120	99.20	60.2	3.5	23	2230	420	10.6	0.0	
0025	248,060	84	11.5	166.0	1655	1772	1536	98	112	147	50,520	65,700	98.76	49.1	3.0	18	3640	480	9.4	0.0	
0026	248,060	93	11.5	184.0	1704	2007	1502	97	118	169	73,615	70,540	99.72	59.9	3.5	18	1000	125	11.6	0.0	
0039	248,060	90	11.5	157.2	1971	1996	1292	88	93	144	73,620	51,510	99.28	52.4	4.5	33	1650	455	10.8	0.0	
0049	243,740	90	11.3	156.5	1953	1952	1468	107	116	154	54,850	58,780	99.72	48.4	3.5	22.5	3020	750	9.9	0.0	
0050	243,740	88	11.3	153.1	1784	1957	1514	106	115	146	44,750	59,510	98.21	45.2	3.0	19	4000	890	9.0	0.0	
0051	243,740	91	11.3	155.0	--	--	--	--	--	--	--	--	--	--	4.0	37	2020	590	10.6	0.0	
0052	241,580	99	11.2	174.2	1784	2006	1490	104	110	158	69,285	66,070	99.88	57.0	4.5	37	550	35	11.8	0.0	
0071	243,740	95	11.3	185.0	1474	1864	1512	85	109	163	27,985	71,935	--	--	--	--	--	--	--	--	
0001	245,900	115	11.4	224.6	2218	1990	1506	330	73	157	111,980	72,240	--	--	--	--	--	--	--	--	High front row temperatures
0002	245,900	115	11.4	224.3	2225	1994	1508	264	77	160	121,250	75,940	--	--	--	--	--	--	--	--	
0003	248,060	110	11.5	224.9	2222	1998	1508	278	81	164	111,980	77,760	99.93	78.2	--	11.5	110	55	11.1	2.0	
0004	248,060	88	11.5	173.0	1846	1669	1603	202	81	134	76,500	66,950	97.92	60.7	--	25	5820	1050	10.0	0.1	
0005	254,520	98	11.8	199.4	2257	1447	1452	241	87	165	112,590	65,985	99.44	72.1	--	35	1950	230	11.7	0.15	
0018	241,580	112	11.2	207.6	2269	1938	1498	423	104	175	102,485	61,815	99.97	69.7	--	22	130	6	10.7	2.3	
0040	243,740	103	11.3	163.1	2073	1821	1306	155	124	178	77,985	54,960	97.58	57.6	5.0	20	1140	2400	10.5	0.86	
0041	243,740	104	11.3	169.3	2128	1840	1318	164	121	185	92,380	53,250	97.53	62.9	6.0	24.5	600	2600	11.0	0.95	
0042	241,580	109	11.2	176.0	2186	1849	1272	185	121	185	90,940	52,160	96.91	62.8	5.0	21	180	3300	10.8	1.9	
0043	241,580	121	11.2	196.1	2031	1885	1301	177	122	185	90,940	59,420	97.86	65.3	7.5	22.5	150	2000	9.5	4.0	
0044	241,580	102	11.2	155.1	1959	1680	1474	164	123	169	70,730	56,075	98.59	54.9	6.0	21.5	1360	1300	10.9	0.45	
0017	241,580	121	11.2	241.8	2067	1933	1506	427	101	168	96,710	71,800	99.88	71.5	--	6	330	53	9.7	4.0	425°F preheat temperature
0019	243,740	102	11.3	201.6	--	--	--	--	--	--	--	--	--	--	--	40	190	1	11.9	0.4	
0020	243,740	82	11.3	168.7	--	--	--	--	--	--	--	--	--	--	--	50	8300	1550	8.8	0.0	

(continued)

TABLE A-13. CONCLUDED

Test I.D. No	Heat release rate (Btu/hr)	TA (%)	Fuel flow (lbm/hr)	Air flow (lbm/hr)	Upstream bed temp (°F)	Down stream bed temp (°F)	$T_{exhaust}$ (°F)	$T_{air+fuel}$ in (°F)	T_{water} in (avg) (°F)	T_{water} out (avg) (°F)	$Q_{water\ tubes}$ (Btu/hr)	$Q_{exhaust}$ (Btu/hr)	Combustion η (%)	Heat balance closure (%)	ΔP (inches water)	NO (ppmv)	CO (ppmv)	UHC (ppmv)	CO_2 (% vol)	O_2 (% vol)	Comments
0006	342,960	105	15.9	280.3	1437	2150	1625	96	90	155	93,820	117,120	99.99	62.7	--	29	30	0	11.6	1.15	Maximum throughput
0007	414,140	104	19.2	329.5	1397	2261	1797	97	95	147	75,060	139,955	99.99	52.9	--	30	30	0	11.7	0.95	
0058	345,170	114	16.0	307.4	1077	2178	1655	96	100	137	53,410	119,030	99.99	51.1	9.0	18	40	2	10.4	2.8	
0059	342,960	120	15.9	359.6	901	2166	1613	92	115	143	40,415	122,130	99.99	48.6	8.5	12	25	2	9.5	3.9	
0060	340,810	120	15.8	347.4	898	2153	1611	92	119	149	40,420	121,050	99.99	48.6	8.5	12	25	2	9.5	3.9	
0061	342,960	111	15.9	264.9	1268	2165	1632	92	126	167	59,180	111,830	99.99	51.0	8.0	10.5	43	2	10.7	2.1	
0062	340,800	104	15.8	254.6	1377	2189	1683	93	129	171	60,625	111,610	99.97	51.7	7.5	20	125	4	11.4	1.0	
0063	340,800	101	15.8	244.8	1464	2214	1700	93	136	173	56,295	100,840	99.92	49.7	7.0	33	400	4	11.6	0.1	
0064	340,800	93	15.8	230.1	1462	2106	1682	94	135	172	53,410	101,370	99.70	46.9	5.5	14.5	1600	6	10.8	--	
0065	340,800	87	15.8	227.0	1437	2093	1693	95	138	175	53,410	100,725	99.69	46.5	5.0	15	2400	16	10.2	--	
0066	340,800	85	15.8	218.8	1315	1762	1664	96	139	166	38,970	95,350	99.23	40.9	3.5	15.5	3500	42	9.3	--	
0067	440,030	110	20.4	307.4	93	1992	1785	93	159	180	30,310	180,050	99.99	48.9	8.5	18	30	2	9.4	3.9	
0068	442,180	120	20.5	359.6	87	2142	1854	91	164	187	33,700	176,240	99.99	48.3	3.0	20.5	45	2	10.0	3.1	
0069	435,710	116	20.2	347.4	89	2220	1885	92	169	196	38,970	173,345	99.98	49.7	3.0	28	75	3	10.6	2.1	
0070	444,340	111	20.6	363.1	130	1920	1754	82	93	112	27,425	167,760	--	--	--	--	--	--	--	--	
0076	243,740	124	11.3	201.6	1243	1913	1409	113	127	157	43,300	75,140	99.15	34.5	6.0	345	1150	560	8.1	4.4	NH_3 Doping 0.5 wt %
0077	241,580	110	11.2	184.3	1507	1892	1420	117	120	169	70,730	65,375	97.44	59.5	5.5	9	300	2400	9.6	3.4	
0078	241,580	120	11.2	183.4	1535	1907	1446	119	118	169	73,615	66,390	99.04	60.2	5.5	385	260	900	9.7	3.0	NH_3 doping 0.5 wt %
0079	241,580	108	11.2	168.5	1097	1898	1450	119	116	175	85,160	61,280	97.14	64.1	5.0	19	300	3000	10.7	1.7	
0080	241,580	103	11.2	169.0	1896	1955	1473	127	113	179	95,265	62,215	99.02	67.5	5.0	520	550	1000	11.4	0.7	NH_3 doping 0.5 wt %
0081	248,060	69	11.5	131.0	1624	1507	1553	608	130	161	44,750	35,110	92.20	36.9	2.5	12	7600	4900	7.0	0.0	
0082	248,060	69	11.5	131.5	1601	1502	1563	613	130	160	43,300	36,030	92.00	36.5	2.5	100	7700	4900	6.8	0.0	NH_3 doping 0.5 wt %
0083	243,740	75	11.3	141.6	1867	1896	1460	630	139	178	56,295	33,610	95.30	40.4	3.5	34	6600	2600	7.7	0.0	
0084	243,740	74	11.3	140.4	1875	1901	1485	624	139	177	54,850	34,600	95.30	40.2	3.5	310	6700	2600	7.5	0.0	NH_3 doping 0.5 wt %
0085	241,580	80	11.2	145.7	2046	1784	1242	599	150	209	85,160	34,330	94.30	54.1	4.0	32	5600	4330	8.2	0.0	
0086	241,580	79	11.2	144.6	2059	1795	1441	595	150	213	90,935	34,960	94.00	57.2	4.0	335	5600	4330	8.1	0.0	NH_3 doping 0.5 wt %
0087	243,740	89	11.3	168.7	--	--	--	--	--	--	--	--	97.37	--	4.0	26	4800	1300	10.0	0.0	
0088	252,370	89	11.7	160.4	1864	2026	1518	183	98	145	67,040	59,345	98.00	--	4.0	330	2850	700	9.9	0.0	NH_3 doping 0.5 wt %
0089	245,900	84	11.4	174.8	1747	1952	1519	170	106	145	56,295	65,650	98.50	52.0	3.5	29	3500	960	9.3	0.0	
0090	245,900	84	11.4	176.1	1711	1926	1512	167	109	143	49,075	66,440	98.37	48.9	3.5	310	3690	860	9.2	0.0	NH_3 doping 0.5 wt %
0091	245,900	94	11.4	174.8	1904	1985	1532	156	116	164	69,285	64,960	99.08	56.7	3.0	28	1760	390	10.8	0.0	
0092	245,900	93	11.4	176.1	1911	1989	1536	152	109	162	76,500	66,040	99.08	60.1	3.0	320	1870	410	10.7	0.0	NH_3 doping 0.5 wt %
0093	250,000	132	13.9	273.2	2315	2118	1595	658	76	144	98,155	61,030	94.97	69.1	--	20	1350	110	11.4	5.6	Diesel fuel 650°F preheat
0094	250,000	124	13.9	223.2	2399	2091	1571	648	79	163	121,250	55,700	97.08	74.6	13.0	46	700	100	12.4	4.4	
0095	250,000	116	13.9	204.3	2413	2069	1530	644	89	178	128,465	49,200	97.89	75.8	12.0	58	650	100	13.2	3.2	
0096	250,000	108	13.9	189.4	2435	2060	1481	636	91	186	137,130	43,720	96.95	76.3	11.0	86	600	105	14.4	1.7	
0097	250,000	103	13.9	178.0	2437	2011	1443	628	95	192	140,010	39,800	97.66	75.2	10.0	120	600	115	15.4	0.5	
0098	250,000	99	13.9	167.9	2383	1912	1472	675	98	201	148,670	36,880	95.23	79.6	9.0	132	1600	160	16.8	0.0	
0099	250,000	99	13.9	150.0	2253	1735	1323	730	94	197	148,670	24,735	91.56	77.5	9.0	225	3550	110	13.3	0.0	

Note: 1. Constant surface losses based on previous data = 4000 Btu/hr
2. Watertube flowrate = 2.9 gpm

(concluded)

Reproduced from best available copy.

TABLE A-14. SUBSCALE CONCENTRIC WATERTUBE SECTION FUEL NITROGEN DATA

Test No.	TA (%)	Dopant conc (ppmv)	Max NH_3 conc (ppmv)	Thermal NO_x (ppmv)	Total NO_x (ppmv)	Fuel NO_x (ppmv)	NH_3 (ppmv)	HCN (ppmv)	Fuel NO_x conv (%)	NH_3 conv (%)	HCN conv (%)	Total conv (%)
0076	124	5778	532.1	4.5	345	340.5	3.2	9.5	65.7	0.6	1.8	68.1
0078	120	5830	581.3	8.8	385	376.2	9.5	3.1	66.2	1.6	0.5	68.3
0080	103	5830	624.3	24	520	496	3.5	46.4	83.3	0.6	7.4	91.3
0082	69	5678	775.7	12	100	88	106.6	688.4	12.9	13.7	88.7	115.3
0084	74	5344	727.1	34	310	276	20.7	180.1	42.6	2.8	24.8	70.2
0086	79	5830	716.6	32	335	303	99.8	271.7	46.7	13.9	37.9	98.5
0088	89	5580	652.1	26	330	304	16.6	281.9	50.6	2.5	43.2	96.3
0090	84	5727	600.6	29	310	281	45.2	235.2	51.6	7.5	39.2	98.3
0092	93	5727	606.7	28	320	292	5.8	218.3	52.7	1.0	34.0	87.7

TABLE A-15. CONCENTRIC WATERTUBE BOILER DATA SUMMARY

Data Point	Heat Release Rate (Btu/hr)	Preheat Temperature (°F)	Air Flow (scfm)	Fuel Flow (scfm)	TA (%)	O_2 (%)	CO_2 (%)	UHC (ppm)	CO (ppm)	NO (ppm)
01	1.08×10^6	422	193	18.7	102	0.4	10.8	120	1600	29
02	↓	434	198	19.5	102	0.4	10.9	60	1300	30
03	↓	444	209	19.5	103	0.5	11.7	2	11	32
04	↓	444	217	19.5	110	2.0	10.8	2	3	27
05	↓	445	204	19.5	106	1.2	11.2	0	3	30
06	↓	455	217	19.3	113	2.65	10.5	↓	2	23
07	↓	454	219	19.2	116	3.15	10.2	↓	↓	21.5
08	↓	454	222	19.0	120	3.8	9.8	↓	↓	19
09	↓	---	---	----	124	4.35	9.4	↓	↓	17.5
10	↓	461	244	19.2	125	4.65	9.3	↓	↓	16
11	↓	463	240	19.4	126	4.85	9.2	↓	↓	15.5
12	↓	467	245	19.4	129	5.3	9.0	↓	↓	14.0
13	↓	470	246	19.9	134	5.7	8.8	12	↓	12.0
14	↓	471	251	19.4	136	6.0	8.4	6	↓	10
15	↓	471	251	19.8	138	6.25	8.4	2	↓	9
16	↓	---	---	----	101	0.1	11.7	0	9	33
17	0.76×10^6	423	139	14.0	101	0.2	11.8	0	20	32
18	↓	425	144	14.0	105	1.1	11.2	↓	2	29
19	↓	429	149	14.0	108	1.6	11.0	↓	2	27
20	↓	433	148	13.8	112	2.4	10.6	↓	↓	24
21	↓	428	146	13.7	109	1.8	10.8	↓	↓	26
22	↓	430	152	13.6	111	2.2	10.6	↓	↓	24
23	↓	435	145	13.4	115	2.9	10.3	↓	↓	21
24	↓	440	149	13.3	118	3.4	10.0	↓	3	19
25	↓	444	151	13.4	119	3.8	9.8	↓	3	15.5
26	↓	446	160	13.4	125	4.4	9.5	↓	3	13
27	↓	450	165	13.2	127	4.9	9.2	↓	2	12
28	↓	456	167	13.3	133	5.6	8.8	↓	2	10
29	↓	458	166	13.3	136	6.0	8.5	↓	2	8
30	1.04×10^6	129	205	18.9	101	0.2	11.8	0	15	25
31	↓	127	205	19.2	103	0.7	11.5	0	2	24
32	↓	124	204	19.0	105	1.15	11.3	1	2	27
33	↓	121	200	19.0	108	1.7	10.9	7	2	20
34	↓	117	212	19.0	112	2.35	10.6	27	2	18
35	↓	115	213	18.8	114	2.8	10.3	20	2	17
36	↓	113	213	18.8	116	3.2	10.1	15	1	15.5
37	↓	109	223	18.5	115	3.0	10.3	11	1	16
38	↓	107	233	18.6	118	3.4	10.0	9	1	15
39	↓	104	232	18.0	119	3.65	9.8	6	2	14
40	↓	102	234	18.3	124	4.45	9.4	5	1	12
41	↓	101	245	18.2	120	3.85	9.7	5	1	14
42	↓	98	234	18.6	125	4.7	9.3	4	1	12
43	↓	97	235	18.4	129	5.1	9.1	4	1	10
44	1.20×10^6	91	234	22.0	104	1.0	11.3	12	2	29
45	↓	89	232	21.7	101	0.2	11.7	11	11	38
46	↓	89	240	21.4	106	1.35	11.1	9	2	25
47	↓	88	238	21.4	109	1.9	10.8	7	2	23
48	↓	87	236	21.4	112	2.35	10.6	7	2	21
49	↓	87	247	21.3	114	2.85	10.3	7	2	19
50	↓	85	283	21.5	120	3.7	9.8	7	2	16
51	↓	85	285	21.6	123	4.2	9.5	10	2	16
52	↓	84	293	21.6	127	4.8	9.2	12	2	18

TABLE A-16. CONCENTRIC WATERTUBE BOILER DATA SUMMARY

Data Point	Heat release rate (Btu/hr)	Preheat temp (°F)	Air flow (scfm)	Fuel flow rate (scfm)	TA (%)	O_2 (%)	CO_2 (%)	UHC (ppm)	CO (ppm)	NO (ppm)	Temperatures						Comments
											1 (°F)	2 (°F)	3 (°F)	4 (°F)	5 (°F)	T_{out} (°F)	
01	735,000	384	127	13.3	102	0.6	10.4	3100	3140	20	2222	2456	1307	1151	623		12/8/81
02	↓	357	133	13.3	101	0.3	9.7	1190	3140	32	2230	2024	1385	1168	571		
03	↓	408	134	13.1	105	1.0	10.6	3200	3140	17	2226	2662	1729	1325	627		
04	↓	443	134	13.0	102	0.6	11.3	450	2730	30	2297	2829	1617	1337	622		
05	↓	467	148	12.9	108	1.7	11.0	20	450	31	2321	2881	1616	1340	652		
06	↓	478	143	12.8	112	2.5	10.7	5	250	31	2318	2889	1593	1376	670		
07	↓	481	144	12.8	115	3.0	10.2	0	180	30	2308	2870	1652	1411	685		
08	↓	487	172	12.8	114	2.9	10.3	0	150	32	2319	2860	1691	1433	686		
09	↓	481	171	12.7	118	3.6	9.9	2	160	26	2305	2821	1720	1453	711		
10	↓	475	178	12.5	124	4.2	9.6	22	240	19	2292	2767	1746	1474	750		
11	↓	467	181	12.5	126	4.7	9.2	57	310	12	2276	2701	1764	1488	759		
12	↓	459	181	12.5	128	5.2	9.0	59	390	9	2270	2653	1776	1495	785		
13	↓	456	195	12.5	132	5.6	8.7	195	800	4	2257	2598	1781	1506	803		
14	↓	451	187	12.5	136	6.0	8.4	370	1180	4	2248	2533	1807	1522	823		
15	1.0×10^6	314	402	17.6	140	6.5	8.2	0	130	18	2087	--	1945	1852	1427		
16	↓	303	408	17.7	127	5.0	8.3	0	90	20	2108	--	2022	1797	1362		
01	0.96×10^6	417	141	16.0	122	4.0	9.8	50	410	7	1948	2454	2055	2344	--	1376	1/11/82
02	0.96×10^6	418	138	16.0	122	3.9	9.8	40	360	8	--	--	--	2332	--	1358	
03	1.04×10^6	424	128	17.3	113	2.3	10.7	20	90	24	--	--	--	2416	--	1400	
04	1.06×10^6	426	132	17.8	110	1.8	11.0	25	90	23	--	--	--	2435	--	1404	
05	1.25×10^6	425	156	20.4	115	2.4	10.5	16	20	28	--	--	--	2162	--	1463	
06	↓	429	144	20.5	110	1.5	11.0	17	30	30	--	--	--	2181	--	1496	
07	↓	431	143	20.4	107	1.1	11.4	20	110	28	--	--	--	2194	--	1475	
08	↓	431	158	20.3	106	0.7	11.5	20	200	30	--	--	--	2182	--	1466	
09	↓	--	--	--	112	2.0	10.8	17	20	29	--	--	--	--	--	--	
10	↓	428	152	20.5	115	2.7	10.5	21	20	27	--	--	--	2168	--	1468	
11	↓	426	165	20.3	118	3.3	10.2	18	30	24	--	--	--	2159	--	1444	
12	↓	419	162	20.2	125	4.2	9.6	22	100	16	--	--	--	2122	--	1420	
13	↓	419	167	20.3	124	4.0	9.7	23	80	18	--	--	--	2118	--	1428	56.0 gal/hr makeup water
14	↓	413	184	20.4	127	4.6	9.4	33	190	9	--	--	--	2091	--	1443	
15	↓	325	177	19.9	134	5.3	8.9	98	640	4	--	--	--	2023	--	1490	
16	↓	--	--	--	121	3.7	9.9	95	440	5	--	--	--	--	--	--	Preheat turned off
17	↓	293	172	19.7	117	3.0	10.3	75	330	11	--	--	--	2008	--	1504	
18	↓	310	168	19.7	112	2.2	10.8	118	380	12	--	--	--	1992	--	1515	
19	↓	275	152	20.0	110	1.7	11.0	230	660	13	--	--	--	1982	--	1537	43.2 gal/hr water
20	↓	220	145	19.7	108	0.8	11.3	840	2160	13	--	--	--	2006	--	1541	
21	↓	157	152	19.6	122	3.9	9.8	52	130	11	--	--	--	2070	--	1625	
22	↓	126	174	19.4	128	4.8	9.3	27	50	15	--	--	--	1944	--	1701	

(continued)

TABLE A-16. CONCLUDED

Data Point	Heat release rate (Btu/hr)	Preheat temp (°F)	Air flow (scfm)	Fuel flow rate (scfm)	TA (%)	O_2 (%)	CO_2 (%)	UHC (ppm)	CO (ppm)	NO (ppm)	Temperatures 1 (°F)	2 (°F)	3 (°F)	4 (°F)	5 (°F)	T_{out} (°F)	Comments
01	1.0×10^6	362	154	16.6	137	6.0	8.7	3	100	9.6				2179		1426	1/13/82
02		363	156	16.7	143	6.6	8.3	3	60	8.5				2167		1446	
03		365	154	16.8	130	5.2	9.2	2	60	15.5				2204		1423	
04		362	153	17.0	123	4.4	9.7	0	10	22.5				2120		1418	46.0 gal/hr
05		355	146	17.0	118	3.4	10.2	0	0	28.0				2051		1435	
06		401	126	17.3	118	3.3	10.2	0	120	25				1926		1433	
07		401	125	16.5	118	3.3	10.2	1	200	20				1912		1401	
08		404	123	16.8	115	2.8	10.5	0	130	26.5				1920		1437	
09		405	117	16.6	110	1.9	11.0	10	180	29.0				1929		1463	
10		423	119	16.6	107	1.2	11.3	98	670	26.0				1926		1470	
11		416	--	--	105	0.6	11.5	500	2300	24.0				1915		1462	
12		334	114	16.5	112	1.3	10.8	4500	0.9%	3.5				1853		1434	Preheat turned off
13		290	117	16.7	113	2.1	10.7	900	1800	4.5				1880		1436	
14		256	115	16.7	116	2.7	10.4	400	1200	4.0				1887		1454	
15		219	130	16.7	118	3.1	10.2	290	880	3.6				1894		1457	28.0 gal/hr
16		218	123	16.8	122	3.8	9.8	300	880	3.2				1897		1470	
17		155	130	16.9	126	4.6	9.5	300	110	15				1888		1584	
18		225	130	17.0	130	5.0	9.2	200	390	15				1705		1597	
19		--	--	--	--	5.5	8.5	--	--	12				1351		1101	
01	1.0×10^6	320	133	16.9	111	2.3	10.7	90	260	22				1880- 1930		1419	1/15/82
02		290	134	16.7	111	2.3	10.7	100	410	18				1960		1423	
03		225	134	16.6	113	2.3	10.7	165	510	16				1907		1448	
04		180	136	16.7	114	2.4	10.6	350	1020	8				1901		1453	
05		155	135	16.5	114	2.4	10.6	600	1270	7				1891		1456	
06		125	134	16.5	113	2.4	10.6	700	1250	5				1915		1477	
07		120	128	16.4	113	2.1	10.8	1000	1620	6				1917		1484	
08		120	121	16.4	108	1.5	10.9	2400	0.6%	5	1726		1540	1940		1485	Flames apparent at back end
09		120	115	16.6	107	1.3	11.0	3200	0.8%	5	1660		1540	1942		1490	
10		120	113	16.2	106	1.2	10.7	8000	1.4%	3	1500		1220	1931		1490	
11		120	110	16.1	103	0.7	10.6	7500	2.2%	7	950		800- 350	1975		1522	

TABLE A-17. WATERTUBE BOILER DATA SUMMARY OF EMISSIONS AND ΔP

Data Point	Heat Input Rate (Btu/hr)	Theoretical Air (%)	Preheat Temp (°F)	Air Flow (scfm)	Fuel* Flow (scfm)	O_2 (%)	CO_2 (%)	UHC (ppm)	CO (ppm/%)	NO (ppm)	ΔP (in. H_2O)
1	683,000	176	803	213	12.3	9.0	7.4	54	85	15	4
2	683,000	132	801	160	12.3	5.2	9.4	0	38	56	4
3	683,000	121	800	147	12.3	2.7	10.3	0	140	94	4
4	683,000	145	800	176	12.3	7.2	8.3	0	35	30	4
5	683,000		743	185	12.3	6.7	8.3	13	68	25	4
1	612,000	133	733	144	11.0	6.2	8.5	150	135	36	3.0
2	728,000	124	741	161	13.1	5.4	8.9	2	60	45	3.7
3	790,000	126	680	176	14.2	4.8	9.2	0	90	42	4.0
4	851,000	117	614	177	15.3	3.7	9.8	7	500	36	4.2
5	973,000	98	556	170	17.5	1.9	10.5	330	0.8%	35	4.2
6	912,000	107	554	173	16.4	2.7	10.2	70	0.4%	31	4.2
7	912,000	104	515	168	16.4	2.7	10.2	160	0.4%	26	4.2
8	912,000	111	648	180	16.4	2.3	10.3	15	0.3%	42	--
9	912,000	134	665	217	16.4	5.5	8.9	4	80	33	--

*Natural gas

TABLE A-18. WATERTUBE BOILER DATA SUMMARY OF GAS AND TUBE TEMPERATURES

Data Point	Heat Input Rate (Btu/hr)	Theoretical Air (%)	Preheat Temp	T_t	T_g	T_g	T_t	T_g	T_g	T_t	T_g	T_g	T_t	T_g	T_g	T_t	T_g	Exit Temp
				1	1	2	2	3	4	3	5	6	4	7	8	5	9	
1	683,000	176	803	1966	2135	1903	1849	1553	1282	1247	1119	992	848	816	707	670	621	475
2	683,000	132	801	2317	2266	1904	1847	1528	1239	1212	1076	936	802	767	658	623	573	472
3	683,000	121	800	2351	2284	1899	1846	1523	1230	1210	1064	924	801	756	647	621	566	472
4	683,000	145	800	2066	2209	1898	1851	1540	1257	1233	1096	961	830	794	684	650	599	497
5	683,000	153	743	2014	2164	1890	1835	1542	1256	1228	1096	965	828	796	686	648	602	499
1	612,000	133	733	2043	2163	1864	1814	1505	1214	1200	1039	899	818	731	627	628	546	427
2	728,000	124	741	2083	2238	1952	1912	1576	1285	1240	1108	965	835	787	676	639	590	484
3	790,000	126	680	1997	2245	1982	1952	1608	1317	1275	1140	966	866	816	702	665	614	498
4	851,000	117	614	1953	2296	2022	2018	1651	1347	1320	1177	1021	899	840	719	694	632	517
5	973,000	98	556	1876	2364	2092	2117	1732	1416	1441	1271	1087	1034	918	768	848	672	542
6	912,000	107	554	1911	2340	2058	2078	1700	1382	1385	1233	1053	964	894	746	772	657	531
7	912,000	104	515	1924	2316	2052	2066	1704	1384	1387	1239	1056	969	893	749	771	657	535
8	912,000	111	648	2152	2390	2052	--	1706	1360	--	1214	1039	928	869	736	740	652	530
9	912,000	134	665	2124	2256	2035	--	1687	1368	--	1206	1064	920	888	766	722	678	556

T_t = Catalyst tube temperature
T_g = Gas temperature